Aix Marseille Université

# THÈSE DE DOCTORAT

Soutenue à Aix-Marseille Université
le 7 mars 2025 par


## Blanche KRIEGUER


# Impact des rayonnements ionisants sur les matériaux polymères utilisés pour des applications biopharmaceutiques et biotechnologiques

**Discipline**
Sciences Chimiques

**École doctorale**
ED 250 – Sciences Chimiques de Marseille

**Laboratoire et Partenaires de recherche**

- ICR (Institut de Chimie Radicalaire)

- IMBE (Institut Méditerranéen de Biodiversité et d'Ecologie)

- Sartorius Stedim FMT S.A.S

**Composition du jury**

| | |
|---|---|
| Christine BRESSY<br>PR, Université de Toulon | Rapporteuse |
| Emmanuel RICHAUD<br>PR, Arts et Métiers Paris Tech | Rapporteur |
| Sophie ROUIF<br>Expert R&D, Ionisos Group | Examinatrice |
| Belkacem OTAZAGHINE<br>MCF, Ecole des mines d'Alès | Examinateur |
| Grégoire DANGER<br>PR, Aix-Marseille Université | Président du jury |
| Sylvain MARQUE<br>PR, Aix-Marseille Université | Directeur de thèse |
| Nathalie DUPUY<br>PR, Aix-Marseille Université | Co-directrice de thèse |
| Fabien GIRARD<br>MCF, Aix-Marseille Université | Co-encadrant de thèse |
| Samuel DOREY<br>Principal Scientist, Sartorius Stedim FMT S.A.S. | Membre invité |

imbe Institut méditerranéen de biodiversité et d'écologie - marine et continentale -

ICR Institut Chimie Radicalaire

SARTORIUS

# Affidavit

Je soussignée, Blanche Krieguer, déclare par la présente que le travail présenté dans ce manuscrit est mon propre travail, réalisé sous la direction scientifique de Sylvain MARQUE (directeur de thèse) et Nathalie DUPUY (co-directrice de thèse), dans le respect des principes d'honnêteté, d'intégrité et de responsabilité inhérents à la mission de recherche. Les travaux de recherche et la rédaction de ce manuscrit ont été réalisés dans le respect à la fois de la charte nationale de déontologie des métiers de la recherche et de la charte d'Aix-Marseille Université relative à la lutte contre le plagiat.

Ce travail n'a pas été précédemment soumis en France ou à l'étranger dans une version identique ou similaire à un organisme examinateur.

Fait à Marseille, le 10 janvier 2025



Cette œuvre est mise à disposition selon les termes de la Licence Creative Commons Attribution - Pas d'Utilisation Commerciale - Pas de Modification 4.0 International.

# Liste des publications et participation aux conférences

1) Liste des publications réalisées dans le cadre du projet de thèse

1. **Gamma, E-beam and X-ray Irradiations on PE/EVOH/PE Multilayer Film: An Industrial Point of View Regarding the Impact on Mechanical Properties**, Nina Girard-Perier, Sylvain R. A. Marque, Nathalie Dupuy, Blanche Krieguer, Samuel Dorey, Polymers **2023**, 15, 2799, doi:10.3390/polym15132799

2. **Comparison of effects from gamma, e-beam and X-ray radiation on multilayer polymer films used in biopharmaceutical devices by chemometric treatment of spectroscopic data**, Blanche Krieguer, Sylvain R.A. Marque, Samuel Dorey, Fabien Girard, Yelin Ni, Donghui Li, Mark K. Murphy, Leonard S. Fifield, Nathalie Dupuy, Radiation Physics and Chemistry **2024**, 218, 111607, doi:10.1016/j.radphyschem.2024.111607

3. **Radical detection and electron-spin resonance (ESR) monitoring in polymer materials irradiated with gamma and X-rays: Polyethylene and polypropylene**, Blanche Krieguer, Sylvain R. A. Marque, Samuel Dorey, Nathalie Dupuy, Fabien Girard, Nina Girard-Perier, Florent Kuntz, Nicolas Ludwig, Journal of Applied Polymer Science **2024**, e55098, doi:10.1002/app.55098

4. **Thermal properties and radical monitoring after gamma, X-ray, and electron beam irradiation in polyamides**, Blanche Krieguer, Nicolas Ludwig, Samuel Dorey, Nathalie Dupuy, Fabien Girard, c Nina Girard-Perier, Florent Kuntz, Sylvain R. A. Marque, Physical Chemistry Chemical Physics **2024**, doi:10.1039/D4CP02358G

5. **Investigating dose rate effects and reactive species formation in irradiated multilayer films – part 1 EVA/EVOH/EVA,** Blanche Krieguer, Samuel Dorey, Nathalie Dupuy, Fabien Girard, Florent Kuntz, Nicolas Ludwig, Sylvain R.A. Marque , soumis dans Physical Chemistry Chemical Physics, 2024

6. **Investigating dose rate effects and reactive species formation in irradiated multilayer films – part 2 PE/EVOH/PE**, Blanche Krieguer, Samuel Dorey, Nicolas Ludwig, Florent Kuntz, Sylvain R.A. Marque, Nathalie Dupuy, Fabien Girard, soumis dans Physical Chemistry Chemical Physics, 2024

7. **How X-rays, e-beam, and gamma irradiation change the chemical and physical properties of polypropylene**, Blanche Krieguer, Sylvain R.A. Marque, Fabien Girard, Nathalie Dupuy, Nicolas Ludwig, Florent Kuntz ,Samuel Dorey, soumis dans Journal of applied polymer science, 2024

## 2) Participation aux conférences et écoles d'été au cours de la période de thèse

1. **Impact of ionizing radiations on polymer materials used for biopharmaceutical and biotechnological applications**, 2023, Journée de la chimie SCF Sud-PACA, France, Marseille. Présentation orale

2. **Investigation of polyethylene, polyamide and polypropylene irradiated by gamma, e-beam and X-ray**, 2024, Vieillissement des Polymères, France, Saint Valery en Caux. Présentation orale

3. **ESR investigation of polymer materials irradiated by gamma, e-beam and X-ray**, 2024, International Meeting on Radiation Processing, Costa Rica, San José. Présentation orale

4. **EPR investigation of gamma and X-ray irradiated polypropylene polymer materials,** 2022, Rencontre Rayonnement Radio-chimie, France, Nice. Présentation poster

# Résumé

Les systèmes en plastique à usage unique sont conçus pour les industries biopharmaceutiques afin de stocker, transporter ou mélanger des solutions biopharmaceutiques. Ces systèmes, fabriqués à partir de polymères, sont actuellement stérilisés par rayonnement gamma. Le contexte sanitaire actuel entraîne une croissance de la production de produits destinés à l'industrie pharmaceutique. Des préoccupations émergent quant à la capacité de stérilisation par rayonnement gamma dans les années à venir. L'irradiation par faisceau d'électrons et par rayonnement X sont comparées pour être utilisées en tant que méthodes alternatives à la stérilisation gamma.

L'objectif de cette thèse est d'examiner l'impact potentiel des irradiations par rayons gamma, rayons X et faisceau d'électrons sur deux types de films (PE/EVOH/PE et EVA/EVOH/EVA) ainsi que sur des matériaux formulés à partir de polypropylène, de polyéthylène et de polyamide.

Les échantillons irradiés ont été analysés à l'aide d'une approche multi-échelle : au niveau moléculaire, macro-moléculaire et au niveau du matériau. Les résultats montrent que, quel que soit le polymère, les trois technologies d'irradiation produisent des effets équivalents : les mêmes types de radicaux sont générés, il n'y a pas de modification de la structure et de la composition des polymères observés dans les conditions d'analyse. Les variations observées entre les différentes classes de polymères sont principalement dues à la composition des matériaux.

# Abstract

Single-use plastic systems are intended for the biopharmaceutical industries to store, transport, or mix biopharmaceutical solutions. These systems, made from polymers, are currently sterilized by gamma radiation. The current health context is leading to an increase in the production of products intended for the pharmaceutical industry. Concerns are emerging about the capacity for gamma radiation sterilization in the coming years. Electron beam irradiation and X-ray irradiation are being compared as alternative methods to gamma sterilization.

The objective of this thesis is to examine the potential impact of gamma, X-ray, and electron beam irradiations on two types of films (PE/EVOH/PE and EVA/EVOH/EVA) as well as on materials formulated from polypropylene, polyethylene, and polyamide.

The irradiated samples were analyzed using a multi-scale approach: at the molecular, macromolecular, and material levels. The results show that, regardless of the polymer, the three irradiation technologies produce equivalent effects: the same types of radicals are generated, and there is no modification of the structure and composition of the polymers observed under the analysis conditions. The variations observed between the different classes of polymers are mainly due to the composition of the materials.

# Remerciements

Je souhaite tout d'abord remercier Grégoire Danger, Professeur à Aix-Marseille Université, pour avoir accepté de présider le jury de ma thèse. Je remercie également Christine Bressy, Professeure à l'Université de Toulon, et Emmanuel Richaud, Professeur à l'ENSAM de Paris, pour avoir accepté d'être rapporteurs de cette thèse. Je remercie également Sophie Rouif, experte R&D chez Ionisos Group, et Belkacem Otazaghine, Maître-assistant à l'École des Mines d'Alès, pour leur participation en tant qu'examinateurs.

Je tiens à remercier mes encadrants de thèse : mon directeur de thèse Sylvain Marque, ma co-directrice de thèse Nathalie Dupuy, et mon co-encadrant Fabien Girard. Sylvain, merci pour votre partage scientifique, votre aide précieuse en RPE et pour avoir toujours apprécié mes pâtisseries lors des réunions. Nathalie, merci pour votre soutien, votre bienveillance et vos conseils avisés. Fabien, merci pour tes nombreux conseils, notamment en informatique (pour la conversion des fichiers en PDF), ainsi que pour l'intérêt que tu m'as porté tout au long de ma thèse. Merci à Nathalie et Fabien pour votre aide dans la préparation de mes échantillons ; sans vous, la préparation de 500 flacons et la découpe de 3000 tranches de polymères n'auraient pas été si simples.

Je remercie Samuel Dorey, mon « co-encadrant » et tuteur industriel. Merci pour tes nombreux conseils, pour m'avoir permis de me perfectionner dans le domaine des polymères et pour m'avoir encouragé à parler anglais.

Merci à vous quatre pour m'avoir encadré de la meilleure des façons pendant cette thèse, et pour nos réunions (et repas au cloître, bien sûr !) mensuelles.

Je remercie Sartorius Stedim FMT S.A.S. pour le financement de ce projet.

Merci à la team Aérial, Florent Kuntz, Nicolas et Abbas, pour votre accueil chaleureux à Strasbourg. Merci à Nicolas d'avoir été présent pour répondre à mes questions sur l'irradiation et la RPE.

Je tiens à remercier tous les membres de l'équipe CHIPS du laboratoire de l'IMBE.
Merci à Yveline et Cathie pour votre aide au labo et vos conseils. Merci à Elodie pour ton écoute, ta bonne humeur et les pauses café.
Un grand merci à Didier pour ta disponibilité, ton aide précieuse et tes nombreux conseils sur l'HPLC.
Je tiens à remercier mon ancienne partenaire de bureau, Rayhane. Sans toi, l'ambiance au laboratoire n'aurait pas été la même durant ces trois années. Merci pour ton soutien sans

faille, ta bonne humeur, ta bienveillance et les nombreux croissants au petit déjeuner. Tu as été un véritable pilier depuis mon arrivée au laboratoire.
Merci aux doctorant et ingénieure, Anthony et Léa, de m'avoir supporté dans le bureau.

Je voudrais remercier toute l'équipe Product Development de Sartorius, Nelly, Lucie et Clémence pour votre accueil chaleureux et pour m'avoir intégré aux événements de l'équipe. Merci à l'équipe des techs pour votre bonne humeur.
Merci à Ludo et Véro G pour votre supervision et la réalisation des manipulations.
Merci aussi à Eric, Christophe, Sandrine et Sergine pour l'accueil dans le labo B lors de la préparation de mes cartons. Merci à José pour ton aide avec l'envoi et la réception de mes colis.
Je remercie la team particules, Manon et Véro C, pour votre accueil dans votre bureau.

Enfin, je tiens à remercier Nina et Fanny. Merci à vous deux pour vos conseils et pour m'avoir rassuré lorsque j'en avais besoin. Merci de m'avoir épaulé pendant ces trois années et de m'avoir intégré chaleureusement dans ce trio de thésardes.

Je remercie également les stagiaires Julie, Céline et Armando. Merci à Céline, pour ton aide précieuse dans la préparation des cartons au labo B pour les envoyer à temps en irradiation.

Enfin, je terminerai par remercier tous mes proches, amis et famille.

Merci à mes copines : Mathilde K, merci pour ta présence et ton soutien sans faille depuis 23 ans ; Lucile, merci pour ton écoute et nos petits moments autour d'un café ; Mathilde G, Pauline et Eloise, merci pour ces moments de décompression et ces week-ends de rigolade entre filles.

Merci à ma belle-famille, Matthieu, Marie, Luc et Béatrice, d'avoir toujours été soucieux de savoir comment se déroulait ma thèse (et ces sympas moments partagés au Paoli).

Merci à mon frère, Emile, tu as toujours été un modèle. Merci pour ta présence et ton encouragement si important à mes yeux. Merci à toi et Hélène.

Merci à mes parents, Papa et Hélène, merci de m'avoir soutenu et encouragé depuis le début de mes études. Maman et Jacquot, merci d'avoir été là dans tous les moments forts de cette thèse, et pour vos conseils très précieux pour moi. Merci à vous quatre d'avoir toujours fait semblant de comprendre ce que je faisais, je ne serais pas là sans vous.

Et comme on dit, le meilleur pour la fin : Thomas, je tiens à te remercier pour ton soutien inconditionnel, ton aide dans la relecture de mes travaux ainsi que ton écoute lors de mes présentations orales. Merci pour ta présence, ta patience, ta bienveillance et surtout ta bonne humeur. Merci d'égayer chacune de mes journées depuis 9 ans.

# Table des matières

**Affidavit** ..... **3**
**Liste des publications et participation aux conférences** ..... **4**
**Résumé** ..... **6**
**Abstract** ..... **7**
**Remerciements** ..... **8**
**Table des matières** ..... **11**
**Liste des figures** ..... **13**
**Liste des tableaux** ..... **14**
**Liste des Abréviations** ..... **15**
**Introduction générale** ..... **17**
**Références introduction générale** ..... **25**
**Chapitre 1 : Étude bibliographique** ..... **29**
1.1. Généralités ..... 31
1.1.1. Interaction rayonnements ionisants-matière ..... 31
1.1.2. Unités de mesure ..... 33
1.1.3. La stérilisation ..... 34
1.1.4. Législation et normes ..... 34
1.2. Généralité sur la stérilisation par irradiations gamma, faisceau d'électrons et rayons X ..... 35
1.2.1. L'irradiation par rayonnement gamma ..... 35
1.2.2. L'irradiation par rayonnements X ..... 36
1.2.3. L'irradiation par faisceau d'électrons ..... 36
1.2.4. Comparaison des trois méthodes ..... 37
1.3. Comportement des polymères sous rayonnements ionisants ..... 38
1.3.1. Comportement des polyoléfines sous irradiation ..... 38
1.3.2. Comportement de l'EVA sous irradiation ..... 42
1.3.3. Comportement du polyamide sous irradiation ..... 42
1.4. Etude de différents paramètres des rayonnements sur la matière ..... 43
1.4.1. Impact de l'énergie du rayonnement sur la matière ..... 44
1.4.2. Impact du débit de dose du rayonnement sur le polymère ..... 45
1.4.3. Impact des additifs ..... 46
**Références Chapitre 1** ..... **47**
**Chapitre 2 : Matériels, méthodes et techniques expérimentales** ..... **51**
2.1. Conditions expérimentales ..... 53
2.1.1. Echantillons ..... 53
2.1.2. Conditions d'irradiations ..... 56

2.2. Techniques analytiques ..... 57
2.3. Traitement de données ..... 58
2.4. Analyses ..... 60
**Références Chapitre 2 ..... 61**
**Chapitre 3 : Comparaison de l'impact de l'irradiation gamma, rayons X et faisceau d'électrons sur le film multicouche EVA/EVOH/EVA ..... 63**
3.1. Étude spectroscopique du film EVA/EVOH/EVA après irradiation ..... 65
3.2. Etude des effets du débit de dose et de la formation d'espèces réactives dans le film EVA/EVOH/EVA ..... 79
**Références Chapitre 3 ..... 92**
**Chapitre 4 : Comparaison de l'impact de l'irradiation gamma, rayons X et faisceau d'électrons sur le film multicouche PE/EVOH/PE ..... 93**
4.1. Étude de l'impact de l'irradiation sur les propriétés mécaniques ..... 95
4.2. Étude des effets du débit de dose et de la formation d'espèces réactives dans le film PE/EVOH/PE ..... 119
**Références Chapitre 4 ..... 134**
**Chapitre 5 : Comparaison de l'impact de l'irradiation gamma, rayons X et faisceau d'électrons sur les matériaux polymères ..... 135**
5.1. Étude par résonnance paramagnétique électronique des radicaux générés dans les polyoléfines ..... 137
5.2. Comportement du polypropylène après irradiation gamma, rayons X et faisceau d'électrons ..... 157
5.3. Comportement du Polyamide après irradiation gamma, rayons X et faisceau d'électrons ..... 189
**Conclusion et perspectives ..... 203**

# Liste des figures

Figure 1 : Schéma d'une installation de stérilisation par rayonnement gamma. Traitement à balancelle (source : Ionisos) ..... 35
Figure 2 : (a) Schéma d'une installation de stérilisation par rayonnement X. (b) Photo d'une installation d'irradiation par rayonnement X chez Aérial. (c) Photo d'une installation d'irradiation par faisceau d'éléctrons chez Aérial (source : Aerial). ..... 36
Figure 3 : Mécanisme d'oxydation du polyamide [31] ..... 43
Figure 4 : Valeurs de TEL en fonction de l'énergie de l'électron en échelle logarithmique [32] ..... 44
Figure 5 : Effet du débit de dose et du temps de stockages post-irradiation sur les rendements en fonctions carbonylées. Les débits de doses sont : A : irradiation gamma à 0,040 kGy/h ; B : irradiation gamma à 0,69 kGy/h ; C : irradiation par faisceau d'électrons à 5400 kGy/h [36]. ..... 45
Figure 6 : Représentation du film multicouche PE/EVOH/PE. ..... 53
Figure 7 : Structure des polymères (a) PE et (b) EVOH ..... 53
Figure 8 : Représentation du film multicouche EVA/EVOH/EVA. ..... 54
Figure 9 : Structure du polymère EVA ..... 54
Figure 10 : (a) Structure du polypropylène. (b) Photo d'un « dogbone » de PP. ..... 55
Figure 11 : Photo d'un « dogbone » de HDPE. ..... 55
Figure 12: Photo de trois échantillons de PA ..... 56
Figure 13 : Structures du (a) Polyamide 6.6 et (b) Polyamide 12. ..... 56
Figure 14 : Techniques analytiques utilisées sur les échantillons formulés à partir de PP après irradiation par rayons gamma, rayons X et faisceau d'électrons à 50 et 100 kGy 157
Figure 15 : Analyse multi-échelle pour caractériser les matériaux après irradiations gamma, rayons X et faisceau d'électrons [1] ..... 207

# Liste des tableaux

Tableau 1 : Tableau comparatif des trois technologies d'irradiation [16,17]. ..... 37
Tableau 2 : Caractéristique du PP non-irradié. ..... 55
Tableau 3 : Techniques analytiques réalisées (✓) et valorisées (✓) des différents polymères étudiés ..... 60
Tableau 4 : Dose et débit de dose d'irradiation du film multicouche EVA/EVOH/EVA. ... 65
Tableau 5 : Dose et débit de dose d'irradiation du film EVA/EVOH/EVA et du film PE/EVOH/PE par rayons gamma, rayons X et faisceaux d'électrons. ..... 79
Tableau 6 : Dose et débit de dose d'irradiation du PA par rayons gamma, rayons X et faisceau d'électrons. ..... 189

# Liste des Abréviations

| | |
|---|---|
| PE | Polyéthylène |
| EVOH | Alcool Ethylène Vinyle |
| EVA | Acétate Ethylène Vinyle |
| PP | Polypropylène |
| PA | Polyamide |
| TPE | Élastomère Thermoplastique |
| RPE | Résonance Paramagnétique Electronique |
| DSC | Calorimétrie Différentielle à Balayage |
| FTIR | Spectroscopie infrarouge à Transformée de Fourier |
| XPS | Spectroscopie de Photoélectrons X |
| DMA | Analyse Mécanique Dynamique |
| HPLC | Chromatographie Liquide à Haute Performance |
| ACP | Analyse en Composantes Principales |
| PC | Composante Principale |
| SIMPLISMA | SIMPLe-to-use Interactive Self-modeling Mixture Analysis |
| PLS | Moindres Carrés Partiels |
| TOST | Test Unilatéral Double |
| MD | Direction Machine |
| TD | Direction Transversale |
| HALS | Stabilisateurs de Lumière à Amine Hinderée |
| TEL | Transfert Linéique d'Énergie |

# Introduction générale

La préparation, le stockage, le mélange et le transport de nombreuses solutions biopharmaceutiques se font à l'aide de dispositifs en plastique à usage unique. Ces dispositifs offrent l'avantage de réduire les risques de contamination croisée par rapport aux cuves en inox [1]. Ces matériaux tels que, les tubes, les filtres et les connecteurs sont principalement fabriqués à partir de polymères formulés comme le polypropylène (PP), le polyamide (PA) ou encore le polyéthylène (PE) [2]. Les principaux polymères utilisés pour la fabrication de poches plastiques sont l'éthylène acétate de vinyle (EVA), l'éthylène alcool vinylique (EVOH), ou le PE.

L'industrie biopharmaceutique a connu une transformation significative avec l'adoption de systèmes en plastique à usage unique pour la préparation, le stockage, le mélange et le transport de solutions biopharmaceutiques. Ces systèmes , qui incluent des tubes, des filtres, des connecteurs et des poches sont devenus essentiels en raison de leur capacité à minimiser les risques de contamination, un problème majeur avec les cuves en inox traditionnelles [1]. L'un des principaux avantages des systèmes en plastique à usage unique est en effet la réduction des risques de contamination croisée. Contrairement aux cuves en inox, qui nécessitent un nettoyage et une stérilisation rigoureux entre chaque utilisation, les dispositifs à usage unique sont éliminés après usage, ce qui élimine le besoin de nettoyage et réduit le risque de contamination [1]. De plus, ces systèmes offrent une flexibilité accrue dans les processus de fabrication. Ils permettent une mise en place rapide et une réduction des temps d'arrêt de la chaine de production, qui est crucial dans un environnement de production où le temps est un facteur critique. Les systèmes à usage unique sont également plus économiques en termes de coûts d'installation et de maintenance, car ils ne nécessitent pas d'infrastructure de nettoyage complexe.

Les matériaux utilisés pour fabriquer ces dispositifs sont principalement des polymères formulés tels que le PP, le PA et le PE [2]. Chaque matériau possède des propriétés spécifiques pour répondre aux besoins d'utilisation. Le PE est reconnu pour ses excellentes propriétés mécaniques [3] et sa capacité à être une barrière à la vapeur d'eau [4]. Le PP offre une résistance chimique, une bonne stabilité thermique, il est caractérisé par une faible densité, ce qui le rend léger et facile à manipuler [5,6]. Le PA, quant à lui, est apprécié pour sa robustesse, sa résistance à l'usure et sa capacité à supporter des températures élevées, ce qui en fait un choix idéal pour des applications nécessitant une durabilité accrue [7]. Les poches plastiques sont souvent fabriquées à partir de polymères tels que l'éthylène acétate de vinyle (EVA), l'éthylène alcool vinylique (EVOH) et le PE. Ces matériaux offrent une barrière efficace contre l'oxygène et l'humidité [8,9], ce qui est essentiel pour préserver l'intégrité des solutions biopharmaceutiques. L'innovation dans le domaine des dispositifs en plastique à usage unique se concentre sur l'amélioration des matériaux pour offrir une meilleure performance et une plus grande sécurité. Des recherches sont en cours pour développer des polymères avec des propriétés barrières améliorées, une résistance accrue aux produits chimiques et une compatibilité élargie avec divers types de solutions biopharmaceutiques.

De plus, l'intégration de capteurs et de dispositifs de suivi dans les systèmes à usage unique est une tendance émergente. Ces technologies permettent un suivi en temps réel des conditions de stockage et de transport, assurant ainsi une meilleure traçabilité et un contrôle de qualité renforcé. Malgré leurs nombreux avantages, les systèmes en plastique à usage unique posent des défis environnementaux. L'augmentation des déchets plastiques est une préoccupation majeure, et l'industrie biopharmaceutique est sous pression pour trouver des solutions durables. Le recyclage et la réutilisation des matériaux plastiques sont des domaines de recherche actifs, avec des initiatives visant à développer des polymères biodégradables ou recyclables.

L'utilisation de systèmes en plastique à usage unique dans l'industrie biopharmaceutique est soumise à des réglementations strictes pour garantir la sécurité et l'efficacité des produits. Les organismes de réglementation, tels que la FDA (Food and Drug Administration) et l'EMA (European Medicines Agency), ont établi des directives pour l'évaluation des matériaux utilisés dans ces dispositifs, y compris des tests de compatibilité et de lixiviation. Ils jouent un rôle crucial dans l'industrie biopharmaceutique moderne et offrent des avantages significatifs en termes de réduction des risques de contamination, de flexibilité et de coût. Cependant, des efforts continus sont nécessaires pour relever les défis environnementaux et réglementaires associés à leur utilisation. L'innovation dans les matériaux et les technologies associées continuera de façonner l'avenir de ces dispositifs, assurant ainsi leur place dans les processus de fabrication biopharmaceutiques.

Pour des applications biotechnologiques et biopharmaceutiques, ces dispositifs sont stérilisés par irradiation gamma, conformément aux normes imposant une dose minimale de 25 kGy avec la méthode sélectionnée [10–13]. Aujourd'hui, les principales technologies de stérilisation sont l'oxyde d'éthylène (50%), l'irradiation gamma (40%), l'irradiation par faisceau d'électrons (4.5%) et d'autres méthodes comme la stérilisation par vapeur d'eau et les rayons X (5%) [14]. Sartorius, spécialisé dans la fabrication de systèmes à usage unique a renoncé à la stérilisation par oxyde d'éthylène il y a une dizaine d'années en raison des résidus laissés dans les produits et de l'impact environnemental négatif de cette technologie.

Le contexte sanitaire actuel, entraînant une forte croissance de la fabrication de produits destinés à l'industrie pharmaceutique et une innovation constante dans ce domaine, pose des problèmes de capacité de stérilisation ainsi que l'accès à des technologies de stérilisation validées et approuvées selon le type de produit. Actuellement deux leaders, Steris et Sterigenics, dominent 85% du marché de l'irradiation gamma [15]. Selon plusieurs études, la demande de stérilisation gamma pour les systèmes à usage unique pourrait dépasser les capacités des sites actuellement en activité. La disponibilité en cobalt 60 nécessaire à ces installations est limitée du fait du temps de fabrication des sources (2 ans) et du fait de l'embargo actuel sur les produits russes [16]. Ces études ne tiennent pas nécessairement compte des autres secteurs qui utilisent l'irradiation gamma, tels que l'industrie des dispositifs médicaux ou l'industrie alimentaire. De plus, des problématiques liées à la production complexe du cobalt 60, aux restrictions

réglementaires, et aux contraintes de manipulation, stockage, transport et distribution de cet isotope existent. Pour garantir la continuité de la production de ces systèmes biopharmaceutiques et réduire les risques associés à l'irradiation gamma, des technologies de stérilisation alternatives sont étudiées. Ces méthodes visent à compléter la stérilisation gamma pour absorber l'excès de demande. La norme ISO 11137-1 [10] utilisée pour la validation de la stérilité des systèmes à usage unique ne dépend pas de la technologie d'irradiation. Les rayons X et l'irradiation par faisceau d'électrons (rayonnements ionisants) pourraient donc être utilisés comme des technologies alternatives à l'irradiation gamma pour stériliser ces systèmes [17–19].

La stérilisation par rayons X a une uniformité de dose et une pénétration similaire, voire meilleure, que l'irradiation gamma. Fondamentalement, l'irradiation gamma et l'irradiation par rayons X reposent sur le même principe d'interaction : les photons pénètrent la matière, et les électrons dispersés détruisent l'ADN des micro-organismes [20]. Cependant, l'origine des rayonnements diffère : les rayons gamma proviennent de la désintégration isotopique des noyaux atomiques, tandis que les rayons X sont produits lorsque des électrons de haute énergie décélèrent en impactant une autre molécule.

La stérilisation par faisceau d'électrons repose sur l'émission d'un flux d'électrons hautement chargés qui agissent directement sur l'ADN des micro-organismes. Cependant, contrairement aux photons émis par l'irradiation gamma générée par le cobalt 60, les électrons ont une charge et une masse non nulle, limitant leur capacité de pénétration. L'irradiation par faisceau d'électrons et par rayons X semblent prometteuse comme méthodes alternatives de stérilisation. Les caractéristiques spectrales d'énergie des rayons X et gamma diffèrent. Le débit de dose est plus élevé pour les technologies de faisceau d'électrons et de rayons X que pour l'irradiation gamma. Il est donc essentiel d'étudier la robustesse des produits après irradiation par faisceau d'électrons et rayons X, en tenant compte des différences de paramètres de procédé [21].

L'impact de l'irradiation gamma sur les diverses propriétés (chimiques, physiques, etc.) de différents matériaux est largement étudié. En revanche, peu de littérature existe sur la comparaison de l'impact de ces trois technologies sur des matériaux polymères. Depuis une décennie, notre équipe étudie l'impact du rayonnement gamma sur des films multicouche irradiés dans des conditions industrielles, puis l'impact des trois technologies d'irradiation sur ces films [22–25,25–41]. Les résultats obtenus constituent un référentiel. Aujourd'hui, l'enjeu est d'analyser l'impact (chimique, physique, biologique, etc.) des irradiations par faisceau d'électrons et rayons X en comparaison avec l'irradiation gamma sur plusieurs familles de polymères afin d'étendre nos connaissances des films multicouches.

Le premier objectif de ce travail de thèse est de poursuivre les études comparatives sur l'impact des trois technologies d'irradiation sur des produits phares commercialisés par Sartorius : deux types de poches constituées d'un film EVA/EVOH/EVA et d'un film

PE/EVOH/PE. Le deuxième objectif est d'évaluer l'effet des différentes irradiations (gamma, faisceau d'électrons et rayon X) sur trois familles de polymères différentes : le polypropylène, le polyéthylène et le polyamide, afin de déterminer si ces technologies d'irradiation peuvent être utilisées pour stériliser les systèmes à usage unique composés de divers composants avec des formulations différentes développés par Sartorius, et sans compromettre leurs performances après irradiation.

Ce mémoire utilise une approche multi-échelle pour étudier les propriétés des matériaux. Au niveau du matériau : les propriétés mécaniques et la colorimétrie. Au niveau macromoléculaire, les propriétés thermiques et chimiques. Enfin, au niveau moléculaire, l'étude porte sur l'oxydation, l'identification des produits de dégradation et des radicaux générés.

L'article publié dans BioProcess International [17] décrit une approche multi-échelle pour étudier les propriétés des matériaux soumis à des radiations ionisantes, notamment dans le cadre des technologies de stérilisation comme les rayons gamma, X et faisceau d'électrons. Cette approche est essentielle pour comprendre comment ces méthodes de stérilisation affectent divers matériaux, en particulier ceux utilisés dans les dispositifs médicaux et les produits biopharmaceutiques. L'étude examine les effets de différentes doses d'irradiation sur les propriétés mécaniques des polymères, telles que la résistance à la traction et la dureté, essentielles pour garantir l'intégrité structurelle des matériaux après stérilisation. L'indice de jaunissement est utilisé pour évaluer la décoloration des matériaux comme le polyoléfine élastomère (POE) et le polypropylène homopolymère (PPH), indicateur de changements chimiques pouvant affecter la performance des matériaux. Des techniques comme la calorimétrie différentielle à balayage (DSC) sont employées pour surveiller les changements dans les propriétés thermiques, influençant la stabilité et la performance des matériaux. La spectroscopie infrarouge à transformée de Fourier (FTIR) et la spectroscopie de photoélectrons X (XPS) détectent les changements chimiques à la surface des matériaux, tels que l'oxydation et la réticulation, qui peuvent affecter les propriétés des matériaux. La spectroscopie de résonance paramagnétique électronique (RPE) est utilisée pour détecter et quantifier les radicaux générés lors de l'irradiation, intermédiaires primaires menant à des changements aux niveaux macromoléculaire et matériel. L'étude examine les processus d'oxydation et la dégradation des antioxydants dans les matériaux après irradiation, cruciaux pour comprendre la stabilité et la performance à long terme des matériaux. La chromatographie liquide à haute performance (HPLC) est utilisée pour détecter et quantifier les produits de dégradation, fournissant des informations sur la stabilité chimique des matériaux. La performance fonctionnelle des dispositifs médicaux, tels que les dispositifs de collecte de sang, est testée après exposition à des doses de stérilisation pertinentes, garantissant leur fonctionnalité et sécurité post-stérilisation. L'étude inclut des évaluations de biocompatibilité pour s'assurer que les matériaux stérilisés n'affectent pas négativement les systèmes biologiques. L'interaction des matériaux stérilisés avec les solutions biopharmaceutiques est analysée, en se concentrant sur les changements potentiels de pH et les processus d'oxydation des acides aminés. La chimiométrie et la

conception de plan d'expériences sont employées pour traiter les vastes quantités de données générées, en se concentrant sur les changements aux niveaux moléculaire et macromoléculaire pouvant avoir un impact significatif sur les propriétés des matériaux. L'approche multi-échelle intègre la recherche technologique, académique et industrielle pour fournir une compréhension complète de l'impact des radiations ionisantes sur les propriétés des matériaux. Cette approche est essentielle pour développer des méthodes de stérilisation alternatives qui peuvent compléter la stérilisation gamma traditionnelle, assurant la sécurité et l'efficacité des dispositifs médicaux et matériaux stérilisés. La collaboration entre l'industrie et le milieu académique facilite la génération de données robustes, aidant à la transition vers des méthodes de stérilisation comme les rayons X et le faisceau d'électrons.

Le premier axe de recherche concerne l'analyse des films polymères multicouche. Cette partie vise à compléter les connaissances sur les propriétés physico-chimique des films après irradiation, tels que la génération d'espèces radicalaires, la modification des propriétés mécaniques et la formation d'espèces oxydées à la surface du film. Le deuxième axe de recherche porte sur l'étude post irradiation des propriétés physiques et chimiques de différents matériaux polymères.

Ce manuscrit est organisé en cinq chapitres :

• Le premier chapitre consiste en une étude bibliographique sur l'interaction rayonnement-polymère, focalisée principalement sur les trois types de rayonnements étudiés au cours de cette thèse : gamma, faisceau d'électrons et rayons X. L'étude aborde également l'impact de différents paramètres des rayonnements sur la matière, tels que l'énergie du rayonnement et le débit de dose, ainsi que le comportement des polymères sous rayonnements ionisants.

• Le deuxième chapitre décrit la composition des polymères étudiés et les différentes techniques analytiques utilisées dans le cadre de cette thèse.

• Le troisième chapitre comprend deux articles, un publié [42] et un soumis, portant sur le film EVA/EVOH/EVA irradié par les trois technologies d'irradiation. Le premier article est une étude spectroscopique du film avec des traitements chimiométriques : Analyse en composante principal (ACP), méthode de résolution de courbe (SIMPLISMA) et modèle de régression des moindres carrés partiels (PLS). Le second article compare l'effet du débit de dose sur le film après irradiation.

• Le quatrième chapitre présente deux articles, un publié [43] et un soumis, portant sur le film PE/EVOH/PE irradié par les trois technologies d'irradiation. Le premier article étudie l'impact de l'irradiation sur les propriétés mécaniques du film. Le deuxième article est la partie 2 de l'étude sur l'impact du débit de dose sur le film PE/EVOH/PE présenté dans le chapitre 3.

• Le cinquième chapitre contient deux articles publiés [44,45] et un soumis. La première étude porte sur la formation des radicaux dans différents polymères (PP et PE) après irradiation. La seconde est une étude multi-échelle sur des échantillons formulés à partir de PP. La dernière étude porte sur les propriétés thermiques et la formation d'espèces radicalaires dans des échantillons formulés à partir de PA.

# Références introduction générale


1. Shukla, A.A.; Gottschalk, U. Single-Use Disposable Technologies for Biopharmaceutical Manufacturing. *Trends in Biotechnology* **2013**, *31*, 147–154, doi:10.1016/j.tibtech.2012.10.004.

2. BPAS Technical Guide X-Rays Sterilization of Single-Use BioProcess Equipment, Part 1: Industry Need; Requirements&Risk Evaluation.; **2021**.

3. Chang, T.; Yuan, C.; Guo, Z. Tribological Behavior of Aged UHMWPE under Water-Lubricated Condition. *Tribology International* **2019**, *133*, 1–11, doi:10.1016/j.triboint.2018.12.038.

4. Propriétés barrières des polymères utilisés en emballage Available online: https://www.techniques.ingenieur.fr/base-documentaire/materiaux-th11/applications-des-plastiques-42141210/proprietes-barrieres-des-polymeres-utilises-en-emballage-am3160/ **2024**.

5. Fintzou, A.T.; Badeka, A.V.; Kontominas, M.G.; Riganakos, K.A. Changes in Physicochemical and Mechanical Properties of γ-Irradiated Polypropylene Syringes as a Function of Irradiation Dose. *Radiation Physics and Chemistry* **2006**, *75*, 87–97, doi:10.1016/j.radphyschem.2005.03.014.

6. *Polypropylene Handbook: Morphology, Blends and Composites*; Karger-Kocsis, J., Bárány, T., Eds.; Springer International Publishing: Cham, **2019**; ISBN 978-3-030-12902-6.

7. Umoren, S.A.; Solomon, M.M.; Saji, V.S. Chapter 23 - Other Synthetic Polymers. In *Polymeric Materials in Corrosion inhibition fundamentals and applications*; **2022**; 541–563 ISBN 978-0-12-823854-7.

8. Osman, A.F.; Alakrach, A.M.; Kalo, H.; Azmi, W.N.W.; Hashim, F. In Vitro Biostability and Biocompatibility of Ethyl Vinyl Acetate (EVA) Nanocomposites for Biomedical Applications. *RSC Advances;* **2015**, *5*, 31485–31495, doi:10.1039/C4RA15116J.

9. Blanchard, A.; Gouanvé, F.; Espuche, E. Effect of Humidity on Mechanical, Thermal and Barrier Properties of EVOH Films. *Journal of Membrane Science* **2017**, *540*, 1–9, doi:10.1016/j.memsci.2017.06.031.

10. ISO 11137-1. International Organization for Standardization, Sterilization of Health Care Products -Radiation - Part 1: Requirements for Development, Validation and Routine Control of a Sterilization Process for Medical Devices. **2006**.

11. ISO 11137-2. International Organization for Standardization, Sterilization of Health Care Products -Radiation - Part 2: Establishing the Sterilization Dose. **2013**.

12. ISO 11137-3. International Organization for Standardization, Sterilization of Health Care Products -Radiation - Part 3: Guidance on Dosimetric Aspects. **2006**.

13. ISO 13485. International Organization for Standardization, Medical Devices - Quality Management Systems - Requirements for Regulatory Purposes. **2012**.

14. GIPA; IIA A Comparison of Gamma, E-Beam, X-Ray and Ethylene Oxide Technologies for the Industrial Sterilization of Medical Devices and Healthcare Products. **2017**.

15. Kroc, T.K.; Cooper, C.A. Accelerator-Driven Medical Sterilization to Replace CO-60 Sources. *Physics Procedia* **2017**, *90*, 92–99, doi:10.1016/j.phpro.2017.09.030.

16. Mineral Commodity Summaries 2022: Cobalt.; U.S. Geological Survey., **2022**.

17. Dupuy, N.; Marque, S.R.A.; Fifield, L.S.; Pharr, M.; Staack, D.; Pillai, S.D.; Nichols, L.; Murphy, M.K.; Dorey, S. Supplementing Gamma Sterilization with X-Ray and E-Beam Technologies. *Bioprocess technical* **2022**, *20*, 24–28.

18. De Brouwer, H. Comparison of the Effects of X-Ray and Gamma Irradiation on Engineering Thermoplastics. *Radiation Physics and Chemistry* **2022**, *193*, 109999, doi:10.1016/j.radphyschem.2022.109999.

19. Darwis, D.; Erizal; Abbas, B.; Nurlidar, F.; Putra, D.P. Radiation Processing of Polymers for Medical and Pharmaceutical Applications. *Macromolecular Symposia* **2015**, *353*, 15–23, doi:10.1002/masy.201550302.

20. Kroc, T.K. Monte Carlo Simulations Demonstrating Physics of Equivalency of Gamma, Electron-Beam, and X-Ray for Radiation Sterilization. *Radiation Physics and Chemistry* **2023**, 204, 110702, doi:10.1016/j.radphyschem.2022.110702.

21. Sadler, G.; Chappas, W.; Pierce, D.E. Evaluation of E-Beam, **γ**- and X-Ray Treatment on the Chemistry and Safety of Polymers Used with Pre-Packaged Irradiated Foods: A Review. *Food Additives and Contaminants* **2001**, *18*, 475–501, doi:10.1080/02652030119263.

22. Audran, G.; Dorey, S.; Dupuy, N.; Gaston, F.; Marque, S.R.A. Degradation of γ-Irradiated Polyethylene-Ethylene Vinyl Alcohol-Polyethylene Multilayer Films: An ESR Study. *Polymer Degradation and Stability* **2015**, *122*, 169–179, doi:10.1016/j.polymdegradstab.2015.10.021.

23. Dorey, S.; Gaston, F.; Girard-Perier, N.; Dupuy, N.; Marque, S.R.A.; Delaunay, L. Generation of $O_2$ -Permeation Barrier during the Gamma-Irradiation of Polyethylene/Ethylene-Vinyl Alcohol/Polyethylene Multilayer Film. *Industrial & Engineering Chemistry Research* **2019**, *58*, 14115–14123, doi:10.1021/acs.iecr.9b02145.

24. Dorey, S.; Gaston, F.; Girard-Perier, N.; Dupuy, N.; Marque, S.R.A.; Delaunay, L. Effect of Gamma Irradiation on the Oxygen Barrier Properties in Ethyl-vinyl Acetate/Ethylene-vinyl Alcohol/Ethyl-vinyl Acetate Multilayer Film. *Journal of Applied Polymer Science* **2020**, *137*, 49361, doi:10.1002/app.49361.

25. Dorey, S.; Gaston, F.; Girard-Perier, N.; Dupuy, N.; Marque, S.R.A.; Barbaroux, M.; Audran, G. Identification of Chemical Species Created during Γ-irradiation of Antioxidant Used in Polyethylene and Polyethylene- *co* -vinyl Acetate Multilayer Film. *Journal of Applied Polymer Science* **2020**, *137*, 49336, doi:10.1002/app.49336.

26. Girard-Perier, N.; Dorey, S.; Marque, S.R.A.; Dupuy, N. Mapping the Scientific Research on the Gamma Irradiated Polymers Degradation (1975–2018). *Radiation Physics and Chemistry* **2020**, *168*, 108577, doi:10.1016/j.radphyschem.2019.108577.

27. Girard-Perier, N.; Claeys-Bruno, M.; Marque, S.R.A.; Dupuy, N.; Gaston, F.; Dorey, S. Monitoring of Peroxide in Gamma Irradiated EVA Multilayer Film Using Methionine Probe. *Polymers* **2020**, *12*, 3024, doi:10.3390/polym12123024.

28. Girard-Perier, N.; Gaston, F.; Dupuy, N.; Marque, S.R.A.; Delaunay, L.; Dorey, S. Study of the Mechanical Behavior of Gamma-Irradiated Single-Use Bag Seals. *Food Packaging and Shelf Life* **2020**, *26*, 100582, doi:10.1016/j.fpsl.2020.100582.

29. Girard-Perier, N.; Claeys-Bruno, M.; Marque, S.R.A.; Dupuy, N.; Gaston, F.; Dorey, S. Effects of X-Ray, Electron Beam and Gamma Irradiation on PE/EVOH/PE Multilayer Film Properties. *Chemical Communications* **2021**, *57*, 11049–11051, doi:10.1039/D1CC02871E.

30. Gaston, F.; Dupuy, N.; Girard-Perier, N.; Marque, S.R.A.; Dorey, S. Investigations at the Product, Macromolecular, and Molecular Level of the Physical and Chemical Properties of a γ-Irradiated Multilayer EVA/EVOH/EVA Film: Comprehensive Analysis and Mechanistic Insights. *Polymers* **2021**, *13*, 2671, doi:10.3390/polym13162671.

31. Girard-Perier, N.; Dorey, S.; Marque, S.R.A.; Dupuy, N. Mapping the Scientific Research on the Ionizing Radiation Impacts on Polymers (1975–2019). *e-Polymers* **2021**, *21*, 770–778, doi:10.1515/epoly-2021-0065.

32. Girard-Perier, N.; Marque, S.R.A.; Dupuy, N.; Claeys-Bruno, M.; Gaston, F.; Dorey, S.; Fifield, L.S.; Ni, Y.; Li, D.; Fuchs, W.K.; et al. Effects of X-Rays, Electron Beam, and Gamma Irradiation on Chemical and Physical Properties of EVA Multilayer Films. *Frontiers in Chemistry* **2022**, *10*, 888285, doi:10.3389/fchem.2022.888285.

33. Girard-Perier, N.; Dorey, S.; Gaston, F.; Girard, F.; Marque, S.R.A.; Dupuy, N. One-Year Ageing FTIR Monitoring of PE/EVOH/PE Film after Gamma or Electron Beam Irradiation. *Polymer Degradation and Stability* **2022**, *195*, 109790, doi:10.1016/j.polymdegradstab.2021.109790.

34. Girard-Perier, N.; Claeys-Bruno, M.; Marque, S.R.A.; Dupuy, N.; Gaston, F.; Dorey, S. Monitoring of Peroxide in Gamma Irradiated PE/EVOH/PE Multilayer Film Using Methionine Probe. *Food and Bioproducts Processing* **2022**, *132*, 226–232, doi:10.1016/j.fbp.2022.02.001.

35. Gaston, F.; Dupuy, N.; Marque, S.R.A.; Dorey, S. Evaluation of Multilayer Film Stability by Raman Spectroscopy after Gamma-Irradiation Sterilization Process. *Vibrational Spectroscopy* **2018**, *96*, 52–59, doi:10.1016/j.vibspec.2018.03.002.

36. Gaston, F.; Dupuy, N.; Marque, S.R.A.; Barbaroux, M.; Dorey, S. FTIR Study of Ageing of γ-Irradiated Biopharmaceutical EVA Based Film. *Polymer Degradation and Stability* **2016**, *129*, 19–25, doi:10.1016/j.polymdegradstab.2016.03.040.

37. Gaston, F.; Dupuy, N.; Marque, S.R.A.; Gigmes, D.; Dorey, S. Monitoring of the Discoloration on Γ-irradiated PE and EVA Films to Evaluate Antioxidant Stability. *Journal of Applied Polymer Science* **2018**, *135*, 46114, doi:10.1002/app.46114.

38. Gaston, F.; Dupuy, N.; Marque, S.R.A.; Barbaroux, M.; Dorey, S. Impact of γ-Irradiation, Ageing and Their Interactions on Multilayer Films Followed by AComDim. *Analytica Chimica Acta* **2017**, *981*, 11–23, doi:10.1016/j.aca.2017.05.021.

39. Gaston, F.; Dupuy, N.; Marque, S.R.A.; Barbaroux, M.; Dorey, S. One Year Monitoring by FTIR of γ-Irradiated Multilayer Film PE/EVOH/PE. *Radiation Physics and Chemistry* **2016**, *125*, 115–121, doi:10.1016/j.radphyschem.2016.03.010.

40. Dorey, S.; Gaston, F.; Dupuy, N.; Barbaroux, M.; Marque, S.R.A. Reconciliation of pH, Conductivity, Total Organic Carbon with Carboxylic Acids Detected by Ion Chromatography in Solution after Contact with Multilayer Films after γ-Irradiation. *European Journal of Pharmaceutical Sciences* **2018**, *117*, 216–226, doi:10.1016/j.ejps.2018.02.023.

41. Dorey, S.; Gaston, F.; Marque, S.R.A.; Bortolotti, B.; Dupuy, N. XPS Analysis of PE and EVA Samples Irradiated at Different γ-Doses. *Applied Surface Science* **2018**, *427*, 966–972, doi:10.1016/j.apsusc.2017.09.001.

42. Krieguer, B.; Marque, S.R.A.; Dorey, S.; Girard, F.; Ni, Y.; Li, D.; Murphy, M.K.; Fifield, L.S.; Dupuy, N. Comparison of Effects from Gamma, e-Beam and X-Ray Radiation on Multilayer Polymer Films Used in Biopharmaceutical Devices by Chemometric Treatment of Spectroscopic Data. *Radiation Physics and Chemistry* **2024**, *218*, 111607, doi:10.1016/j.radphyschem.2024.111607.

43. Girard-Perier, N.; Marque, S.R.A.; Dupuy, N.; Krieguer, B.; Dorey, S. Gamma, E-Beam and X-Ray Irradiations on PE/EVOH/PE Multilayer Film: An Industrial Point of View Regarding the Impact on Mechanical Properties. *Polymers* **2023**, *15*, 2799, doi:10.3390/polym15132799.

44. Krieguer, B.; Marque, S.R.A.; Dorey, S.; Dupuy, N.; Girard, F.; Girard-Perier, N.; Kuntz, F.; Ludwig, N. Radical Detection and Electron-Spin Resonance (ESR) Monitoring in Polymer Materials Irradiated with Gamma and X-Rays: Polyethylene and Polypropylene. *Journal of Applied Polymer Science* **2024**, e55098, doi:10.1002/app.55098.

45. Krieguer, B.; Ludwig, N.; Dorey, S.; Dupuy, N.; Girard, F.; Girard-Perier, N.; Kuntz, F.; Marque, S.R.A. Thermal Properties and Radical Monitoring after Gamma, X-Ray, and Electron Beam Irradiation in Polyamides. *Physical Chemistry Chemical Physics* **2024**, 10.1039.D4CP02358G, doi:10.1039/D4CP02358G.

# Chapitre 1 : Étude bibliographique

# 1.1. Généralités

## 1.1.1. Interaction rayonnements ionisants-matière

Le rayonnement est généralement défini comme l'émission ou la transmission d'énergie sous forme d'ondes ou de particules. On parle de rayonnement ionisant lorsqu'il possède suffisamment d'énergie pour provoquer une ionisation, c'est-à-dire une interaction avec les électrons de la matière. L'énergie des rayonnements ionisants dépasse celle nécessaire pour dissocier les liaisons chimiques, ce qui leur permet de transformer des molécules initialement neutres en molécules ionisées [1–3]. Il existe différents types de rayonnements ionisants, classés selon les particules impliquées. On distingue les rayonnements directement ionisants (particules chargées) comme les rayonnements α ou β, et les rayonnements indirectement ionisants (particules non chargées) comme les rayonnements γ, X ou les neutrons.

Lors de l'interaction avec la matière, les particules ionisantes transfèrent partiellement ou totalement leur énergie cinétique en fonction de l'épaisseur de la matière traversée qui les ralentit. Le Transfert Linéique d'Énergie (TEL) mesure ce ralentissement et représente l'énergie transférée au milieu par unité de longueur de la trajectoire parcourue [4]. Un TEL élevé signifie qu'une grande quantité d'énergie est transmise sur une faible épaisseur. Les rayonnements (α, β) à parcours limité perdent toute leur énergie en traversant la matière et peuvent donc être arrêtés, tandis que les rayonnements (X, γ, neutrons) à parcours non limité subissent une atténuation progressive de leur énergie.

L'interaction rayonnement ionisant-matière sera différente selon le type de particules transportées.

Pour cette étude, l'interaction de la matière avec les rayons gamma, rayons X et faisceau d'électrons sera détaillée.

### *Rayons gamma et rayons X*

Le rayonnement gamma et le rayonnement X sont deux types de rayonnements électromagnétiques, mais ils diffèrent par leur origine. Le rayonnement gamma est émis par des noyaux radioactifs, ce qui lui confère une origine nucléaire. En revanche, le rayonnement X est produit lorsque des électrons accélérés interagissent avec les noyaux d'atomes dans une cible, résultant en une origine électronique. Ce processus, connu sous le nom de rayonnement de Bremsstrahlung [4], se produit lorsque des électrons de haute énergie sont ralentis par l'interaction avec les atomes du matériau cible, libérant ainsi de l'énergie sous forme de rayons X.

Les photons gamma et X, lorsqu'ils traversent la matière, perdent une partie de leur énergie en interagissant avec les électrons. Selon l'énergie initiale de ces photons, trois

types d'interactions peuvent se produire : l'effet photoélectrique, formation de paires ioniques (e+ e-) et l'effet Compton [5].

- L’effet photoélectrique : Cet effet se manifeste principalement dans les matériaux métalliques. Un photon de basse énergie (<70 keV) éjecte un électron lié à l'atome depuis une couche interne, plaçant ainsi l'atome dans un état excité.

- La formation de paires d’électrons : Ce phénomène ne se produit que si l'énergie du photon incident dépasse 1,02 MeV, seuil requis par la relation d'Einstein pour créer la masse d'un électron et d'un positon. Lors de l'interaction avec le noyau de l’atome cible, le photon incident génère un électron et un positon.

- L’effet Compton : Cet effet est représenté par la collision entre un photon d’énergie élevé et un électron quasi libre. Le photon cède, par collision avec un électron, une partie de son énergie initiale. L’électron ciblé perd ensuite son énergie par ionisation comme un électron β et le photon secondaire (ou diffusé) continue à propager dans la matière sans déposer d’énergie jusqu’à ce qu’il interagisse de nouveau. L'effet Compton est un phénomène qui peut se produire avec les deux types de rayonnements, gamma et X, lorsque leurs énergies se situent dans la même gamme (entre 100 keV et 10 MeV). Cela signifie que, du point de vue de l'interaction Compton, les photons gamma et X peuvent être considérés comme équivalents, car ils subissent le même type de processus physique lorsqu'ils interagissent avec la matière.

Dans les applications courantes des rayons X et des radionucléides émetteurs gamma (dont les énergies varient entre 50 keV et quelques MeV), l'effet Compton est prédominant. Le photon transfère une partie de son énergie à un électron, émettant un photon secondaire dans une autre direction. L'électron éjecté, ayant une énergie trop élevée pour être absorbée directement, interagit à son tour avec la matière en éjectant d'autres électrons secondaires de plus faibles énergies. Lorsque l'énergie de l'électron devient comparable à celle des énergies de dissociation des liaisons chimiques du matériau, des ruptures homolytiques des liaisons covalentes se produisent, formant des radicaux libres. Ces radicaux libres sont à l'origine de nombreuses réactions chimiques (oxydation, scission, réticulation) et sont responsables de la dégradation des matériaux polymères exposés aux rayonnements ionisants [6,7].

### *Faisceau d'électrons*

Le rayonnement par faisceau d'électrons est constitué de particules chargées (électrons) ayant une masse de $9{,}11.10^{-31}$ kg, contrairement aux photons non chargés des rayonnements gamma et X. Lorsqu'un électron incident traverse la matière, il transfère son énergie par deux processus distincts, en fonction de son énergie initiale :

- La diffusion inélastique avec les électrons des atomes environnants, entraînant des ionisations ou des excitations des atomes du milieu traversé, ce qui provoque une perte d'énergie de l'électron incident. Ce processus se produit pour les électrons de faible énergie (< 2 MeV) [8].

- La diffusion inélastique avec les noyaux des atomes cibles, accompagnée de l'émission d'un rayonnement électromagnétique de freinage (Bremsstrahlung) chaque fois que l'électron est dévié de sa trajectoire. Ce processus se produit pour les électrons de haute énergie (> 10 MeV) [9].

Ainsi, l'énergie cinétique des électrons est dissipée par diffusion inélastique, entraînant soit une ionisation, soit la production de photons par rayonnement de freinage. La perte d'énergie des électrons dépend de leur énergie initiale ainsi que de la densité électronique du milieu traversé.

## 1.1.2. Unités de mesure

### *Energie des rayonnements ionisants*

Pour le rayonnement gamma, le cobalt 60 est le radionucléide le plus couramment utilisé pour produire des photons. Il sert de source de radiation avec des énergies de 1,17 et 1,33 MeV, et possède une demi-vie de 5,26 ans [7]. Le becquerel (Bq) mesure l'activité (nombre de désintégration par seconde) de la matière radioactive. Anciennement, l'unité de mesure utilisée était le curie (Ci). Un curie (1 Ci) équivaut à 3,7.1010 Bq [10].

Concernant l'irradiation par faisceau d'éléctrons, dans le cadre des applications de stérilisation des dispositifs médicaux, l'énergie des électrons générés par les accélérateurs industriels varie entre 3 et 10 MeV.

Pour la production de rayons X destinés à la stérilisation des dispositifs médicaux, les accélérateurs industriels produisent des faisceaux d'électrons avec des énergies comprises entre 5 et 7 MeV.

### *Dose et débit de dose*

Lorsqu'un matériau est bombardé par des particules, il se produit un dépôt d'énergie. Ce dépôt est quantifié par le terme de dose absorbée ou de débit de dose Ce dernier, exprimé en unités telles que Gy/s ou kGy/h, varie considérablement selon la technologie d'irradiation utilisée : environ 1 à 2 kGy/h pour les rayons gamma, 12 kGy/h pour les rayons X, et jusqu'à 18 000 kGy/h pour l'irradiation par faisceau d'électrons.

La dose absorbée correspond à la quantité d'énergie déposée par unité de masse dans un matériau irradié. Dans le Système international d'unités (SI), cette dose est mesurée en Gray (Gy). Un Gray équivaut à l'absorption d'une énergie de 1 joule par kilogramme (1 J/kg).

## 1.1.3. La stérilisation

La stérilisation est un processus visant à éliminer les microorganismes présents sur un matériau, exerçant ainsi un effet bactéricide. Un produit stérile est dépourvu de tout microorganisme viable. La radio-stérilisation, qui utilise des rayonnements ionisants, provoque la rupture de la double hélice d'ADN, empêchant toute réplication.

Les plastiques sont omniprésents dans de nombreux dispositifs médicaux tels que les seringues, les gants, les appareils de perfusion et de prélèvement, ainsi que les poches à usage unique. Ces matériaux peuvent être sensibles à la chaleur (rendant la stérilisation par autoclave inappropriée) et aux agents stérilisants chimiques (rendant la stérilisation par oxyde d'éthylène également inappropriée). Par conséquent, la radio-stérilisation s'avère nécessaire.

Aujourd'hui, la radio-stérilisation des dispositifs médicaux est principalement réalisée par rayons gamma.

## 1.1.4. Législation et normes

Il existe un certain nombre de normes qui imposent aux industriels biopharmaceutiques et biotechnologiques d'utiliser des dispositifs stérilisés à une dose minimale de 25 kGy [11–14]. En effet cette dose est définie comme la dose de référence qui garantit un Niveau d'Assurance de Sécurité (NAS) destiné aux dispositifs médicaux. Ce NAS traduit la probabilité qu'un micro-organisme sur 1 000 000 soit viable après la stérilisation à 25 kGy du matériau.

## 1.2. Généralité sur la stérilisation par irradiations gamma, faisceau d'électrons et rayons X

### 1.2.1. L'irradiation par rayonnement gamma

Depuis l'introduction des dispositifs médicaux stériles à usage unique dans les années 1960, l'irradiation par rayonnements gamma est devenue une méthode de stérilisation majeure dans le domaines biopharmaceutiques [15]. Le premier irradiateur a été installé en 1963 dans le New Jersey, et aujourd'hui, environ 200 installations sont opérationnelles à travers le monde. Ce procédé est non seulement fiable mais aussi extrêmement efficace pour le traitement des systèmes en plastique à usage unique, car il permet de stériliser les produits directement dans leur emballage final.

La source d'énergie pour l'irradiation gamma est le cobalt 60, un radio-isotope qui émet deux photons d'énergie de 1,17 et 1,33 MeV. L'installation de sites de stérilisation par rayonnement gamma, illustré en Figure 1, implique que les produits à stériliser soient transportés dans la cellule d'irradiation par un système automatique. Ils suivent un circuit prédéfini à une vitesse contrôlée, passant devant la source de rayonnement avant de ressortir. L'irradiation gamma possède une grande capacité de pénétration, ce qui facilite le traitement de produits modérément denses ou emballés, ainsi que ceux en palettes. La dose absorbée dépend de la densité du produit, de l'épaisseur de l'emballage, du débit de dose, de la durée d'exposition, et, dans une certaine mesure, de la conception des installations.

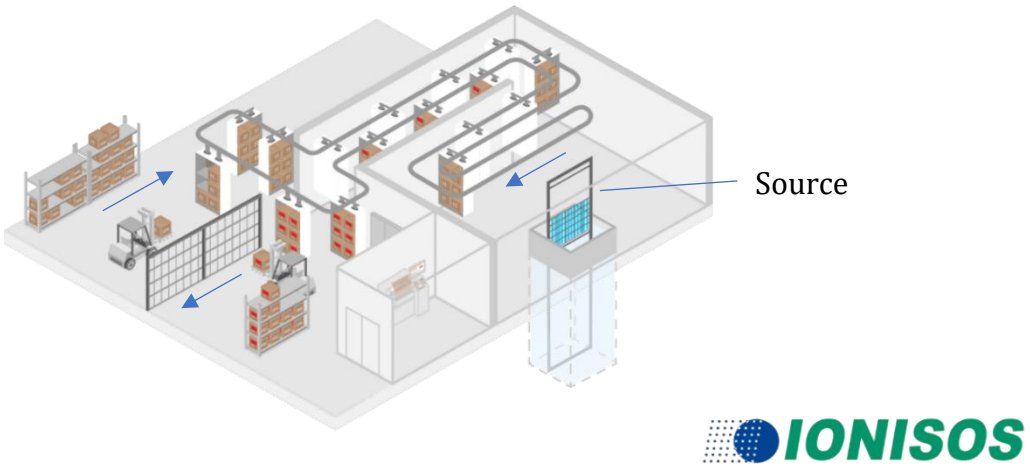


Figure 1 : Schéma d'une installation de stérilisation par rayonnement gamma. Traitement à balancelle (source : Ionisos)

### 1.2.2. L'irradiation par rayonnements X

L'irradiation par rayons X est une méthode plus récente, introduite avec la création du premier irradiateur à palette de grande capacité en Suisse en 2010. Ce traitement constitue une alternative pratique aux autres méthodes de stérilisation. Alimenté par des appareils électriques utilisant des électrons à haute énergie (7 MeV), le traitement par rayons X offre un temps de traitement court et une excellente capacité de pénétration. La Figure 2 représente le schéma de l'irradiation par rayonnement X chez Aérial.

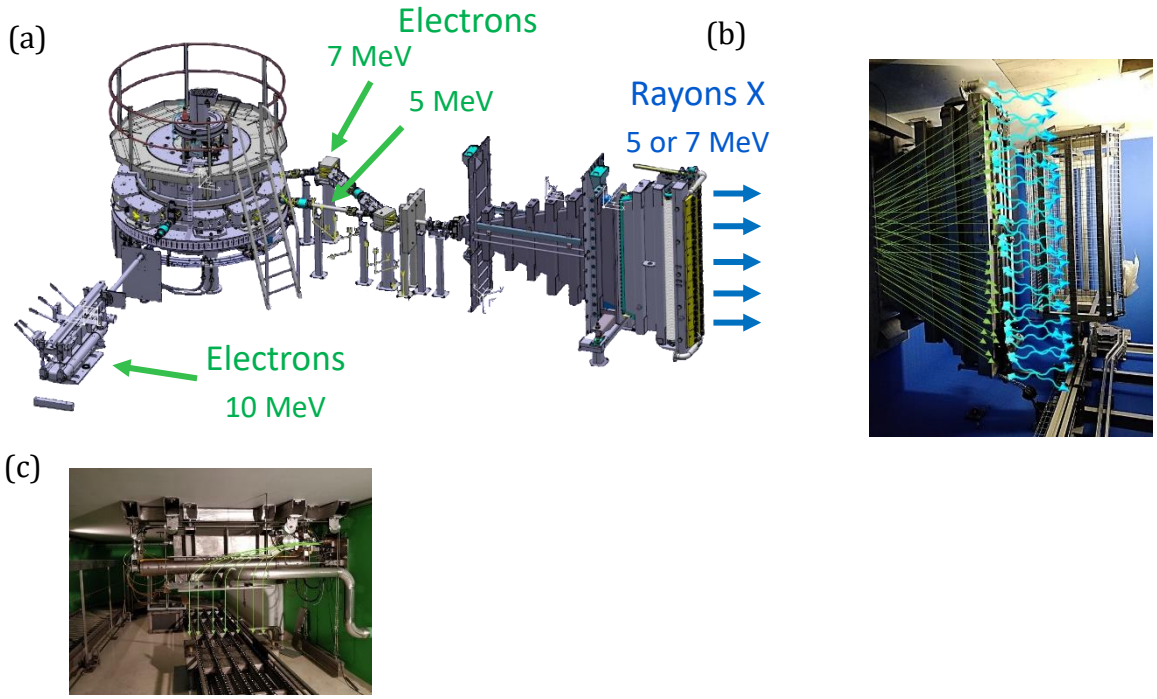


Figure 2 : (a) Schéma d'une installation de stérilisation par rayonnement X. (b) Photo d'une installation d'irradiation par rayonnement X chez Aérial. (c) Photo d'une installation d'irradiation par faisceau d'éléctrons chez Aérial (source : Aerial).

### 1.2.3. L'irradiation par faisceau d'électrons

L'irradiation par faisceau d'électrons est utilisée depuis plus de 50 ans, avec des centaines d'accélérateurs d'électrons installés à travers le monde. Cette méthode est principalement employée pour la réticulation du polyéthylène (avec une énergie allant jusqu'à 5 MeV) et pour la stérilisation de dispositifs médicaux (avec des énergies entre 5 et 7 MeV).

Le faisceau d'électrons est produit par des appareils électriques utilisant des électrons à haute énergie (10 MeV). Le traitement par faisceau d'électrons est extrêmement rapide (quelques secondes). Les produits sont transportés dans la cellule d'irradiation par un

système de convoyeur automatique, puis passent sous le faisceau à une vitesse ajustée selon la dose et la nature du produit (Figure 2 a et c).

### 1.2.4. Comparaison des trois méthodes

Le Tableau 1 présente une comparaison des trois technologies d'irradiation abordées dans cette thèse. Les irradiations par rayons gamma et X permettent de stériliser des palettes, tandis que le faisceau d'électrons est limité à la stérilisation de cartons de faible épaisseur. Ces trois méthodes respectent la norme ISO 11137 [12–14], qui définit les exigences pour la stérilisation des dispositifs médicaux. Le traitement par rayons X entraîne une variation de température plus faible. Le débit de dose est beaucoup plus élevé pour le faisceau d'électrons que pour les rayonnements gamma et X, ce qui réduit le temps de traitement. Enfin, les rayons gamma sont la technologie dominante dans la stérilisation des dispositifs à usage unique en raison de leur capacité à pénétrer profondément dans les matériaux, assurant ainsi une stérilisation uniforme et efficace de matériaux polymères.

Tableau 1 : Tableau comparatif des trois technologies d'irradiation [16,17].

| **Caractéristique** | **Gamma** | **Rayons X** | **Faisceau d'électrons** |
|---|---|---|---|
| **Source d'énergie** | Isotopes radioactifs ($^{60}$Co) | Electricité | Electricité |
| **Energie** | 1,17 et 1,33 MeV | 7 MeV | 10 MeV |
| **Débit de dose** | ~2 kGy/h | ~12 kGy/h | 18 000 kGy/h |
| **Pénétration** | Profonde | Profonde | Limité (15 cm pour une face) |
| **Homogénéité (DUR)** | Bonne : ~ 1,5 pour des palettes de 400 kg | Bonne : ~ 1,3 pour des palettes de 400 kg | Bonne à moyenne : ~1,5 (une face) à 2,8 (traitement bi-face) |
| **ISO 11137 accepté** | Oui | Oui | Oui |

## 1.3. Comportement des polymères sous rayonnements ionisants

Dans le cadre de notre étude, nous nous intéressons aux comportements des polyoléfines (PE et PP), de l'éthylène acétate de vinyle et du polyamide.

### 1.3.1. Comportement des polyoléfines sous irradiation

Les polyoléfines sont une classe de polymères produits à partir d'oléfines (ou alcènes), qui sont des hydrocarbures insaturés contenant une double liaison carbone-carbone. Les polyoléfines les plus courantes sont le polyéthylène (PE) et le polypropylène (PP).

Le PP est un polymère utilisé pour fabriquer des connecteurs et des filtres en raison de sa rigidité et de sa résistance. Il est produit par la polymérisation du propylène.

Le PE est un polymère fréquemment utilisé pour le stockage de produits chimiques en raison de sa faible réactivité chimique et de sa grande résistance physique. Il est produit par la polymérisation de l'éthylène :

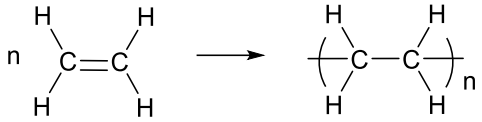

(1)

Le polyéthylène est un polymère semi-cristallin, composé d'une phase cristalline où les chaînes polymères sont régulièrement agencées, et d'une phase amorphe où les macromolécules sont désordonnées. Le taux de cristallinité influence fortement ses propriétés mécaniques. Il existe plusieurs types de polyéthylène selon leur densité théorique :

- Polyéthylène très basse densité (PEtBD) : densité entre 0,860 et 0,910 ;
- Polyéthylène basse densité (PEBD) : densité entre 0,910 et 0,925 ;
- Polyéthylène basse densité linéaire (PEBDL) ;
- Polyéthylène moyenne densité (PEMD) : densité entre 0,926 et 0,940 ;
- Polyéthylène haute densité (PEHD) : densité entre 0,940 et 0,970.

Une densité de 0,860 indique un polyéthylène totalement amorphe, tandis qu'une densité de 1,01 indique un polyéthylène entièrement cristallin. Bien que le polyéthylène soit perméable à l'oxygène, il est peu perméable à l'eau. Sa perméabilité diminue avec l'augmentation du taux de cristallinité et la diminution de la température.

Depuis les années 60, le comportement des polymères sous irradiation a fait l'objet de nombreuses études, avec Charlesby et Chapiro en tant que pionniers [18,19]. Dans cette thèse, nous allons décrire le comportement du polyéthylène, mais il est important de noter que le polypropylène présente un comportement similaire [20–23].

Le polyéthylène, en raison de sa simplicité chimique, a été particulièrement étudié. Lorsqu'il est exposé à des rayonnements ionisants, il subit des processus impliquant des radicaux :




(2)

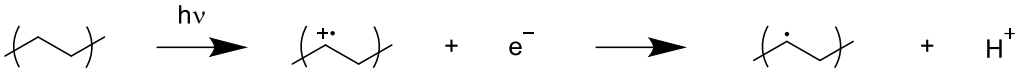


(3)

Ces radicaux peuvent réagir soit par :

- Couplage avec la formation de liaison C-C inter chaine appelé réticulation (4).

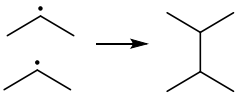

(4)

- Soit par dismutation, c'est-à-dire par transfert d'atome hydrogène pour former un alcane et un alcène (5).

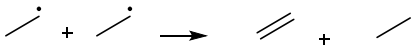


(5)

Une autre voie de disparition est la formation d'une molécule de dihydrogène conduisant à la formation d'une double liaison, menant à un radical allyle plus stable :

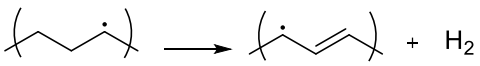


(6)

Lorsque l'atmosphère environnante contient de l'oxygène (conditions aérobies) pendant la radiolyse du polyéthylène, l'oxygène réagit avec les radicaux pour former des radicaux alkyl, peroxyles ou des hydroperoxyle. Ce phénomène est particulièrement notable à la surface de l'échantillon, où l'oxygène est constamment renouvelé. En revanche, au cœur du matériau, l'oxydation se poursuit uniquement jusqu'à ce que l'oxygène dissous soit entièrement consommé. Par la suite, l'oxydation ne se produit que si le débit de dose est suffisamment bas pour permettre à l'oxygène de diffuser dans le

matériau et de rencontrer des radicaux. Cette réaction est favorisée lorsque les radicaux ont une longue durée de vie.

Les radicaux HOO• formés en (7) et ROO• formés en (8) disparaissent suivant plusieurs voies : (9-11) pour HOO• et (12-14) pour ROO•.

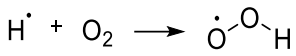
(7)

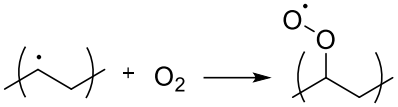
(8)

L'oxygène conduit à la formation de fonctions oxygénées ainsi que d'eau, de monoxyde de carbone et de dioxyde de carbone. Les mécanismes de disparition du radical HOO• formés en (7) et ceux formés au cours de ces réactions sont détaillés ci-dessous (9–11).

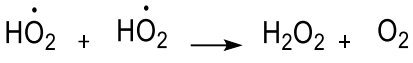
(9)

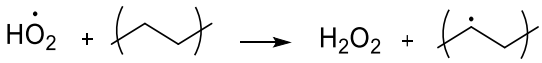
(10)

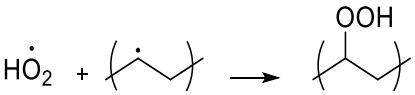
(11)

Ces réactions illustrent la formation de peroxyde d'hydrogène dans le polymère et de fonctions hydroperoxydes sur les chaînes de polyéthylène. En effet le couplage de HOO• conduit à la formation de $H_2O_2$ et $O_2$ (9). Ces deux espèces pouvant être à nouveau impliqués dans un cycle d'oxydation en fonction des conditions de radiolyses. HOO• peut arracher un atome d'hydrogène d'une chaine polymère amorçant ainsi un nouveau cycle (10). Finalement, HOO• peut se coupler avec un radical alkyl pour former un hydroperoxyde (11). Ce dernier en fonctions des conditions de radiolyse peut amorcer à nouveaux des cycles de dégradation du polymère.

Les mécanismes de réaction formés en (8) et ceux formés au cours de ces réactions sont détaillés ci-dessous (12-15).

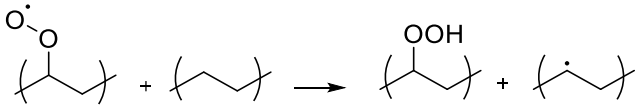
(12)

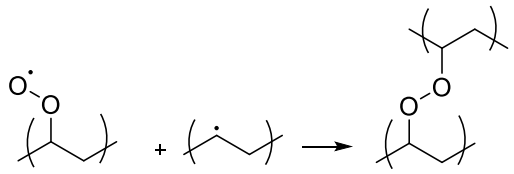

(13)

De son côté, ROO• peut arracher un atome d'hydrogène sur une chaine polymère et ainsi amorcer un nouveau cycle de dégradation (12). ROO• peut aussi se coupler avec un radical alkyl pour former un peroxyde de diallyle (13). Ce dernier en fonction des conditions de radiolyse peut produire des radicaux alkyl et réamorcer des processus de dégradation.

Les ROO• peuvent aussi dimériser pour former un tetroxyde (14) qui se décompose pour donner soit des produits « inertes » hydroxyalkyle, carbonyles, soit se décompose en RO• et $O_2$ (15). Les radicaux alkoxyl sont capables de réamorcer des cycles de dégradations.

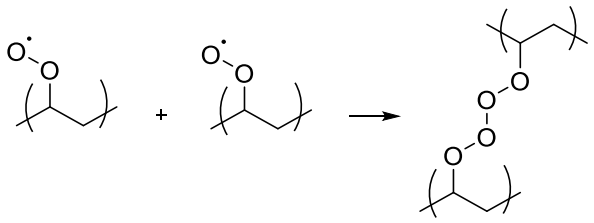

(14)

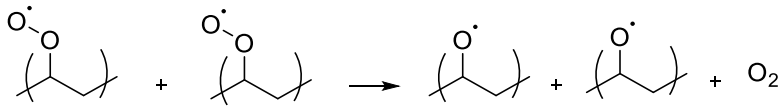

(15)

Les fonctions tétraoxydes formées en (14) sont instables et se décomposent pour créer deux fonctions stables, un alcool et une cétone (16) :

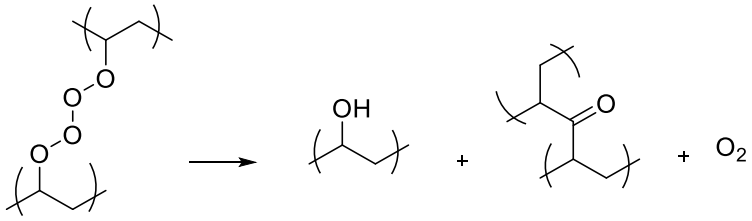

(16)

Les principaux sous-produits du polyéthylène sont les alcools, les cétones, les aldéhydes, les acides carboxyliques, les chaines vinyliques et les esters.[24–27]

## 1.3.2. Comportement de l'EVA sous irradiation

L'éthylène-acétate de vinyle présente un intérêt particulier dans l'étude des effets de l'irradiation, grâce à sa structure (17) qui allie la robustesse des polyoléfines à la flexibilité apportée par les groupes acétates.

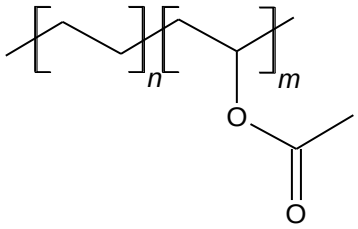


(17)

Lorsque l'EVA est soumis à une irradiation gamma en conditions aérobies, une scission peut se produire au niveau de la fonction acétate (18) ou une hydro peroxydation peut survenir sur le carbone en α portant la fonction acétate (19). La probabilité qu'une réaction soit privilégiée par rapport à l'autre dépend de l'énergie de dissociation des liaisons concernées[28,29].

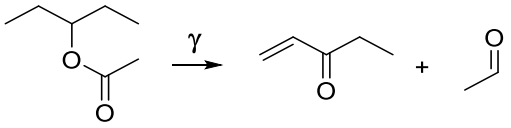


(18)

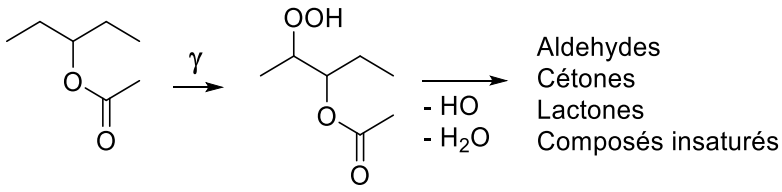


(19)

Les principaux sous-produits de l'EVA incluent les aldéhydes, les cétones, les lactones et les composés insaturés. La formation d'acide acétique est également très probable, résultant de l'hydrolyse de l'EVA [30] (20).

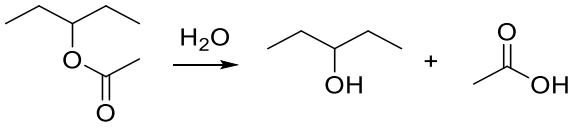


(20)

## 1.3.3. Comportement du polyamide sous irradiation

Dans le cadre de notre étude du comportement des matériaux polymères sous irradiation, il est essentiel de se pencher sur le polyamide, un polymère dont la structure chimique complexe et la présence d'hétéroatomes influence significativement sa réactivité face aux rayonnements ionisants. Contrairement à des polymères plus simples

comme le polyéthylène, le polyamide présente des sites réactifs d'oxydation spécifiques, dictés par l'effet inductif des fonctions amide, nécessitant une compréhension approfondie des mécanismes d'oxydation pour évaluer son comportement sous irradiation, comme suggéré par les travaux de Dong et Gijsman [31].

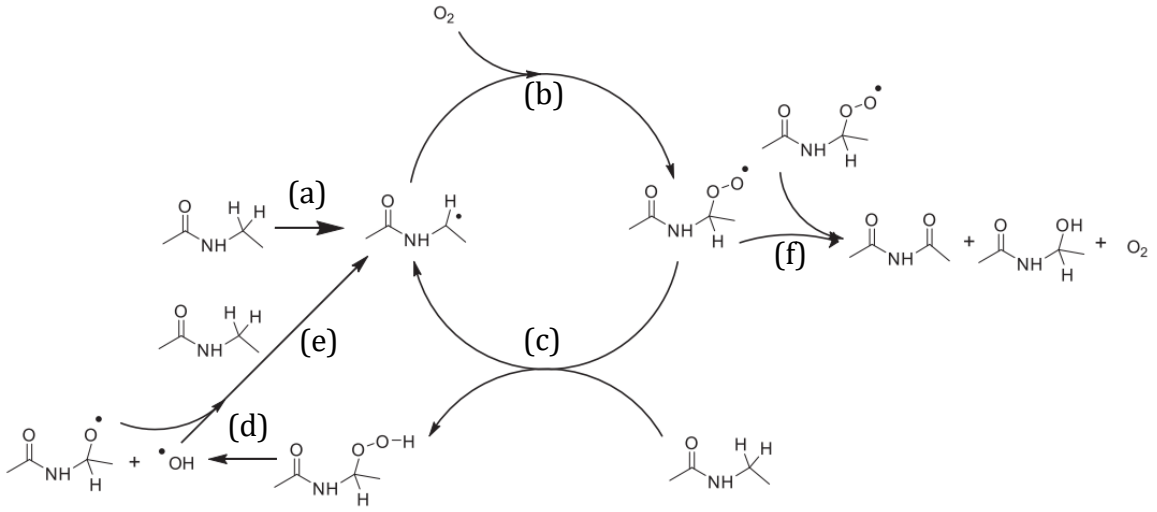


Figure 3 : Mécanisme d'oxydation du polyamide [31]

La réaction (a) correspond à l'amorçage extrinsèque de l'oxydation (par opposition aux réactions (d) et (e) qui constituent des amorçages intrinsèques) et conduit à la formation du premier radical alkyle, qui réagira très rapidement avec l'oxygène au cours de la réaction (b) pour former un radical peroxyle. Au cours de la réaction (c), le radical peroxyle va arracher l'hydrogène sur un méthylène, et former un hydroperoxyde. Cette réaction conduit aussi à la formation d'un nouveau radical. La décomposition homolytique de l'hydroperoxyde (d) conduit à la formation des radicaux α-N-alkoxyle et hydroxyle. La réaction (e) décrit uniquement une autre voie de formation du radical, de même que la réaction (c), le fait que la réaction produise son propre amorceur explique le caractère auto-entretenu de l'oxydation qui génère les radicaux dans le milieu.

## 1.4. Etude de différents paramètres des rayonnements sur la matière

Dans la plupart des cas, l'interaction initiale entre un rayonnement et un polymère résulte d'une rupture homolytique, générant ainsi un radical. La formation de ce radical est influencée par divers facteurs, notamment l'énergie du rayonnement et le débit de dose. L'objectif ici est d'examiner si ces facteurs provoquent des variations dans la matière lorsqu'elle est exposée à des rayonnements gamma, X ou electron-beam.

### 1.4.1. Impact de l'énergie du rayonnement sur la matière

Il a été établi que chaque type de rayonnement étudié ici possède une énergie incidente distincte. Une question pertinente est : l'impact sur la matière sera-t-il identique selon l'énergie du rayonnement ? Pour analyser l'influence de ce paramètre, la notion de rendement radiolytique G est considérée. Ce rendement est défini comme le nombre d'atomes formés ou transformés par unité d'énergie absorbée, exprimé en molécules/100 eV.

Pour le rayonnement gamma, l'électron secondaire atteint une énergie maximale de 1,33 MeV, tandis que pour le rayonnement X, il peut atteindre jusqu'à 7 MeV, et pour le rayonnement par électrons, entre 0,1 et 10 MeV. Chaque énergie correspond à une valeur de TEL (lors de la radiolyse dans l'eau). La Figure 4 ci-dessous illustre les TEL en fonction de l'énergie de l'électron. Pour des électrons dont l'énergie est comprise entre 10 keV et 10 MeV, les valeurs de TEL sont inférieures à 2 eV/nm.

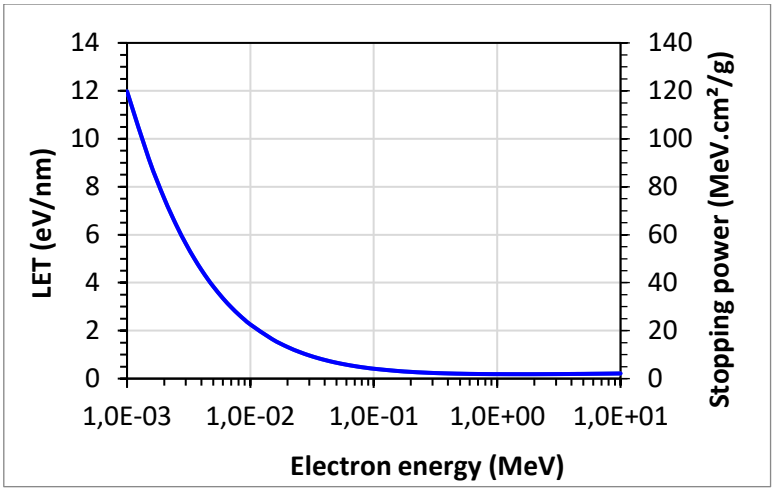


Figure 4 : Valeurs de TEL en fonction de l'énergie de l'électron en échelle logarithmique [32].

Une étude menée sur le PMMA [33] révèle que les rendements de scission sont peu affectés dans une gamme de TEL allant jusqu'à 10 eV/nm. Au-delà de cette valeur, les rendements de scission diminuent au profit de ceux de réticulation. La valeur de TEL de 10 eV/nm, nettement supérieure à celles observées pour les rayonnements dans l'eau (<2 eV/nm), s'explique par la structure rigide du matériau et sa faible mobilité. En raison du manque de littérature sur ce sujet, il est difficile de conclure sur l'impact de l'énergie du rayonnement sur le polymère. Toutefois, l'étude du PMMA suggère que des modifications similaires pourraient être observées entre les rayonnements gamma, X et le faisceau d'électrons. Une autre étude [34], utilisant des rayonnements gamma et X à même débit de dose mais à différentes énergies sur divers polymères, corrobore cette hypothèse.

### 1.4.2. Impact du débit de dose du rayonnement sur le polymère

Le rôle du débit de dose dans l'exposition aux radiations ionisantes est complexe et multifacette. Dans les systèmes biologiques, il influence des processus allant des dommages à l'ADN aux réponses cellulaires globales. Les faibles débits de dose (LDR) peuvent activer des mécanismes de réparation adaptatifs, tandis que les hauts débits de dose (HDR) entraînent souvent des dommages plus immédiats et sévères [35].

Dans les systèmes polymères, le débit de dose est crucial pour déterminer les propriétés des matériaux. Les polymères subissent des changements chimiques et physiques, tels que la réticulation et l'oxydation, qui peuvent altérer leurs propriétés mécaniques, thermiques et chimiques, influençant ainsi leur adéquation pour des applications spécifiques [36].

Par exemple, des débits de dose plus faibles tendent à augmenter l'oxydation et la dégradation des polymères comme les polyoléfines [36–38]. La Figure 5 présente différentes valeurs de rendements en formation de fonctions carbonylées lorsque le polyéthylène est irradié par rayonnements gamma et par faisceau d'électrons à plusieurs débits de dose.

Dans des conditions de faible débit de dose gamma, les rendements en hydroperoxydes et carbonyles augmentent, ce qui accélère l'oxydation [39]. En revanche, à des débits de dose élevés, la recombinaison des radicaux prédomine, réduisant ainsi l'oxydation [36].

L'étude de Clough et Gillen [40] souligne que le débit de dose influence fortement la dégradation des matériaux polymères, y compris pour le PVC, en raison de mécanismes de dégradation par ramification de chaîne impliquant la décomposition thermique des peroxydes formés lors de l'exposition aux radiations.

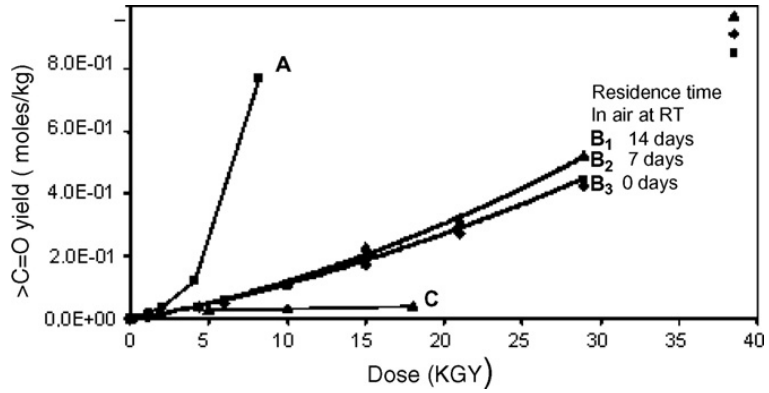


Figure 5 : Effet du débit de dose et du temps de stockages post-irradiation sur les rendements en fonctions carbonylées. Les débits de doses sont : A : irradiation gamma à 0,040 kGy/h ; B : irradiation gamma à 0,69 kGy/h ; C : irradiation par faisceau d'électrons à 5400 kGy/h [36].

### 1.4.3. Impact des additifs

Divers additifs sont contenus dans la formulation des matériaux polymères pour prévenir leur dégradation pendant la fabrication et pour optimiser leur performance et durabilité. Ces additifs, bien que présents en quantités inférieures à 5%, jouent un rôle crucial dans la préservation des propriétés des polymères. Parmi eux, on trouve des antioxydants, des agents anti-UV, des stabilisants, des lubrifiants, et des colorants.

Les antioxydants (AO) sont particulièrement importants, ils jouent un rôle dans la protection du polymère en présence d'$O_2$. Il existe deux types d'AO : les AO primaires, tels que les phénols substitués et les AO secondaires, tels que les phosphites.
Les AO permettent de réduire la réticulation des polymères. Cependant, l'exposition aux rayonnements ionisants peut affecter à la fois les polymères et les additifs, entraînant la formation de sous-produits. Ces sous-produits peuvent migrer à travers le matériau, posant des risques potentiels lors de l'utilisation du produit final. Ainsi, bien que les additifs soient essentiels pour la protection et l'amélioration des polymères, il est crucial de comprendre et de gérer les interactions complexes entre les polymères, les additifs, et les conditions d'irradiation pour garantir la sécurité et l'efficacité des matériaux [24,41].

# Références Chapitre 1


1. Blanc, D. *Les Rayonnements ionisants : détection, dosimétrie, spectrométrie*; Masson: Paris, **1997**; ISBN 978-2-225-83079-2.

2. Blanc, D. *La chimie nucléaire*; Que sais-je ?; Presses universitaires de France: Paris, **1987**; ISBN 978-2-13-039463-1.

3. Verdu, J. *Vieillissement des plastiques*; Association française de normalisation: Paris, **1985**; ISBN 978-2-12-425111-7.

4. Loveland, W.D.; Morrissey, D.J.; Seaborg, G.T. *Modern Nuclear Chemistry*; 1st ed.; Wiley, **2017**; ISBN 978-0-470-90673-6.

5. Bourgeois, C. Interaction particules-matière - Détecteurs. *Physique Chimie* **1998**, doi:10.51257/a-v1-af3531.

6. Kroc, T.K. Monte Carlo Simulations Demonstrating Physics of Equivalency of Gamma, Electron- Beam, and X-Ray for Radiation Sterilization. *Radiation Physics and Chemistry* **2022**, *204*, 110702, doi:10.1016/j.radphyschem.2022.110702.

7. Makuuchi, K.; Cheng, S. *Radiation Processing of Polymer Materials and Its Industrial Applications*; 1st ed.; Wiley, **2012**; ISBN 978-0-470-58769-0.

8. Su, H.; Cheng, X.; Cooper, B.; Tennyson, J.; Zhang, H. Elastic and Inelastic Low-Energy Electron Scattering from Pyridine. *The Journal of Chemical Physics* **2023**, *158*, 024301, doi:10.1063/5.0127540.

9. Jakubassa-Amundsen, D.H. Relativistic Theory for the Elementary Process of Bremsstrahlung Induced by Heavy Spin-Zero Nuclei. *Physical Review A* **2016**, *93*, 052716, doi:10.1103/PhysRevA.93.052716.

10. Basic Concepts of Radiation Processing. In *Radiation Processing of Polymer Materials and its Industrial Applications*; John Wiley & Sons, Inc.: Hoboken, NJ, USA, **2012**; 1–25 ISBN 978-1-118-16279-8.

11. ISO 13485. International Organization for Standardization, Medical Devices - Quality Management Systems - Requirements for Regulatory Purposes. **2012**.

12. ISO 11137-1. International Organization for Standardization, Sterilization of Health Care Products -Radiation - Part 1: Requirements for Development, Validation and Routine Control of a Sterilization Process for Medical Devices. **2006**.

13. ISO 11137-2. International Organization for Standardization, Sterilization of Health Care Products -Radiation - Part 2: Establishing the Sterilization Dose. **2013**.

14. ISO 11137-3. International Organization for Standardization, Sterilization of Health Care Products -Radiation - Part 3: Guidance on Dosimetric Aspects. **2006**.

15. Dupuy, N.; Marque, S.R.A.; Fifield, L.S.; Pharr, M.; Staack, D.; Pillai, S.D.; Nichols, L.; Murphy, M.K.; Dorey, S. Supplementing Gamma Sterilization with X-Ray and E-Beam Technologies. *Bioprocess technical* **2022**, *20*, 24–28.

16. GIPA; IIA A Comparison of Gamma, E-Beam, X-Ray and Ethylene Oxide Technologies for the Industrial Sterilization of Medical Devices and Healthcare Products. **2017**.

17. Darwis, D.; Erizal; Abbas, B.; Nurlidar, F.; Putra, D.P. Radiation Processing of Polymers for Medical and Pharmaceutical Applications. *Macromolecular Symposia* **2015**, *353*, 15–23, doi:10.1002/masy.201550302.

18. Charlesby, A. *Atomic Radiation and Polymers*; International Series of Monographs on Radiation Effects in Materials; Pergamon Press Ltd: Oxford [England], **1960**; ISBN 978-1-4831-9776-0.

19. Chapiro, A. Radiation Chemistry of Polymers. *Radiation Research Supplement* **1964**, *4*, 179, doi:10.2307/3583578.

20. Lacoste, J.; Vaillant, D.; Chmela, S. Gamma, Photo and Thermally initiated oxidation of polyolefines used in packaging. *Journal of Polymer Engineering* **1995**, *15*, doi:10.1515/POLYENG.1995.15.1-2.139.

21. Niki, E.; Decker, C.; Mayo, F.R. Aging and Degradation of Polyolefins. I. Peroxide-Initiated Oxidations of Atactic Polypropylene. *Journal of Polymer Science: Polymer Chemistry Edition* **1973**, *11*, 2813–2845, doi:10.1002/pol.1973.170111108.

22. Decker, C.; Mayo, F.R. Aging and Degradation of Polyolefins. II. γ-Initiated Oxidations of Atactic Polypropylene. *Journal of Polymer Science: Polymer Chemistry Edition* **1973**, *11*, 2847–2877, doi:10.1002/pol.1973.170111109.

23. Decker, C.; Mayo, F.R.; Richardson, H. Aging and Degradation of Polyolefins. III. Polyethylene and Ethylene–Propylene Copolymers. *Journal of Polymer Science: Polymer Chemistry Edition* **1973**, *11*, 2879–2898, doi:10.1002/pol.1973.170111110.

24. Driffield, M.; Bradley, E.L.; Leon, I.; Lister, L.; Speck, D.R.; Castle, L.; Potter, E.L.J. Analytical Screening Studies on Irradiated Food Packaging. *Food Additives & Contaminants: Part A* **2014**, *31*, 556–565, doi:10.1080/19440049.2013.865087.

25. Liu, Z.; Chen, S.; Zhang, J. Photodegradation of Ethylene–Octene Copolymers with Different Octene Contents. *Polymer Degradation and Stability* **2011**, *96*, 1961–1972, doi:10.1016/j.polymdegradstab.2011.08.009.

26. Tidjani, A.; Wilkie, C.A. TGA Analysis of Γ-irradiated Linear Low-density Polyethylene. *Journal of Applied Polymer Science* **2006**, *100*, 2790–2795, doi:10.1002/app.23556.

27. Buchalla, R.; Boess, C.; Bögl, K.W. Characterization of Volatile Radiolysis Products in Radiation-Sterilized Plastics by Thermal Desorption–Gas Chromatography–Mass

Spectrometry: Screening of Six Medical Polymers. *Radiation Physics and Chemistry* **1999**, *56*, 353–367, doi:10.1016/S0969-806X(99)00311-4.

28. Giurginca, M.; Popa, L.; Zaharescu, T. Thermo-Oxidative Degradation and Radio-Processing of Ethylene Vinyl Acetate Elastomers. *Polymer Degradation and Stability* **2003**, *82*, 463–466, doi:10.1016/S0141-3910(03)00200-3.

29. Jin, J.; Chen, S.; Zhang, J. UV Aging Behaviour of Ethylene-Vinyl Acetate Copolymers (EVA) with Different Vinyl Acetate Contents. *Polymer Degradation and Stability* **2010**, *95*, 725–732, doi:10.1016/j.polymdegradstab.2010.02.020.

30. Wenwei, Z.; Xiaoguang, Z.; Li, Y.; Yuefang, Z.; Jiazhen, S. Determination of the Vinyl Acetate Content in Ethylene-Vinyl Acetate Copolymers by Thermogravimetric Analysis. *Polymer* **1994**, *35*, 3348–3350, doi:10.1016/0032-3861(94)90148-1.

31. Dong, W.; Gijsman, P. Influence of Temperature on the Thermo-Oxidative Degradation of Polyamide 6 Films. *Polymer Degradation and Stability* **2010**, *95*, 1054–1062, doi:10.1016/j.polymdegradstab.2010.02.030.

32. Seltzer, S. Stopping-Powers and Range Tables for Electrons, Protons, and Helium Ions, NIST Standard Reference Database 124 **1993**.

33. Lee, E.H.; Rao, G.R.; Mansur, L.K. LET Effect on Cross-Linking and Scission Mechanisms of PMMA during Irradiation. *Radiation Physics and Chemistry* **1999**, *55*, 293–305.

34. Croonenborghs, B.; Smith, M.A.; Strain, P. X-Ray versus Gamma Irradiation Effects on Polymers. *Radiation Physics and Chemistry* **2007**, *76*, 1676–1678, doi:10.1016/j.radphyschem.2007.01.014.

35. Lowe, D.; Roy, L.; Tabocchini, M.A.; Rühm, W.; Wakeford, R.; Woloschak, G.E.; Laurier, D. Radiation Dose Rate Effects: What Is New and What Is Needed? *Radiation and Environmental Biophysics* **2022**, *61*, 507–543, doi:10.1007/s00411-022-00996-0.

36. Buttafava, A.; Tavares, A.; Arimondi, M.; Zaopo, A.; Nesti, S.; Dondi, D.; Mariani, M.; Faucitano, A. Dose Rate Effects on the Radiation Induced Oxidation of Polyethylene. *Nuclear Instruments and Methods in Physics Research Section B: Beam Interactions with Materials and Atoms* **2007**, *265*, 221–226, doi:10.1016/j.nimb.2007.08.091.

37. Alariqi, S.A.S.; Singh, R.P. Effect of γ-Dose Rate on Biodegradation of γ-Sterilized Biomedical Polyolefins. *Journal of Polymers and the Environment* **2010**, *18*, 600–607, doi:10.1007/s10924-010-0217-9.

38. Alariqi, S.A.S.; Kumar, A.P.; Rao, B.S.M.; Singh, R.P. Effect of γ-Dose Rate on Crystallinity and Morphological Changes of γ-Sterilized Biomedical Polypropylene. *Polymer Degradation and Stability* **2009**, *94*, 272–277, doi:10.1016/j.polymdegradstab.2008.10.027.

39. Singh, A. Irradiation of Polyethylene: Some Aspects of Crosslinking and Oxidative Degradation p. *Radiation Physics and Chemistry* **1999**, *56*, 375–380.

40. Clough, R.L.; Gillen, K.T. Radiation-Thermal Degradation of PE and PVC: Mechanism of Synergism and Dose Rate Effects. *Radiation Physics and Chemistry* **1981**, *18*, 661–669, doi:10.1016/0146-5724(81)90189-8.

41. Bourges, F.; Bureau, G.; Dumonceau, J.; Pascat, B. Effects of Electron Beam Irradiation on Antioxidants in Commercial Polyolefins: Determination and Quantification of Products Formed. *Packaging Technology and Science* **1992**, *5*, 205–209, doi:10.1002/pts.2770050406.

# Chapitre 2 : Matériels, méthodes et techniques expérimentales

# 2.1. Conditions expérimentales

## 2.1.1. Echantillons

Les échantillons étudiés ont été fournis par la société Sartorius Stedim FMT S.A.S. (Aubagne, France).

### *Film PE/EVOH/PE*

Le film PE/EVOH/PE est produit par co-extrusion à partir de résines de LDPE (polyéthylène basse densité) et d'EVOH (avec 71 % mol de VOH) stabilisées par des additifs. Le polyéthylène basse densité est un PE très ramifié. L'épaisseur totale du film est d'environ 400 µm. La structure de ce film est représentée en Figure 6. Les structures des polymères PE et EVOH sont représentées respectivement sur la Figure 7a et b.

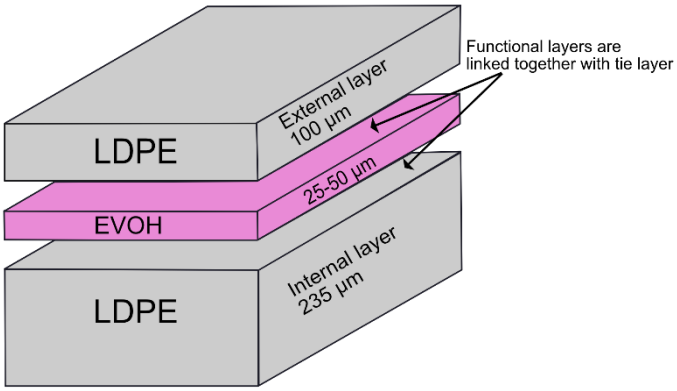


Figure 6 : Représentation du film multicouche PE/EVOH/PE.

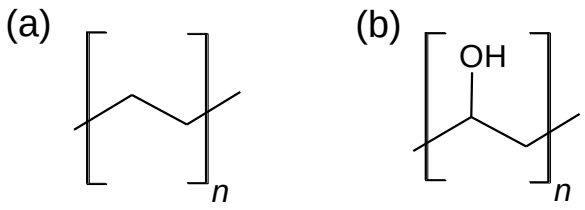


Figure 7 : Structure des polymères (a) PE et (b) EVOH.

Le film PE/EVOH/PE est utilisé pour fabriquer des poches principalement destinées à la culture cellulaire pour la production d'anticorps thérapeutiques, de protéines et de vaccins, avec des volumes pouvant varier de 20 mL à 3000 L selon la poche. La couche interne correspond à la couche qui sera en contact avec la solution contenue dans la

poche, tandis que la couche externe correspond à la couche qui sera en contact avec le milieu extérieur.

### *Film EVA/EVOH/EVA*

Les couches externes de ce film sont fabriquées par co-extrusion à partir de résines d'EVA et d'EVOH (contenant 56 %mol de VOH), tandis que la couche interne (de contact) est produite par extrusion-gonflage. La couche externe est laminée à chaud avec la couche interne lors d'une seconde phase.
Les différentes couches de ce film contiennent des additifs, incluant au moins un antioxydant (phénol ou phosphite) et des agents anti-bloquants. Ces antioxydants stabilisent chimiquement le film pendant les phases de fabrication et de conservation. L'épaisseur totale du film est de 360 µm.
La structure du film EVA/EVOH/EVA est représentée dans la Figure 8 et la structure du polymère EVA est représentée dans la Figure 9.

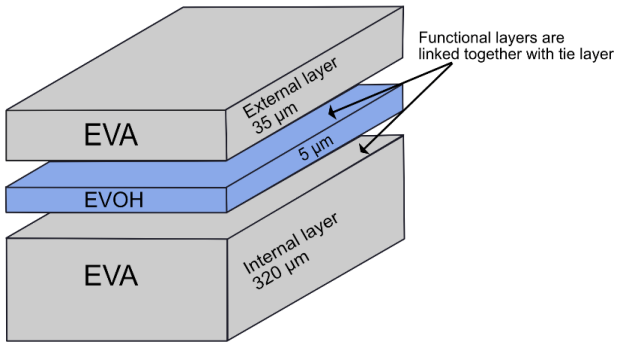


Figure 8 : Représentation du film multicouche EVA/EVOH/EVA.

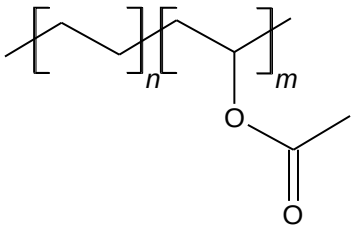


Figure 9 : Structure du polymère EVA.

Ce film est utilisé pour la fabrication de poches destinées au stockage de solutions biopharmaceutiques, de produits intermédiaires et finaux, avec des volumes allant de 5 mL à 50 L et une plage de température de -70 °C à 45 °C. La couche interne est en contact avec la solution contenue dans la poche, tandis que la couche externe est en contact avec le milieu extérieur.

## *Echantillons de polypropylène*

Cinq échantillons de polypropylène avec des formulations et utilisations différentes ont été étudiés dans cette thèse sous forme de « dogbones » (Figure 10a et Tableau 2). La structure du PP est représentée dans la Figure 10b. Ces échantillons, fournis par Sartorius, ont une densité d'environ 0,9 g/cm$^3$ et sont conçus pour diverses applications spécifiques telles que les pinces coulissantes, les filtres à cartouche, les connecteurs et les boîtiers de filtre.

(a) (b)



Figure 10 : (a) Structure du polypropylène. (b) Photo d'un « dogbone » de PP.

Tableau 2 : Caractéristique du PP non-irradié.

| **Polymères** | **Polypropylène (PP)** | | | | |
|---|---|---|---|---|---|
| **Numéro d'identification** | PP-1 | PP-2 | PP-3 | PP-4 | PP-5 |
| **Application industriel** | Pince coulissante | Filtres à cartouche | Connecteur | Boitier de filtre | Connecteur |
| **Densité (g·cm$^{-3}$)** | 0,9 | 0,9 | 0,9 | 0,905 | 0,905 |
| **Type de Polymère** | Homopolymère | Homopolymère | Copolymère | Homopolymère | Homopolymère |

## *Echantillon de polyéthylène*

Treize échantillons de polyéthylène (PE) avec des formulations différentes ont été étudiés dans cette thèse sous forme de dogbones (Figure 11). Ces échantillons incluent du HDPE, du LLDPE et du LDPE. La structure de ces échantillons est représentée dans la Figure 11. Ces échantillons fournis par Sartorius ont des densités typiques variant selon le type de PE : 0,94-0,97 g/cm$^3$ pour le HDPE, 0,91-0,94 g/cm$^3$ pour le LLDPE, et 0,91-0,93 g/cm$^3$ pour le LDPE.



Figure 11 : Photo d'un « dogbone » de HDPE.

Les connecteurs, les sacs de mélange ou les sacs STR sont composés de HDPE (High-Density PolyEthylene). Le LDPE (Low-Density PolyEthylene) est utilisé dans le corps principal des capteurs de pH et le LLDPE (Linear Low-Density PolyEthylene) est utilisé comme port d'électrode de pH et d'hélice de composants.

### *Echantillons de polyamide*

Quatre échantillons de polyamide (PA) avec des formulations différentes ont été étudiés dans cette thèse sous forme de colliers de serrage (Figure 12). Les structures du PA 6.6 et du PA 12 sont représentées dans la Figure 13. Ces échantillons, fournis par Sartorius, incluent plusieurs formes de PA : du PA 6.6, du PA 12 et du PA renforcé de verre. Ils sont conçus pour diverses applications spécifiques telles que les colliers de serrage ou les pinces.



Figure 12: Photo de trois échantillons de PA.

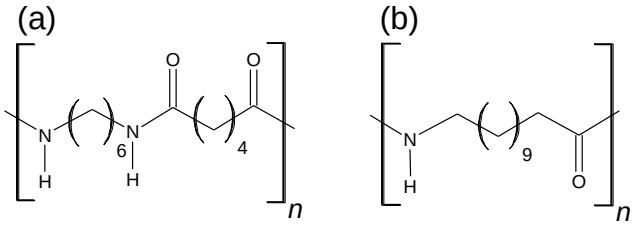


Figure 13 : Structures du (a) Polyamide 6.6 et (b) Polyamide 12.

## 2.1.2. Conditions d'irradiations

Les matériaux ont été emballés dans des sachets (fabriqués en PE/PA/PE) et un vide partiel a été réalisé. Les sachets ont ensuite été placés dans des cartons pour chaque technologie d'irradiation. Le détail des irradiations utilisées pour réaliser les études présentées dans ce mémoire est présenté dans la partie matériel et méthodes de chaque article et en début de chaque chapitre.

## 2.2. Techniques analytiques

Tous les paramètres des techniques analytiques employées dans cette thèse pour caractériser les matériaux polymères après irradiation sont détaillés dans les articles des chapitres suivants. Les techniques d'analyse utilisées sont énumérées ci-dessous :

La Résonance Paramagnétique Électronique (RPE) a été employée pour détecter, identifier et quantifier les radicaux produits dans les échantillons après irradiation. Cette technique a été appliquée aux échantillons irradiés par rayonnement gamma, faisceau d'électrons et rayons X.

La Calorimétrie Différentielle à Balayage (DSC) est une technique d'analyse thermique utilisée pour déterminer les transitions de phase, telles que la température de transition vitreuse ou les températures de fusion des matériaux. Elle a été utilisée pour comparer les effets des irradiations gamma, faisceau d'électrons et rayons X, et pour identifier tout changement macromoléculaire.

La Chromatographie Liquide à Haute Performance (HPLC) est une méthode extrêmement sensible (détection de l'ordre du µM), de séparation analytique des molécules en solution. Dans cette thèse, elle a été utilisée pour mesurer la première forme oxydée de la méthionine (méthionine sulfoxyde). La solution de méthionine est stockée dans les poches PE et EVA ou dans des flacons contenant les échantillons de PP découpé en morceaux afin d'avoir une surface de contact égale à 6 $cm^2$/mL.

Le test de traction est un essai mécanique qui détermine le comportement élastique et la résistance à la rupture d'un matériau.

L'infrarouge (FTIR : Fourrier Transform InfraRed) est utilisé pour obtenir des informations sur la composition et la structure de l'échantillon. La micro-FTIR combine la spectroscopie infrarouge avec la microscopie pour obtenir des informations détaillées sur la composition chimique et la structure des matériaux à une échelle microscopique [1,2].

La spectrophotométrie UV-Visible est utilisée pour mesurer l'absorption de la lumière ultraviolette et visible par un échantillon, cette technique permet de déterminer la concentration de composés dans une solution [3,4].

La Colorimétrie permet de mesurer la concentration de substances colorées dans une solution en utilisant la relation entre la couleur et la concentration de l'analyte. Par exemple, dans le cas des matériaux polymères, des mesures de couleur sont effectuées pour évaluer les changements de couleur avant et après irradiation.

L’Analyse Mécanique Dynamique (DMA) permet de mesurer les propriétés mécaniques d'un matériau en fonction de la température, de la fréquence ou du temps, fournissant des informations sur la rigidité, la viscosité et le comportement viscoélastique des matériaux [5].

## 2.3. Traitement de données

Tous les paramètres des méthodes de traitement de données utilisées dans cette thèse pour évaluer l’équivalence de l’impact de l’irradiation sur les matériaux polymères sont détaillés dans les articles des chapitres suivants. Les méthodes de traitement de données employées sont énumérées ci-dessous :

L'Analyse en Composantes Principales (ACP) est une méthode statistique exploratoire qui identifie les relations entre les variables étudiées [6,7]. Elle organise les données sous forme de matrice, avec les spectres des échantillons en lignes et les mesures spectrales en colonnes. L'ACP simplifie un nuage de points multidimensionnel en réduisant les dimensions tout en conservant l'essentiel des informations. Elle transforme les variables corrélées en composantes principales décorrélées, permettant de visualiser les similitudes entre échantillons. Les premières composantes expliquent la majorité de la variance, et les résultats sont interprétés à l'aide des scores et des loadings. Les analyses ACP ont été réalisées avec le logiciel Unscrambler X 10.3.

La méthode SIMPLISMA (SIMPLe-to-use Interactive Self-modeling Mixture Analysis) extrait les spectres purs et les profils de concentration d'un mélange complexe. Appliquée aux signaux RPE par exemple, cette méthode permet d’identifier la composition des espèces radicalaires générées au sein des polymères après irradiation et leurs profils de concentration. SIMPLISMA recherche les variables pures, permettant d'estimer les composants du mélange et de reconstituer les spectres initiaux. Les analyses SIMPLISMA ont été effectuées avec le logiciel Matlab 7.14 (R2012a) [8–13].

Le modèle de Régression des Moindres Carrés Partiels (PLS) est utilisé pour prédire la dose absorbée par les polymères à partir des données spectroscopiques. Les spectres des polymères sont obtenus via des techniques spectroscopiques comme la spectroscopie UV-Vis ou infrarouge. Le modèle PLS décompose les données spectroscopiques en composantes latentes, puis effectue une régression entre ces composantes et la dose absorbée, maximisant la covariance entre elles. Le modèle est validé par validation croisée pour garantir sa robustesse et précision, puis utilisé pour prédire la dose absorbée par de nouveaux échantillons [14–16].

Les modèles multiparamétriques linéaires identifient et quantifient les facteurs influençant les propriétés des polymères. Les données sont collectées pour plusieurs

variables indépendantes susceptibles d'influencer les propriétés des polymères. Les coefficients sont estimés par régression linéaire, quantifiant l'impact de chaque variable indépendante sur les propriétés des polymères. Ce modèle permet d'évaluer l'impact significatif de chaque variable indépendante, avec un intervalle de confiance de 95 % ($\alpha$=0,05). Le diagramme de Pareto montre les valeurs absolues des effets standardisés du plus grand au plus petit effet. Le diagramme trace également une ligne pointillée de référence indiquant si les effets sont statistiquement significatifs. La ligne de référence pour la significativité statistique dépend du niveau de significativité (noté par $\alpha$), du nombre d'échantillons et du degré de liberté. Le modèle peut ensuite être utilisé pour optimiser les conditions de traitement ou la composition des polymères [17].

Le test d'équivalence à deux tests unilatéraux (TOST) est une méthode statistique utilisée pour déterminer si deux groupes ou conditions sont équivalents. Contrairement à un test d'hypothèse traditionnel qui cherche à détecter une différence significative, le TOST vérifie si la différence entre les moyennes des deux groupes se situe à l'intérieur d'un intervalle d'équivalence prédéfini. Cet intervalle représente la plage de différences jugées acceptables pour l'application. Si les résultats tombent dans cet intervalle, on conclut que les deux groupes sont équivalents [18].

Le test de Student est une méthode statistique utilisée pour comparer les moyennes de deux ensembles de données. Ce test repose sur des hypothèses de normalité des données et d'égalité des variances. Il est couramment utilisé dans l'analyse de variance et d'autres analyses statistiques pour déterminer la signification des différences observées entre les groupes [19].

## 2.4. Analyses

Les films multicouches PE/EVOH/PE et EVA/EVOH/EVA, ainsi que les polymères PE, PP et PA ont été analysés avec plusieurs techniques analytiques décrites ci-dessus. Dans ce manuscrit, nous avons effectué une analyse de ces différents polymères multi-échelle. Le Tableau 3 résume toute les techniques analytiques réalisées et valorisées dans ce manuscrit.

Tableau 3 : Techniques analytiques réalisées (✓) et valorisées (✓) des différents polymères étudiés

| | RPE | IR | Traction | DSC | DMA | HPLC | Colorimétrie |
|---|---|---|---|---|---|---|---|
| Films EVA/EVOH/EVA | ✓ | ✓ | ✓ | ✓ | | ✓ | |
| Films PE/EVOH/PE | ✓ | ✓ | ✓ | ✓ | ✓ | ✓ | |
| PE | ✓ | ✓ | ✓ | ✓ | | ✓ | ✓ |
| PP | ✓ | ✓ | ✓ | ✓ | | ✓ | ✓ |
| PA | ✓ | | | ✓ | | | |

# Références Chapitre 2


1. Voronko, Y.; Chernev, B.S.; Eder, G.C. Spectroscopic Investigations on Thin Adhesive Layers in Multi-Material Laminates. *Applied Spectroscopy* **2014**, *68*, 584–592, doi:10.1366/13-07291.

2. Wrobel, T.P.; Vichi, A.; Baranska, M.; Kazarian, S.G. Micro-Attenuated Total Reflection Fourier Transform Infrared (Micro ATR FT-IR) Spectroscopic Imaging with Variable Angles of Incidence. *Applied Spectroscopy* **2015**, *69*, 1170–1174, doi:10.1366/15-07963.

3. Di Benedetto, D.; Breuil, P. Spectrophotométrie d'absorption dans l'ultraviolet et le visible. *Techniques d'analyse* **2007**, doi:10.51257/a-v2-p2795.

4. NicDaéid, N. Systematic Drug Identification ☆. In *Reference Module in Chemistry, Molecular Sciences and Chemical Engineering*; Elsevier, **2018**; ISBN 978-0-12-409547-2.

5. *Thermal Analysis of Polymers: Fundamentals and Applications*; Menczel, J.D., Prime, R.B., Eds.; John Wiley: Hoboken, N.J, **2009**; ISBN 978-0-471-76917-0.

6. Kumar, N.; Bansal, A.; Sarma, G.S.; Rawal, R.K. Chemometrics Tools Used in Analytical Chemistry: An Overview. *Talanta* **2014**, *123*, 186–199, doi:10.1016/j.talanta.2014.02.003.

7. Martens, H.; Naes, T. *Multivariate Calibration*; Wiley: Chichester, **2002**; ISBN 978-0-471-93047-1.

8. Gemperline, P.J. Mixture Analysis Using Factor Analysis I: Calibration and Quantitation. *J. Chemometrics* **1989**, *3*, 549–568, doi:10.1002/cem.1180030404.

9. Hamilton, J.C.; Gemperline, P.J. Mixture Analysis Using Factor Analysis. II: Self-Modeling Curve Resolution. *Journal of Chemometrics* **1990**, *4*, 1–13, doi:10.1002/cem.1180040103.

10. Windig, W. The Use of Second-Derivative Spectra for Pure-Variable Based Self-Modeling Mixture Analysis Techniques. *Chemometrics and Intelligent Laboratory Systems* **1994**, *23*, 71–86, doi:10.1016/0169-7439(93)E0058-C.

11. Windig, W. Spectral Data Files for Self-Modeling Curve Resolution with Examples Using the Simplisma Approach. *Chemometrics and Intelligent Laboratory Systems* **1997**, *36*, 3–16, doi:10.1016/S0169-7439(96)00061-5.

12. Windig, W.; Stephenson, D.A. Self-Modeling Mixture Analysis of Second-Derivative near-Infrared Spectral Data Using the SIMPLISMA Approach. *Analytical Chemistry* **1992**, *64*, 2735–2742, doi:10.1021/ac00046a015.

13. Windig, Willem.; Guilment, Jean. Interactive Self-Modeling Mixture Analysis. *Analytical Chemistry* **1991**, *63*, 1425–1432, doi:10.1021/ac00014a016.

14. Daszykowski, M.; Kaczmarek, K.; Vander Heyden, Y.; Walczak, B. Robust Statistics in Data Analysis — A Review. *Chemometrics and Intelligent Laboratory Systems* **2007**, *85*, 203–219, doi:10.1016/j.chemolab.2006.06.016.

15. Ergon, R.; Esbensen, K.H. PCR/PLSR Optimization Based on Noise Covariance Estimation and Kalman Filtering Theory. *J. Chemometrics* **2002**, *16*, 401–407, doi:10.1002/cem.732.

16. Liang, Y.-Z.; Kvalheim, O.M. Robust Methods for Multivariate Analysis — a Tutorial Review. *Chemometrics and Intelligent Laboratory Systems* **1996**, *32*, 1–10, doi:10.1016/0169-7439(95)00006-2.

17. Malashin, I.P.; Tynchenko, V.S.; Nelyub, V.A.; Borodulin, A.S.; Gantimurov, A.P. Estimation and Prediction of the Polymers' Physical Characteristics Using the Machine Learning Models. *Polymers* **2023**, *16*, 115, doi:10.3390/polym16010115.

18. Lakens, D. Equivalence Tests: A Practical Primer for *t* Tests, Correlations, and Meta-Analyses. *Social Psychological and Personality Science* **2017**, *8*, 355–362, doi:10.1177/1948550617697177.

19. Poirier, J. Estimateurs et tests d'hypothèses. *Instrumentation et méthodes de mesure* **1992**, doi:10.51257/a-v1-r250.

# Chapitre 3 : Comparaison de l'impact de l'irradiation gamma, rayons X et faisceau d'électrons sur le film multicouche EVA/EVOH/EVA

L'objectif de ce chapitre est d'analyser l'impact de la stérilisation par rayons gamma, X et faisceau d'électrons sur les propriétés chimiques du film multicouches EVA/EVOH/EVA, irradié à différentes doses. Ce chapitre s'articule autour de deux articles.

Dans le premier article, une approche analytique multi-échelle a été employée afin de détecter les modifications potentielles des propriétés chimiques du matériau après irradiation. L'objectif est d'analyser l'oxydation des couches EVA et EVOH du film en utilisant un film non irradié comme référence.

Des modèles PLS basés sur les données spectroscopiques ont été développés pour chaque technologie d'irradiation, permettant de prédire la dose reçue par le film et d'évaluer l'équivalence de l'impact des différentes technologies.

Les poches commercialisées par la société Sartorius sont principalement utilisées pour la production de produits et substances médicamenteuses telles que des vaccins, des protéines recombinantes et des anticorps monoclonaux. Ces substances seront par la suite utilisées pour le développement de biomolécules au stade des phases cliniques. Un des principaux inconvénients causés par l'irradiation est la formation d'espèces oxydante qui pourraient être relargués dans la solution contenue dans la poche [1].

Le second article porte sur la détection de ces espèces après irradiation. L'impact des trois technologies d'irradiation a été analysé en examinant la formation de peracides pouvant altérer les solutions biologiques contenue dans la poche. Une solution de méthionine a été choisie car l'oxydation de la méthionine représente une voie de dégradation majeure des protéines thérapeutiques ainsi que des anticorps monoclonaux [2]. De plus, la méthionine constitue l'un des principaux acides aminés sujet à l'oxydation à cause de son atome de soufre, très réactif vis-à-vis des espèces réactives dérivées de l'oxygène. En étudiant l'oxydation de la méthionine contenue dans la poche EVA par HPLC, la formation d'agents oxydants après irradiation par rayons gamma, X et faisceau d'électrons sera alors mise en évidence.

La principale différence entre les irradiations gamma, rayons X et faisceau d'électrons réside dans les débits de dose moyens délivrés, qui sont très différents (de l'ordre de

quelques kGy/h pour les rayons gamma, ~12 kGy/h pour les rayons X et kGy/s pour faisceau d'électrons). Cet article analyse l'impact de ces trois technologies en fonction de leurs débits de dose respectifs.

De plus, nous avons analysé par RPE la formation d'espèces radicalaire après irradiation afin de corréler les résultats obtenus par HPLC. L'étude montre l'équivalence des trois technologies en analysant la nature et la quantité des espèces radicalaires générées par RPE, et l'impact du débit de dose qui est étroitement lié à la technologie en analysant l'oxydation de la méthionine contenue dans la solution.

# 3.1. Étude spectroscopique du film EVA/EVOH/EVA après irradiation

Dans cet article publié dans la revue *Radiation Physics and chemistry* en 2024, le film multicouche EVA/EVOH/EVA a été analysé après irradiation gamma, rayons X et faisceau d'électrons afin d'évaluer l'impact des trois technologies d'irradiation. Les analyses sont issues de la base de données de Sartorius et de la team Nablo (Tableau 4 ).

Tableau 4 : Dose et débit de dose d'irradiation du film multicouche EVA/EVOH/EVA.

| **Techniques analytiques** | **Gamma** | | **Rayons X** | | **Faisceau d'électrons** | |
|---|---|---|---|---|---|---|
| | Dose (kGy) | Débit de dose (kGy/h) | Dose (kGy) | Débit de dose (kGy/h) | Dose (kGy) | Débit de dose (kGy/h) |
| **Micro FTIR** | 25, 50, 100 | 2 | 25, 50, 100 | 12 | 25, 50 | 18000 |
| **ATR-FTIR** | 30, 45, 60 | 2 | 30, 45, 100 | 12 | 30, 45, 60 | 18000 |
| **UV-Vis** | | | | | | |

Une approche analytique à plusieurs niveaux est utilisée :

- Une analyse au niveau macromoléculaire afin d'obtenir des informations sur les potentiels changements chimiques conduisant à la modification du matériau après irradiation par spectroscopie infrarouge (micro infrarouge et ATR/FTIR).
- Une analyse au niveau moléculaire afin de comprendre le comportement des antioxydants après irradiation par spectroscopie UV-Vis.

La spectroscopie infrarouge (micro infrarouge et ATR/FTIR) dans cette étude permet d'obtenir des informations sur l'oxydation potentielle des couches EVOH et EVA du film. Une telle approche a produit une énorme quantité de données ; ainsi, les analyses de ces données ont été effectuées en utilisant des méthodes chimiométriques décrites dans l'article telles que l'analyse en composantes principales, SIMPLISMA (SIMPLe-to-use Interactive Self-modeling Mixture Analysis) et la régression par moindres carrés partiels.

L'étude de l'oxydation à la surface des films multicouches après irradiation a déjà fait l'objet de publications[3–5]. L'objectif de cette étude est d'analyser l'oxydation potentielle dans la tranche du film, afin d'évaluer les modifications après irradiation dans la couche EVA et dans la couche EVOH. Pour cela nous avons utilisé la spectroscopie micro-infrarouge pour évaluer et comparer les effets de l'irradiation gamma, rayons X et

faisceaux d'électrons sur le film à différentes doses, en utilisant un film non-irradié comme référence. Les résultats obtenus avec l'ACP sont présentés dans la figure 6 dans l'article.

Des modèles PLS ont été construits à partir des données spectroscopiques ATR pour chaque technologie d'irradiation ainsi que pour les données spectroscopiques obtenues par ATR. Une fois validés pour une technologie d'irradiation, ces modèles sont ensuite utilisés pour prédire la dose reçue par le film avec les résultats spectroscopiques obtenus après irradiation avec d'autres technologies, afin d'évaluer l'équivalence de l'impact des différentes technologies d'irradiation. Les résultats obtenus par ces modèles sont représentés dans l'article.

Les conclusions principales de cette étude sont :

- Aucune modification de la couche EVOH et EVA n'a été observée dans le film quelle que soit la technologie d'irradiation avec la méthode d'analyse micro-infrarouge jusqu'à une dose absorbée de 100 kGy.
- La dose absorbée par le film peut être modélisée en utilisant les données UV-Vis ou ATR/FTIR et ainsi l'impact de l'irradiation peut être évalué. Il est important de noter que les modèles de dose ne s'appliquent pas de manière uniforme à toutes les technologies d'irradiation. Par exemple, la dose absorbée estimée pour le film irradié par faisceau d'électrons est sous-évaluée lorsqu'on utilise des modèles basés sur les rayons gamma ou X.
- L'impact de l'irradiation par faisceau d'électrons, tel qu'évalué par UV-Vis et FTIR, diffère de celui des rayons gamma et X sur le film multicouche.
- Les rayons gamma et X ont un impact équivalent sur le film permettant une prédiction cohérente tandis que l'irradiation par faisceau d'électrons a un impact plus faible sur le film.

Radiation Physics and Chemistry 218 (2024) 111607

Contents lists available at ScienceDirect

Radiation Physics and Chemistry

journal homepage: www.elsevier.com/locate/radphyschem

# Comparison of effects from gamma, e-beam and X-ray radiation on multilayer polymer films used in biopharmaceutical devices by chemometric treatment of spectroscopic data

Blanche Krieguer [a,b,c,*], Sylvain R.A. Marque [b], Samuel Dorey [a,**], Fabien Girard [c], Yelin Ni [d], Donghui Li [d], Mark K. Murphy [d], Leonard S. Fifield [d], Nathalie Dupuy [c,***]

[a] Sartorius Stedim FMT S.A.S, Z.I. Les paluds, Avenue de Jouques CS91051, 13781, Aubagne Cedex, France
[b] Aix Marseille Univ, CNRS, ICR, Case 551, 13397 Marseille, France
[c] Aix Marseille Univ, Avignon Univ, CNRS, IRD, IMBE, Marseille, France
[d] Pacific Northwest National Laboratory, Richland, WA 99354, USA

ARTICLE INFO

Handling Editor: Piotr Ulanski

*Keywords:*
FTIR
UV-VIS
Chemometrics
Gamma-ray
X-ray
e-beam

ABSTRACT

The present study investigated the effects of gamma-ray, electron beam, and X-ray radiation on polymers in EVA/EVOH/EVA multilayer films. Spectroscopic methods, including FTIR and UV–Vis, were employed in conjunction with chemometric treatments such as PCA, SIMPLISMA treatments, and PLS models. The feasibility of dose prediction on multilayer film, given a known dose, is attainable across various irradiation technologies. Both gamma ray and X-ray exhibit comparable effects on the multilayer film, and it is feasible to anticipate the dose released on the film by utilizing UV–Vis spectra or infrared spectra for gamma ray or X-ray of a predetermined dose.

## 1. Introduction

In a wide range of industrial sectors, including the production of single-use systems with multilayer plastic film for biopharmaceutical applications, gamma sterilization is utilized as a necessary and standardized process. Due to its extremely low residual toxicity, radiation sterilization offers a considerable benefit. Alternative irradiation technologies have emerged (Armenante and Akiti, 2019; Darwis et al., 2015; Dupuy et al., 2022; Komolprasert, 2016; Moondra et al., 2018), including electron beam (e-beam) and X-ray, despite the long history of gamma irradiation in the sterilizing process.

Polymers are used in a variety of medical and pharmaceutical products (Valente et al., 2016), including consumable plastic bags, gloves, and syringes. E-beam and X-ray sterilization are becoming more and more popular and numerous studies on the impact of this sterilization on medicinal goods, have been conducted since the technologies have become commercially available.

Previous studies have extensively examined the effects of gamma irradiation on EVOH and EVA polymers (Dinesh and Chikkakuntappa, 2013; Ji et al., 2019), while only a few studies have investigated the effects of e-beam and X-ray irradiation (Ahmed et al., 2020; Entezam et al., 2017; Matsui et al., 1992). Few studies have compared the effects of gamma and e-beam irradiation on EVA, with gamma irradiation having a greater impact on physical, mechanical, and thermal properties (Girard-Perier et al., 2022b). Other studies have compared the effects of gamma and electron beam irradiation on EVA shelf life, with no significant changes observed. Similarly, the effects of gamma and X-ray irradiation on the mechanical properties of EVA were found to be similar. For the EVA/EVOH/EVA multilayer film in this paper, various analytical techniques have been used to study the effects of gamma irradiation on different levels, but there is a lack of data on the effects of electron beam and X-ray irradiation on the spectroscopic properties of

* Corresponding author. Sartorius Stedim FMT S.A.S, Z.I. Les paluds, Avenue de Jouques CS91051, 13781, Aubagne Cedex, France.
** Corresponding author.
*** Corresponding author.
*E-mail addresses:* blanche.krieguer@sartorius.com (B. Krieguer), sylvain.marque@univ-amu.fr (S.R.A. Marque), samuel.dorey@sartorius.com (S. Dorey), fabien.girard@univ-amu.fr (F. Girard), yelin.ni@pnnl.gov (Y. Ni), donghui.li@pnnl.gov (D. Li), Mark.Murphy@pnnl.gov (M.K. Murphy), leo.fifield@pnnl.gov (L.S. Fifield), nathalie.dupuy@univ-amu.fr (N. Dupuy).

https://doi.org/10.1016/j.radphyschem.2024.111607
Received 13 June 2023; Received in revised form 18 December 2023; Accepted 11 February 2024
Available online 16 February 2024
0969-806X/© 2024 The Authors. Published by Elsevier Ltd. This is an open access article under the CC BY-NC license (http://creativecommons.org/licenses/by-nc/4.0/).

multilayer materials. The use of ionizing irradiation as a sterilization method can cause bond cleavage and cross-linking, which may alter the physical and mechanical properties of the polymers. The chemical composition of polymers, the presence of additives, or the amount of oxygen in the surrounding environment all have an impact on polymers when exposed to radiation: radicals are created (Audran et al., 2015), the molecular weight of the polymer changes due to crosslinking, oxidized molecules are created, scission and other species like ions, excited macromolecules, etc (Darwis et al., 2015; Fifield et al., 2021; Matsui et al., 1992; Tarantili and Kiose, 2008).

The literature describes the cross-linking and chain scission events related to the effect of radiation on molecular weight distribution.

All these analyses (Driffield et al., 2014; Gaston et al., 2016a; Girard-Perier et al., 2022a; Tarantili and Kiose, 2008; Fifield et al., 2021) were performed on ready-to-use materials prepared in the factory and the several irradiations were performed in sterilization companies in classic industrial conditions. This approach has a strong limitation due to the non-controlled environment, which was circumvented by taking care on repeatability and reproducibility on the experiments.

In this study, an ethylene vinyl acetate (EVA)/ethylene vinyl alcohol (EVOH)/EVA multilayer film was analyzed after irradiation with gamma, X-ray, and e-beam in order to evaluate the effects of the three irradiation technologies on the film from a spectroscopic point of view.

A multilevel analytic approach is used for the investigation of EVA/EVOH/EVA multi-layer films: (i) analysis at the macromolecular level to get insights into the chemical changes leading to deterioration of material integrity by infrared spectroscopy (micro infrared and classic ATR/FTIR); and (ii) analysis at the molecular level to understand the behaviour of additive (antioxidants) by UV–Vis spectroscopy. Such approach generates a huge amount of data; thus, analyses of these data are performed using chemometrics methods such as Principal Component Analysis PCA and partial least square regressions (PLS). The goal of this study is to use infrared and UV–Vis spectroscopy to compare the effects of gamma, X-ray and e-beam radiation on multilayer films at various doses using the same unirradiated films as a reference. Quantitative models are built for each irradiation technology to predict the dose received. These models, once validated for an irradiation technology, are then used to predict the dose received for other irradiation technologies, in order to understand if the impact of the different irradiation technologies is similar.

## 2. Materials and methods

### 2.1. EVA/EVOH/EVA multilayer film and additives

The two batches of EVA single-use plastic bags investigated are made from a multilayer film composed of one layer of EVOH sandwiched between two layers of EVA, with a total thickness of approximately 360 μm. Sample bags are provided by Sartorius Stedim FMT S.A.S., Aubagne, France. Two different batches were examined in order to consider batch-to-batch variation. The different layers of these films contain additives such as antiblocking agents and antioxidants (AO) to stabilize them during the manufacturing process and during their shelf life.

### 2.2. Irradiation technologies

Precut EVA/EVOH/EVA samples were irradiated in gamma, e-beam and X-ray facilities. Samples were packed and wrapped in 100 ± 20 μm thick packaging films made of polyethylene (PE)/polyamide (PA)/PE during irradiation.

- Gamma irradiation

Gamma irradiation was carried out at room temperature with a cobalt-60 source at Ionisos (Dagneux, France) at a dose rate of 1–2 kGy $h^{-1}$. Co-60 has 1.17 and 1.33 MeV gamma energies. Multiple sterilization cycles were performed to obtain target doses. The waiting time between cycles and storage conditions were not specifically controlled. The actual delivered dose was measured using alanine dosimeters on a cardboard box (±5%). For the UV–Vis and ATR-FTIR analyze the doses delivered are 30, 44 and 61 kGy and for the micro-ATR FTIR the doses delivered are 30, 59 and 106 kGy.

- Electron beam irradiation

For the ATR-FTIR and UV–Vis spectroscopy, e-beam irradiation was performed using two 10 MeV, 20 kW Mevex accelerators at Steri-Tek (Fremont, California, USA), the dose rate being 18 MGy $h^{-1}$. The delivered doses are 31, 47 and 59 kGy for double sided irradiation.

Model B3 dosimeters were used on cardboard boxes to assess the radiation delivered to the film samples (±5%). For the micro-ATR-FTIR, e-beam irradiation was performed using a 10 MeV Rhodotron (Ionisos, Chaumesnil, France) with a power source at 28 kW, the dose rate being 18 MGy $h^{-1}$ (Chmielewski and Sun, 2017; Kroc, 2023). Alanine dosimeters were used on the cardboard to assess the radiation delivered (±5%) to the single-use bag samples. The delivered doses are 25 and 52 kGy for double sided irradiation.

•X-ray irradiation.

X-ray irradiation has been performed at Aerial-CRT on Feerix facilities. This facility is based on a Rhodotron (TT300 – IBA) and delivers X-ray beams. In this study, 7 MeV X-rays have been obtained from the conversion of 7 MeV electrons in a tantalum target. Irradiation has been performed with a vertical scan and a horizontal translation of products. The average dose rate was about 12 kGy $h^{-1}$. This, together with the adapted packaging of plastic parts in thin craft boxes, provides good treatment uniformity.

Delivered doses are 33, 45, 60 and 99 kGy ±10% for the UV–Vis and ATR-FTIR analysis and for the micro-ATR FTIR the delivered doses are 25, 50 and 100 kGy. The dose was verified by placing dosimeters in the cardboard box volume. Dosimetry has been performed using alanine.

### 2.3. Micro ATR FTIR

Micro-ATR-FTIR (μIR) is an extremely useful technique for confirming the identity of pure compounds (Voronko et al., 2014; Wrobel et al., 2015). The technique is based upon the identification of functional groups within molecules where such groups vibrations intensify through infrared radiation absorption (either through stretching torsion or bending in various ways). These vibrations and their intensity (reflectance) are plotted against the wavenumbers ($cm^{-1}$) to which the sample is exposed to produce an FTIR spectrum. Micro-ATR-FTIR makes it possible to analyze surfaces that are theoretically as small as the limit imposed by the diffraction of infrared radiation. Using the most powerful microscopes equipped with sophisticated optical systems and highly sensitive detectors, it is possible to analyze areas as small as 10 μm × 10 μm (Gardette, 1998). The obtain spectra are not saturated. The cross-section (Fig. 1) of each EVA/EVOH/EVA film sample was analyzed starting from the external face to the internal face. The set of spectra produced is called a mapping. The spectrometer used was a Thermo Nicolet Scientific MIR spectrometer with a microscope and ATR module, model IN10, with MCT detectors cooled with liquid nitrogen for better sensitivity. The spectrometer was placed in an air-conditioned room at 22 °C. Between each analysis, the KBr/Ge beam splitter was cleaned with an ethanol solution. At the beginning of each analysis, a reference spectrum was recorded, and the spectra were recorded with 16 scans and a resolution of 8 $cm^{-1}$. Each mapping was recorded in line form (Fig. 1) and the spectra were acquired every 10 μm. We did not consider spectra with too low signal-to-noise ratio; a total of 293 recorded spectra are available for chemometric analysis.

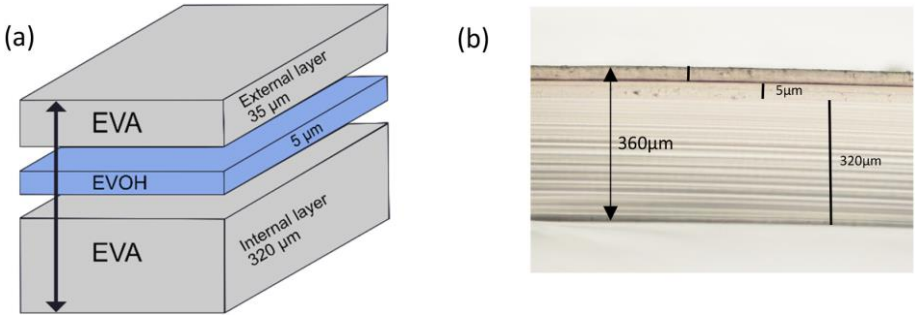


**Fig. 1.** (a) Representation of EVA/EVOH/EVA multilayer film; arrow represents the cross-section (b) microscopic image of cross-section of multilayer film.

### 2.4. ATR-FTIR

Fourier transform infrared spectroscopy (FTIR) was used to characterize chemical property changes on the polymer surface. After conditioning (23 °C and 50% relative humidity for at least 40 h), the samples were measured by Alpha II FTIR spectrometer (Bruker Corporation, MA, USA) with a diamond attenuated total reflection (ATR) crystal. The spectra of each sample were recorded from 4000 to 400 $cm^{-1}$ with 64 scans and a resolution at 4 $cm^{-1}$. For each sample, spectra were measured at four locations near the four edges of the sample. We did not consider spectra with too low a signal-to-noise ratio; a total of 220 recorded spectra are available for chemometric analysis.

### 2.5. Ultraviolet spectroscopy (UV–Vis)

UV–Vis spectroscopy is one of the most simple and economical methods for analysis of polymer film (Di Benedetto and Breuil, 2007; NicDaéid, 2018). UV–Vis transmittance from 200 nm to 800 nm was measured on a Cary 5000 UV–Vis–NIR spectrophotometer (Agilent Technologies, Inc.) with a solid sample holder. Three films irradiated at 30, 45, 60 kGy by gamma, e-beam and X-ray technologies were tested. Each film sample was tested three times. Prior to testing, the incident beam in the spectrometer was turned on for at least 30 min until it fully stabilized. Baseline scans (100% transmittance) were performed using the sample holder. Stabilization of the beam source was checked by examining the smoothness of the baseline.

### 2.6. Curve resolution method (SIMPLISMA)

The SIMPLe-to-use Interactive Self-modelling Mixture Analysis (SIMPLISMA) method, described in the literature (Gemperline, 1989; Hamilton and Gemperline, 1990; Windig, 1994, 1997; Windig and Stephenson, 1992; Windig and Guilment, 1991), was used for self-modelling mixture analysis by resolving mixture data into pure component signal and concentration profiles without the help of prior information about the mixture. Plastics are always a mixture of polymers and additives. SIMPLISMA will consider as "pure" either a mono-material or a mixture which evolves in a consistent way after irradiation (Gaston et al., 2018). When the radicals have the same kinetic trend and the same concentration profile, this tool is unable to differentiate the characteristics of different components. SIMPLISMA analysis is based on least squares optimization to determine the pure signal that has received the contributions from only one component. To properly handle noise, peak shifts, and instrument drift, user interactions are required (Audran et al., 2015).

The fitting of the SIMPLISMA results is calculated using the Relative Residual Sum of Squares (RRSSQ) (Windig, 1994), square sum between the calculated and the original spectra. The SIMPLISMA data treatments are performed with MATLAB 2009 software.

### 2.7. Principal Component Analysis (PCA)

Principal component analysis (PCA) is a tool commonly used in chemometrics (Kumar et al., 2014; Martens and Naes, 1989) and was described in a previous study (Audran et al., 2015). Each principal component (PC) is constructed to maximize the variance extracted from the remaining data. The projection of the scores in the space defined by the PCs gives an overview of the similarities and differences between the samples, while the loadings indicate which variables bring more information to each PC. In this study, we considered for each model only the PCs containing more than 15% of the variance. Thus, in some cases only the first PC was relevant, and the scores could be represented as a bar chart. In other cases, the first two PCs were relevant, and the scores could be represented as a scatter plot.

PCA was performed on spectra acquired in µIR on irradiated film EVA/EVOH/EVA by gamma, e-beam, and X-ray at 25, 50 and 100 kGy. To highlight the impact of the irradiation technology, only two ageing scenarios were selected (12 months for non-irradiated samples and 6 months). The spectra were corrected with a baseline and standard normal variate (SNV) pretreatment to correct for additive and multiplicative effects. PCA models were performed using CAMO (Computer Aided Modelling, Trondheim, Norway) software UNSCRAMBLER *X*.1.

### 2.8. Partial least square model (PLS)

Partial least squares (PLS) regression (Daszykowski et al., 2007; Ergon and Esbensen, 2002; Liang and Kvalheim, 1996; Martens, 1979; Sjöström et al., 1983) is a supervised method which is based on the relation between signal intensity (spectrum) and the characteristics of the sample (Y variable). Interference and overlapping information may be overcome by using a powerful multicomponent analysis such as PLS. The algorithm is based on the ability to mathematically correlate spectral data to a property or a concentration. PLS models were performed using CAMO (Computer Aided Modelling, Trondheim, Norway) software UNSCRAMBLER *X*.1.

## 3. Results and discussion

The modifications of the film after irradiation by gamma, e-beam and X-ray are analyzed on several scales: to the $cm^2$ with analysis in UV–Vis, to the $mm^2$ with analysis in infrared and to some $\mu m^2$ with analysis in µIR.

### 3.1. ATR-FTIR

The infrared spectra of the EVA/EVOH/EVA multilayer film non-irradiated and irradiated by gamma, e-beam, and X-ray doses ranging from 30 to 60 kGy displayed in Fig. 2. According to the literature (Gaston et al., 2016a), the main signal changes are observed in the

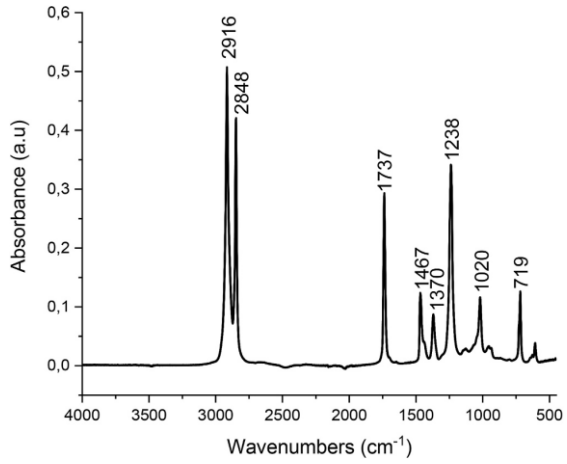


**Fig. 2.** Overlay of 220 EVA/EVOH FTIR spectra for non-irradiated samples.

carboxylic acid region (1737 $cm^{-1}$). The IR assignments of the EVA and EVOH spectra are given in Table S1 in accordance with the literature (Gaston et al., 2016a; Wool et al., 1986). The peak at 2916 $cm^{-1}$ corresponds to the antisymmetric stretching ($\nu CH_2$), the peak at 2848 $cm^{-1}$ corresponds to the symmetric stretching ($\nu CH_2$), and the peak at 1737 $cm^{-1}$ corresponds to the νCO of the ester. Peaks included between 1470 and 1360 $cm^{-1}$ correspond to the deformation in the plane of the $\delta CH_2$ and $\delta CH_3$ groups. Peaks included between 1300 and 1020 $cm^{-1}$ correspond to the stretching νCO, the peak at 730 $cm^{-1}$ (shoulder) corresponds to the inner rocking vibration of $CH_2$ in the crystalline part ($\delta CH_2$), and the peak at 719 $cm^{-1}$ corresponds to the inner rocking vibration of $CH_2$ in the amorphous part ($\delta CH_2$) (Gaston et al., 2016a).

### 3.1.1. Principal component analysis

The PCA displayed in Fig. 3 concerns the FTIR fingerprint spectral region [1800–700 $cm^{-1}$] and is performed on the 220 spectra representing the effects of all irradiation doses and technologies. For this region, the EVA spectra are baseline corrected and normalized. The first principal component (PC1) represents 52% of the total variance of the modification of the spectra. The second component (PC2) represents 22% of the total variance. In PCA approach, the data are clustered based on the similarities between samples by plotting two principal components relative to each other. All changes observed in PC1 and PC2 are correlated with the irradiation dose, regardless of the technology. Principal components (PCs) describe the variations among the objects in decreasing order, from the greatest to the smallest.

Fig. 3a displays then two different groups, the irradiated and the non-irradiated samples. Neither the effect of the different radiation technologies is visible, nor is the effect of the dose received at 30, 45 and 60 kGy. The first two components are the difference between the irradiated and non-irradiated spectra. Representation of variables PC1 and PC2 (Fig. 3b and c) highlight the wavenumbers contributing to the difference. No difference is observed on the investigated irradiation technologies.

When irradiated the primary signal change is noticeable in the carbonyl zone (1720-1740 cm-1). No signal changes are noticeable in the carboxylic acid zone (around 1714 cm-1) and the trans alkene zone (between 880 and 980 cm-1). The extent of these changes do not varies clearly depending on the absorbed dose with a different technologies, as shown in Fig. 3a and emphasized by the PCA. The peaks observed in the 730–700 cm-1 zone do not exhibit strong variation in the absorbed doses.

### 3.1.2. PLS regression

As the PCA showed that the unirradiated samples were slightly different from the irradiated samples, we quantified the dose received by those samples. A PLS regression was modeled to do so. The purpose of the PLS model is to extrapolate the effect of irradiation on the EVA/EVOH/EVA film to simulate the radiation dose received by the polymers regardless of the radiation source. We applied 3 PLS models, one for each irradiation technology.

Half of the non-irradiated samples and all samples irradiated at 30 and 60 kGy using gamma radiation were used for modelling. Samples irradiated at 45 kGy by gamma rays and half of the non-irradiated samples are used for prediction (Table S2). The modelling results ($R^2$ = 0.99, RMSEC = 1.52) show that a good correlation is obtained between the infrared spectra and the absorbed gamma radiation dose. The model was then used to predict the absorbed dose for samples irradiated by X-ray or e-beam at 30, 45 and 60 kGy (Fig. 4a). The results show that X-ray doses are correctly predicted while e-beam doses are underestimated.

A similar model was built for the X-ray irradiated samples. Half of the non-irradiated samples and all samples irradiated at 30 and 60 kGy using X-ray irradiation were used for modelling. Samples irradiated at 45 kGy by X-ray and half of the non-irradiated samples are used for prediction (Table S2 in SI). The modelling results ($R^2$ = 0.99, RMSEC = 1.94) show that a good correlation is obtained between the infrared spectra and the X-ray absorbed radiation dose. The model was then used to predict the absorbed dose for samples irradiated by Gamma or e-beam at 30, 45 and 60 kGy (Fig. 4a). The results show that gamma doses are correctly predicted while e-beam doses are underestimated.

A model was then built for the e-beam irradiated samples. Half of the non-irradiated samples and all samples irradiated at 30 and 60 kGy using e-beam were used for modelling. Samples irradiated at 45 kGy, and half of the unirradiated samples are used for prediction. The modelling results ($R^2$ = 0.99, RMSEC = 3.38) show that a good correlation is obtained between the infrared spectra and the received e-beam doses. The prediction results (Table S2) show that the model is applicable: non-irradiated samples are predicted with an average dose of 1 kGy, the dose of samples irradiated at 45 kGy by e-beam is predicted as 43.6 kGy. The model used to predict the absorbed dose for samples irradiated by gamma or X-ray at 30, 45 and 60 kGy show that X-ray doses and gamma doses are overestimated. Consequently, e-beam irradiation produces effects in different proportion on polymers than gamma and X-ray irradiation technologies, and the PLS models underestimate the expected dose for the electron beam. The gamma and the X-ray impact prediction are both in good agreement as they are both photon based technologies delivering doses in similar dose rate range. X-ray technology can deliver dose with dose rate <100 kGy $h^{-1}$ and gamma technology deliver dose with dose rate <10 kGy $h^{-1}$. E-beam technology can deliver dose with dose rate <30,000 kGy $h^{-1}$. We know according to ISO11137 that normally the higher the dose rate, the lower the impact on polymers without details on this statement. This could explain that e-beam production is not in agreement with the other ones.

The plot of the spectra (Fig. 5) displays that the effects of three irradiation technologies are different. The effect on the band at 720 $cm^{-1}$, which corresponds to the inner rocking vibration of $CH_2$ in the amorphous part ($\delta CH_2$) varies with the technology used. e-beam irradiation has a lesser effect on the crystallinity of the polymer compared to gamma and X-ray irradiation.

## 3.2. Micro infrared (μIR)

To complement the previous ATR study on the surface of the multilayer film, we analyzed the cross section of the film by μIR (Fig. 1). The aim of this analysis is to evaluate the effects inside the film and to conclude on the homogeneity of the film after irradiation with gamma, e-beam and X-ray.

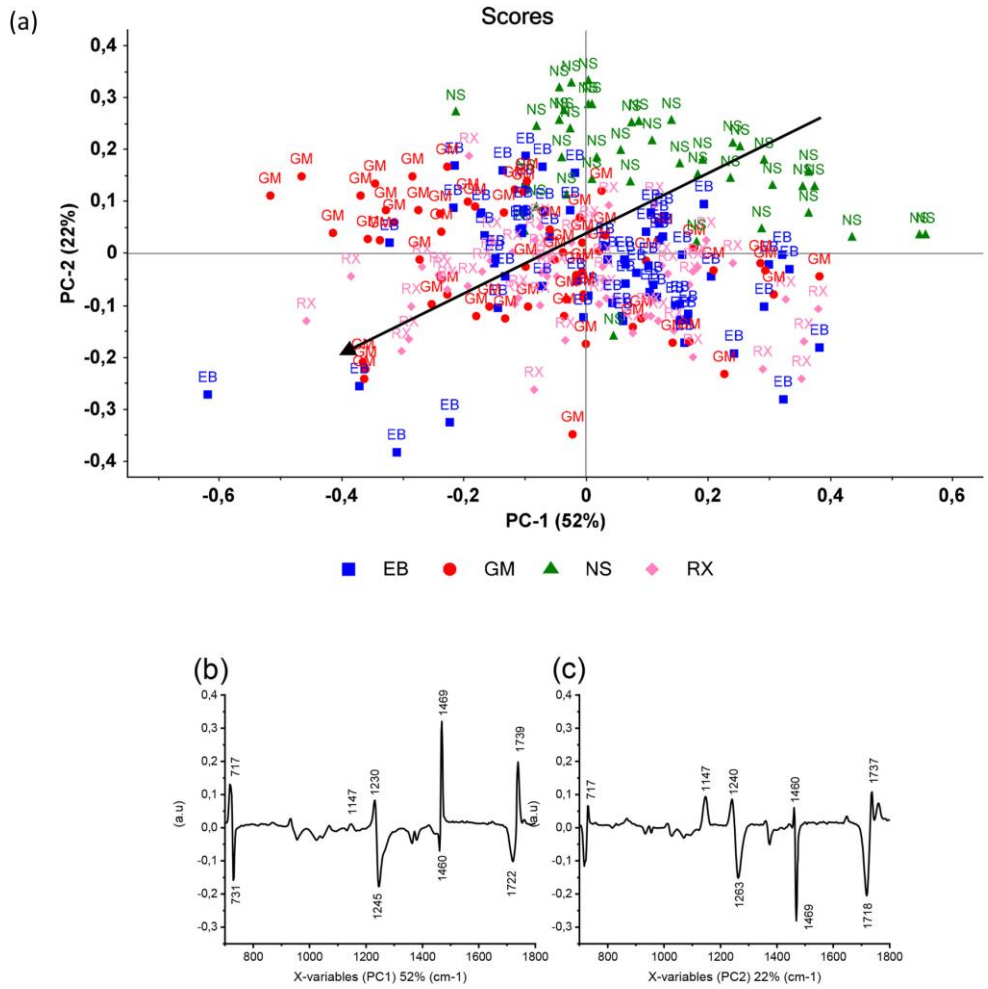


**Fig. 3.** PCA of 220 EVA spectra of non-irradiated and gamma, e-beam and X-ray irradiated samples at 30, 45 et 60 ± 10% kGy•h$^{-1}$. Spectra are baseline corrected and normalized. a) Score plot of PCA with irradiation technology (NS: non-irradiated, EB: e-beam irradiation, GM: gamma irradiation, RX: X-ray irradiation). (b) Loading plot of PC-1. (c) Loading plot of PC-2.

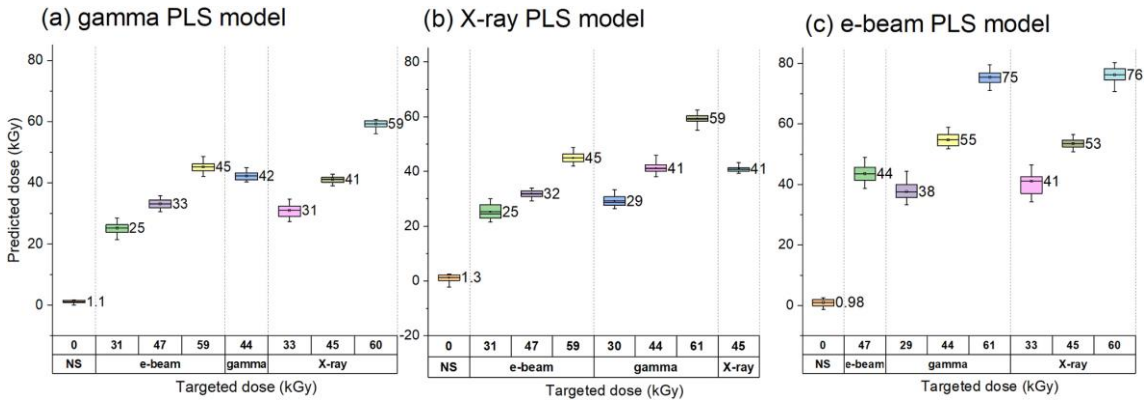


**Fig. 4.** PLS model using ATR spectra of (a) gamma irradiated samples. (b) X-ray irradiated samples. (c) e-beam irradiated samples. Labels correspond to predicted doses. Missing data were used to build models.

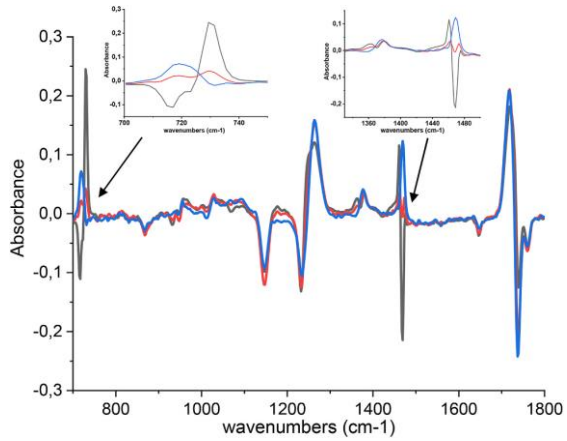


**Fig. 5.** Spectra representing model PLS (black line) with gamma irradiated samples, (red line) with X-ray irradiated samples and (blue line) with e-beam irradiated samples at 25, 50 and 100 kGy ± 10%.

### 3.2.1. PCA

The PCA displayed in Fig. 6 concerns the carbonyl and ester zones [1800–700 $cm^{-1}$] and is based on the 293 spectra measured on the cross-section, 6 months after irradiation for each dose and irradiation technology. The cross-section spectra are baseline corrected and normalized. The first principal component (PC1) represents 73% of the total variance of the modification of the spectra. The second component (PC2) represents 11% of the total variance.

Fig. 6 displays the PCA score, and the variable plot displays the μIR spectra of the main species present in the cross-section. The presence of oxidized EVA cannot be detected, as the acid peak at 1714 $cm^{-1}$ is not visible in the spectrum obtained after PCA. The intensity of the characteristic peak of the ester at 1739 and 1238 $cm^{-1}$ is high, so PC1 represents the pure EVA spectra. Similarly, it is not possible to detect the EVOH layer with this analysis method, the typical EVOH peak is the deformation of –OH peak at 1100 $cm^{-1}$. The PC1 score displays no effect of dose or irradiation technology. The samples are not grouped with their irradiation mode, or with the absorbed radiation dose of the film as no changes in the apparent cross-section of EVA layer after irradiation are observed. As the EVOH layer is not detected, only the score of the EVA spectra was analyzed. There would be no correlation between the doses or the irradiation technologies if the main species present in all spectra analyzed after irradiation are similar to those present before the irradiation. Detailed explanation of PCA could be find in reference (Gaston et al., 2016b).

### 3.2.2. SIMPLISMA

To further examine the results on the μIR spectra, SIMPLISMA treatment was applied. This method is applied to the 293 spectra recorded for non-irradiated and irradiated samples by gamma, e-beam, and X-ray. The analysis gives a result corresponding to a pure spectrum of the main species; a reconstructed spectrum is sufficient to take into account in the data set (RRSSQ = 0.02). The concentration profile of the pure component is used to define the presence of that component in each spectrum analyzed. Profiles are obtained for each irradiation technology at different doses after processing data with SIMPLISMA.

The extracted spectrum represents the EVA spectrum (Fig. S1 in SI), involve 98% of the species present in the spectra analyzed by μIR on the cross-section. The narrow thickness of the EVOH layer (5 μm) does not allow its analysis by this technique. The μIR method supports the conclusion that there is no modification of the EVA layer in the multilayer film after irradiation by gamma, X-ray, or e-beam radiation at a dose below 100 kGy.

### 3.3. UV–visible spectroscopy (UV–Vis)

Fig. 7b displays the UV–Vis spectra of multilayer EVA/EVOH/EVA film non-irradiated and irradiated at 50 and 100 kGy by gammas, e-beam and X-ray radiation.

The spectra of non-irradiated and irradiated films are different (Fig. 7), it can be due to radiation affects the antioxidants present in samples (Tao et al., 2020). For the three irradiation technologies, the UV–Vis band present on the spectrum between 250 and 300 nm (Fig. 7) is similar, but the intensity of this band differs between gamma, e-beam and X-ray.

The aim of the PLS model is to extrapolate the effect of irradiation on the EVA/EVOH/EVA film, to know the radiation absorbed dose to the polymers regardless of the irradiation technologies. We performed three PLS models, one for each irradiation technology.

For the three PLS models, half of the non-irradiated samples and all of the 30 and 60 kGy irradiated samples were used. Samples irradiated at 45 kGy and half of the non-irradiated samples are used for prediction. The model was then used to predict the dose absorbed by samples irradiated by two other irradiations at 30, 45 and 60 kGy (Table S3 in SI).

#### 3.3.1. Gamma irradiation partial least square model

The first model calibration is based on the UV–Vis spectra of samples irradiated by gamma. The modelling results ($R^2$ = 0.99, RMSEC = 3.03) show that a good correlation is obtained between the UV–Vis spectra and the absorbed gamma dose. The prediction results show that the model is applicable: the dose of non-irradiated samples is predicted with an average dose of 0 kGy, and the dose of samples irradiated by gamma at 44 kGy is predicted with an average dose of 43 kGy (Fig. 8). The model was then used to predict the dose received for samples irradiated by X-ray at 30,45, 60 and 100 kGy or e-beam at 30, 45 and 60 kGy. The results show that X-ray and e-beam doses are underestimated.

#### 3.3.2. X-ray partial least square model

The second model (Fig. 9) is based on the UV–Vis spectra of samples irradiated by X-ray, the modelling results ($R^2$ = 0.97, RMSEC = 7.1) show that a good correlation is obtained between the UV–Vis spectra and the X-ray dose absorbed. The prediction results show that the model is applicable: the dose of non-irradiated samples is predicted with an average dose of 3 kGy, and the dose of samples irradiated at 45 kGy is predicted at 45 kGy. The model was then used to predict the dose received for samples irradiated by gamma or e-beam at 30, 45 and 60 kGy. The results show that gamma doses are correctly predicted while e-beam doses are underestimated.

#### 3.3.3. e-beam partial least square model

The model (Fig. 10) is based on the UV–Vis spectra of samples irradiated by e-beam, the modelling results ($R^2$ = 0.99, RMSEC = 2.31) show that a good correlation is obtained between the UV–Vis spectra and the e-beam dose absorbed. The prediction results show that the model is applicable: The dose of non-irradiated samples predicted with an average dose of −1 kG y, and the dose of samples irradiated by e-beam at 47 kGy is predicted at 47 kGy. The model was then used to predict the dose received for samples irradiated by gamma or X-ray at 30, 45 and 60 kGy. The results show that gamma and X-ray are overestimated.

The three loadings (Fig. 11) represent the wavelength most correlated to the irradiation doses in each PLS model. The representation of the loadings differs according to the irradiation technology. As already explained in FTIR-ATR section, the gamma and the X-ray impact prediction are in good agreement certainly due to the fact dose rate are quite similar. The extend of the by-product concentration could be different. Their identification is provided in another reference (Dorey et al., 2020).

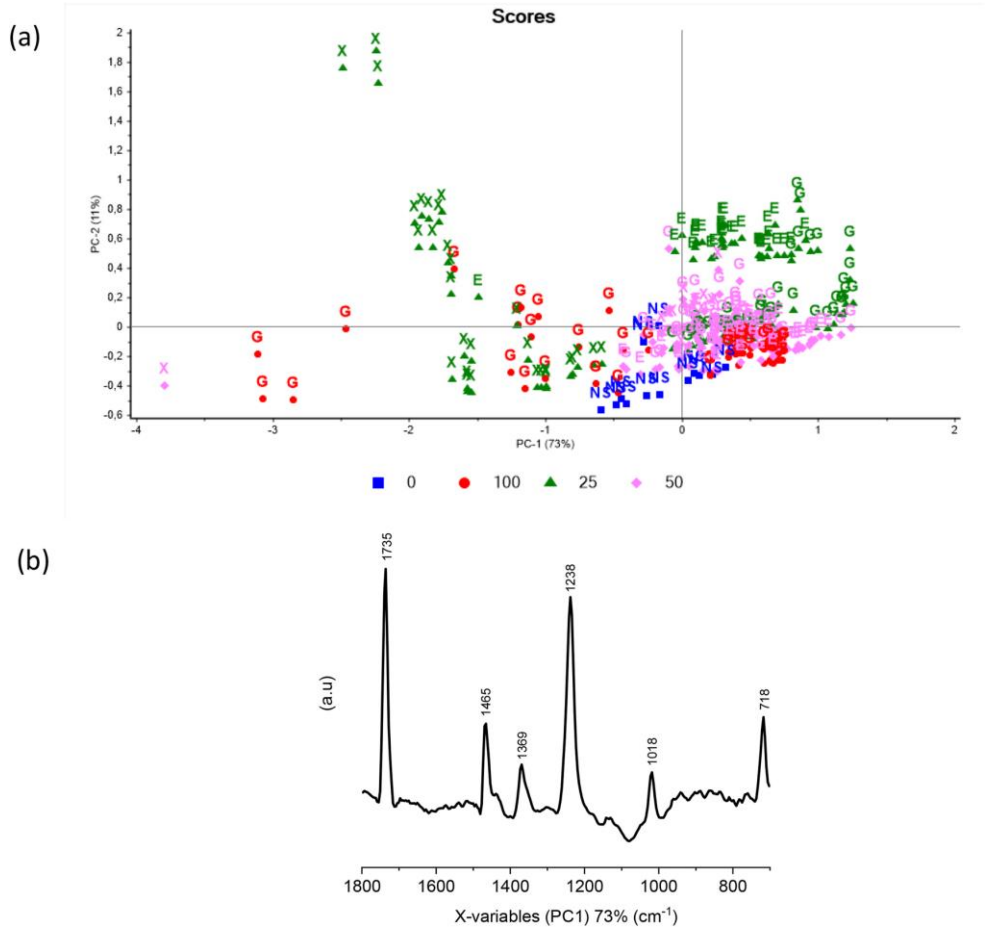


**Fig. 6.** PCA of 293 EVA spectra of non-irradiated and gamma, e-beam and X-ray irradiated samples at 25, 50 et 100 ± 10%. Spectra are baseline corrected and normalized. (a) Score plot of PCA with dose labels (b) Loading plot of PC1. G, X, E, NS stand for gamma, X-ray, e-beam, non-sterile respectively. The peak at 1737 $cm^{-1}$ corresponds to the νCO of the ester. Peaks included between 1470 and 1360 $cm^{-1}$ correspond to the deformation in the plane of the $\delta CH_2$ and $\delta CH_3$ groups. Peaks included between 1300 and 1020 $cm^{-1}$ correspond to the stretching νCO, and the peak at 719 $cm^{-1}$ corresponds to the inner rocking vibration of $CH_2$ in the amorphous part ($\delta CH_2$).

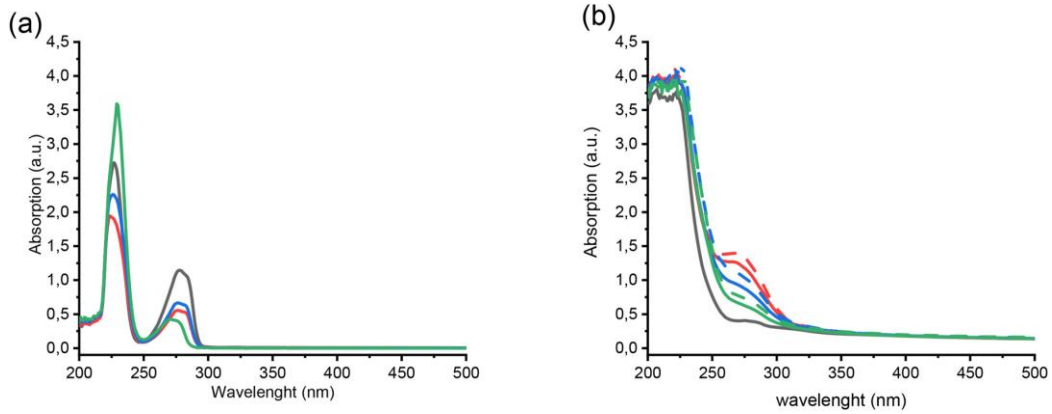


**Fig. 7.** (a) UV–Vis spectra of antioxidants dissolved in DCM: BHT (black line), Irganox® 1076 (red line), Irganox® 1010 (blue line) and Irgafos® 168 (green line). (b) Multilayer film non irradiated (black line), irradiated at 50 kGy (solid line) and 100 kGy (dotted line) by gamma (red line), X-ray (green line) and e-beam (blue line).

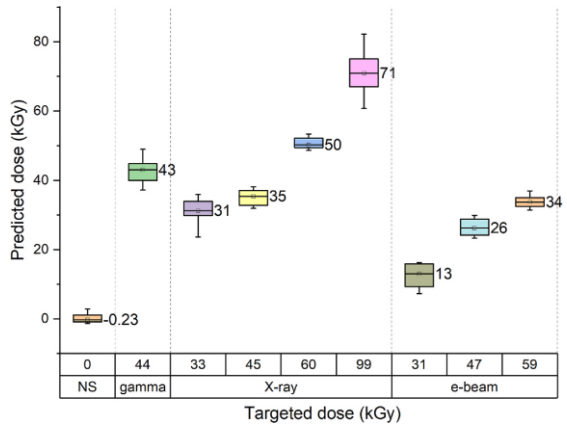


**Fig. 8.** (a) PLS model using UV spectra of gamma irradiated samples. Labels correspond to predicted doses. Missing data were used to build models: Non irradiated samples and samples irradiated at 30 and 60 kGy ± 10%.

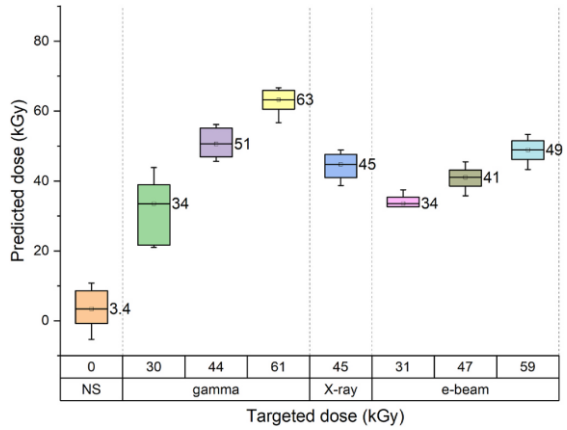


**Fig. 9.** PLS model using UV–Vis spectra of X-ray irradiated samples. Labels correspond to predicted doses. Missing data were used to build models. Non irradiated samples and samples irradiated at 30,60 and 100 kGy ± 10%.

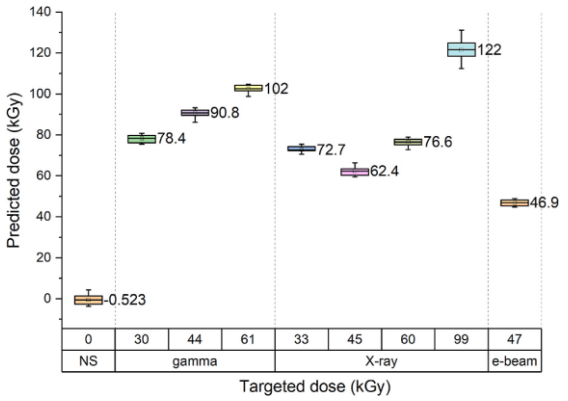


**Fig. 10.** PLS model using UV–Vis spectra of e-beam irradiated samples. Labels correspond to predicted doses. Missing data were used to build models. Non irradiated samples and samples irradiated at 30 and 60 kGy ± 10%.

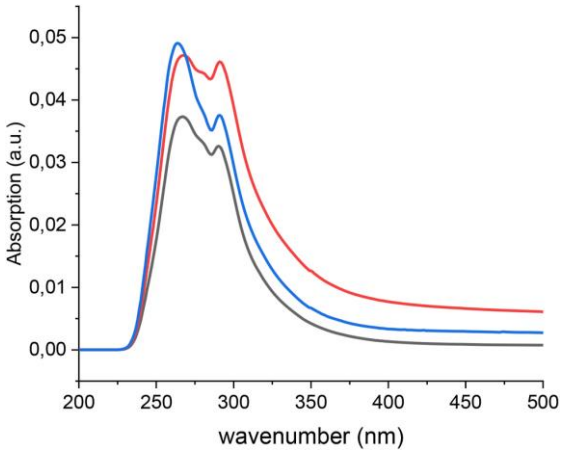


**Fig. 11.** Loading of the UV–Vis spectra of EVA/EVOH/EVA film irradiated by gamma (black line), e-beam (blue line) and X-ray (red line).

## 4. Conclusions

The multilayer film composed of EVA/EVOH/EVA underwent analysis subsequent to gamma, e-beam, and X-ray irradiation at various scales. The analysis was conducted at a $cm^2$ scale using UV–Vis analysis, at a $mm^2$ scale using infrared analysis, and at a few $\mu m^2$ scale using micro infrared method.

The utilization of micro-infrared analysis does not discern the varying effects of the three irradiation technologies on polymers.

The feasibility of estimating the absorbed dose of a multilayer film can be achieved through UV–Vis or FTIR analysis of the impact of irradiation on the film, given a predetermined irradiation dose. Nonetheless, the extrapolation of the absorbed dose modelling is not universally applicable to all irradiation technologies. The estimation of absorbed dose in e-beam irradiated films is undervalued when projected from models based on gamma or X-ray. The impact of e-beam irradiation, as assessed through UV–Vis and FTIR analysis, differs from that of gamma and X-ray irradiation on the multilayer film.

Both gamma ray and X-ray exhibit comparable effects on the multilayer film, and it is feasible to anticipate the absorbed dosage of the film by utilizing UV–Vis spectra or infrared spectra for gamma ray or X-ray of a predetermined dose. The modifications after gamma and X-ray irradiations are close to the methodology detection capability, revealing the modifications happen in low extent.

## Funding

Support for PNNL participation in this research was provided by the USDOE National Nuclear Security Administration Office of Radiological Security.

## CRediT authorship contribution statement

**Blanche Krieguer:** Data curation, Investigation, Methodology, Validation, Visualization, Writing – original draft, Writing – review & editing. **Sylvain R.A. Marque:** Conceptualization, Data curation, Funding acquisition, Investigation, Methodology, Project administration, Resources, Supervision, Validation, Visualization, Writing – review & editing. **Samuel Dorey:** Conceptualization, Data curation, Funding acquisition, Investigation, Methodology, Project administration, Resources, Supervision, Validation, Visualization, Writing – review &

editing. **Fabien Girard:** Conceptualization, Data curation, Funding acquisition, Investigation, Methodology, Project administration, Resources, Supervision, Validation, Visualization, Writing – review & editing. **Yelin Ni:** Formal analysis, Investigation, Methodology, Validation, Visualization, Writing – review & editing. **Donghui Li:** Formal analysis, Methodology, Validation, Visualization, Writing – review & editing. **Mark K. Murphy:** Conceptualization, Data curation, Funding acquisition, Investigation, Methodology, Project administration, Resources, Supervision, Validation, Visualization, Writing – review & editing. **Leonard S. Fifield:** Conceptualization, Data curation, Funding acquisition, Investigation, Methodology, Project administration, Resources, Supervision, Validation, Visualization, Writing – review & editing. **Nathalie Dupuy:** Conceptualization, Data curation, Funding acquisition, Investigation, Methodology, Project administration, Resources, Supervision, Validation, Visualization, Writing – review & editing.

## Declaration of competing interest

The authors declare the following financial interests/personal relationships which may be considered as potential competing interests: Samuel Dorey reports equipment, drugs, or supplies, statistical analysis, and writing assistance were provided by Sartorius Stedim FMT SAS.

## Data availability

The data that has been used is confidential.

## Acknowledgements

We acknowledge Sartorius Stedim FMT S.A.S for the financial support of this work. N. D, F.G and S.R.A.M are thankful to AMU and CNRS for support. We acknowledge Nina Girard-Perier for her technical assistance. The Pacific Northwest National Laboratory (PNNL) is operated by Battelle for the U.S. Department of Energy (USDOE) under Contract DE-AC05-76RL01830.

## Appendix A. Supplementary data

Supplementary data to this article can be found online at https://doi.org/10.1016/j.radphyschem.2024.111607.

## References

Ahmed, J., Wu, J., Mushtaq, S., Zhang, Y., 2020. Effects of electron beam irradiation and multi-functional monomer/co-agents on the mechanical and thermal properties of ethylene-vinyl acetate copolymer/polyamide blends. Mater. Today Commun. 23, 100840 https://doi.org/10.1016/j.mtcomm.2019.100840.

Armenante, P.M., Akiti, O., 2019. Sterilization processes in the pharmaceutical industry. In: am Ende, D.J., am Ende, M.T. (Eds.), Chemical Engineering in the Pharmaceutical Industry. John Wiley & Sons, Inc., Hoboken, NJ, USA, pp. 311–379. https://doi.org/10.1002/9781119600800.ch64.

Audran, G., Dorey, S., Dupuy, N., Gaston, F., Marque, S.R.A., 2015. Degradation of γ-irradiated polyethylene-ethylene vinyl alcohol-polyethylene multilayer films: an ESR study. Polym. Degrad. Stabil. 122, 169–179. https://doi.org/10.1016/j.polymdegradstab.2015.10.021.

Chmielewski, A.G., Sun, Y. (Eds.), 2017. Applications of Ionizing Radiation in Materials Processing, vol. 1. Institute of Nuclear Chemistry and Technology, Warszawa.

Darwis, D., Erizal, Abbas, B., Nurlidar, F., Putra, D.P., 2015. Radiation processing of polymers for medical and pharmaceutical applications. Macromol. Symp. 353, 15–23. https://doi.org/10.1002/masy.201550302.

Daszykowski, M., Kaczmarek, K., Vander Heyden, Y., Walczak, B., 2007. Robust statistics in data analysis — a review. Chemometr. Intell. Lab. Syst. 85, 203–219. https://doi.org/10.1016/j.chemolab.2006.06.016.

Di Benedetto, D., Breuil, P., 2007. Spectrophotométrie d'absorption dans l'ultraviolet et le visible. Tech. Anal. https://doi.org/10.51257/a-v2-p2795.

Dinesh, M., Chikkakuntappa, R., 2013. Microwave irradiation induced modifications on the interfaces in SAN/EVA/PVC and PVAc/BPA/PVP ternary polymer blends: positron lifetime study. Nucl. Instrum. Methods Phys. Res. Sect. B Beam Interact. Mater. Atoms 310, 67–74. https://doi.org/10.1016/j.nimb.2013.05.020.

Dorey, S., Gaston, F., Girard-Perier, N., Dupuy, N., Marque, S.R.A., Barbaroux, M., Audran, G., 2020. Identification of chemical species created during γ-irradiation of antioxidant used in polyethylene and polyethylene- *co* -vinyl acetate multilayer film. J. Appl. Polym. Sci. 137, 49336 https://doi.org/10.1002/app.49336.

Driffield, M., Bradley, E.L., Leon, I., Lister, L., Speck, D.R., Castle, L., Potter, E.L.J., 2014. Analytical screening studies on irradiated food packaging. Food Addit. Contam. 31, 556–565. https://doi.org/10.1080/19440049.2013.865087.

Dupuy, N., Marque, S.R.A., Fifield, L.S., Pharr, M., Staack, D., Pillai, S.D., Nichols, L., Murphy, M.K., Dorey, S., 2022. Supplementing gamma sterilization with X-ray and E-beam technologies. Bioproc. Technol. 20, 24–28.

Entezam, M., Aghjeh, M.K.R., Ghaffari, M., 2017. Electron beam irradiation induced compatibilization of immiscible polyethylene/ethylene vinyl acetate (PE/EVA) blends: mechanical properties and morphology stability. Radiat. Phys. Chem. 131, 22–27. https://doi.org/10.1016/j.radphyschem.2016.10.016.

Ergon, R., Esbensen, K.H., 2002. PCR/PLSR optimization based on noise covariance estimation and Kalman filtering theory. J. Chemom. 16, 401–407. https://doi.org/10.1002/cem.732.

Fifield, L.S., Pharr, M., Staack, D., Pillai, S.D., Nichols, L., McCoy, J., Faucette, T., Bisel, T.T., Huang, M., Hasan, M.K., Perkins, L., Cooley, S.K., Murphy, M.K., 2021. Direct comparison of gamma, electron beam and X-ray irradiation effects on single-use blood collection devices with plastic components. Radiat. Phys. Chem. 180, 109282 https://doi.org/10.1016/j.radphyschem.2020.109282.

Gardette, J.-L., 1998. Caractérisation des polymères par spectrométrie optique.

Gaston, F., Dupuy, N., Marque, S.R.A., Barbaroux, M., Dorey, S., 2016a. FTIR study of ageing of γ-irradiated biopharmaceutical EVA based film. Polym. Degrad. Stabil. 129, 19–25. https://doi.org/10.1016/j.polymdegradstab.2016.03.040.

Gaston, F., Dupuy, N., Marque, S.R.A., Barbaroux, M., Dorey, S., 2016b. One year monitoring by FTIR of γ-irradiated multilayer film PE/EVOH/PE. Radiat. Phys. Chem. 125, 115–121. https://doi.org/10.1016/j.radphyschem.2016.03.010.

Gaston, F., Dupuy, N., Marque, S.R.A., Dorey, S., 2018. Evaluation of multilayer film stability by Raman spectroscopy after gamma-irradiation sterilization process. Vib. Spectrosc. 96, 52–59. https://doi.org/10.1016/j.vibspec.2018.03.002.

Gemperline, P.J., 1989. Mixture analysis using factor analysis I: calibration and quantitation. J. Chemom. 3, 549–568. https://doi.org/10.1002/cem.1180030404.

Girard-Perier, N., Dorey, S., Gaston, F., Girard, F., Marque, S.R.A., Dupuy, N., 2022a. One-year ageing FTIR monitoring of PE/EVOH/PE film after gamma or electron beam irradiation. Polym. Degrad. Stabil. 195, 109790 https://doi.org/10.1016/j.polymdegradstab.2021.109790.

Girard-Perier, N., Marque, S.R.A., Dupuy, N., Claeys-Bruno, M., Gaston, F., Dorey, S., Fifield, L.S., Ni, Y., Li, D., Fuchs, W.K., Murphy, M.K., Pillai, S.D., Pharr, M., Nichols, L., 2022b. Effects of X-rays, electron beam, and gamma irradiation on chemical and physical properties of EVA multilayer films. Front. Chem. 10, 888285 https://doi.org/10.3389/fchem.2022.888285.

Hamilton, J.C., Gemperline, P.J., 1990. Mixture analysis using factor analysis. II: self-modeling curve resolution. J. Chemom. 4, 1–13. https://doi.org/10.1002/cem.1180040103.

Ji, Y.-Y., Chang, H.-S., Lim, T., Lee, W., 2019. Application of a SrI2(Eu) scintillation detector to in situ gamma-ray spectrometry in the environment. Radiat. Meas. 122, 67–72. https://doi.org/10.1016/j.radmeas.2019.01.014.

Komolprasert, V., 2016. Packaging food for radiation processing. Radiat. Phys. Chem. 129, 35–38. https://doi.org/10.1016/j.radphyschem.2016.07.023.

Kroc, T.K., 2023. Monte Carlo simulations demonstrating physics of equivalency of gamma, electron-beam, and X-ray for radiation sterilization. Radiat. Phys. Chem. 204, 110702 https://doi.org/10.1016/j.radphyschem.2022.110702.

Kumar, N., Bansal, A., Sarma, G.S., Rawal, R.K., 2014. Chemometrics tools used in analytical chemistry: an overview. Talanta 123, 186–199. https://doi.org/10.1016/j.talanta.2014.02.003.

Liang, Y.-Z., Kvalheim, O.M., 1996. Robust methods for multivariate analysis — a tutorial review. Chemometr. Intell. Lab. Syst. 32, 1–10. https://doi.org/10.1016/0169-7439(95)00006-2.

Martens, H., 1979. Factor analysis of chemical mixtures. Anal. Chim. Acta 112, 423–442. https://doi.org/10.1016/S0003-2670(01)85040-6.

Martens, H., Naes, T., 1989. Multivariate Calibration. Wiley.

Matsui, T., Shimoda, M., Osajima, Y., 1992. Mechanical changes of electron beam irradiated ethylene–vinyl acetate copolymer (EVA) film (I). Polym. Int. 29, 85–90. https://doi.org/10.1002/pi.4990290204.

Moondra, S., Raval, N., Kuche, K., Maheshwari, R., Tekade, M., Tekade, R.K., 2018. Sterilization of pharmaceuticals. In: Dosage Form Design Parameters. Elsevier, pp. 467–519. https://doi.org/10.1016/B978-0-12-814421-3.00014-2.

NicDaéid, N., 2018. Systematic drug identification. In: Reference Module in Chemistry, Molecular Sciences and Chemical Engineering. Elsevier, B9780124095472144579. https://doi.org/10.1016/B978-0-12-409547-2.14457-9.

Sjöström, M., Wold, S., Lindberg, W., Persson, J.-Å., Martens, H., 1983. A multivariate calibration problem in analytical chemistry solved by partial least-squares models in latent variables. Anal. Chim. Acta 150, 61–70. https://doi.org/10.1016/S0003-2670(00)85460-4.

Tao, B., Wang, G., Yin, Z., Pu, X., Jiang, Y., Zhang, L., Cheng, J., Li, Y., Zhang, J., 2020. Determination of the contents of antioxidants and their degradation products in sodium chloride injection for blood transfusion. J. Anal. Methods Chem. 2020, 1–12. https://doi.org/10.1155/2020/8869576.

Tarantili, P.A., Kiose, V., 2008. Effect of accelerated aging on the structure and properties of monolayer and multilayer packaging films. J. Appl. Polym. Sci. 109, 674–682. https://doi.org/10.1002/app.28091.

Valente, T.A.M., Silva, D.M., Gomes, P.S., Fernandes, M.H., Santos, J.D., Sencadas, V., 2016. Effect of sterilization methods on electrospun poly(lactic acid) (PLA) fiber alignment for biomedical applications. ACS Appl. Mater. Interfaces 8, 3241–3249. https://doi.org/10.1021/acsami.5b10869.

Voronko, Y., Chernev, B.S., Eder, G.C., 2014. Spectroscopic investigations on thin adhesive layers in multi-material laminates. Appl. Spectrosc. 68, 584–592. https://doi.org/10.1366/13-07291.

Windig, W., 1997. Spectral data files for self-modeling curve resolution with examples using the Simplisma approach. Chemometr. Intell. Lab. Syst. 36, 3–16. https://doi.org/10.1016/S0169-7439(96)00061-5.

Windig, W., 1994. The use of second-derivative spectra for pure-variable based self-modeling mixture analysis techniques. Chemometr. Intell. Lab. Syst. 23, 71–86. https://doi.org/10.1016/0169-7439(93)E0058-C.

Windig, W., Stephenson, D.A., 1992. Self-modeling mixture analysis of second-derivative near-infrared spectral data using the SIMPLISMA approach. Anal. Chem. 64, 2735–2742. https://doi.org/10.1021/ac00046a015.

Windig, Willem, Guilment, Jean, 1991. Interactive self-modeling mixture analysis. Anal. Chem. 63, 1425–1432. https://doi.org/10.1021/ac00014a016.

Wool, R.P., Bretzlaff, R.S., Li, B.Y., Wang, C.H., Boyd, R.H., 1986. Infrared and Raman spectroscopy of stressed polyethylene. J. Polym. Sci., Part B: Polym. Phys. 24, 1039–1066. https://doi.org/10.1002/polb.1986.090240508.

Wrobel, T.P., Vichi, A., Baranska, M., Kazarian, S.G., 2015. Micro-attenuated total reflection fourier transform infrared (micro ATR FT-IR) spectroscopic imaging with variable angles of incidence. Appl. Spectrosc. 69, 1170–1174. https://doi.org/10.1366/15-07963.

# Supporting Information: Sterilization of polymer-based healthcare devices, and the comparison of effects from gamma-ray, E-beam and X-ray radiation

## ATR-FTR

Table S1: IR assignments of bands for EVA spectra.

| Wavenumber ($cm^{-1}$) | Functional group | Type of vibration |
|---|---|---|
| 2916 | $\nu CH_2$ | Antisymmetric stretching |
| 2848 | $\nu CH_2$ | Symmetric stretching |
| 1737 | νCO ester | Stretching |
| 1714 | νCO carboxylic acid | Stretching |
| 1467-1438 | $\delta CH_2$ | Deformation in the plane |
| 1370 | $\delta CH_3$ | Deformation in the plane |
| 1300-1020 | νCO | Stretching |
| 964 | $R_1CHCHR_2$ | *Trans* vinylene group |
| 730 (shoulder) | $\delta CH_2$ | Inner rocking vibration of $CH_2$ in the crystalline part |
| 719 | $\delta CH_2$ | Inner rocking vibration of $CH_2$ in the amorphous part |

Table S2 : Parameters of PLS models with ATR data

| Model PLS | Sterilization | Calibration Dose (kGy) | Validation Dose (kGy) | Prediction Dose (kGy) |
|---|---|---|---|---|
| 1 : Gamma | Non-irradiated | 0 | 0 | / |
| | Gamma | 30,61 | 44 | / |
| | X-ray | / | / | 33,45,60 |
| | E-beam | / | / | 31,47,59 |
| 2: X-ray | Non-irradiated | 0 | 0 | / |
| | Gamma | / | / | 30,44,61 |
| | X-ray | 33,60 | 45 | / |
| | E-beam | / | / | 31,47,59 |
| 3: E-beam | Non-irradiated | 0 | 0 | / |
| | Gamma | / | / | 30,44,61 |
| | X-ray | / | / | 33,45,60 |
| | E-beam | 31,59 | 47 | / |

### Micro-infrared : SIMPLISMA

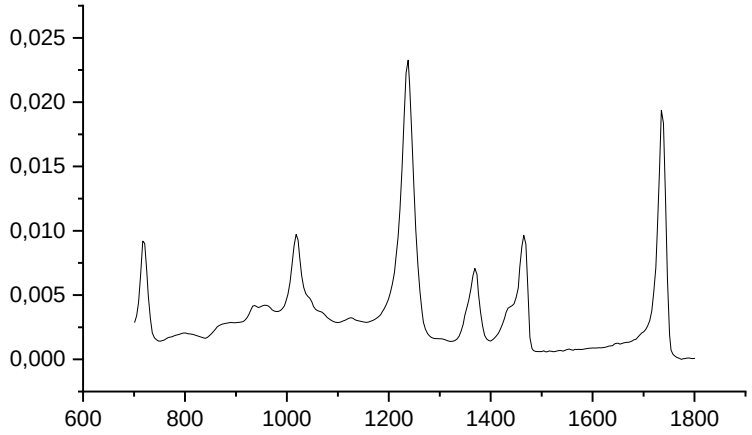


Figure S1: Reconstructed spectrum with SIMPLISMA analysis

## UV-Vis

Table S3: parameters of PLS models with UV-Vis data

| Model PLS | Sterilization | Calibration Dose (kGy) | Validation Dose (kGy) | Prediction Dose (kGy) |
|---|---|---|---|---|
| 1: Gamma | Non-irradiated | 0 | 0 | / |
| | Gamma | 30,61 | 44 | / |
| | X-ray | / | / | 33,45,60,99 |
| | E-beam | / | / | 31,47,59 |
| 2: X-ray | Non-irradiated | 0 | 0 | / |
| | Gamma | / | / | 30,44,61 |
| | X-ray | 33,60,99 | 45 | / |
| | E-beam | / | / | 31,47,59 |
| 3: E-beam | Non-irradiated | 0 | 0 | / |
| | Gamma | / | / | 30,44,61 |
| | X-ray | / | / | 33,45,60,99 |
| | E-beam | 31,59 | 47 | / |

## 3.2. Etude des effets du débit de dose et de la formation d'espèces réactives dans le film EVA/EVOH/EVA

Des études précédentes [1,5,6] ont démontré que les espèces transitoires produites par les rayons gamma produisent une large gamme de molécules, telles que les acides carboxyliques et le peroxyde d'hydrogène. La combinaison de ces espèces peut engendrer des peracides, modifiant ainsi par oxydation les solutions biologiques contenues dans les poches. Pour modéliser l'impact potentiel de l'irradiation sur l'interaction entre le film et les substances médicamenteuse contenue dans la solution, une solution de méthionine a été choisie.

Dans les systèmes polymères, le débit de dose des radiations ionisantes peut être un des paramètres essentiels influençant les propriétés et les performances des matériaux. Les polymères exposés aux radiations subissent divers changements chimiques et physiques, tels que la réticulation, la scission de chaînes et l'oxydation. Ces transformations peuvent modifier les propriétés mécaniques, thermiques et chimiques du polymère, influençant ainsi son adéquation pour des applications spécifiques. Cet article, soumis à la revue *Physical Chemistry Chemical Physics* en 2024, adopte une approche multidisciplinaire, intégrant la biologie chimique et l'étude des polymères, pour approfondir la compréhension du rôle du débit de dose dans l'exposition aux radiations ionisantes. Le détail des doses et des débits de dose d'irradiation sont détaillés dans le Tableau 5.

Tableau 5 : Dose et débit de dose d'irradiation du film EVA/EVOH/EVA et du film PE/EVOH/PE par rayons gamma, rayons X et faisceaux d'électrons.

| Techniques analytiques | Gamma | | Rayons X | | Faisceau d'électrons | |
|---|---|---|---|---|---|---|
| | Dose (kGy) | Débit de dose (kGy/h) | Dose (kGy) | Débit de dose (kGy/h) | Dose (kGy) | Débit de dose (kGy/h) |
| **RPE** | 50, 100 | 2 | 50, 100 | 12 | 50, 100 | 18000 |
| **HPLC** | 30, 50 | 2 | 30, 50, 100 | 13 | 30, 50 | 18000 |
| | 30, 50 | 8 | 70 | 80 | 30, 50 | 18000 |

L'étude compare l'impact de trois technologies d'irradiation sur la modification des polymères à travers des radicaux générés après irradiations. L'objectif de cet article est de mesurer l'impact du débit de dose, qui ne peut être dissocié de chaque technologie

d'irradiation, sur la génération d'espèces réactives tels que les peroxydes et les peracides. Pour cela, la nature et la quantité des espèces radicalaires générées (analysées par RPE) et l'oxydation de la solution de méthionine contenue dans la poche (analysée par HP LC) ont été étudiées.

L'analyse RPE a révélé que les trois technologies d'irradiation produisent des radicaux hydroxyalkyles dans le film EVA/EVOH/EVA. Les mécanismes de formation de ces radicaux sont décrits dans la figure 4 de l'article. Ces radicaux instables ne peuvent être quantifiés au maximum qu'un jour après l'irradiation. La cinétique et les espèces radicalaires engendrées sont équivalentes pour les trois technologies d'irradiation.

Dans l'article, un modèle de régression a été utilisé pour analyser les données obtenues après irradiation gamma, rayons X et faisceau d'électrons. Ce modèle, représenté dans la figure 6, a montré que le débit de dose a un effet significatif sur la concentration de méthionine oxydée dans la solution en contact avec le film EVA. Par la suite, des modèles distincts, représentés dans la figure 7, ont été réalisés pour les technologies d'irradiation gamma et rayons X. Les résultats ont révélé que, pour l'irradiation gamma, la variation du débit de dose influence la quantité de méthionine oxydée dans la solution de contact. Des résultats similaires ont été observés pour l'irradiation par rayons X, confirmant l'impact du débit de dose pour chaque technologie.

Deux processus d'irradiation gamma utilisant le même irradiateur chez Ionisos (France) avec un débit de dose constant (2 kGy/h) ont également été comparés. Le premier processus consiste à irradier l'échantillon en plusieurs passages devant la source sans temps d'arrêt entre les passages jusqu'à obtention de la dose souhaitée (single-run), tandis que le second accumule également la dose en plusieurs passages dans le bunker d'irradiation, avec des temps de repos inconnus entre les passages (multiple-runs).

Le modèle de régression comparant l'impact des deux processus d'irradiation gamma représenté dans la figure 8 révèle que la concentration de méthionine oxydée contenue dans la solution en contact avec la poche est équivalente, quel que soit le processus d'irradiation utilisé.

ARTICLE

# Investigating dose rate effects and reactive species formation in irradiated multilayer films – part 1 EVA/EVOH/EVA

Received 00th January 20xx,
Accepted 00th January 20xx

DOI: 10.1039/x0xx00000x

Blanche Krieguer,*[a,b,c] Samuel Dorey,*[a] Nathalie Dupuy,*[c] Fabien Girard,[c] Florent Kuntz[d], Nicolas Ludwig,[d] Sylvain R.A. Marque ,*[b]

This study investigates the effects of gamma rays, X-ray, and electron beams on ethylene vinyl acetate (EVA) multilayer films, commonly used in biotechnological applications. Electron Spin Resonnance (ESR) analysis showed that irradiation generates unstable hydroxyalkyl radicals, quantifiable one day post-exposure, with concentrations decreasing within nine days, and similar kinetics observed across all three irradiation technologies. The research focuses on dose rate impacts, which significantly influence polymer properties. Reactive species like hydrogen peroxide and hydroxyl radicals, generated during irradiation, can affect protein function through methionine oxidation. Advanced analytical techniques reveal that the dose rate significantly impacted the levels of reactive species, impacting the film's structural integrity and chemical stability comparably. Gamma irradiation generates more oxidative species. The study concludes that dose rate is crucial in methionine sulfoxide generation, with longer exposure leading to increased concentrations, particularly in gamma irradiation. These findings underscore the importance of considering dose rate and irradiation technology to optimize the stability and performance of multilayer films.

## Introduction

Single-use plastic bags are extensively used in the biotechnological and biopharmaceutical industries for storing, shipping, and preparing intermediates, biopharmaceutical preparations, solutions, and final products [1,2]. These bags are typically constructed from multilayer films, such as ethylene vinyl acetate/ethylene vinyl alcohol/ethylene vinyl acetate (EVA/EVOH/EVA), selected for their barrier protection and flexibility to ensure the integrity of the contents. To eliminate microorganisms, these single-use plastic bags require sterilization, usually within a dose range of 25–45 kGy [3,4]. Currently, gamma radiation is the most prevalent sterilization method for pharmaceutical devices. However, the growing production of biopharmaceutical products and concerns about the future capacity of gamma radiation sterilization have prompted the exploration of alternative methods, such as electron beam (e-beam) and X-ray irradiation [5–12].

Electron-beam irradiation is a continuous process that employs an electron accelerator to convert electricity into a radiation beam[13]. These accelerators can be used for direct electron beam irradiation or to produce X-ray fields *via* the Bremsstrahlung effect, typically involving a tantalum converter [14].

[a] Sartorius Stedim FMT S.A.S, Z.I. Les paluds, Avenue de Jouques CS91051, 13781, Aubagne Cedex, France
[b] Aix Marseille Univ, CNRS, ICR, Case 551, 13397 Marseille, France
[c] Aix Marseille Univ, Avignon Univ, CNRS, IRD, IMBE, Marseille, France
[d] Aerial, 250 Rue Laurent Fries, 67400 Illkirch, France

Both X-ray and gamma rays are photons; however, gamma rays originate from radioactive sources and are emitted during disintegration. Due to their similar nature, the energy deposition patterns (dose profiles) of X-ray and gamma rays are quite comparable, facilitating an easy transition from gamma-ray to X-ray technologies. X-ray may even achieve superior dose uniformity due to specific energy spectrum and easily adjustable radiation field properties [11]. In similarly irradiated materials, e-beams exhibit significantly less penetration compared to photons because their interaction with matter is much stronger. The main difference of the three irradiation technologies is the dose rate.

The role of dose rate in ionizing radiation exposure is complex and multifaceted. In biological systems, the dose rate of ionizing radiation influences a variety of outcomes, from DNA damages and repair mechanisms to cellular responses and whole organism effects [15]. Low-Dose-Rate (LDR) exposures tend to induce different biological responses compared to High-Dose-Rate (HDR) exposures. For instance, LDR radiation can activate adaptive responses that enhance cellular repair mechanisms and reduce mutation rates, while HDR radiation often leads to more immediate and severe damages [15]. Similarly, in polymer systems, the dose rate of ionizing radiation is one of the parameters playing a crucial role in determining the material's properties and performances[16]. Polymers exposed to radiation undergo various chemical and physical changes, such as cross-linking, chain scission, and oxidation. These changes could alter the mechanical, thermal, and chemical properties of the polymer, affecting its suitability for specific applications.

To address these challenges, a multidisciplinary approach is needed, integrating chemical biology, and polymer

investigation. This comprehensive strategy will help to bridge the gap between experimental findings on sterilized polymer systems and their applications, providing among others a more accurate understanding of the role of dose rate in ionizing radiation exposure. Recently, the effects of gamma irradiation on the physical/mechanical/chemical properties of a multilayer film composed of EVA/EVOH/EVA were thoroughly studied using various different techniques[17–27]. The impacts of the three irradiation technologies (X-ray, e-beam, and gamma irradiations) have also been investigated by our team [28,29].

Besides modifications on polymers, other studies highlight that irradiation source and dose rate can influence the formation of transient species and final products [30]. In previous investigation, we show that transient species generated by gamma rays afford a broad range of molecular species such as carboxylic acids and $H_2O_2$. Combination of these species may highly afford oxidant peracids species spoiling biological solutions. Hence, to model such event, we used the easily and specifically oxidizing methionine proxy[31].

The oxidation of methionine residues in proteins can have varying effects on protein function. In some cases, it maintains structural integrity and function (cysteine), while in others, it decreases functional activity [32]. Methionine oxidation can alter the structural conformation of proteins, potentially affecting their stability, binding affinity, and overall biological activity. This can compromise the efficacy of therapeutic proteins and antibodies [33].

In a previous article [25], it was explained how methionine is oxidized into methionine sulfoxide in gamma irradiated samples and it was shown that if no radical species were detected in the samples, the oxidation was likely due to the presence of hydrogen peroxide, peracids, *or in situ* generated peracids. The effects of X-ray, electron beam, and gamma irradiation on EVA multilayer films at 50 kGy [28], revealed significant differences in the generation of reactive species among the irradiation technologies. Both gamma and X-ray irradiations produced similar levels of reactive species, while electron beam irradiation resulted in a reduced quantity.

This study aims to compare the effects of three irradiation technologies on polymer modification, providing insights into the attributes of multilayer structures for biopharmaceutical applications and their interactions with biopharmaceutical solutions. Our investigations are focused on how dose rate, associated with each irradiation technology, on the generation of reactive species such as peroxides and peracids, due to radical post reactivity impact the quality of the materials. It was probed by investigating the nature and amount of generated radical species (Electron Spin Resonance investigation), and by analyzing the oxidation of methionine (High-Performance Liquid Chromatography investigation).

## Materials and methods

### Samples

EVA single-use plastic bags investigated are made from a multilayer film, namely the S71 film, composed of one layer of EVOH sandwiched between two layers of EVA, with a total thickness of approximately 360 µm (Figure 1). Sample bags are provided by Sartorius Stedim FMT S.AS, Aubagne, France.

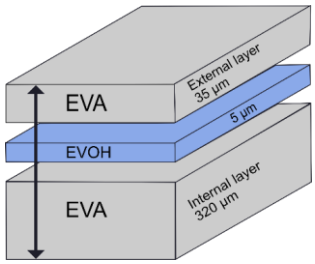


Figure 1: Representation of EVA/EVOH/EVA multilayer film (S71 film)

### Packaging

EVA bags were individually wrapped in multilayer packaging (polyethylene/polyamide/polyethylene). Samples were stored in boxes in the dark following irradiation, in an air-conditioned room at 20 ± 2°C.

### Samples irradiation

#### Gamma rays

EVA bags were irradiated with gamma rays sourced from $^{60}$Co at Ionisos in Dagneux, France, with an average dose rate of 2 kGy/h. There were two irradiation processes: the first spanned over several days, accumulating the dose over multiple runs within the irradiation bunker, while the second was completed in a single run.

EVA bags were also irradiated with gamma rays sourced from $^{60}$Co at Steris in the USA, with an average dose rate of 8 kGy/h.

#### X-ray

EVA bags were irradiated with a 7 MeV Rhodotron (Steris, Däniken, Switzerland) at an average dose rate of 80 kGy/h with a maximum power source of 560 kW.

EVA bags were also irradiated with a 7 MeV Rhodotron at Aerial in Strasbourg, France, with an average dose rate of 13 kGy/h.

#### e-beam

EVA bags were irradiated with a 10 MeV Rhodotron (Ionisos, Chaumesnil, France) at a dose rate of 18,000 kGy/h with a power source of 28 kW.

EVA bags were also irradiated with an e-beam at Aerial-CRT using the same Feerix® facility as the X-ray treatment. A 10 MeV vertical electron beam was utilized, with an average dose rate of 18 MGy/h (5 kGy/s). The irradiation was performed in increments of 50 kGy to prevent critical temperature increases in the samples.

### Dosimetry

The targeted delivered doses were approximately 30, 50, 70 and 100 kGy depending on the irradiation technologies, with a target dose uniformity of ± 10%. There were two phases of irradiation. Table 1 summarizes the dosimetry for the RPE study and


This journal is © The Royal Society of Chemistry 20xx

Table 2 for the HPLC study. To accurately measure the absorbed dose, alanine pellets combined with ESR spectroscopy (Magnettech MS5000 ESR, Bruker) were used, along with AerEDE® dosimetry software (Aerial, France). Dosimetry readings were taken in a manner traceable to an international standard.

Table 1: Effective doses on samples irradiated by gamma, X-ray, and e-beam for ESR analysis

| Target doses (kGy; ± 10%) | | 50 | 100 |
|---|---|---|---|
| Gamma | Ionisos, France (2 kGy/h) | 51 | 90 |
| X-ray | Aerial, France (13 kGy/h) | 50 | 99 |
| e-beam | Aerial, France (18,000 kGy/h) | 55 | 109 |

Table 2: Effective doses on samples irradiated by gamma, X-ray, and e-beam for HPLC analysis

| Target doses (kGy; ± 10%) | | 30 | 50 | 70 | 100 |
|---|---|---|---|---|---|
| Gamma | Ionisos, France (1.9 kGy/h) | 29 | 59 | / | / |
| | Ionisos, France (2.4 kGy/h) | 32 | 52 | / | / |
| | Steris, USA (8 kGy/h) | 28 | 54 | / | / |
| X-ray | Aerial, France (13 kGy/h) | 26 | 51 | / | 100 |
| | Steris, Suisse (80 kGy/h) | / | / | 68 | / |
| e-beam | Ionisos, France (18,000 kGy/h) | 25 | 52 | / | / |
| | Aerial, France (18,000 kGy/h) | 25 | 52 | / | / |

**Electron Spin Resonance**

ESR measurements were performed using a Magnettech MS5000X ESR spectrometer, manufactured by Bruker in Switzerland, and operated with ESR studio software for control. More details are given in a previous article [13].

**High Performance Liquid Chromatography**

Three and six months after irradiation, bags were filled with a 50 µM solution of methionine in buffer (10mM $NaH_2PO_4$, 10mM $Na_2B_4O_7 \bullet 10H_2O$, 5 mM $NaN_3$, pH=8.2). To determine the concentrations of methionine and methionine sulfoxide, an Agilent 1260 HPLC system (Waghaeusel-Wiesental, Germany) equipped with a quaternary pump (G1311C), an autosampler (G1329B), and a fluorescence detector (G1321B) was used. The automated online derivatization (in the autosampler) using an injection program is detailed in Figure 2. The derivatization reagent used was the ortho-phthaldehyde (OPA).

The gradient program was as follows: 0–13.4 min, 2% phase B; 13.4 min, 57% phase B; 13.5–15.8 min, 100% phase B; 18 min, 2% phase B. Separation was carried out on an Agilent Poroshell HPH-C18 column (4.6 mm x 100 mm, 2.7 µm particles—Waghaeusel-Wiesental, Germany) used with a pre-column, UHPLC guard Poroshell HPH-C18, 4.6 mm. The column was maintained at 40 °C ± 0.8 °C in a thermostatted column compartment (G1316A) during the analyses. The fluorescence detector was set to an excitation wavelength of 340 nm and an emission wavelength of 450 nm. The total runtime of the method was 20 min. Chromatographic data were acquired and evaluated with the HPLC 1260 OpenLAB software (Waghaeusel-Wiesental, Germany). Internal calibration was done by spiking 20 µL of L-Norvaline in each sample and standard [25].

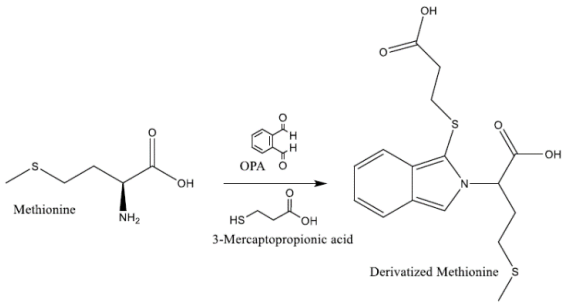


Figure 2: Automatic derivatization reaction for detecting methionine with a fluorescence detector

**Equivalency analysis**

Regression models were performed using the Minitab software to assess the effect of doses, the effect of ageing post irradiation, the effect of methionine contact days and the effect of dose rate on the concentration of methionine sulfoxide generated in solution in contact to the multilayer film. This model allows for the evaluation of the significant impact of each independent variable, with confidence interval at 95% (α=0.05). The Pareto chart shows the absolute values of the standardized effects from the largest to the smallest effect. The chart also plots a reference dotted line indicating if the effects are statistically significant. The reference line for statistical significance depends on the significance level (denoted by α), the number of samples, and the degree of freedom[34].

## Results and discussion

**Electron Spin Resonance**

Figure 3 presents the ESR detection of radical species in the EVA/EVOH/EVA multilayer film after one and nine days of irradiation. Due to transport time, the sample irradiated by

gamma rays cannot be analyzed by ESR one day post-irradiation.

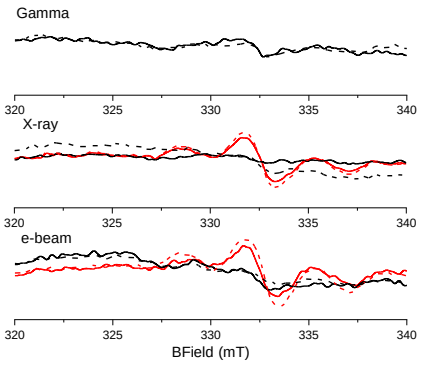


Figure 3: ESR signal of EVA/EVOH/EVA multilayer film one day (red line) and nine days (black line) after gamma, X-ray and e-beam irradiation at 50 kGy (solid line) and 100 kGy (dashed line).

The ESR signals and the monitoring of radical species concentration in the sample post-irradiation reveal that the generated radical species are unstable and can only be quantified one day after irradiation. The amount of radicals presenting nine days post-irradiation decreased below the Limit Of Quantification (LOQ) (Figure S1 in SI).

The radical species generated in the EVA/EVOH/EVA multilayer film are identified as hydroxyalkyl radicals in EVOH (Figure 4), consistent with the literature [28,35] and the different radical pathways are depicted in a previous study [22].

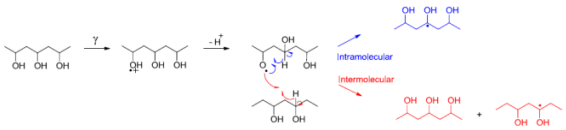


Figure 4: Different radical pathways to generate hydroxyalkyl radical[22].

**Oxidation assay by high Performance Liquid Chromatography**

**Comparison of irradiation technology**

In the present study, multilayer films were irradiated at different radiation processing facilities ~~locations~~ with different dose rates for each irradiation technology, and the quantity of methionine sulfoxide formed was measured three months and six months after irradiation, the methionine sulfoxide concentrations are represented in Figure 5.

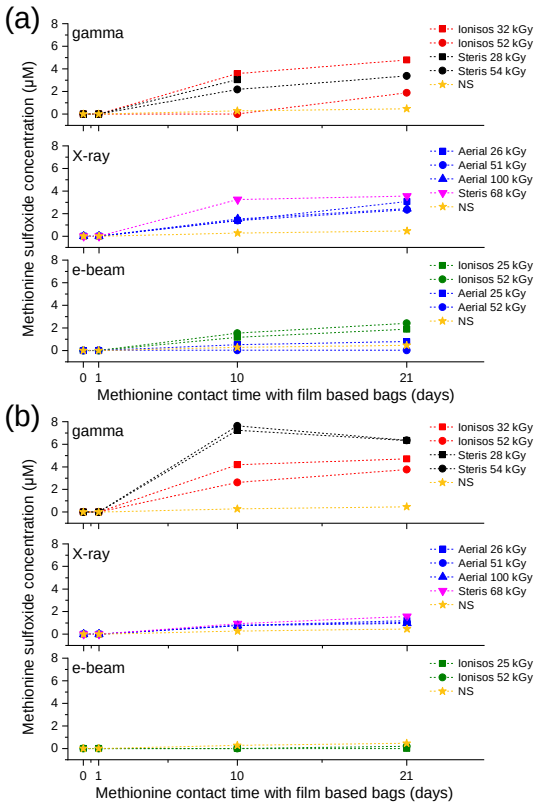


Figure 5: (a) Three months after irradiation. (b) Six months after irradiation. Methionine sulfoxide concentration (µM) in stored solution for 0, 1, 10 and 21 days after irradiation and analyzed by HPLC. Irradiation doses were 30 kGy (square), 50 kGy (circle), 70 kGy (down triangle) and 100 kGy (up triangle). Non irradiated sample (NS) are represented in yellow. Irradiations at Ionisos, Dagneux, France were represented in Red (2kGy/h), at Steris, USA, were represented in black (8 kGy/h), at Aerial, France were represented in blue (13 kGy/h for X-ray and 18000 kGy/h for e-beam), at Steris, Daniken, Switzerland were represented in pink (80 kGy/h) and at Ionisos, Chausmenil, France in green (18000 kGy/h).

Regression models were developed to assess whether the dose, ageing post irradiation, methionine contact time and dose rate can have a significant effect on the methionine sulfoxide concentration generated in the multilayer film (
Figure 6).

The results from the regression model, depicted in
Figure 6, indicate that both the contact time with the methionine solution and the dose rate significantly influence methionine oxidation. The equation model is represented in (1).


This journal is © The Royal Society of Chemistry 20xx

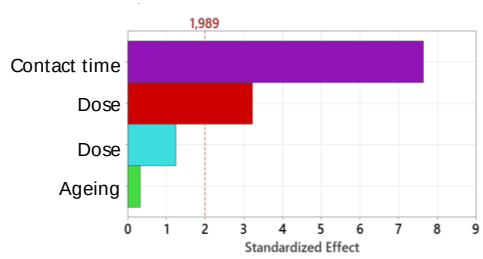


Figure 6: Pareto analysis of significant effects on methionine sulfoxide concentration: Dose (kGy) (blue), Ageing post irradiation (green), methionine contact day (days) (purple) and dose rate (kGy/h) (red).

$$\text{Methionine sulfoxide concentration} = 0.676 - 0.00877\ \text{Dose} + 0.0332\ \text{Ageing post irradiation} + 0.1329\ \text{Methionine contact time} - 0.000062\ \text{Dose rate} \quad (1)$$

The positive coefficient of the contact time indicates that the methionine sulfoxide concentration increased over time when the methionine solution is in contact with the film. This result is in accordance with the Figure 5.

In this model, the dose rate is influenced by the irradiation technology, as each technology has a specific range of dose rates. Electron beam irradiation uses an accelerator to convert electricity into a radiation beam. The dose rates differ significantly among technologies: gamma rays range from 2 to 8 kGy/h, X-rays from 13 to 80 kGy/h, and electron beams can reach up to 18,000 kGy/h. This higher dose rate of electron beams is directly linked to the irradiation technology, affecting the production of methionine sulfoxide over time when the methionine solution is in contact with the multilayer films. Therefore, the dose rate can be attributed to the irradiation technology and multilayer films irradiated by gamma radiation generated more methionine sulfoxide.

**Variation of dose rate**

A multiparametric regression model was developed for each irradiation technology to assess whether variations in dose rate within the same technology affect the concentration of methionine sulfoxide in methionine solution in contact with the film. For e-beam technology, the dose rate remains consistent between the two irradiation sites, thereby preventing any comparison of the dose rate for this technology. The gamma equation model is represented in (2) and the X-ray equation model is represented in (3).

$$\text{Methionine sulfoxide concentration} = -1.43 - 0.0356\ \text{Dose} + 0.471\ \text{Ageing post irradiation} + 0.2359\ \text{Methionine contact time} + 0.1991\ \text{Dose rate} \quad (2)$$

$$\text{Methionine sulfoxide concentration} = + 0.925 - 0.00102\ \text{Dose} - 0.2278\ \text{Ageing post irradiation} + 0.1016\ \text{Methionine contact time} - 0.00652\ \text{Dose rate} \quad (3)$$

The regression model results indicate that for gamma irradiation (Figure 7a), the dose rate significantly impacts methionine oxidation with a p-value equal to 0.04. In contrast, for X-ray irradiation, the dose rate does not have a significant effect on methionine oxidation with a p-value equal to 0.059 (Figure 7b). Given the limit of 0.05, the results are close for both technologies, and this difference may be attributed to experimental error.

Additionally, the contact time of the methionine solution with the film and the post-irradiation ageing process significantly influence the concentration of methionine sulfoxide due to the oxidant species released by the film for the three irradiation technologies.

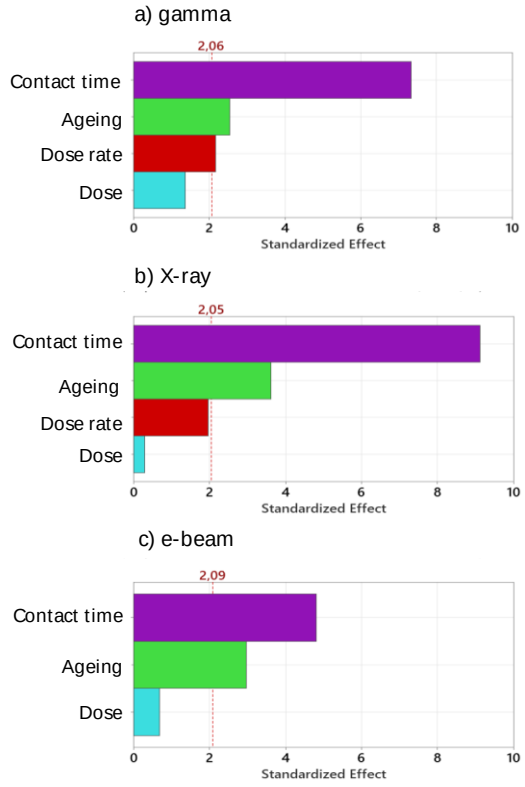


Figure 7: (a) multilayer film irradiated by gamma. (b) multilayer film irradiated by X-ray. (c) multilayer film irradiated by e-beam. Pareto analysis of significant effects on methionine sulfoxide concentration: Dose (kGy) (blue), Ageing post irradiation (green), methionine contact time (days) (purple) and dose rate (kGy/h) (red).

**Gamma radiation process**

To complete the study, we conducted an HPLC investigation to compare two gamma irradiation processes using the same irradiator at Ionisos in France, with a consistent dose rate of 2 kGy/h. The first process involved irradiating the sample in a single run, while the second process accumulated the dose over multiple runs within the irradiation bunker, with unknown rest times between runs.

The concentration of methionine sulfoxide formed in the solution in contact with the bag was measured by HPLC in samples after 1, 2, 3, 6, 12, 24, and 36 months irradiation at 30 kGy and 50 kGy (Figure S2 in SI).
A regression model was generated to determine whether the irradiation process, ageing post irradiation, contact time with the solution, and dose had a significant impact on the concentration of methionine sulfoxide formed.

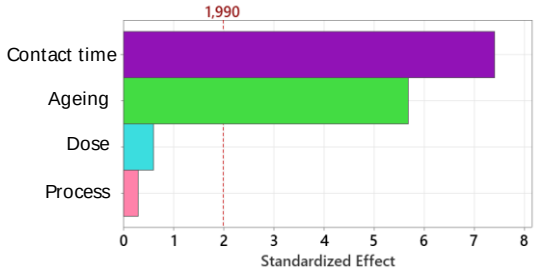


Figure 8: Pareto analysis of significant effects on methionine sulfoxide concentration: Dose (kGy) (blue), Ageing post irradiation (green), methionine contact time (days) (purple) and different process of gamma irradiation (pink).

The regression model (Figure 8) reveals that the contact time with the solution and the multilayer film significantly influence methionine oxidation. Post-irradiation ageing plays a crucial role, indicating that less methionine sulfoxide forms in the solution when the irradiation occurred a long time ago (refer to the coefficient model in the Supplementary Information).
On the other hand, dose and processing have no significant effect on methionine oxidation.

## Conclusion

This study offers insights into the behavior and stability of single-use plastic bags made from EVA/EVOH/EVA multilayer films, extensively used in the biotechnological and biopharmaceutical industries. These materials require sterilization, and the research examined the effects of gamma, X-ray, and electron beam irradiation on these films.
ESR analysis revealed that irradiation generates reactive species such as hydroxyalkyl radicals, which are unstable and can only be quantified one day post-exposure, with concentrations decaying dramatically within nine days. In sharp contrast to the report on PE/EVOH/PE films [22]. The study highlighted that the kinetics and radical species generated are similar across the three irradiation technologies.
The study concludes that the dose rate is one of the parameters which could play a crucial role in the generation of methionine sulfoxide when methionine in solution in contact with the film. This effect is closely tied to the irradiation technology used. Notably, the impact of dose rate is not significantly different for X-ray and gamma irradiation. The high dose rate is inherently linked to the e-beam technology.

A regression model examining different gamma irradiation processes reveals that the concentration of oxidized methionine remains statistically equivalent whatever the processes. Post-irradiation ageing significantly affects the results, with materials irradiated 36 months prior exhibiting lower oxidative effects.
These findings underscore the importance of considering dose rate and irradiation technology in optimizing the stability and performance of multilayer films. The research provides valuable insights into the long-term effects of irradiation, guiding future material handling and application strategies. The interdisciplinary approach of this research provides valuable information on the generation and stability of radical species induced by different irradiation technologies.

## Data availability

The data supporting this article have been included as part of the ESI.

## Conflicts of interest

There are no conflicts to declare.

## Acknowledgements

N.D., F.G. and S.R.A.M. are thankful to Aix-Marseille Université (AMU), Institut de Recherche pour le Développement (IRD) and Centre National pour la Recherche Scientifique (CNRS) for support.

## Notes and references

1 J. D. Vogel, The Maturation of Single-Use Applications, *BioProcess Int.*, 2012, 10–19.
2 E. Mahajan, G. Lye and R. Eibl-Schindler, Brinding polymer Science to Biotechnology Applications: A Single-Use Technology Conference Report, *BioProcess Int*, 2018.
3 ISO 11137-1; Sterilization of HealthCare Products-Radiation-Part 1: Requirements for Development, Validation and Routine control of a Sterilization Process for MedicalDevices. ISO: Geneva, Switzerland, 2006.
4 Guide to Irradiation and Sterilization Validation of Single-Use Bioprocess Systems, *BioProcess Int*, 2008.
5 N. Dupuy, S. R. A. Marque, L. S. Fifield, M. Pharr, D. Staack, S. D. Pillai, L. Nichols, M. K. Murphy and S. Dorey, Supplementing Gamma Sterilization with X-Ray and E-Beam Technologies, *Bioprocess technical*, 2022, 20, 24–28.
6 BPAS Technical Guide, *X-rays Sterilization of single-Use BioProcess Equipment, Part 1: Industry Need*, Requirements&Risk Evaluation., 2021.
7 P. M. Armenante and O. Akiti, in *Chemical Engineering in the Pharmaceutical Industry*, eds. D. J. am Ende and M. T. am Ende, John Wiley & Sons, Inc., Hoboken, NJ, USA, 2019, pp. 311–379.
8 D. Darwis, Erizal, B. Abbas, F. Nurlidar and D. P. Putra, Radiation Processing of Polymers for Medical and Pharmaceutical Applications, *Macromolecular Symposia*, 2015, 353, 15–23.


This journal is © The Royal Society of Chemistry 20xx

9 H. De Brouwer, Comparison of the effects of x-ray and gamma irradiation on engineering thermoplastics, *Radiat. Phys. Chem.*, 2022, 193, 109999.

10 B. Croonenborghs, M. A. Smith and P. Strain, X-ray versus gamma irradiation effects on polymers, *Radiat. Phys. Chem.*, 2007, 76, 1676–1678.

11 T. K. Kroc, Monte Carlo simulations demonstrating physics of equivalency of gamma, electron-beam, and X-ray for radiation sterilization, *Radiat. Phys. Chem.*, 2023, 204, 110702.

12 A. T. Fintzou, A. V. Badeka, M. G. Kontominas and K. A. Riganakos, Changes in physicochemical and mechanical properties of γ-irradiated polypropylene syringes as a function of irradiation dose, *Radiat. Phys. Chem.*, 2006, 75, 87–97.

13 B. Krieguer, N. Ludwig, S. Dorey, N. Dupuy, F. Girard, N. Girard-Perier, F. Kuntz and S. R. A. Marque, Thermal properties and radical monitoring after gamma, X-ray, and electron beam irradiation in polyamides, *Phys. Chem. Chem. Phys.*, 2024, 10.1039.D4CP02358G.

14 G. Sadler, W. Chappas and D. E. Pierce, Evaluation of e-beam, **γ-** and X-ray treatment on the chemistry and safety of polymers used with pre-packaged irradiated foods: a review, *Food Addit. Contam.*, 2001, 18, 475–501.

15 D. Lowe, L. Roy, M. A. Tabocchini, W. Rühm, R. Wakeford, G. E. Woloschak and D. Laurier, Radiation dose rate effects: what is new and what is needed?, *Radiat Environ Biophys*, 2022, 61, 507–543.

16 A. Buttafava, A. Tavares, M. Arimondi, A. Zaopo, S. Nesti, D. Dondi, M. Mariani and A. Faucitano, Dose rate effects on the radiation induced oxidation of polyethylene, *Nuclear Instruments and Methods in Physics Research Section B: Beam Interactions with Materials and Atoms*, 2007, **265**, 221–226.

17 F. Gaston, N. Dupuy, S. R. A. Marque, M. Barbaroux and S. Dorey, Impact of γ-irradiation, ageing and their interactions on multilayer films followed by AComDim, *Analytica Chimica Acta*, 2017, **981**, 11–23.

18 F. Gaston, N. Dupuy, S. R. A. Marque, D. Gigmes and S. Dorey, Monitoring of the discoloration on γ-irradiated PE and EVA films to evaluate antioxidant stability, *J of Applied Polymer Sci*, 2018, **135**, 46114.

19 F. Gaston, N. Dupuy, S. R. A. Marque, M. Barbaroux and S. Dorey, FTIR study of ageing of γ-irradiated biopharmaceutical EVA based film, *Polym. Degrad. Stab.*, 2016, **129**, 19–25.

20 S. Dorey, F. Gaston, N. Dupuy, M. Barbaroux and S. R. A. Marque, Reconciliation of pH, conductivity, total organic carbon with carboxylic acids detected by ion chromatography in solution after contact with multilayer films after γ-irradiation, *European Journal of Pharmaceutical Sciences*, 2018, **117**, 216–226.

21 F. Gaston, N. Dupuy, S. R. A. Marque and S. Dorey, Evaluation of multilayer film stability by Raman spectroscopy after gamma-irradiation sterilization process, *Vib. Spectrosc.*, 2018, 96, 52–59.

22 G. Audran, S. Dorey, N. Dupuy, F. Gaston and S. R. A. Marque, Degradation of γ-irradiated polyethylene-ethylene vinyl alcohol-polyethylene multilayer films: An ESR study, *Polym. Degrad. Stab.*, 2015, 122, 169–179.

23 S. Dorey, F. Gaston, S. R. A. Marque, B. Bortolotti and N. Dupuy, XPS analysis of PE and EVA samples irradiated at different γ-doses, *Appl. Surf. Sci*, 2018, 427, 966–972.

24 S. Dorey, F. Gaston, N. Girard-Perier, N. Dupuy, S. R. A. Marque and L. Delaunay, Effect of gamma irradiation on the oxygen barrier properties in ethyl-vinyl acetate/ethylene-vinyl alcohol/ethyl-vinyl acetate multilayer film, *J of Applied Polymer Sci*, 2020, 137, 49361.

25 N. Girard-Perier, M. Claeys-Bruno, S. R. A. Marque, N. Dupuy, F. Gaston and S. Dorey, Monitoring of Peroxide in Gamma Irradiated EVA Multilayer Film Using Methionine Probe, *Polymers*, 2020, 12, 3024.

26 N. Girard-Perier, F. Gaston, N. Dupuy, S. R. A. Marque, L. Delaunay and S. Dorey, Study of the mechanical behavior of gamma-irradiated single-use bag seals, *Food Packaging and Shelf Life*, 2020, **26**, 100582.

27 F. Gaston, N. Dupuy, N. Girard-Perier, S. R. A. Marque and S. Dorey, Investigations at the Product, Macromolecular, and Molecular Level of the Physical and Chemical Properties of a γ-Irradiated Multilayer EVA/EVOH/EVA Film: Comprehensive Analysis and Mechanistic Insights, *Polymers*, 2021, 13, 2671.

28 N. Girard-Perier, S. R. A. Marque, N. Dupuy, M. Claeys-Bruno, F. Gaston, S. Dorey, L. S. Fifield, Y. Ni, D. Li, W. K. Fuchs, M. K. Murphy, S. D. Pillai, M. Pharr and L. Nichols, Effects of X-Rays, Electron Beam, and Gamma Irradiation on Chemical and Physical Properties of EVA Multilayer Films, *Front. Chem.*, 2022, 10, 888285.

29 B. Krieguer, S. R. A. Marque, S. Dorey, F. Girard, Y. Ni, D. Li, M. K. Murphy, L. S. Fifield and N. Dupuy, Comparison of effects from gamma, e-beam and X-ray radiation on multilayer polymer films used in biopharmaceutical devices by chemometric treatment of spectroscopic data, *Radiation Physics and Chemistry*, 2024, **218**, 111607.

30 T. Pędzinski, K. Grzyb, K. Skotnicki, P. Filipiak, K. Bobrowski, C. Chatgilialoglu and B. Marciniak, Radiation- and Photo-Induced Oxidation Pathways of Methionine in Model Peptide Backbone under Anoxic Conditions, *Int J Mol Sci*, 2021, 22, 4773.

31 V. Gold, Ed., *The IUPAC Compendium of Chemical Terminology: The Gold Book*, International Union of Pure and Applied Chemistry (IUPAC), Research Triangle Park, NC, 4th edn., 2019.

32 M. A. Rosenfeld, L. V. Yurina and A. D. Vasilyeva, Antioxidant role of methionine-containing intra- and extracellular proteins, *Biophys Rev*, 2023, 15, 367–383.

33 D. Tavella, D. R. Ouellette, R. Garofalo, K. Zhu, J. Xu, E. O. Oloo, C. Negron and P. M. Ihnat, A novel method for in silico assessment of Methionine oxidation risk in monoclonal antibodies: Improvement over the 2-shell model, *PLoS One*, 2022, 17, e0279689.

34 Minitab Statistical software, 2022. Minitab Help. Retrieved from https://support.minitab.com/en-us/minitab/21/help-and-how-to/.

35 A. G. Davies, J. A. Howard and M. Lehnig, *Magnetic properties of free radicals- Organic O-, P-, Se-, Si-, Ge-, Sn-, Pb-, As-, Sb-Centered Radicals*, 1979, vol. 9 c2.

# Supporting Information: Investigating dose rate effects and reactive species formation in irradiated multilayer films – part 1 EVA/EVOH/EVA

## Electron spin Resonance

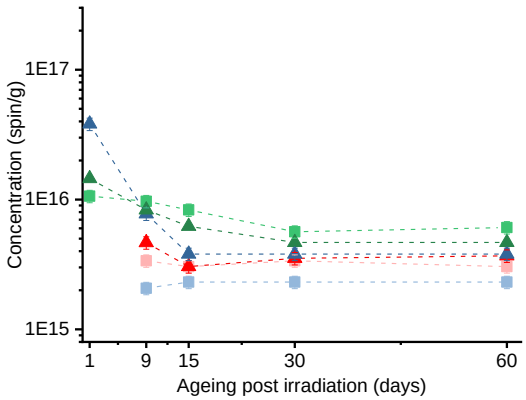


Figure 1: Monitoring of the concentration of radicals by ESR as concentration (Spin/g) vs ageing (days). Squares correspond to sample irradiated at 50 kGy and up triangle correspond to sample irradiated at 100 kGy, red for gamma, blue for X-ray and green for e-beam.

## HPLC

### Regression Analysis: Gamma, e-beam and X-ray

#### Regression Equation

Methionine sulfoxide concentration = 0,676 - 0,00877 Dose + 0,0332 Ageing post irradiation + 0,1329 Methionine contact time - 0,000062 Dose rate

#### Coefficients

| Term | Coef | SE Coef | T-Value | P-Value | VIF |
|---|---|---|---|---|---|
| Constant | 0,676 | 0,598 | 1,13 | 0,262 | |
| Dose | -0,00877 | 0,00701 | -1,25 | 0,214 | 1,10 |
| Ageing post irradiation | 0,0332 | 0,0989 | 0,34 | 0,738 | 1,03 |
| Methionine contact time | 0,1329 | 0,0174 | 7,65 | 0,000 | 1,00 |
| Dose rate | -0,000062 | 0,000019 | -3,23 | 0,002 | 1,11 |

#### Model Summary

| S | R-sq | R-sq(adj) | R-sq(pred) |
|---|---|---|---|
| 1,35971 | 45,62% | 42,97% | 40,00% |

#### Analysis of Variance

| Source | DF | Adj SS | Adj MS | F-Value | P-Value |
|---|---|---|---|---|---|
| Regression | 4 | 127,183 | 31,796 | 17,20 | 0,000 |
| Dose | 1 | 2,895 | 2,895 | 1,57 | 0,214 |
| Ageing post irradiation | 1 | 0,209 | 0,209 | 0,11 | 0,738 |
| Methionine contact time | 1 | 108,087 | 108,087 | 58,46 | 0,000 |
| Dose rate | 1 | 19,299 | 19,299 | 10,44 | 0,002 |
| Error | 82 | 151,603 | 1,849 | | |
| Lack-of-Fit | 70 | 149,588 | 2,137 | 12,73 | 0,000 |

| | | | |
|---|---|---|---|
| Pure Error | 12 | 2,015 | 0,168 |
| Total | 86 | 278,786 | |

### Fits and Diagnostics for Unusual Observations

| Obs | Methionine sulfoxide | Fit | Resid | Std Resid | |
|---|---|---|---|---|---|
| 18 | 7,245 | 1,766 | 5,480 | 4,09 | R |
| 19 | 6,333 | 3,228 | 3,105 | 2,35 | R |
| 22 | 7,623 | 1,766 | 5,857 | 4,37 | R |
| 23 | 6,350 | 3,228 | 3,122 | 2,36 | R |

*R Large residual*

## Regression analysis: Gamma irradiation

### Regression Equation

Methionine sulfoxide = -1,43 - 0,0356 Dose + 0,471 Ageing post irradiation + 0,2359 Methionine contact time + 0,1991 Dose rate concentration

### Coefficients

| Term | Coef | SE Coef | T-Value | P-Value | VIF |
|---|---|---|---|---|---|
| Constant | -1,43 | 1,18 | -1,21 | 0,235 | |
| Dose | -0,0356 | 0,0258 | -1,38 | 0,180 | 1,20 |
| Ageing post irradiation | 0,471 | 0,185 | 2,55 | 0,017 | 1,10 |
| Methionine contact time | 0,2359 | 0,0321 | 7,34 | 0,000 | 1,01 |
| Dose rate | 0,1991 | 0,0920 | 2,16 | 0,040 | 1,09 |

### Model Summary

| S | R-sq | R-sq(adj) | R-sq(pred) |
|---|---|---|---|
| 1,46859 | 71,05% | 66,60% | 61,38% |

### Analysis of Variance

| Source | DF | Adj SS | Adj MS | F-Value | P-Value |
|---|---|---|---|---|---|
| Regression | 4 | 137,646 | 34,411 | 15,96 | 0,000 |
| Dose | 1 | 4,097 | 4,097 | 1,90 | 0,180 |
| Ageing post irradiation | 1 | 14,040 | 14,040 | 6,51 | 0,017 |
| Methionine contact tim | 1 | 116,167 | 116,167 | 53,86 | 0,000 |
| Dose rate | 1 | 10,099 | 10,099 | 4,68 | 0,040 |
| Error | 26 | 56,076 | 2,157 | | |
| Lack-of-Fit | 22 | 56,004 | 2,546 | 142,69 | 0,000 |
| Pure Error | 4 | 0,071 | 0,018 | | |
| Total | 30 | 193,721 | | | |

### Fits and Diagnostics for Unusual Observations

| Obs | Methionine sulfoxide | Fit | Resid | Std Resid | |
|---|---|---|---|---|---|
| 26 | 7,245 | 3,568 | 3,678 | 2,64 | R |
| 30 | 7,623 | 3,568 | 4,055 | 2,91 | R |

*R Large residual*

## Regression analysis: X-ray irradiation

### Regression Equation

Methionine sulfoxide = 0,925 - 0,00102 Dose - 0,2278 Ageing post irradiation + 0,1016 Methionine contact time + 0,00652 Dose rate concentration

### Coefficients

| Term | Coef | SE Coef | T-Value | P-Value | VIF |
|---|---|---|---|---|---|
| Constant | 0,925 | 0,380 | 2,43 | 0,022 | |
| Dose | -0,00102 | 0,00349 | -0,29 | 0,773 | 1,03 |
| Ageing post irradiation | -0,2278 | 0,0628 | -3,62 | 0,001 | 1,00 |
| Methionine contact time | 0,1016 | 0,0111 | 9,12 | 0,000 | 1,00 |
| Dose rate | 0,00652 | 0,00331 | 1,97 | 0,059 | 1,04 |

### Model Summary

| S | R-sq | R-sq(adj) | R-sq(pred) |
|---|---|---|---|
| 0,533171 | 78,76% | 75,62% | 68,85% |

### Analysis of Variance

| Source | DF | Adj SS | Adj MS | F-Value | P-Value |
|---|---|---|---|---|---|
| Regression | 4 | 28,4634 | 7,1159 | 25,03 | 0,000 |
| Dose | 1 | 0,0242 | 0,0242 | 0,09 | 0,773 |
| Ageing post irradiation | 1 | 3,7354 | 3,7354 | 13,14 | 0,001 |
| Methionine contact time | 1 | 23,6193 | 23,6193 | 83,09 | 0,000 |
| Dose rate | 1 | 1,1073 | 1,1073 | 3,90 | 0,059 |
| Error | 27 | 7,6753 | 0,2843 | | |
| Total | 31 | 36,1388 | | | |

### Fits and Diagnostics for Unusual Observations

| Obs | Methionine sulfoxide | Fit | Resid | Std Resid | |
|---|---|---|---|---|---|
| 15 | 3,250 | 1,708 | 1,542 | 3,15 | R |

*R Large residual*

## Regression analysis: e-beam irradiation

### Regression Equation

Methionine sulfoxide concentration = 0,604 + 0,00536 Dose - 0,2030 Ageing post irradiation + 0,0548 Methionine contact time

### Coefficients

| Term | Coef | SE Coef | T-Value | P-Value | VIF |
|---|---|---|---|---|---|
| Constant | 0,604 | 0,419 | 1,44 | 0,165 | |
| Dose | 0,00536 | 0,00771 | 0,70 | 0,495 | 1,00 |
| Ageing post irradiation | -0,2030 | 0,0681 | -2,98 | 0,007 | 1,00 |
| Methionine contact time | 0,0548 | 0,0114 | 4,81 | 0,000 | 1,00 |

### Model Summary

| S | R-sq | R-sq(adj) | R-sq(pred) |
|---|---|---|---|
| 0,471887 | 61,92% | 56,21% | 41,66% |

### Analysis of Variance

| Source | DF | Adj SS | Adj MS | F-Value | P-Value |
|---|---|---|---|---|---|
| Regression | 3 | 7,2425 | 2,4142 | 10,84 | 0,000 |
| Dose | 1 | 0,1077 | 0,1077 | 0,48 | 0,495 |
| Ageing post irradiation | 1 | 1,9784 | 1,9784 | 8,88 | 0,007 |
| Methionine contact time | 1 | 5,1564 | 5,1564 | 23,16 | 0,000 |
| Error | 20 | 4,4536 | 0,2227 | | |
| Lack-of-Fit | 12 | 2,5099 | 0,2092 | 0,86 | 0,607 |
| Pure Error | 8 | 1,9436 | 0,2430 | | |
| Total | 23 | 11,6961 | | | |

### Fits and Diagnostics for Unusual Observations

| Obs | Methionine sulfoxide | Fit | Resid | Std Resid | |
|---|---|---|---|---|---|
| 8 | 2,415 | 1,414 | 1,002 | 2,38 | R |

*R Large residual*

## Regression Analysis: gamma irradiation processes

### Method

Categorical predictor coding (1; 0)

### Regression Equation

| Ster | | | |
|---|---|---|---|
| S1 | metox | = | 0,748 + 0,0089 Dose - 0,0688 Ageing + 0,1348 days |

S2 metox = 0,659 + 0,0089 Dose - 0,0688 Ageing + 0,1348 days

## Coefficients

| Term | Coef | SE Coef | T-Value | P-Value | VIF |
|---|---|---|---|---|---|
| Constant | 0,659 | 0,676 | 0,97 | 0,333 | |
| Dose | 0,0089 | 0,0149 | 0,60 | 0,551 | 1,00 |
| Ageing | -0,0688 | 0,0121 | -5,69 | 0,000 | 1,00 |
| Contact time | 0,1348 | 0,0182 | 7,41 | 0,000 | 1,00 |
| Ster process | 0,089 | 0,297 | 0,30 | 0,764 | 1,00 |

## Model Summary

| S | R-sq | R-sq(adj) | R-sq(pred) |
|---|---|---|---|
| 1,36329 | 52,62% | 50,22% | 46,76% |

## Analysis of Variance

| Source | DF | Adj SS | Adj MS | F-Value | P-Value |
|---|---|---|---|---|---|
| Regression | 4 | 163,039 | 40,760 | 21,93 | 0,000 |
| Dose | 1 | 0,667 | 0,667 | 0,36 | 0,551 |
| Ageing | 1 | 60,156 | 60,156 | 32,37 | 0,000 |
| Contact time | 1 | 102,048 | 102,048 | 54,91 | 0,000 |
| Process | 1 | 0,168 | 0,168 | 0,09 | 0,764 |
| Error | 79 | 146,826 | 1,859 | | |
| Total | 83 | 309,865 | | | |

## Fits and Diagnostics for Unusual Observations

| Obs | metox | Fit | Resid | Std Resid | |
|---|---|---|---|---|---|
| 8 | 4,936 | 2,205 | 2,731 | 2,05 | R |
| 9 | 6,922 | 3,687 | 3,235 | 2,45 | R |
| 23 | 5,278 | 2,314 | 2,964 | 2,22 | R |

*R Large residual*

# Références Chapitre 3

1. Girard-Perier, N.; Claeys-Bruno, M.; Marque, S.R.A.; Dupuy, N.; Gaston, F.; Dorey, S. Monitoring of Peroxide in Gamma Irradiated EVA Multilayer Film Using Methionine Probe. *Polymers* **2020**, *12*, 3024, doi:10.3390/polym12123024.

2. Balakrishnan, G.; Barnett, G.V.; Kar, S.R.; Das, T.K. Detection and Identification of the Vibrational Markers for the Quantification of Methionine Oxidation in Therapeutic Proteins. *Anal. Chem.* **2018**, *90*, 6959–6966, doi:10.1021/acs.analchem.8b01238.

3. Gaston, F.; Dupuy, N.; Marque, S.R.A.; Barbaroux, M.; Dorey, S. FTIR Study of Ageing of γ-Irradiated Biopharmaceutical EVA Based Film. *Polymer Degradation and Stability* **2016**, *129*, 19–25, doi:10.1016/j.polymdegradstab.2016.03.040.

4. Gaston, F.; Dupuy, N.; Marque, S.R.A.; Barbaroux, M.; Dorey, S. Impact of γ-Irradiation, Ageing and Their Interactions on Multilayer Films Followed by AComDim. *Analytica Chimica Acta* **2017**, *981*, 11–23, doi:10.1016/j.aca.2017.05.021.

5. Girard-Perier, N.; Marque, S.R.A.; Dupuy, N.; Claeys-Bruno, M.; Gaston, F.; Dorey, S.; Fifield, L.S.; Ni, Y.; Li, D.; Fuchs, W.K.; et al. Effects of X-Rays, Electron Beam, and Gamma Irradiation on Chemical and Physical Properties of EVA Multilayer Films. *Frontiers in Chemistry* **2022**, *10*, 888285, doi:10.3389/fchem.2022.888285.

6. Gaston, F.; Dupuy, N.; Girard-Perier, N.; Marque, S.R.A.; Dorey, S. Investigations at the Product, Macromolecular, and Molecular Level of the Physical and Chemical Properties of a γ-Irradiated Multilayer EVA/EVOH/EVA Film: Comprehensive Analysis and Mechanistic Insights. *Polymers* **2021**, *13*, 2671, doi:10.3390/polym13162671.

# Chapitre 4 : Comparaison de l'impact de l'irradiation gamma, rayons X et faisceau d'électrons sur le film multicouche PE/EVOH/PE

Ce chapitre se concentre sur la comparaison des effets des trois technologies d'irradiation sur le film multicouche PE/EVOH/PE, en analysant ses propriétés mécaniques et chimiques.

Le premier article explore l'effet des rayons X, faisceau d'électrons et rayons gamma sur le film PE à une dose de 50 kGy. L'objectif est de vérifier l'équivalence des résultats obtenus avec ces trois technologies d'irradiation. Des méthodes statistiques, comme le test TOST (Two One-Sided T-Test), et le test de Student [1], ont été employées pour vérifier l'hypothèse d'équivalence et de différence, respectivement, des propriétés mécaniques et viscoélastiques du film après irradiations.

Le deuxième article présenté dans ce chapitre est la seconde partie de l'article du chapitre 3. Cette étude reprend les mêmes objectifs et les mêmes méthodologies utilisés sur le film EVA pour le film PE. L'étude compare l'impact des trois technologies d'irradiation en analysant les radicaux générés dans le matériau après irradiation et l'impact du débit de dose sur l'oxydation d'une solution en contact avec le film.

# 4.1. Étude de l’impact de l’irradiation sur les propriétés mécaniques

En vue de la qualification du film PE/EVOH/PE pour chaque technologie d’irradiation, il est nécessaire de démontrer l'équivalence de l’impact des trois technologies d’irradiations. En général, les tests d'hypothèse sont utilisés comme méthode d'analyse des données pour évaluer leurs équivalences ou leurs différences.

Dans l'article publié en 2023 dans la revue *Polymers*, l'impact de trois technologies d'irradiation, les rayons X, le faisceau d'électrons et les rayons gamma, a été étudié dans des conditions industrielles à une dose unique de 50 kGy sur un film multicouche PE/EVOH/PE. Les propriétés de ce film ont été analysées dans deux directions : la direction de l'extrusion (Machine Direction, MD) et la direction perpendiculaire à celle-ci (Transverse Direction, TD). Ces deux orientations sont essentielles pour comprendre le comportement mécanique des films polymères sous contrainte, car elles peuvent révéler des propriétés distinctes en fonction de l'orientation des chaînes polymères et des conditions de traitement.

Notre approche vise à reproduire au mieux les conditions industrielles d'irradiation. L’équivalence potentielles de l’impact entre les technologies d'irradiation ont été analysées à l'aide du test de Student et du test d'équivalence TOST. Le test d’équivalence TOST est couramment accepté pour l'évaluation de l’impact des trois technologies d’irradiation. Deux ensembles de données sont considérés comme équivalente si la différence de leurs moyennes n'est pas statistiquement significative. Le t-test a été utilisé pour comparer les différences de moyennes entre les groupes, permettant de déterminer si ces différences étaient statistiquement significatives.

Dans cet article, les tests statistiques ont été appliqués aux propriétés mécaniques et viscoélastiques du film, mesurées à l'aide de tests de traction et d'analyses mécaniques dynamiques (DMA).

Les t-tests, réalisés à partir des données obtenues par les tests de tractions, ont révélé que certaines différences de moyennes entre les groupes étaient statistiquement significatives, notamment pour les échantillons testés dans la direction machine (MD). En revanche, les résultats obtenus avec les tests d'équivalence TOST ont montré que ces différences n'étaient pas suffisamment importantes pour être considérées comme significatives. Par exemple, les films irradiés par gamma et rayons X présentent une résistance à la traction ultime (UTS) similaire à celle des films non stériles (~17 MPa en MD), tandis que les films irradiés par faisceau d'électrons affichent une UTS légèrement plus élevée (~19 MPa). Ces résultats sont détaillés dans les Figures 3a et 3b, qui illustrent les valeurs d'UTS pour les directions MD et TD. Cette analyse souligne l'importance

d'utiliser plusieurs méthodes statistiques pour obtenir une évaluation complète et précise des effets des irradiations sur les films polymères.
En complément, les analyses DMA ont montré que les températures de transition thermique (γ et β) sont similaires pour toutes les technologies d'irradiation, indiquant que les mouvements de chaîne dans la phase amorphe du polymère n'étaient pas affectés. Les valeurs des transitions γ et β après irradiation sont représentées dans la figure 6 de l'article.

Dans cet article nous avons montré que ces méthodes peuvent conduire à des conclusions différentes concernant l'impact des technologies d'irradiation sur les propriétés mécaniques. Nous avons observé que les critères d'acceptation d'équivalence (EAC) dépendent de la taille de l'échantillon, de l'homogénéité de l'échantillonnage et de l'écart-type du ou des groupes de référence. Ils peuvent devenir très élevés pour de petites tailles d'échantillons et de grands écarts types. Le critère d'équivalence peut ne pas être suffisamment strict dans ce cas. Quelle que soit la méthode statistique, les différences observées sont faibles entre chaque technologie d'irradiation et reflètent plutôt la variation dans la méthodologie d'échantillonnage et de test.
L'irradiation gamma, faisceau d'électrons et rayons X ont un impact équivalent sur les propriétés mécaniques du film multicouche PE/EVOH/PE, ce qui suggère que les irradiations par rayons X et faisceau d'électrons pourraient convenir aux applications biopharmaceutiques.

polymers

MDPI

*Article*

# Gamma, E-Beam and X-ray Irradiations on PE/EVOH/PE Multilayer Film: An Industrial Point of View Regarding the Impact on Mechanical Properties

**Nina Girard-Perier [1,*], Sylvain R. A. Marque [2], Nathalie Dupuy [3], Blanche Krieguer [1,2,3] and Samuel Dorey [1,*]**

[1] Sartorius Stedim FMT S.A.S, Z.I. Les Paluds, Avenue de Jouques CS91051, CEDEX, 13781 Aubagne, France; blanche.krieguer@sartorius.com
[2] Aix Marseille Univ, CNRS, ICR, Case 551, 13397 Marseille, France; sylvain.marque@univ-amu.fr
[3] Aix Marseille Univ, Avignon Université, CNRS, IRD, IMBE, 13013 Marseille, France; nathalie.dupuy@univ-amu.fr
* Correspondence: nina.perier@sartorius.com (N.G.-P.); samuel.dorey@sartorius.com (S.D.)

**Abstract:** X-ray and electron-beam (E-beam) sterilization technologies were assessed to supplement gamma sterilization, the most common radiation technology used today for biopharmaceutical product sterilization. The mechanical properties of a PE/EVOH/PE film were studied using tensile tests and dynamical mechanical analysis after each irradiation technology (i.e., gamma, electron beam and X-ray irradiations). The effects of each irradiation were compared using two statistical methods. The results indicate that the three irradiation technologies induce no difference in mechanical properties in the investigated dose range for this material.

**Keywords:** irradiation technology; gamma; X-rays; polyethylene; mechanical properties; thermal and viscoelastic properties

check for updates

**Citation:** Girard-Perier, N.; Marque, S.R.A.; Dupuy, N.; Krieguer, B.; Dorey, S. Gamma, E-Beam and X-ray Irradiations on PE/EVOH/PE Multilayer Film: An Industrial Point of View Regarding the Impact on Mechanical Properties. *Polymers* **2023**, *15*, 2799. https://doi.org/10.3390/polym15132799

Academic Editor: Nadege Follain

Received: 29 March 2023
Revised: 31 May 2023
Accepted: 16 June 2023
Published: 24 June 2023

**Copyright:** © 2023 by the authors. Licensee MDPI, Basel, Switzerland. This article is an open access article distributed under the terms and conditions of the Creative Commons Attribution (CC BY) license (https://creativecommons.org/licenses/by/4.0/).

## 1. Introduction

Single-use plastic bags are frequently used by the biotechnological and biopharmaceutical industries for the storage, shipping or preparation of intermediates, biopharmaceutical preparations and solutions and final products [1–3]. Films used in single-use systems are mainly made, for example, of polyethylene/ethylene vinyl alcohol/polyethylene (PE/EVOH/PE) multilayer film. These polymers are selected for their properties of barrier protection and flexibility to ensure the integrity of the solution. Single-use plastic bags in biopharmaceutical and biotechnological environments require sterilization to be free of microorganisms [4]. The dose range usually used for biopharmaceutical industries is 25–45 kGy [5]. Nowadays, the most common radiation technology for pharmaceutical devices is gamma radiation. The current healthcare context leads to a strong growth in the manufacture of biopharmaceutical products. In addition, there are concerns about the capacity of sterilization using gamma radiation in future years [6]. Two alternative methods, electron beam irradiation and X-ray irradiation, are being considered for use as additional technologies to gamma sterilization.

Electron beam irradiation is generated when electrons are accelerated by an electromagnetic field in an accelerator. X-rays are photons that are generated using an electron beam accelerator. The electron beam is converted to photons by accelerating the electrons into a high-density material (tungsten, tantalum) with an energy in the same range as gamma. It is important to investigate the impact of these two additional sources on single-use systems. For both irradiation modalities, a sterility assurance level (SAL) of $10^{-6}$ can be achieved. The ionizing radiation energy for the gamma, E-beam and X-ray radiations considered is used to define the absorbed dose (in kGy) because it is the ionizing ability of the radiation—the ability to ionize or kick electrons off the shell of atoms through Compton

scattering—that initiates the killing effect on microorganisms. Up to now, the impact of gamma irradiation on both EVOH and PE polymers has been exhaustively studied [7–21]. Few studies report on the impact of the two other irradiation technologies (i.e., E-beam and X-rays) [22–25]. Two studies report on the effect of gamma irradiation and E-beam irradiation on polypropylene [26,27]. The authors observed that gamma irradiation has a greater effect on physical, mechanical and thermal properties than E-beam irradiation. Badia et al. [28] compared gamma and electron beam irradiation on high-density polyethylene shelf life and found no change. Croonenborghs et al. [29] observed a similar effect between gamma and X-ray irradiations on the mechanical properties of polyethylene.

Regarding the PE/EVOH/PE multilayer film in this paper, many studies were performed on the impact of gamma irradiation using various analytical techniques and at different analysis levels, such as molecular level with electron spin resonance [30] (to monitor radicals) or High-Pressure Liquid Chromatography [31] (to monitor oxidations), analysis at macromolecular level with X-ray Photoelectron Spectroscopy [32] or analysis at material level with permeation or mechanical properties [33]. However, the lack of data in the literature on the impact of electron beam and X-ray irradiations on the mechanical properties of multilayer materials could hamper their use.

The use of ionizing irradiation as a sterilizing method implies the occurrence of two mains reactions: bond cleavage and cross-linking—which may alter the physical and mechanical properties of the polymers. The cross-linking and chain scission events related to the effect of radiation on molecular weight distribution are well described in the literature [34,35].

For characterization and qualification studies, equivalence between process parameter outputs needs to be shown. The impact of three irradiation technologies, X-ray, E-beam and gamma irradiations is investigated in industrial conditions at a single dose of 50 kGy on single-use bags made up of PE/EVOH/PE multilayer film. This approach has a strong limitation due to the non-controlled environment, which was circumvented by paying attention to the repeatability and reproducibility of the experiments. Typically, hypothesis testing is used as a data analysis technique to evaluate the comparability of data. Our approach here aims to be as close as possible to the industrial conditions of irradiations, and two datasets are comparable if their difference in means is of no practical and statistical significance such that it is accepted as nearly zero [36]. Today, a simple equivalence test first introduced by Schuirmann et al. [37] is accepted, for example, as standard for bioequivalence assessment [38], namely, the two one-sided *t*-test (TOST). In contrast to the two-sample *t*-test, the null hypothesis of the TOST states that the two means are not equivalent [36]. The impact of the null hypothesis is that in the case of small sample sizes and/or poor precision (large variance) in one or both groups, equivalence is rejected, resulting in low numbers of false-positive test results [39]. With such test results, conclusions can also be difficult to draw from very large sample sizes. A very large sample size in the reference data leads to a narrow equivalency acceptance criterion (EAC), and therefore, equivalence is easily rejected even though the groups are practically equivalent [40]. Modifications induced upon irradiation were monitored, and the potential differences induced between irradiation technologies were investigated with the Student test (i.e., *t*-test) and the two one-sided test (TOST) equivalence test. In this paper all these statistical tests are performed on mechanical performances [1].

## 2. Materials and Methods

### *2.1. PE/EVOH/PE Multilayer Film*

The structure of the PE/EVOH/PE multilayer film analyzed in this article is depicted in Figure 1. It has a total thickness of 400 µm.

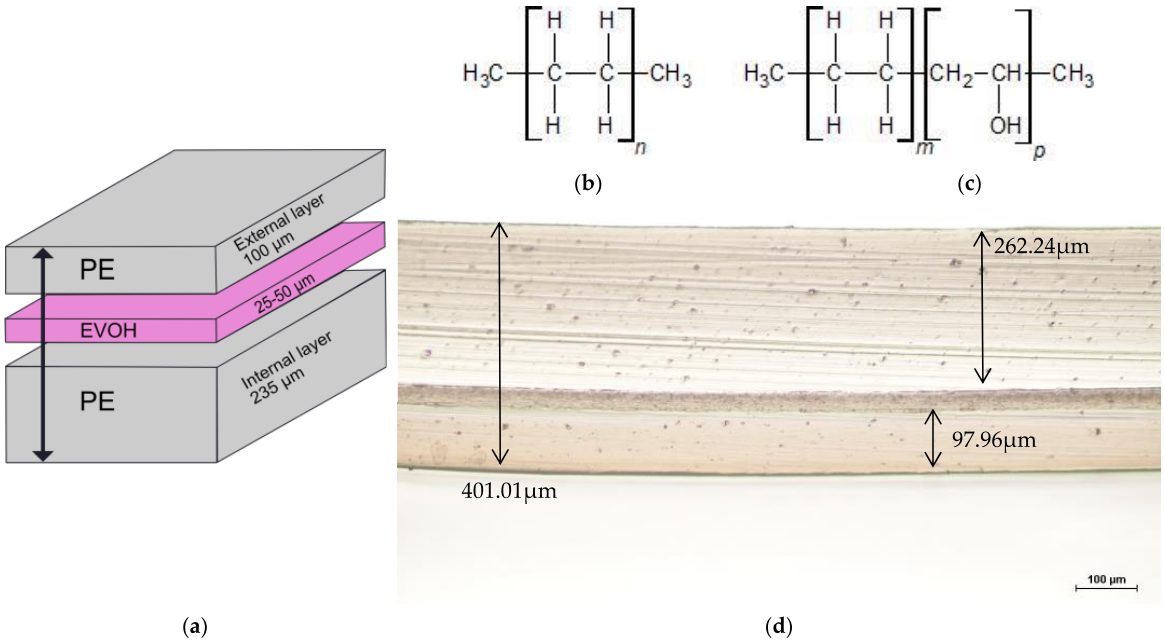


(**a**) (**b**) (**c**) (**d**)

**Figure 1.** (**a**) Representation of PE/EVOH/PE multilayer film, (**b**) chemical structure of PE, (**c**) chemical structure of EVOH, (**d**) image of cross-section of multilayer film.

### 2.2. Storage Conditions

Before irradiation, each sample was wrapped in a packaging bag (PE/Polyamide/PE), and a partial vacuum (not controlled) was formed [27]. However, materials were not $O_2$-degassed and therefore contained some level of $O_2$. The packaging bags were placed in a cardboard box and then irradiated. After irradiation and before analysis, the cardboard box was stored in the dark, in an air-conditioned room at 20 ± 2 °C. The details of storage time (ageing) after irradiation are shown in Table 1.

**Table 1.** Mechanical properties investigated: tensile test and dynamical mechanical analysis (DMA) for different batches, irradiation doses (kGy) and ageing between irradiation and mechanical tests.

| | Tensile Test | | | DMA | | |
|---|---|---|---|---|---|---|
| | **Batch #** | **Dose (kGy)** | **Ageing (Months)** | **Batch #** | **Dose (kGy)** | **Ageing (Months)** |
| Gamma | Batch 1 | 54.3 ± 2.7 | 2 | Batch 3 | 55.2 ± 2.8 | 6 |
| | Batch 2 | 48.2 ± 2.1 | 2 | Batch 2 | 48.2 ± 2.1 | 4 |
| X-rays | Batch 3 | 55.2 ± 2.8 | 2 | Batch 6 | 50.8 ± 1.4 | 6 |
| | Batch 2 | 54.7 ± 2.5 | 2 | Batch 2 | 53.1 ± 1.7 | 4 |
| E-beam | Batch 4 | 52.0 ± 2.6 | 2 | Batch 7 | 54.1 ± 9.5 | 12 |
| | Batch 5 | 54.8 ± 2.8 | 2 | n.a. | n.a. | n.a. |
| Non-sterile | Batch 2 | 0 | n.a. [a] | Batch 7 | 0 | n.a. |

[a] n.a.: not applicable.

### *2.3. Irradiation Methods*

- Gamma

PE/EVOH/PE multilayer films were irradiated at room temperature with a $^{60}$Co gamma source at BGS—Beta Gamma Service GmbH & Co. KG, Wiehl, Germany. The dose rate provided was 1–2 kGy/h. The irradiation was performed at room temperature under an environmental atmosphere. The detail of doses received for each sample depending on analysis is reported in Table 1.

- Electron beam

PE/EVOH/PE multilayer films were packed and wrapped in a packaging bag (PE/Polyamide/PE) and placed side by side in an 8 cm thin cardboard box to have the same thickness of plastic material. They were irradiated with a 10 MeV Rhodotron (Ionisos, Chaumesnil, France), with a power source at 28 kW. The dose rate was 300 kGy/min. Alanine dosimeters were used on the cardboard box to assess the radiation delivered to the single-use bag samples ($\pm$ 5%). The doses received for each sample depending on analysis are reported in Table 1.

- X-ray

PE/EVOH/PE multilayer films were irradiated with a 7 MeV Rhodotron (Steris, Däniken, Switzerland), with a power source at 360 kW. The average dose rate was 80 kGy/h. The doses received for each sample depending on analysis are reported in Table 1.

### *2.4. Tensile Strength Measurement*

Yields, ultimate tensile strength (UTS) and elongation were measured, with specimens along the machine direction (MD) and transverse direction (TD). The MD corresponds to the direction the film was extruded (main direction of the polymer chains), while TD is perpendicular to MD.

The specimens were cut according to the ISO527-3 [41] (150 mm length, 15 mm width). The crosshead speed used was 500 mm/min. The initial gauge length was 100 mm. Six to eight specimens per direction were used for each sample.

The tensile strengths of irradiated PE/EVOH/PE multilayer films were measured using a universal testing machine (Zwick Z005) at 23 $\pm$ 3 °C. UTS is the maximum tensile load a material can withstand prior to fracture and is calculated by dividing the maximum load by the original cross-sectional area of the specimen. All raw data can be found in the supporting information file (Tables S1 and S2).

### *2.5. DMA (Dynamic Mechanical Analysis)*

DMA was performed using the DMA 850 Discovery model from TA instruments. Tests were performed according to ASTM 1640-04. The storage (elasticity) modulus (E′), the loss (viscosity) modulus (E″) and the tangent delta (tan δ, ratio of the loss to the storage curves) were studied as a function of temperature. The storage modulus is a measure of the elastic character of the material [42]. The loss modulus is a measure of the viscous character of the material [42]. The tan δ is defined as the ratio of the loss modulus to the storage modulus (i.e., $\tan\delta = \frac{E''}{E}$). It represents the ratio of energy dissipated to energy stored per cycle of deformation [42]. We considered maxima in curves to assess the different thermal transitions. The γ transition (or glass transition) of the PE of the PE/EVOH/PE multilayer film is obtained with the maximum of the tan δ curve. The β transition is defined as the maximum of the loss modulus curve. The α transition was not studied as there are some variations due to a specimen slipping effect from approx. 50 °C and the overlapping of the glass transition of EVOH and the α transition temperature of PE.

Measurements were performed with 1 Hz by increasing the temperature from −150 °C to 110 °C. Between 2 and 6 specimens were tested per irradiation technology; the details and all the raw data are in the supporting information file (Tables S5 and S6).

### *2.6. Statistical Analyses*

#### 2.6.1. Equivalency Assessment

The statistical evaluation was conducted with a two one-sided test (TOST) equivalence test using the software Minitab®. The equivalency acceptance criterion (EAC) is used to check if the measurement results obtained from one type of irradiation to another fall within the equivalence interval. It is defined as the limit outside which the difference in mean values should be considered practically and statistically significant [39].

#### 2.6.2. Tensile Strength EAC

The first parameter that must be specified before an analyst performs statistical testing is δ, i.e., the equivalence acceptance criterion (EAC), the absolute value of the true difference between the groups' mean values. δ is a hypothetical value such that if the absolute value of the observed difference is no more than δ, there is a strong probability of concluding that the two datasets represent equivalent results [40]. There are different methods to calculate the equivalence acceptance criterion [36], such as the 3-sigma rule (the one used in this paper), Limentani's EAC, Limentani modified, Cohen's standardized difference—effect sizes—and tolerance interval.

To allow the acceptance of a measurable impact on the polymer, criterion δ needs to consider the intrinsic variabilities of the materials and variabilities from the methodology. These variabilities were studied on UTS (Ultimate Tensile Stress) and elongation. The output summary is available in Table 2. These variations reproduce the potential variations during a comparative study over time. The different factors involved in characterizing the materials and method measurements are close to potential variations met during a comparative study, meaning at least different sampling in one batch (destructive tests) and two operators.

**Table 2.** Summary of tensile strength reproducibility study outputs performed on PE/EVOH/PE multilayer film and defined δ (EAC).

| | **UTS (Ultimate Tensile Stress)** | **Elongation** |
|---|---|---|
| Six-sigma variation | 22% | 21% |
| Criteria δ | 35% | 25% |

The equivalence criteria δ are drawn to exceed the six-sigma variations of the materials and the methodology variabilities to significantly discriminate and to conclude on the impact of the studied factor. Therefore, for the UTS, to conclude on a potential impact, the criterion selected is 35% to also embed other films to assess (reproducibility not shown here). The ratio ($UTS_{X\text{-}rays}/UTS_{gamma}$) must be between 0.65 and 1.35 to claim equivalency. For the elongation, the criterion of 25% is selected to conclude on a potential impact on the materials in accordance with other studies [43]. The ratio ($Elongation_{X\text{-}rays}/Elongation_{gamma}$) must be between 0.75 and 1.25. The six-sigma variation for films was evaluated in the transversal direction. The criteria determined are also applicable for the machine direction. As a reminder, in TOST, $p\text{-value}_{TOST}$ must be <0.05 with $\alpha = 5\%$ to claim equivalency, while with the *t*-test, two means are not considered different when $p\text{-value}_{t\text{-test}} > 0.05$.

#### 2.6.3. Thermal Properties EAC

As DMA analysis allows us to study the thermal properties as Differential Scanning Calorimetry (DSC) does, we selected the same criterion for both experiments. With repetitive DSC measurements on one batch of several materials, two sample picking and by two operators, a variability of 5 °C was defined as the DSC criterion. A temperature of 5 °C was then also chosen for DMA analysis to evaluate a potential impact on the material. The statistical evaluation was performed on thermal transitions observed in the storage modulus (E′), loss modulus (E″) and tangent delta (tan δ) curves.

The null hypothesis H0 in TOST is either $H0_1$ = difference $\leq -5$ °C or $H0_2$ = difference $\geq 5$ °C. When both these one-sided tests can be statistically rejected, we can conclude that the alternative hypothesis H1 = $-5$ °C < difference < 5 °C is true and that the observed effect falls within the equivalence bounds and is crossing or touching zero and is, therefore, practically equivalent (or, in other words, statistically not different).

## 3. Results

### *3.1. Tensile Strength Evaluation*

An overview of the tensile curves of the PE/EVOH/PE film obtained after each irradiation technology (i.e., gamma in red, X-rays in blue and electron beam in green) is plotted in Figure 2.

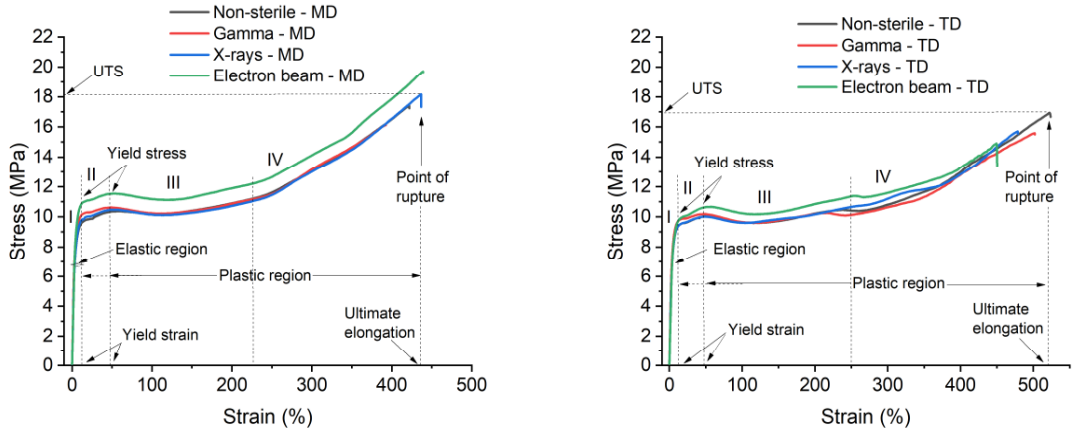


(**a**) (**b**)

**Figure 2.** Tensile curves of PE/EVOH/PE in MD (**a**) and TD (**b**) (one batch, one specimen for each direction)—non-sterile in black, gamma-irradiated sample in red, X-ray-irradiated sample in blue, electron-beam-irradiated sample in green. A dose of 50 ± 5 KGy was used for all technologies. UTS and ultimate elongation values are shown in Figures 3 and 4.

For the non-sterile and sterile samples, four zones can be defined. Two yields, at ≈15% and ≈50%, are observed as zones I and II. From ≈50% elongation, there is a plateau to ≈200% elongation for zone III. From ≈200% (zone IV), strain hardening starts until the complete rupture of the film up to ≈500%. The UTS results obtained for the irradiated multilayer film are depicted in Figure 3a for MD and Figure 3b for TD. Each tensile curve was decomposed into six characteristic values: ultimate tensile strength at break (UTS), ultimate elongation or elongation at break, 1st Yield Strength (Y1 Strength), 1st Yield Strain (Y1 Strain), 2nd Yield Strength (Y2 Strength) and 2nd Yield Strain (Y2 Strain) (for more details see SI). The gamma- and X-ray-irradiated PE/EVOH/PE films tested in the MD have a similar UTS to the non-sterile film (~17 MPa). Regarding the PE/EVOH/PE film tested in the TD (Figure 3b), the gamma and X-ray irradiations seem to have a lower UTS (~16 MPa) compared to the non-sterile film (~17.5 MPa). The tensile curves follow the same tendency regardless of the irradiation technology. They show a double yield characteristic of LDPE [33] in engineering stress–strain curves, and no yield shift is observed. This gives us the indication that crystallites are not impacted, regardless of the irradiation technology used. The yield stress seems to be higher for the electron-beam-irradiated sample than for the other irradiation technologies, probably due to the use of a different lot. The UTS obtained for the electron-beam-irradiated sample is also slightly higher (~19 MPa). All observations are in accordance with results observed in other studies [44,45].

The UTS data were further compared between irradiation technologies (gamma vs. X-rays, gamma vs. E-beam, X-rays vs. E-beam) with a *t*-test. All $p$-values$_{t\text{-test}}$ are reported in the supporting information file (Table S3a,b). Regarding the UTS results obtained for the MD samples, the $p$-values$_{t\text{-test}}$ are <0.05, and we cannot draw conclusions on the equivalency with this current dataset. The *t*-test does not consider the variabilities of the methodology, as reported during our reproducibility study (Table 2) and used to draw the UTS plots (Figure 3). For the UTS results obtained for the TD samples, only the difference between the non-sterile vs. electron-beam-irradiated samples is not significantly different.

Hypothesis tests (TOST) were also performed ($p$-values$_{TOST}$ are in Table S4a,b), and for all conditions, $p$-values$_{TOST}$ are <0.05. Equivalences were observed for UTS in the MD and TD.

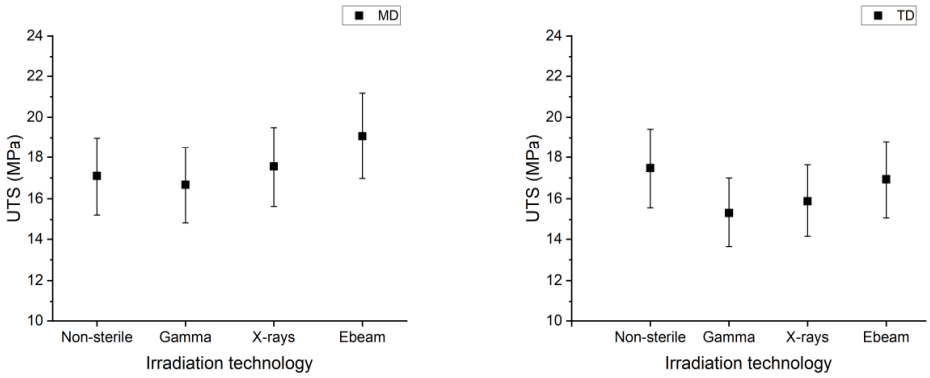


**Figure 3.** Ultimate tensile strength (UTS) for MD (**a**) and for TD (**b**) as a function of the irradiation technology. The mean is plotted with a variability (±3δ) defined in the reproducibility study outputs in Table 2. Average data of two batches. Raw data are given in the supporting information file (Tables S1 and S2).

Figure 4 displays the elongation at break of the PE/EVOH/PE film irradiated at 50 kGy under three irradiation technologies. The elongation at break for the film tested in the MD (Figure 4a) is obtained at ~420%, regardless of the irradiation technology. There is no difference between the non-sterile film and the irradiated films. For the film tested in the TD (Figure 4b), the elongation at break is ~540% for the non-sterile, whereas for the irradiated films, it is obtained at ~480% for gamma, X-ray and electron beam irradiation. No difference is observed regarding the stress hardening position (mainly observed ~250% in the TD and present for each irradiation technology). It can indicate that the cross-linking of the PE and the modification of EVOH occur in the same proportion in all radiation process conditions (dose and sources). This also indicates that the whole film keeps the same flexibility, regardless of the irradiation technology.

All the TOST equivalence tests performed in parallel show no impact of the irradiation technologies on the elongation at break (MD or TD). All $p$-values$_{TOST}$ are recorded in the supporting information file—Table S4c,d. The *t*-tests performed on the MD elongation results reveal that non-sterile vs. X-ray, gamma vs. X-ray irradiation and electron beam vs. X-ray irradiation are statistically significant different. The *t*-tests results on TD elongation show that only X-ray vs. gamma irradiation results are statistically non-significantly different. All $p$-values$_{t\text{-test}}$ are recorded Table S3c,d.

Greene et al. reports that an increase in the tensile strength is characterized by a higher molecular weight, whereas a decrease in the tensile strength is characterized by a broader molecular weight distribution [46]. The similar tensile strength obtained with the three irradiation technologies indicates that the molecular weight is modified in an equivalent proportion, regardless of the irradiation technology used [46]. It also shows that the number

of entanglements in the polymer remains at an equivalent amount in the assessed materials with the three irradiation technologies. Bond cleavage and cross-linking occurring upon irradiation do not impact the overall mechanical properties of the multilayer film. This conclusion agrees with a previous study [33].

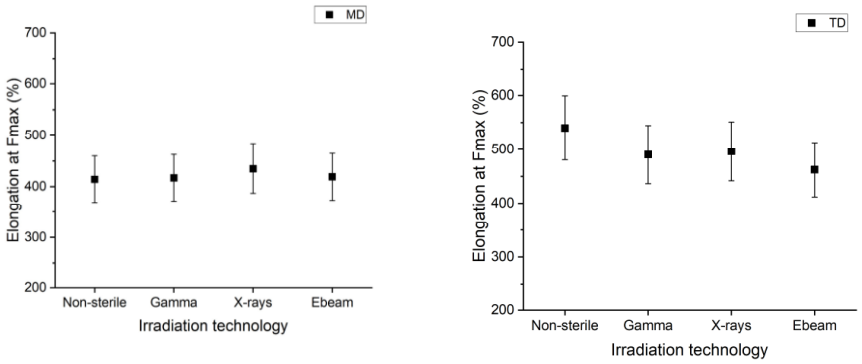


(**a**) (**b**)

**Figure 4.** Elongation for MD (**a**) and for TD (**b**) as a function of the irradiation technology. The mean is plotted with a variability (±3δ) defined in the reproducibility study outputs in Table 2 and relies on two batches and from six to eight specimens/batch. Raw data are given in the supporting information file (Tables S1 and S2).

### *3.2. Thermal Relaxations*

DMA (Dynamic mechanical analysis) was performed on the PE/EVOH/PE multilayer film to investigate the thermal and viscoelastic properties. Figure 5 shows three curves: the storage modulus E′ (triangles), the loss modulus E″ (squares) and tan δ (circles) in the machine direction (MD) without irradiation (non-sterile, black) and after gamma, X-ray and electron beam irradiations (red, blue and pink curves, respectively).

The storage modulus E′ is proportional to the stored energy, the loss modulus is proportional to the energy irreversibly converted to heat and tan delta is the loss factor. The maximum values of the loss modulus and tan δ correspond to the value of the β transition and γ transition for the non-sterile and sterile samples.

Polyethylene is well known to have three relaxation mechanisms, referred to as α, β and γ [47–49]. α relaxation is ascribed to chain motion in the crystalline phase, whereas the β and γ relaxations are related to chain motion in the amorphous phase. The γ relaxation, in some studies, is defined as the glass transition temperature [47], while in other studies, the glass transition in polyethylene and polyethylene/α-olefin-copolymers is the β and not the γ transition [48].

All phenomena (such as cross-linking, chain scission, etc.) happened to an extent that did not change the motion in the molecular chain segment, as observed per DMA.

The glass transition (γ transition) and β transition temperatures are displayed in Figure 6. A similar temperature is obtained for the γ transition (for TD and MD samples; Figure 6a and 6b, respectively), regardless of the irradiation technology. Regarding the β transition (for TD and MD samples; Figure 6c and 6d, respectively), the temperature for the electron-beam-irradiated samples is slightly lower than the non-sterile, gamma- and X-ray-irradiated samples, surely due to curve processing variations.

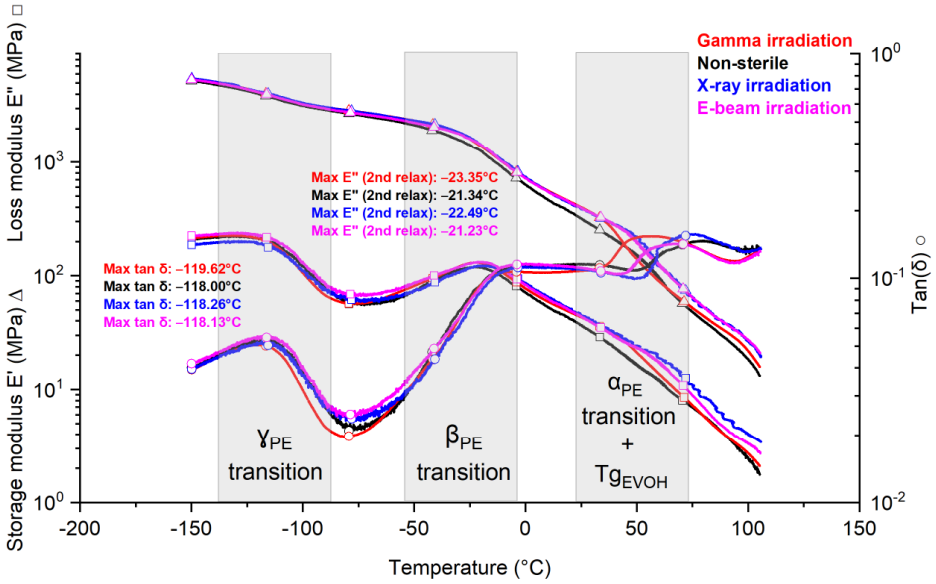


**Figure 5.** Example of DMA curves of PE/EVOH/PE in MD (one batch, one specimen). Δ for storage modulus E′, □ for loss modulus E″ and ○ for tan δ. Gamma irradiation curves are red, non-sterile curves are black, X-ray curves are blue and electron beam curves are pink. TD curves show similar trends between gamma- and X-ray-irradiated samples and are available in the supporting information file—Figure S2.

The *t*-tests performed on MD-γ transition results revealed that non-sterile vs. E-beam irradiation and gamma vs. X-ray irradiations are statistically non-different. The *t*-test results on TD-γ transition data show that only X-ray vs. E-beam irradiation results are statistically significantly different. All $p$-values$_{t\text{-test}}$ are recorded Table S7a,b.

The *t*-tests performed on MD-β transition results revealed that E-beam vs. non-sterile, E-beam vs. gamma irradiations and E-beam vs. X-ray irradiations are statistically significantly different. The *t*-test results on the TD-β transition show that the E-beam vs. non-sterile and E-beam vs. gamma irradiations results are statistically significantly different. All $p$-values$_{t\text{-test}}$ are recorded Table S7c,d.

Hypothesis tests (TOST) were also performed ($p$-values$_{TOST}$ are in Table S8a–d), and for all conditions, $p$-values$_{TOST}$ are <0.05. Equivalences are observed for γ and β transition temperatures (MD or TD).

There is no shift in the relaxation temperatures in irradiated samples (within methodology uncertainties), meaning that the chain motions in the amorphous phase (related to β and γ transitions) are equivalent under gamma and X-ray irradiations. No further crystallization processes occur during irradiation with the different radiation sources.

Polyethylene is a semicrystalline synthetic polymer containing some regions with order (arrangement of the polymer chains) and some other disordered amorphous regions. The manufacturing process creates preferential polymer chain orientation in thin films. There is no influence of the irradiation technology in the crystalline and amorphous parts of the polymers after the film manufacturing process. We showed no change in the thermal and viscoelastic properties for the PE layer, denoting also the absence of significant alteration in structuration (molecular size and cross-linking).

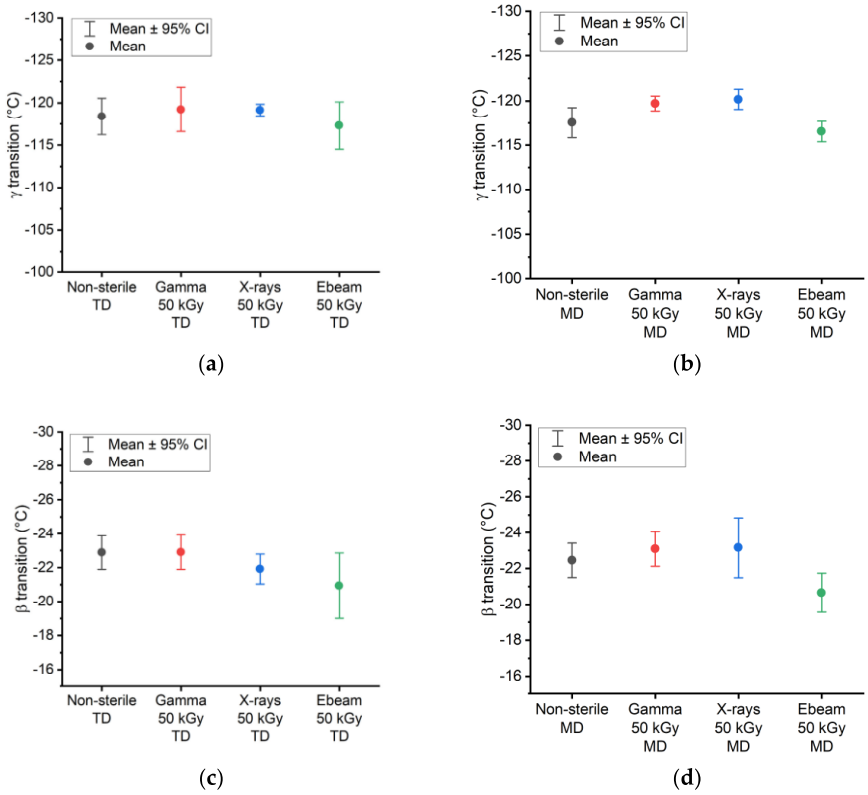


**Figure 6.** γ transition TD (**a**), γ transition MD (**b**), β transition TD (**c**) and β transition MD (**d**) for different irradiation technologies. The error bars were calculated based on two batches (except for E-beam) and from two to five specimens/batch. Raw data are given in the supporting information file—Tables S5 and S6.

## 4. Conclusions

Variations which may have an impact on the quality or performance of a biopharmaceutical film, such as changes in the manufacturing process, e.g., the sterilization technology, were assessed after irradiation. In this paper, tensile (with UTS and elongation at break parameters) and DMA tests were used to monitor mechanical, thermal and viscoelastic properties. It has been shown that no difference is induced, regardless of the irradiation technology used on the material at 50 kGy (using TOST method). These observations are in good agreement with one of our previous studies, which showed no modification in thermal relaxations recorded by DSC [50]. Gamma, electron beam and X-ray irradiation have the same impact on PE/EVOH/PE multilayer film mechanical properties, even for low temperatures, meaning that X-ray and electron beam irradiations could be possible for freeze and thaw applications.

The comparison between gamma, E-beam or X-ray irradiations on the mechanical property effects of PE/EVOH/PE multilayer film have been studied in this paper. To compare and conclude on any potential difference regarding the impact of the irradiation technologies, two statistical methods were used: the two-sample *t*-test and the TOST. We showed that these can afford different conclusions regarding the impact of irradiation technologies on mechanical properties. We observed that the EACs are dependent on sample size, sampling homogeneity and standard deviation of the reference group(s). They can become very high for small sample sizes and large standard deviations. The equivalence criterion may not be strict enough in this case. Whatever the statistical method,

the differences observed are small between each irradiation technology and rather reflect the variation in sampling and testing methodology.

**Supplementary Materials:** The following supporting information can be downloaded at https://www.mdpi.com/article/10.3390/polym15132799/s1, Table S1: Raw data of the mechanical properties obtained by the tensile test on PE/EVOH/PE film (TD); Table S2: Raw data of the mechanical properties obtained by the tensile test on PE/EVOH/PE film (MD); Table S3: *t*-test summary. *p*-values obtained for UTS MD (a), UTS TD (b), elongation MD c) and elongation TD d); Table S4: Equivalence test summary. Null hypothesis: ratio $\leq$ 0.75 or ratio $\geq$ 1.25. Alternative hypothesis: 0.75 < ratio < 1.25. *p*-values obtained for UTS MD (a), UTS TD (b), elongation MD (c) and elongation TD (d); Table S5: Raw data of the thermal transitions obtained by DMA on PE/EVOH/PE film (TD); Table S6: Raw data of the thermal transitions obtained by DMA on PE/EVOH/PE film (MD); Figure S1: Tensile curves of PE/EVOH/PE in MD; Figure S2: Example of DMA curves of PE/EVOH/PE in TD (1 batch, 1 specimen); Table S7: *t*-test summary. *p*-values obtained for $\gamma$ transition MD (a), $\gamma$ transition TD (b), $\beta$ transition MD (c) and $\beta$ transition TD (d); Table S8: Equivalence test summary. Null hypothesis: difference $\leq -5$ or difference $\geq 5$. Alternative hypothesis: $-5$ < difference < 5. *p*-values obtained for $\gamma$ transition MD (a), $\gamma$ transition TD (b), $\beta$ transition MD (c) and $\beta$ transition TD (d).

**Author Contributions:** Conceptualization, N.G.-P., S.R.A.M., N.D. and S.D.; methodology, N.G.-P., S.R.A.M., N.D., B.K. and S.D.; writing—original draft preparation, N.G.-P.; writing—review and editing, N.G.-P., S.R.A.M., N.D., B.K. and S.D. All authors have read and agreed to the published version of the manuscript.

**Funding:** This research received no external funding.

**Institutional Review Board Statement:** Not applicable.

**Data Availability Statement:** Research data are provided in supplementary files.

**Acknowledgments:** We acknowledge Sartorius Stedim FMT S.A.S. for the financial support of this work. N.D. and S.R.A.M. are thankful to AMU and CNRS for their support.

**Conflicts of Interest:** The authors declare no conflict of interest.

## References

1. Vogel, J.D. The Maturation of Single-Use Applications. *BioProcess Int.* **2012**, *10* (Suppl. 5), 10–19.
2. Mahajan, E.; Lye, G.; Eibl-Schindler, R. Bridging Polymer Science to Biotechnology Applications: A Single-Use Technology Conference Report. *BioProcess Int.* 2018. Available online: https://bioprocessintl.com/manufacturing/single-use/bridging-polymer-science-to-biotechnology-applications-a-single-use-technology-conference-report/ (accessed on 1 March 2023).
3. Scott, C. Downstream Disposables: The Latest Single-Use Solutions for Downstream Processing. *BioProcess Int.* 2017. Available online: https://bioprocessintl.com/downstream-processing/downstream-single-use-technologies/downstream-processing-single-use-solutions/ (accessed on 1 March 2023).
4. Guide to Irradiation and Sterilization Validation of Single-Use Bioprocess Systems. *BioProcess Int.* 2008. Available online: https://bioprocessintl.com/upstream-processing/upstream-single-use-technologies/guide-to-irradiation-and-sterilization-validation-of-single-use-bioprocess-systems-183975/ (accessed on 1 March 2023).
5. *ISO 11137-1*; Sterilization of HealthCare Products-Radiation-Part 1: Requirements for Development, Validation and Routine Control of a Sterilization Process for MedicalDevices. ISO: Geneva, Switzerland, 2006.
6. BPSA. *X-ray Sterilization of Single-Use BioProcess Equipment, Part 1: Industry Need, Requirements & Risk Evaluation*; BPSA: Washington, WA, USA, 2021.
7. Dutta, A.; Ghosh, A.K. Investigation on $\gamma$-irradiated PP/ethylene acrylic elastomer TPVs by rheological and thermal approaches. *Radiat. Phys. Chem.* **2018**, *144*, 149–158. [CrossRef]
8. Abdel Tawab, K.; Ibrahim, S.M.; Magida, M.M. The effect of gamma irradiation on mechanical, and thermal properties of recycling polyethylene terephthalate and low density polyethylene (R-PET/LDPE) blend compatibilized by ethylene vinyl acetate (EVA). *J. Radioanal. Nucl. Chem.* **2013**, *295*, 1313–1319. [CrossRef]
9. Buttafava, A.; Consolati, G.; Mariani, M.; Quasso, F.; Ravasio, U. Effects induced by gamma irradiation of different polyesters studied by viscometry, thermal analysis and positron annihilation spectroscopy. *Polym. Degrad. Stab.* **2005**, *89*, 133–139. [CrossRef]
10. Hyun Kang, P. The effect of $\gamma$-irradiation on ultra-high molecular weight polyethylene recrystallized under different cooling conditions. *Radiat. Phys. Chem.* **2001**, *60*, 79–87. [CrossRef]
11. Montanari, L.; Costantini, M.; Signoretti, E.C.; Valvo, L.; Santucci, M.; Bartolomei, M.; Fattibene, P.; Onori, S.; Faucitano, A.; Conti, B.; et al. Gamma irradiation effects on poly(dl-lactictide-co-glycolide) microspheres. *J. Control. Release* **1998**, *56*, 219–229. [CrossRef] [PubMed]

12. Hemmerich, K.J. Medical Device and Diagnostic Industry. 2000. Available online: https://www.mddionline.com/materials/polymer-materials-selection-radiation-sterilized-products (accessed on 1 March 2023).
13. Şen, M.; Çopuroğlu, M. A comparative study of gamma irradiation of poly(ethylene-co-vinyl acetate) and poly(ethylene-co-vinyl acetate)/carbon black mixture. *Mater. Chem. Phys.* **2005**, *93*, 154–158. [CrossRef]
14. Stoffers, N.H.; Linssen, J.P.H.; Franz, R.; Welle, F. Migration and sensory evaluation of irradiated polymers. *Radiat. Phys. Chem.* **2004**, *71*, 205–208. [CrossRef]
15. Dutta, S.K.; Bhowmick, A.K.; Mukunda, P.G.; Chaki, T.K. Thermal degradation studies of electron beam cured ethylene-vinyl acetate copolymer. *Polym. Degrad. Stab.* **1995**, *50*, 75–82. [CrossRef]
16. Demertzis, P.G.; Franz, R.; Welle, F. The effects of γ-irradiation on compositional changes in plastic packaging films. *Packag. Technol. Sci.* **1999**, *12*, 119–130. [CrossRef]
17. Milosavljevic, B.H.; Thomas, J.K. Effects of the degree of hydrolysis on radiation induced reactions in the poly(vinyl alcohol)–poly(vinyl acetate) system. *Radiat. Phys. Chem.* **2001**, *62*, 3–10. [CrossRef]
18. Zainuddin, Z.; Hill, D.J.T.; Le, T.T. An ESR study on γ-irradiated poly(vinyl alcohol). *Radiat. Phys. Chem.* **2001**, *62*, 283–291. [CrossRef]
19. Rao, B.S.; Murthy, M.R. Electron spin resonance and UV absorption of irradiated poly(vinyl alcohol). *J. Polym. Sci. Part B Polym. Phys.* **1987**, *25*, 1897–1902. [CrossRef]
20. Suarez, J.C.M.; Mano, E.B. Characterization of degradation on gamma-irradiated recycled polyethylene blends by scanning electron microscopy. *Polym. Degrad. Stab.* **2001**, *72*, 217–221. [CrossRef]
21. Chapiro, A. Radiation chemistry of polymers. *Radiat. Res.* **1964**, *4*, 179–191. [CrossRef]
22. Fifield, L.S.; Pharr, M.; Staack, D.; Pillai, S.D.; Nichols, L.; McCoy, J.; Faucette, T.; Bisel, T.T.; Huang, M.; Hasan, M.K.; et al. Direct comparison of gamma, electron beam and X-ray irradiation effects on single-use blood collection devices with plastic components. *Radiat. Phys. Chem.* **2021**, *180*, 109282. [CrossRef]
23. Brouwer, H.D. Comparison of the effects of X-ray and gamma irradiation on engineering thermoplastics. *Radiat. Phys. Chem.* **2022**, *193*, 109999. [CrossRef]
24. Manfredini, M.; Atzei, D.; Elsener, B.; Marchetti, A.; Rossi, A. Degradation of plasticized PVC for biomedical disposable device under soft X-ray irradiation. *Surf. Interface Anal.* **2003**, *35*, 294–300. [CrossRef]
25. Nouh, S.A.; El-Nabarawy, H.A.; Abutalib, M.M.; Bahareth, R.A. Effect of X-ray irradiation on the structure, thermal and mechanical properties of polyester. *Eur. Phys. J. Appl. Phys.* **2013**, *62*, 30201. [CrossRef]
26. Fintzou, A.T.; Kontominas, M.G.; Badeka, A.V.; Stahl, M.R.; Riganakos, K.A. Effect of electron-beam and gamma-irradiation on physicochemical and mechanical properties of polypropylene syringes as a function of irradiation dose: Study under vacuum. *Radiat. Phys. Chem.* **2007**, *76*, 1147–1155. [CrossRef]
27. Hassan, M.M.; El-kelesh, N.A.; Dessouki, A.M. The effect of gamma and electron beam irradiation on the thermal and mechanical properties of injection-moulded high crystallinity poly(propylene). *Polym. Compos.* **2008**, *29*, 883–889. [CrossRef]
28. Badia, A.; Duplâtre, G. Electron beam and gamma irradiation effects on high density polyethylene studied via positron annihilation lifetime spectroscopy. *Radiat. Phys. Chem.* **1999**, *54*, 151–158. [CrossRef]
29. Croonenborghs, B.; Smith, M.A.; Strain, P. X-ray versus gamma irradiation effects on polymers. *Radiat. Phys. Chem.* **2007**, *76*, 1676–1678. [CrossRef]
30. Audran, G.; Dorey, S.; Dupuy, N.; Gaston, F.; Marque, S.R.A. Degradation of γ-irradiated polyethylene-ethylene vinyl alcohol-polyethylene multilayer films: An ESR study. *Polym. Degrad. Stab.* **2015**, *122*, 169–179. [CrossRef]
31. Girard-Perier, N.; Claeys-Bruno, M.; Marque, S.R.A.; Dupuy, N.; Gaston, F.; Dorey, S. Monitoring of peroxide in gamma irradiated PE/EVOH/PE multilayer film using methionine probe. *Food Bioprod. Process.* **2022**, *132*, 226–232. [CrossRef]
32. Dorey, S.; Gaston, F.; Marque, S.R.A.; Bortolotti, B.; Dupuy, N. XPS analysis of PE and EVA samples irradiated at different γ-doses. *Appl. Surf. Sci.* **2018**, *427*, 966–972. [CrossRef]
33. Dorey, S.; Gaston, F.; Girard-Perier, N.; Dupuy, N.; Marque, S.R.A.; Delaunay, L. Generation of O 2 -Permeation Barrier during the Gamma-Irradiation of Polyethylene/Ethylene-Vinyl Alcohol/Polyethylene Multilayer Film. *Ind. Eng. Chem. Res.* **2019**, *58*, 14115–14123. [CrossRef]
34. Saito, O. On the Effect of High Energy Radiation to Polymers I. Cross-linking and Degradation. *J. Phys. Soc. Jpn.* **1958**, *13*, 198–206. [CrossRef]
35. Saito, O. Effects of High Energy Radiation on Polymers II. End-linking and Gel Fraction. *J. Phys. Soc. Jpn.* **1958**, *13*, 1451–1464. [CrossRef]
36. Yassouridis, C.; Dürauer, A.; Scharl, T.; Leisch, F.; Brocard, C.; Tscheliessnig, A.-L. Strategy to equivalence testing for development and scale up of biopharmaceutical downstream processes. *Chem. Eng. Sci.* **2021**, *235*, 116497. [CrossRef]
37. Schuirmann, D.J. A comparison of the two one-sided tests procedure and the power approach for assessing the equivalence of average bioavailability. *J. Pharmacokinet. Biopharm.* **1987**, *15*, 657–680. [CrossRef] [PubMed]
38. Food and Drug Administration. *Statistical Approaches to Establishing Bioequivalence: Guidance for Industry*; Food and Drug Administration: Silver Spring, MD, USA, 2001.
39. Limentani, G.B.; Ringo, M.C.; Ye, F.; Berquist, M.L.; McSorley, E.O. Beyond the t-test: Statistical equivalence testing. *Anal. Chem.* **2005**, *77*, 221A–226A. [CrossRef] [PubMed]

40. Lakens, D. Equivalence Tests: A Practical Primer for t Tests, Correlations, and Meta-Analyses. *Soc. Psychol. Personal. Sci.* **2017**, *8*, 355–362. [CrossRef]
41. *ISO527-3:1995*; Plastics—Determination of Tensile Properties—Part 3: Test Conditions for Films and Sheets. ISO: Geneva, Switzerla, 1995.
42. Menczel, J.D.; Prime, R.B. (Eds.) *Thermal Analysis of Polymers: Fundamentals and Applications*; John Wiley & Sons: Hoboken, NJ, USA, 2009; ISBN 978-0-471-76917-0.
43. AAMI: Association for the Advancement of Medical Instrumentation. *Compatibility of Materials Subject to Sterilization*; AAMI: Arlington, VA, USA, 2017.
44. Denardin, E.L.G.; Tokumoto, S.; Samios, D. Stress–strain behaviour of poly(ethylene terephthalate) (PET) during large plastic deformation by plane strain compression: The relation between stress–strain curve and thermal history, temperature and strain rate. *Rheol Acta* **2005**, *45*, 142–150. [CrossRef]
45. Nitta, K.-h.; Uchida, Y.; Tanaka, A. Analysis of Stress-Strain Curve of Polyethylene Films by Toda-Lattice Model. *Polym. J.* **1991**, *23*, 895–901. [CrossRef]
46. Greene, J.P. Microstructures of Polymers. In *Automotive Plastics and Composites*; Elsevier: Amsterdam, The Netherlands, 2021; pp. 27–37. ISBN 9780128180082.
47. Munaro, M.; Akcelrud, L. Correlations between composition and crystallinity of LDPE/HDPE blends. *J. Polym. Res.* **2008**, *15*, 83–88. [CrossRef]
48. Nitta, K.-H.; Tanaka, A. Dynamic mechanical properties of metallocene catalyzed linear polyethylenes. *Polymer* **2001**, *42*, 1219–1226. [CrossRef]
49. Matsuo, M.; Bin, Y.; Xu, C.; Ma, L.; Nakaoki, T.; Suzuki, T. Relaxation mechanism in several kinds of polyethylene estimated by dynamic mechanical measurements, positron annihilation, X-ray and 13C solid-state NMR. *Polymer* **2003**, *44*, 4325–4340. [CrossRef]
50. Girard-Perier, N.; Claeys-Bruno, M.; Marque, S.R.A.; Dupuy, N.; Gaston, F.; Dorey, S. Effects of X-ray, electron beam and gamma irradiation on PE/EVOH/PE multilayer film properties. *Chem. Commun.* **2021**, *57*, 11049–11051. [CrossRef]


**Disclaimer/Publisher's Note:** The statements, opinions and data contained in all publications are solely those of the individual author(s) and contributor(s) and not of MDPI and/or the editor(s). MDPI and/or the editor(s) disclaim responsibility for any injury to people or property resulting from any ideas, methods, instructions or products referred to in the content.

# Supporting information : Comparison of gamma, e-beam or X-ray irradiations effects on mechanical properties of PE/EVOH/PE multilayer

Table S1: Raw data of the mechanical properties obtained by tensile test on PE/EVOH/PE film (TD)

| | Irradiation modality (#Batch) | S80 Transversal Direction (TD) | | | | | | |
|---|---|---|---|---|---|---|---|---|
| | | Sample 1 | Sample 2 | Sample 3 | Sample 4 | Sample 5 | Sample 6 | Sample 7 |
| Elongation at Fmax (%) | Gamma 50kGy Batch 2 | 497 | 501 | 488 | 462 | 506 | 491 | - |
| | X-ray 50kGy Batch 3 | 515 | 485 | 508 | 519 | 524 | 527 | - |
| | Gamma 50kGy Batch 2 | 502 | 487 | 484 | 487 | 492 | 488 | - |
| | X-ray 50kGy Batch 2 | 479 | 490 | 478 | 476 | 461 | 495 | - |
| | Non sterile Batch 2 | 522 | 548 | 538 | 540 | 545 | 546 | - |
| | E-beam 50kGy Batch 4 | 461 | 483 | 474 | 461 | 459 | 465 | 477 |
| | E-beam 50kGy Batch 5 | 448 | 455 | 455 | 449 | 474 | 454 | 458 |
| Ultimate Tensile Strength (MPa) | Gamma 50kGy Batch 1 | 15.6 | 15.5 | 15.2 | 14.3 | 15.9 | 15.4 | - |
| | X-ray 50kGy Batch 3 | 16.0 | 15.3 | 16.0 | 16.1 | 16.1 | 16.6 | - |
| | Gamma 50kGy Batch 2 | 15.6 | 15.4 | 15.4 | 15.1 | 15.2 | 15.2 | - |
| | X-ray 50kGy Batch 2 | 15.7 | 15.8 | 15.9 | 15.8 | 15.3 | 16.0 | - |
| | Non sterile Batch 2 | 16.9 | 17.6 | 17.2 | 17.8 | 17.8 | 17.6 | - |
| | E-beam 50kGy Batch 4 | 17.1 | 17.8 | 17.9 | 17.1 | 16.8 | 17.5 | 17.4 |
| | E-beam 50kGy Batch 4 | 16.4 | 16.4 | 16.3 | 16.0 | 17.3 | 16.7 | 16.6 |

Table S2: Raw data of the mechanical properties obtained by tensile test on PE/EVOH/PE film (MD)

| | Irradiation modality | S80 Machine Direction (MD) | | | | | | | |
|---|---|---|---|---|---|---|---|---|---|
| | | Sample 1 | Sample 2 | Sample 3 | Sample 4 | Sample 5 | Sample 6 | Sample 7 | Sample 8 |
| Elongation at Fmax (%) | Gamma 50kGy Batch 1 | 432 | 428 | 438 | 441 | 442 | 427 | - | - |
| | X-ray 50kGy Batch 3 | 439 | 456 | 452 | 458 | 448 | 429 | - | - |
| | Gamma 50kGy Batch 2 | 392 | 408 | 409 | 388 | 395 | 406 | - | - |
| | X-ray 50kGy Batch 2 | 437 | 422 | 410 | 430 | 421 | 416 | - | - |
| | Non sterile Batch 2 | 422 | 423 | 409 | 413 | 415 | 404 | - | - |
| | E-beam 50kGy Batch 4 | 416 | 406 | 393 | 448 | 413 | 411 | 406 | 389 |
| | E-beam 50kGy Batch 5 | 437 | 434 | 437 | 418 | 403 | 437 | 442 | 413 |
| Ultimate Tensile Strength (MPa) | Gamma 50kGy Batch 1 | 16.9 | 16.8 | 17.3 | 17.0 | 17.0 | 16.9 | - | - |
| | X-ray 50kGy Batch 3 | 17.4 | 17.8 | 18.2 | 18.3 | 17.4 | 17.1 | - | - |
| | Gamma 50kGy Batch 2 | 16.1 | 16.6 | 16.6 | 16.1 | 16.4 | 16.4 | - | - |

| | | | | | | | | | |
|---|---|---|---|---|---|---|---|---|---|
| | X-ray 50kGy Batch 2 | 18.2 | 17.2 | 17.0 | 17.5 | 17.5 | 17.1 | - | - |
| | Non sterile Batch 2 | 17.4 | 16.9 | 17.0 | 17.1 | 17.5 | 16.7 | - | - |
| | E-beam 50kGy Batch 4 | 19.1 | 18.5 | 17.9 | 20.3 | 18.8 | 19.7 | 18.9 | 18.0 |
| | E-beam 50kGy Batch 5 | 19.7 | 19.3 | 19.5 | 18.9 | 18.2 | 19.4 | 19.4 | 18.7 |

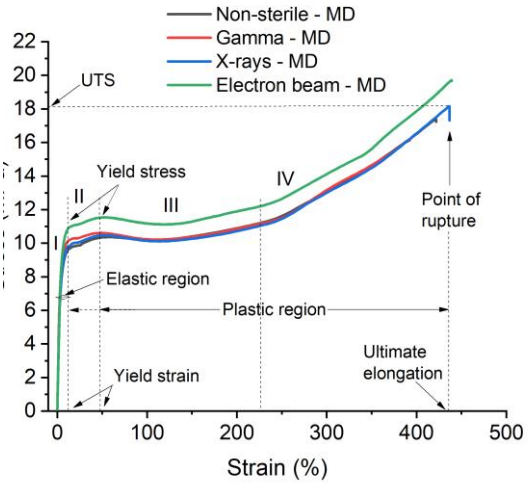


(a)

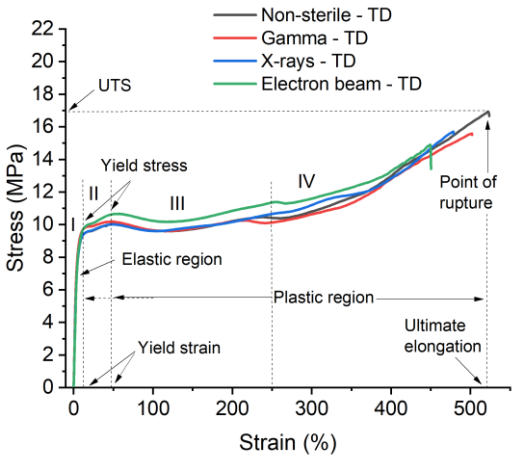


(b)

Figure S1: Tensile curves of PE/EVOH/PE in MD a) and TD b) (1 batch, 1 specimen for each direction) – non sterile in black, gamma irradiated sample in red, X-rays irradiated sample in blue, Electron beam irradiated sample in green. 50+/-5 KGy use for all technologies. UTS and Ultimate elongation values are used for Figure 3 and 4.

Ultimate tensile strength at break and ultimate elongation are defined as the maximum strength and maximum elongation which the material can withstand (ISO 527-1, 2019). Yield strength (or strain) is the strength (or strain) level at which plastic deformation initiates. Importantly, in this section, regarding the EVA and PE bags, the seal part is never damaged during the mechanical test. This means that only the film part is broken by the strain applied (Fig. 3). As observed in Fig. 3b-d, the seal shows no opening or tear and no delamination takes place. Once the interpenetration of the polymer chains has occurred, the seal then keeps its function of sealing, whatever the gamma irradiation dose and the seal location.

Table S3 : T-test summary. p-values obtained for UTS MD a), UTS TD b), Elongation MD c) and Elongation TD d). * means that the difference between 2 values is statistically significant and p-value <5%. ** means that the difference between 2 values is statistically significant and p-value <1%.

a)

| UTS MD | Non-sterile | Gamma | X-rays | E-beam |
|---|---|---|---|---|
| Non-sterile | | * P=0.0288 | * P=0.0439 | ** P=4.10E-7 |
| Gamma | * P=0.0288 | | ** P=3.72E-5 | ** P=7.47E-12 |
| X-rays | * P=0.0439 | ** P=3.72E-5 | | ** P=1.70E-7 |

| | | | | |
|---|---|---|---|---|
| E-beam | ** P=4.10E-7 | ** P=7.47E-12 | ** P=1.70E-7 | |

b)

| UTS TD | Non-sterile | Gamma | X-rays | E-beam |
|---|---|---|---|---|
| Non-sterile | | ** P=4.49E-9 | ** P=1.17E-7 | Non significant |
| Gamma | ** P=4.49E-9 | | ** P=0.00117 | ** P=2.12E-8 |
| X-rays | ** P=1.17E-7 | ** P=0.00117 | | ** P=1.30E-5 |
| E-beam | Non significant | ** P=2.12E-8 | ** P=1.30E-5 | |

c)

| Elong MD | Non-sterile | Gamma | X-rays | E-beam |
|---|---|---|---|---|
| Non-sterile | | Non significant | ** P=0.00979 | Non significant |
| Gamma | Non significant | | * P=0.0254 | Non significant |
| X-rays | ** P=0.00979 | * P=0.0254 | | * P=0.0243 |
| E-beam | Non significant | Non significant | * P=0.0243 | |

d)

| Elong TD | Non-sterile | Gamma | X-rays | E-beam |
|---|---|---|---|---|
| Non-sterile | | ** P=9.49E-8 | ** P=2.78E-4 | ** P=1.11E-11 |
| Gamma | ** P=9.49E-8 | | Non significant | ** P=1.13E-6 |
| X-rays | ** P=2.78E-4 | Non significant | | ** P=2.54E-5 |
| E-beam | ** P=1.11E-11 | ** P=1.13E-6 | ** P=2.54E-5 | |

Test results:

**Test**

Null hypothesis: Ratio ≤ 0,65 or Ratio ≥ 1,35
Alternative hypothesis: 0,65 < Ratio < 1,35
α level: 0,05

| **Null Hypothesis** | **DF** | **T-Value** | **P-Value** |
|---|---|---|---|
| Ratio ≤ 0,65 | 24 | 45,464 | 0,000 |
| Ratio ≥ 1,35 | 24 | -15,821 | 0,000 |

*The greater of the two P-Values is 0,000. Can claim equivalence.*

Table S4 : Equivalence test summary. Null hypothesis: Ratio≤0.75 or Ratio≥1.25. Alternative hypothesis: 0.75<Ratio<1.25. p-values obtained for UTS MD a), UTS TD b), Elongation MD c) and Elongation TD d).

a)

| UTS MD | Non-sterile | Gamma | X-rays | E-beam |
|---|---|---|---|---|
| Non-sterile | | ✓ Ratio ≤0.65: 0.000 Ratio ≥1.35: 0.000 | ✓ Ratio ≤0.65: 0.000 Ratio ≥1.35: 0.000 | ✓ Ratio ≤0.65: 0.000 Ratio ≥1.35: 0.000 |
| Gamma | ✓ Ratio ≤0.65: 0.000 Ratio ≥1.35: 0.000 | | ✓ Ratio ≤0.65: 0.000 Ratio ≥1.35: 0.000 | ✓ Ratio ≤0.65: 0.000 Ratio ≥1.35: 0.000 |
| X-rays | ✓ Ratio ≤0.65: 0.000 Ratio ≥1.35: 0.000 | ✓ Ratio ≤0.65: 0.000 Ratio ≥1.35: 0.000 | | ✓ Ratio ≤0.65: 0.000 Ratio ≥1.35: 0.000 |
| E-beam | ✓ Ratio ≤0.65: 0.000 Ratio ≥1.35: 0.000 | ✓ Ratio ≤0.65: 0.000 Ratio ≥1.35: 0.000 | ✓ Ratio ≤0.65: 0.000 Ratio ≥1.35: 0.000 | |

b)

| UTS TD | Non-sterile | Gamma | X-rays | E-beam |
|---|---|---|---|---|
| Non-sterile | | ✓ Ratio ≤0.65: 0.000 Ratio ≥1.35: 0.000 | ✓ Ratio ≤0.65: 0.000 Ratio ≥1.35: 0.000 | ✓ Ratio ≤0.65: 0.000 Ratio ≥1.35: 0.000 |
| Gamma | ✓ Ratio ≤0.65: 0.000 Ratio ≥1.35: 0.000 | | ✓ Ratio ≤0.65: 0.000 Ratio ≥1.35: 0.000 | ✓ Ratio ≤0.65: 0.000 Ratio ≥1.35: 0.000 |
| X-rays | ✓ Ratio ≤0.65: 0.000 Ratio ≥1.35: 0.000 | ✓ Ratio ≤0.65: 0.000 Ratio ≥1.35: 0.000 | | ✓ Ratio ≤0.65: 0.000 Ratio ≥1.35: 0.000 |
| E-beam | ✓ Ratio ≤0.65: 0.000 Ratio ≥1.35: 0.000 | ✓ Ratio ≤0.65: 0.000 Ratio ≥1.35: 0.000 | ✓ Ratio ≤0.65: 0.000 Ratio ≥1.35: 0.000 | |

c)

| Elong MD | Non-sterile | Gamma | X-rays | E-beam |
|---|---|---|---|---|
| Non-sterile | | ✓ Ratio ≤0.75: 0.000 Ratio ≥1.25: 0.000 | ✓ Ratio ≤0.75: 0.000 Ratio ≥1.25: 0.000 | ✓ Ratio ≤0.75: 0.000 Ratio ≥1.25: 0.000 |
| Gamma | ✓ Ratio ≤0.75: 0.000 Ratio ≥1.25: 0.000 | | ✓ Ratio ≤0.75: 0.000 Ratio ≥1.25: 0.000 | ✓ Ratio ≤0.75: 0.000 Ratio ≥1.25: 0.000 |
| X-rays | ✓ Ratio ≤0.75: 0.000 Ratio ≥1.25: 0.000 | ✓ Ratio ≤0.75: 0.000 Ratio ≥1.25: 0.000 | | ✓ Ratio ≤0.75: 0.000 Ratio ≥1.25: 0.000 |
| E-beam | ✓ Ratio ≤0.75: 0.000 Ratio ≥1.25: 0.000 | ✓ Ratio ≤0.75: 0.000 Ratio ≥1.25: 0.000 | ✓ Ratio ≤0.75: 0.000 Ratio ≥1.25: 0.000 | |

d)

| Elong TD | Non-sterile | Gamma | X-rays | E-beam |
|---|---|---|---|---|
| Non-sterile | | ✓ Ratio ≤0.75: 0.000 Ratio ≥1.25: 0.000 | ✓ Ratio ≤0.75: 0.000 Ratio ≥1.25: 0.000 | ✓ Ratio ≤0.75: 0.000 Ratio ≥1.25: 0.000 |

| | | | | |
|---|---|---|---|---|
| Gamma | ✓<br>Ratio ≤0.75: 0.000<br>Ratio ≥1.25: 0.000 | | ✓<br>Ratio ≤0.75: 0.000<br>Ratio ≥1.25: 0.000 | ✓<br>Ratio ≤0.75: 0.000<br>Ratio ≥1.25: 0.000 |
| X-rays | ✓<br>Ratio ≤0.75: 0.000<br>Ratio ≥1.25: 0.000 | ✓<br>Ratio ≤0.75: 0.000<br>Ratio ≥1.25: 0.000 | | ✓<br>Ratio ≤0.75: 0.000<br>Ratio ≥1.25: 0.000 |
| E-beam | ✓<br>Ratio ≤0.75: 0.000<br>Ratio ≥1.25: 0.000 | ✓<br>Ratio ≤0.75: 0.000<br>Ratio ≥1.25: 0.000 | ✓<br>Ratio ≤0.75: 0.000<br>Ratio ≥1.25: 0.000 | |

Table S5 : Raw data of the thermal transitions obtained by DMA on PE/EVOH/PE film (TD)

| Irradiation modality | Samples | Relaxation 1<br>Max Tan Delta (°C) | Relaxation 2<br>Max E" (°C) |
|---|---|---|---|
| Non sterile<br>Batch 7 | Sample 1 | -121.9 | -23.8 |
| | Sample 2 | -116.7 | -23.7 |
| | Sample 3 | -117.6 | -22.3 |
| | Sample 4 | -119.4 | -21.9 |
| | Sample 5 | -116.3 | -23.7 |
| | Sample 6 | -118.4 | -21.9 |
| E-beam 50 kGy<br>Batch 7 | Sample 1 | -116 | -21.8 |
| | Sample 2 | -117.9 | -20.7 |
| | Sample 3 | -118 | -20.3 |
| Gamma 50kGy<br>Batch 3 | Sample 1 | -118.4 | -21.5 |
| | Sample 2 | -116.2 | -22.7 |
| | Sample 3 | -116.2 | -22.7 |
| | Sample 4 | -120.0 | -24.4 |
| | Sample 5 | -118.0 | -24.2 |
| X-ray 50kGy<br>Batch 6 | Sample 1 | -119.8 | -20.4 |
| | Sample 2 | -119.8 | -21.8 |
| | Sample 3 | -118.0 | -21.7 |
| | Sample 4 | -118.5 | -22.7 |
| | Sample 5 | -119.6 | -22.8 |
| | Sample 6 | -120.4 | -23.5 |
| Gamma 50kGy<br>Batch 2 | Sample 1 | -122.2 | -23.0 |
| | Sample 2 | -123.5 | -21.8 |
| X-ray 50kGy<br>Batch 2 | Sample 1 | -118.6 | -21.1 |
| | Sample 2 | -119.7 | -22.9 |

*Table S6 : Raw data of the thermal transitions obtained by DMA on PE/EVOH/PE film (MD)*

| Irradiation modality | Samples | Relaxation 1<br>Max Tan Delta (°C) | Relaxation 2<br>Max E" (°C) |
|---|---|---|---|
| Non sterile<br>Batch 7 | Sample 1 | -115.7 | -23.2 |
| | Sample 2 | -119.6 | -22.4 |
| | Sample 3 | -117.9 | -21.3 |
| | Sample 4 | -117.1 | -23.1 |
| | Sample 5 | -119.1 | -21.4 |
| | Sample 6 | -115.9 | -23.3 |
| E-beam 50 kGy<br>Batch 7 | Sample 1 | -118.1 | -21.2 |
| | Sample 2 | -115.5 | -19.5 |
| | Sample 3 | -117.2 | -19.7 |
| | Sample 4 | -115.3 | -20.3 |
| | Sample 5 | -116 | -22.3 |
| | Sample 6 | -117.1 | -20.9 |
| Gamma 50kGy<br>Batch 3 | Sample 1 | -118.3 | -23.7 |
| | Sample 2 | -120.5 | -24.1 |
| | Sample 3 | -119.5 | -21.7 |
| | Sample 4 | -119.0 | -22.7 |
| | Sample 5 | -120.9 | -24.2 |
| X-ray 50kGy<br>Batch 6 | Sample 1 | -121.3 | -25.4 |
| | Sample 2 | -120.4 | -25.2 |
| | Sample 3 | -119.9 | -21.1 |
| | Sample 4 | -122.0 | -21.4 |
| | Sample 5 | -119.7 | -24.4 |
| Gamma 50kGy<br>Batch 2 | Sample 1 | -119.6 | -23.4 |
| | Sample 2 | -120.2 | -21.8 |
| X-ray 50kGy<br>Batch 2 | Sample 1 | -118.3 | -22.5 |
| | Sample 2 | -119.6 | -22.1 |

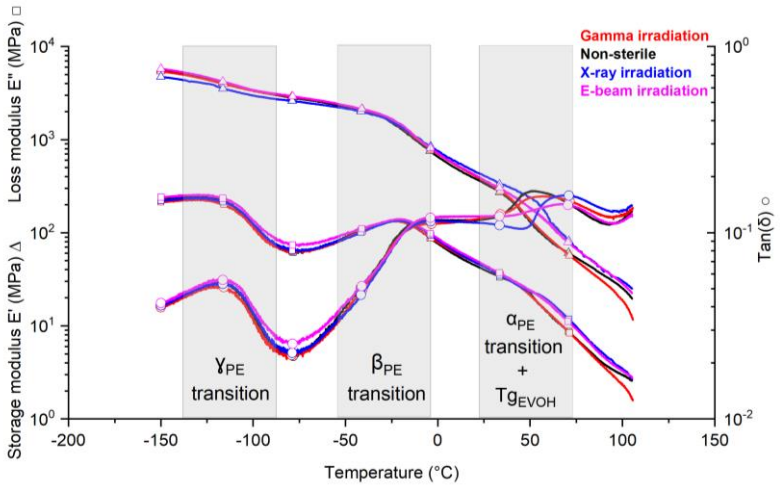


*Figure S2 : Example of DMA curves of PE/EVOH/PE in TD (1 batch, 1 specimen). Δ for Storage modulus E', □ for Loss modulus E" and ○ for tan δ Gamma irradiation curves are red, non-sterile are black, X-rays are blue and electron beam are pink. Gamma irradiation curves are red, non-sterile are black, X-rays are blue and electron beam are pink.*

*Table S7: T-test summary. p-values obtained for γ transition MD a), γ transition TD b), β transition MD c) and β transition TD d). * means that the difference between 2 values is statistically significant and p-value <5%. ** means that the difference between 2 values is statistically significant and p-value <1%.*

a)

| γ transition MD | Non-sterile | Gamma | X-rays | E-beam |
|---|---|---|---|---|
| Non-sterile | | * P=0.0111 | ** P=0.00657 | Non significant |
| Gamma | * P=0.0111 | | Non significant | ** P=1.31E-4 |
| X-rays | ** P=0.00657 | Non significant | | ** P=1.55E-4 |
| E-beam | Non significant | ** P=1.31E-4 | ** P=1.55E-4 | |

b)

| γ transition TD | Non-sterile | Gamma | X-rays | E-beam |
|---|---|---|---|---|
| Non-sterile | | Non significant | Non significant | Non significant |
| Gamma | Non significant | | Non significant | Non significant |
| X-rays | Non significant | Non significant | | * P=0.0147 |
| E-beam | Non significant | Non significant | * P=0.0147 | |

c)

| β transition MD | Non-sterile | Gamma | X-rays | E-beam |
|---|---|---|---|---|
| Non-sterile | | Non significant | Non significant | ** P=0.00970 |
| Gamma | Non significant | | Non significant | ** P=0.00146 |
| X-rays | Non significant | Non significant | | * P=0.0124 |

| | | | | |
|---|---|---|---|---|
| E-beam | **<br>P=0.00970 | **<br>P=0.00146 | *<br>P=0.0124 | |

d)

| β transition TD | Non-sterile | Gamma | X-rays | E-beam |
|---|---|---|---|---|
| Non-sterile | | Non significant | Non significant | *<br>P=0.0187 |
| Gamma | Non significant | | Non significant | *<br>P=0.0239 |
| X-rays | Non significant | Non significant | | Non significant |
| E-beam | *<br>P=0.0187 | *<br>P=0.0239 | Non significant | |

*Table S8: Equivalence test summary. Null hypothesis: Difference≤-5 or Difference≥5. Alternative hypothesis: -5<Difference<5. p-values obtained for γ transition MD a), γ transition TD b), β transition MD c), β transition TD d) ü: equivalence*

a)

| γ transition MD | Non-sterile | Gamma | X-rays | E-beam |
|---|---|---|---|---|
| Non-sterile | | ✓<br>Difference≤-5: 0.003<br>Difference≥5: 0.000 | ✓<br>Difference≤-5: 0.008<br>Difference≥5: 0.000 | ✓<br>Difference≤-5: 0.000<br>Difference≥5: 0.001 |
| Gamma | ✓<br>Difference≤-5: 0.003<br>Difference≥5: 0.000 | | ✓<br>Difference≤-5: 0.000<br>Difference≥5: 0.000 | ✓<br>Difference≤-5: 0.000<br>Difference≥5: 0.005 |
| X-rays | ✓<br>Difference≤-5: 0.008<br>Difference≥5: 0.000 | ✓<br>Difference≤-5: 0.000<br>Difference≥5: 0.000 | | ✓<br>Difference≤-5: 0.000<br>Difference≥5: 0.030 |
| E-beam | ✓<br>Difference≤-5: 0.000<br>Difference≥5: 0.001 | ✓<br>Difference≤-5: 0.000<br>Difference≥5: 0.005 | ✓<br>Difference≤-5: 0.000<br>Difference≥5: 0.030 | |

b)

| γ transition TD | Non-sterile | Gamma | X-rays | E-beam |
|---|---|---|---|---|
| Non-sterile | | ✓<br>Difference≤-5: 0.007<br>Difference≥5: 0.001 | ✓<br>Difference≤-5: 0.002<br>Difference≥5: 0.000 | ✓<br>Difference≤-5: 0.001<br>Difference≥5: 0.005 |
| Gamma | ✓<br>Difference≤-5: 0.007<br>Difference≥5: 0.001 | | ✓<br>Difference≤-5: 0.002<br>Difference≥5: 0.002 | ✓<br>Difference≤-5: 0.000<br>Difference≥5: 0.024 |
| X-rays | ✓<br>Difference≤-5: 0.002<br>Difference≥5: 0.000 | ✓<br>Difference≤-5: 0.002<br>Difference≥5: 0.002 | | ✓<br>Difference≤-5: 0.005<br>Difference≥5: 0.026 |
| E-beam | ✓<br>Difference≤-5: 0.001<br>Difference≥5: 0.005 | ✓<br>Difference≤-5: 0.000<br>Difference≥5: 0.024 | ✓<br>Difference≤-5: 0.005<br>Difference≥5: 0.026 | |

c)

| β transition MD | Non-sterile | Gamma | X-rays | E-beam |
|---|---|---|---|---|
| Non-sterile | | ✓<br>Difference≤-5: 0.000<br>Difference≥5: 0.000 | ✓<br>Difference≤-5: 0.000<br>Difference≥5: 0.000 | ✓<br>Difference≤-5: 0.000<br>Difference≥5: 0.000 |
| Gamma | ✓<br>Difference≤-5: 0.000<br>Difference≥5: 0.000 | | ✓<br>Difference≤-5: 0.000<br>Difference≥5: 0.000 | ✓<br>Difference≤-5: 0.000<br>Difference≥5: 0.001 |
| X-rays | ✓<br>Difference≤-5: 0.000<br>Difference≥5: 0.000 | ✓<br>Difference≤-5: 0.000<br>Difference≥5: 0.000 | | ✓<br>Difference≤-5: 0.000<br>Difference≥5: 0.006 |
| E-beam | ✓<br>Difference≤-5: 0.000<br>Difference≥5: 0.000 | ✓<br>Difference≤-5: 0.000<br>Difference≥5: 0.001 | ✓<br>Difference≤-5: 0.000<br>Difference≥5: 0.006 | |

d)

| β transition TD | Non-sterile | Gamma | X-rays | E-beam |
|---|---|---|---|---|
| Non-sterile | | ✓<br>Difference≤-5: 0.000<br>Difference≥5: 0.000 | ✓<br>Difference≤-5: 0.000<br>Difference≥5: 0.000 | ✓<br>Difference≤-5: 0.000<br>Difference≥5: 0.003 |
| Gamma | ✓<br>Difference≤-5: 0.000<br>Difference≥5: 0.000 | | ✓<br>Difference≤-5: 0.000<br>Difference≥5: 0.000 | ✓<br>Difference≤-5: 0.000<br>Difference≥5: 0.002 |
| X-rays | ✓<br>Difference≤-5: 0.000<br>Difference≥5: 0.000 | ✓<br>Difference≤-5: 0.000<br>Difference≥5: 0.000 | | ✓<br>Difference≤-5: 0.000<br>Difference≥5: 0.001 |
| E-beam | ✓<br>Difference≤-5: 0.000<br>Difference≥5: 0.003 | ✓<br>Difference≤-5: 0.000<br>Difference≥5: 0.002 | ✓<br>Difference≤-5: 0.000<br>Difference≥5: 0.001 | |

# 4.2. Étude des effets du débit de dose et de la formation d'espèces réactives dans le film PE/EVOH/PE

Ce chapitre constitue la deuxième partie de l'article présenté dans le chapitre 3.2 [3]. Les deux études s'appuient sur des analyses identiques, mais elles portent sur des matériaux différents. L'article présenté dans ce chapitre est sur le film multicouche PE/EVOH/PE et a été soumis dans la revue *Physical Chemistry Chemical Physics* en 2024. Les conditions expérimentales sont décrites dans le Tableau 5.

L'analyse RPE met en évidence la formation de radicaux hydroxyalkyles après irradiations gamma, rayons X et faisceau d'électrons, avec des cinétiques de décroissance de radicaux équivalentes jusqu'à 60 jours après irradiations. Les signaux RPE obtenus après irradiation sont représentés dans la figure 2 de l'article.

L'étude sur l'oxydation de la méthionine dans la solution de contact avec le film révèle que le débit de dose n'a pas d'impact significatif sur la formation de méthionine sulfoxyde. Le temps de contact avec la solution de méthionine étant le principal facteur influençant l'oxydation.

Les différents processus d'irradiation gamma présentés dans le chapitre 3 ont un impact équivalent sur le film PE/EVOH/PE.

Pour le film EVA et le film PE, quelle que soit la technologie utilisée, un radical identique est généré. La concentration en radical est équivalentes après irradiation par rayons gamma, X et faisceau d'électrons pour chaque film indépendamment. Les cinétiques de décroissance diffèrent entre les deux films. Dans le film EVA/EVOH/EVA, les radicaux disparaissent dans les neuf jours suivant l'irradiation, tandis que dans le film PE/EVOH/PE, ils persistent jusqu'à 60 jours après irradiation. Cette différence pourrait être attribuée à l'épaisseur de la couche d'EVOH et à la différence de formulation des deux films. La couche d'EVOH plus épaisse dans le film PE/EVOH/PE contribue probablement à la formation de radicaux plus stables au fil du temps.

Le film EVA/EVOH/EVA génère plus de méthionine sulfoxyde en contact avec la solution de méthionine que le film PE/EVOH/PE en raison d'une formation accrue de peracides. Dans le film EVA/EVOH/EVA, les radicaux hydroxyalkyles réagissent avec l'oxygène pour former des radicaux peroxyles, qui oxydent ensuite la méthionine. Le film EVA/EVOH/EVA produit plus d'acides carboxyliques, qui réagissent avec le peroxyde d'hydrogène pour former des peracides, augmentant ainsi l'oxydation. En revanche, le film PE/EVOH/PE génère moins d'acides carboxyliques, limitant la formation de

peracides et donc l'oxydation de la méthionine, les mécanismes sont présentés dans l'article et dans la littérature [4].

Pour les deux films, le temps de contact de la solution de méthionine avec le film est un facteur significatif. Pour le film EVA/EVOH/EVA, le débit de dose influence l'oxydation de la solution de méthionine. Ce n'est pas le cas pour le film PE/EVOH/PE.

Pour les deux films, le procédé d'irradiation par rayons gamma mené en milieu industriel a été étudié : single-run (passage devant la source sans temps de repos entre les différents passage) et multiples-runs (plusieurs passages dans le bunker avec des temps de repos inconnus entre les passages). Le procédé d'irradiation n'a pas d'effet significatif sur l'oxydation de la méthionine qui est en contact avec des échantillons irradiés.

Les trois technologies d'irradiation (gamma, rayons X et faisceau d'électrons) ont un impact équivalent sur le film EVA/EVOH/EVA et sur le film PE/EVOH/PE.

ARTICLE

# Investigating dose rate effects and reactive species formation in irradiated multilayer films – part 2 PE/EVOH/PE

Received 00th January 20xx,
Accepted 00th January 20xx

DOI: 10.1039/x0xx00000x

Blanche Krieguer,*[a,b,c] Samuel Dorey,*[a] Nicolas Ludwig,[d] Florent Kuntz[d], Sylvain R.A. Marque ,*[b] Nathalie Dupuy,*[c] Fabien Girard,[c]

This study investigates the impact of gamma rays, X-ray, and electron beam irradiation on PE/EVOH/PE multilayer films focusing on how dose rate influences polymer modifications and the formation of reactive species like peroxides and methionine sulfoxide from methionine solution, which can affect protein stability. Using advanced analytical techniques such as Electron Spin Resonance (ESR) and High-Performance Liquid Chromatography (HPLC), the study measures radical formation and methionine oxidation. Results indicate that post-irradiation ageing and contact time with methionine significantly affect methionine sulfoxide levels, while the impact of dose rate varies by irradiation technology. Oxidation of methionine solution in contact with irradiated film remains consistent whatever gamma, X-ray and e-beam technologies used to irradiate the film.

## Introduction

Following our previous study on ethylene vinyl acetate / ethylene vinyl alcohol / ethylene vinyl acetate (EVA/EVOH/EVA) films[1], this study investigates the impacts of irradiation technologies on polyethylene / ethylene vinyl alcohol / polyethylene (PE/EVOH/PE) multilayer films, essential in the biotechnological and biopharmaceutical sectors. These films are used for storing and transporting biopharmaceutical products and require sterilization, typically through gamma radiation [2–5]. The increasing production of biopharmaceutical products and concerns about the future capacity of gamma radiation sterilization have led to the investigation of alternative methods, including electron beam (e-beam) and X-ray irradiation[6–12].

Electron-beam irradiation uses an electron accelerator to convert electricity into a radiation beam, which can be used directly or to produce X-ray via the Bremsstrahlung effect[13,14]. Both X-ray and gamma rays are photons, but gamma rays come from radioactive sources. Their similar energy deposition patterns allow for an easy transition from gamma-ray to X-ray technologies, with X-ray potentially offering better dose uniformity[12]. E-beams, however, have less penetration due to stronger interactions with matter. One of the key differences among X-ray, e-beam, and gamma-ray technologies is the dose rate, which significantly influences biological and polymer systems. Low-dose-rate (LDR) exposures can enhance cellular repair, while high-dose-rate (HDR) exposures often cause more severe damage. In polymers, dose rate affects properties like cross-linking and oxidation, impacting their application suitability[15].

A multiscale approach is essential to understand the role of dose rate in ionizing radiation exposure, especially in sterilized polymer systems used in biopharmaceuticals. Recent studies have focused on the effects of irradiation on multilayer films, revealing changes in physical, mechanical, and chemical properties[16–27,27–29]. Additionally, irradiation influences the formation of transient species like hydrogen peroxide and hydroxyl radicals, which can affect protein oxidation and function[30,31]. Methionine oxidation, for example, can alter protein stability and efficacy, impacting therapeutic proteins and antibodies[32,33].

This study aims to compare the effects of X-ray, e-beam, and gamma irradiation on PE/EVOH/PE films, focusing on polymer modifications and interactions with biopharmaceutical solutions. We investigate the generation of reactive species, such as peroxides and peracids, through methionine oxidation, using High-Performance Liquid Chromatography (HPLC) and Electron Spin Resonance (ESR) to assess the impacts of each technology. This research extends the observations from Part 1[1], providing deeper insights into the role of dose rate and irradiation technology in polymer applications.

## Materials and methods

### Samples

PE single-use plastics bags investigated are made from a multilayer film, namely the S80 film, composed of one layer of EVOH sandwiched between two layers of PE, with a total

[a] Sartorius Stedim FMT S.A.S, Z.I. Les paluds, Avenue de Jouques CS91051, 13781, Aubagne Cedex, France
[b] Aix Marseille Univ, CNRS, ICR, Case 551, 13397 Marseille, France
[c] Aix Marseille Univ, Avignon Univ, CNRS, IRD, IMBE, Marseille, France
[d] Aerial, 250 Rue Laurent Fries, 67400 Illkirch, France

thickness of approximately 360 µm (Figure 1). Sample bags are provided by Sartorius stedim FMT S.A.S., Aubagne, France.

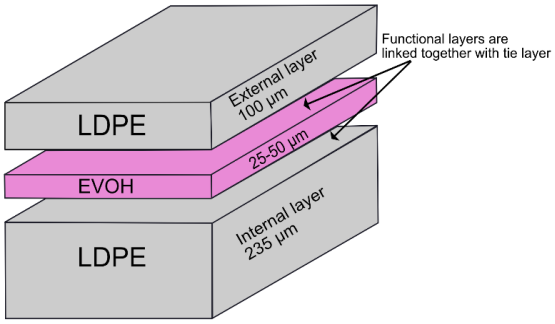


Figure 1: Representation of PE/EVOH/PE multilayer film (S80 film), Low Density PolyEthylene (LDPE) is noted as PE all along the text.

**Samples irradiation**

**Gamma rays**

PE bags were irradiated with gamma rays from $^{60}$Co at Ionisos in Dagneux, France, at an average dose rate of 2 kGy/h. A first process needed several days, accumulating the dose over multiple runs in the irradiation bunker, while the second was completed in a single run. Additionally, PE bags were irradiated with gamma rays from $^{60}$Co at Steris in the USA, with an average dose rate of 8 kGy/h.

**X-ray**

PE bags were irradiated using a 7 MeV Rhodotron at Steris in Däniken, Switzerland, with an average dose rate of 80 kGy/h and a maximum power of 560 kW. Additionally, PE bags were irradiated at Aerial-CRT in Strasbourg, France, using the Feerix facility based on a Rhodotron. A 7 MV X-ray beam was generated by converting a 7 MeV electron beam in a tantalum target. The average dose rate was 13 kGy/h.

**e-beam**

PE bags were irradiated with a 10 MeV Rhodotron at Ionisos in Chaumesnil, France, at a dose rate of 18,000 kGy/h with a power source of 28 kW. Additionally, PE bags underwent e-beam irradiation at Aerial-CRT using the same Feerix® facility as the X-ray treatment. A 10 MeV vertical electron beam was used, with an average dose rate of 18 MGy/h (5 kGy/s), and the irradiation was performed in 50 kGy increments to prevent critical temperature increases in the samples.

**Dosimetry**

The targeted doses were approximately 30, 50, 70, and 100 kGy, depending on the irradiation technology, with a dose accuracy target of ± 10%. There were two phases of irradiation. Table 1 summarizes the dosimetry for the ESR study and Table 2 for the HPLC study. To accurately measure the absorbed dose, alanine pellets with ESR spectroscopy (Magnettech MS5000 ESR, Bruker) were used, along with AerEDE® dosimetry software (Aerial, France). Dosimetry readings were traceable to an international standard. Dosimeters were placed inside the sample box to ensure dose uniformity.

Table 1: Effective doses on samples irradiated by gamma, X-ray and e-beam for ESR analysis

| Target doses (kGy; ± 10%) | | 50 | 100 |
|---|---|---|---|
| Gamma | Ionisos, France (2 kGy/h) | 51 | 90 |
| X-ray | Aerial, France (13 kGy/h) | 50 | 99 |
| e-beam | Aerial, France (18,000 kGy/h) | 55 | 109 |

Table 2: Effective doses on samples irradiated by gamma, X-ray and e-beam for HPLC analysis

| Target doses (kGy; ± 10%) | | 30 | 50 | 70 | 100 |
|---|---|---|---|---|---|
| Gamma | Ionisos, France (1.9 kGy/h) | 29 | 59 | / | / |
| | Ionisos, France (2.4 kGy/h) | 32 | 52 | / | / |
| | Steris, USA (8 kGy/h) | 28 | 54 | / | / |
| X-ray | Aerial, France (13 kGy/h) | 26 | 51 | / | 100 |
| | Steris, Suisse (80 kGy/h) | / | / | 68 | / |
| e-beam | Ionisos, France (18,000 kGy/h) | 25 | 52 | / | / |
| | Aerial, France (18,000 kGy/h) | 25 | 52 | / | / |

**Analytical Methods**

The analytical methods, including ESR, HPLC, and equivalency analysis are described in Part 1.[1]

## Results and discussion

**Electron Spin Resonance**

Figure 2 displays ESR signal of radical species in PE/EVOH/PE multilayer film nine days after irradiation by gamma, X-ray and e-beam at 50 kGy and 100 kGy.

A three-peak signal is observed, and the radical species generated in the PE/EVOH/PE multilayer film are identified as hydroxyalkyl radicals in EVOH, similar to those in the EVA/EVOH/EVA multilayer film[1,20,34].


This journal is © The Royal Society of Chemistry 20xx

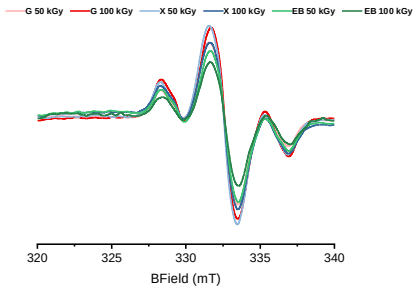


Figure 2: ESR signal of PE/EVOH/PE multilayer film nine days after gamma (red line), X-ray (blue line) and e-beam (green line)

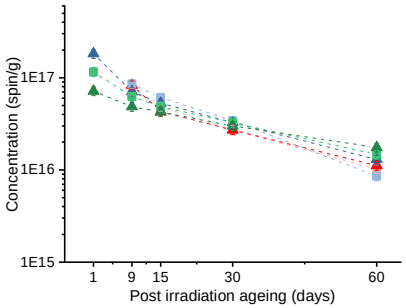


Figure 3: Monitoring of the radicals concentration by ESR as concentration (Spin/g) vs ageing post irradiation (days). Squares correspond to sample irradiated at 50 kGy and triangle correspond to sample irradiated at 100 kGy. Red for gamma, blue for X-ray and green for e-beam

Figure 3 shows small difference in concentration of radical species generated one day after X-ray and e-beam irradiation. Over a longer period, there are no significant differences between the three irradiation technologies, meaning a likely similar process of decay.

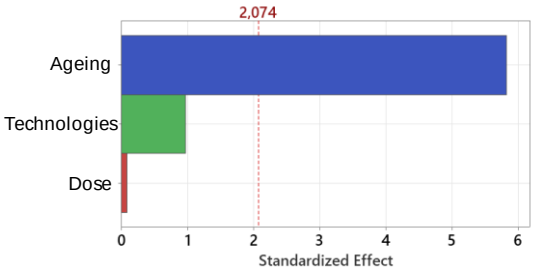


Figure 4: Pareto analysis of significant effects on radical concentration: Ageing post irradiation (blue); Dose (red) and irradiation technologies (gamma, X-ray and e-beam) (green)

Regression model was performed to assess whether the doses, post irradiation ageing, and irradiation technologies significantly influence the amount of radicals generated in the samples (Figure 4).

Only post-irradiation ageing significantly affects the radical concentration, which decreases after irradiation. Equivalent radical species are generated in samples irradiated by the three technologies, regardless of the dose. The equations and coefficients of the regression models obtained for each sample are reported in the SI.

**Oxidation assay by High Performance Liquid Chromatography**

**Comparison of irradiation technology**

As in Part 1[1], the multilayer films were irradiated in different irradiation facilities with varying dose rates for each irradiation technology. The quantity of methionine sulfoxide from methionine solution in contact with the film formed was measured three and six months after irradiation, with the concentrations presented in Figure 5.

The concentration of methionine sulfoxide obtained in contact with the PE/EVOH/PE film is very low compared to that with the EVA/EVOH/EVA film[1,27,35].

Regression models were developed to assess whether the dose rate, the dose, ageing post irradiation, methionine contact time and dose rate can have a significant effect on the methionine sulfoxide concentration generated in the multilayer film. The equation model is represented in (1).

$$\text{Methionine sulfoxide concentration} = 0.132 + 0.00102\ \text{Dose} - 0.0464\ \text{Ageing post irradiation} + 0.04487\ \text{Methionine contact time} + 0.000002\ \text{Dose rate} \quad (1)$$

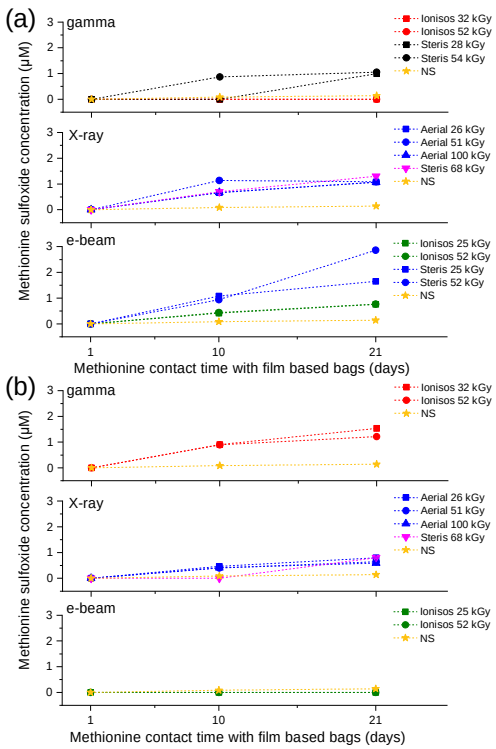


Figure 5: (a) Three months after irradiation. (b) Six months after irradiation. Methionine sulfoxide concentration (µM) in stored solution for 0, 1, 10 and 21 days after irradiation and analyzed by HPLC. Irradiation doses were 30 kGy (square), 50 kGy (circle), 70 kGy (down triangle) and 100 kGy (up triangle). Non irradiated sample are represented in yellow. Irradiations at Ionisos, Dagneux, France were represented in Red (2kGy/h), at Steris, USA, were represented in black (8 kGy/h), at Aerial, France were represented in blue (13 kGy/h for X-ray and 18000 kGy/h for e-beam), at Steris, Daniken, Switzerland were represented in pink (80 kGy/h) and at Ionisos, Chausmenil, France in green (18000 kGy/h).

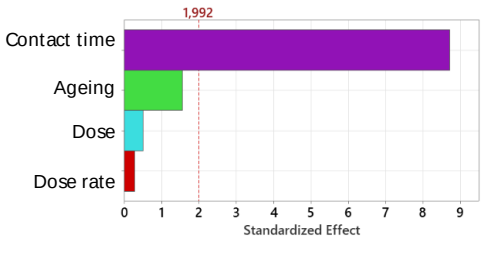


Figure 6: Pareto analysis of significant effects on methionine sulfoxide concentration: Dose (kGy) (blue), Ageing post irradiation (green), methionine contact day (days) (purple) and dose rate (kGy/h) (red).

The regression model results, shown in Figure 6, reveal that only the contact time with the methionine solution significantly affects methionine oxidation, with a coefficient of 0.045 indicating a slight increase in methionine sulfoxide over time. This is in accordance with the results observed in **Erreur ! Source du renvoi introuvable.**. The dose rate, influenced by irradiation technology, does not significantly impact methionine oxidation. Despite varying dose rates among technologies—gamma rays (2 to 8 kGy/h), X-ray (13 to 80 kGy/h), and electron beams (up to 18,000 kGy/h)—the irradiation itself does not seem affect the production of methionine sulfoxide in multilayer films.

### Variation of dose rate

A multiparametric regression model was performed for each irradiation technology to evaluate if variations in dose rate within the same technology impact methionine sulfoxide concentration Figure 7. For e-beam technology, the dose rate is consistent across both irradiation sites, making dose rate comparison for this technology impossible. The gamma equation model is represented in (2) and the X-ray equation model is given as (3).

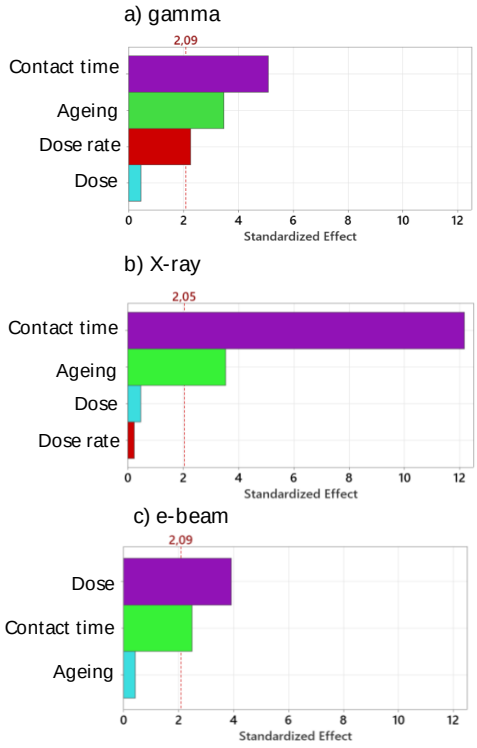


Figure 7: (a) multilayer film irradiated by gamma. (b) multilayer film irradiated by X-ray. (c) multilayer film irradiated by e-beam. Pareto analysis of significant effects on methionine sulfoxide concentration: Dose (kGy) (blue), Ageing post irradiation (green), methionine contact time (days) (purple) and dose rate (kGy/h) (red).

$$\text{Methionine sulfoxide concentration} = -1.095 + 0.00252\ \text{Dose} + 0.1875\ \text{Ageing post irradiation} + 0.03953\ \text{Methionine contact time} + 0.0610\ \text{Dose rate} \quad (2)$$


This journal is © The Royal Society of Chemistry 20xx

Methionine sulfoxide concentration = -0.384 – 0.00057 Dose – 0.0750 Ageing post irradiation + 0.04569 Methionine contact time – 0.00028 Dose rate

(3)

The results from the regression model, depicted in Figure 7, indicate that both the contact time with the methionine solution and the ageing post irradiation significantly influence methionine oxidation for the three irradiation technologies.
The regression model results indicate that for gamma irradiation (Figure 7a), the dose rate significantly impacts methionine oxidation with a p-value equal to 0.035. In contrast, for X-ray irradiation, the dose rate does not have a significant effect on methionine oxidation with a p-value equal to 0.805 (Figure 7b).

**Single-run and multiple-runs gamma irradiation processes**

To complete the study, an HPLC analysis was performed to compare two gamma irradiation processes using the same irradiator at Ionisos in France, maintaining a consistent dose rate of 2 kGy/h. The single run consisted in irradiating continuously samples until reaching the desired dose. The multiple-runs consisted in irradiating samples over multiple runs within the irradiation bunker, with unknown rest times between runs.
Methionine sulfoxide concentration in the solution in contact with the bag was measured by HPLC in samples after 1, 2, 3, 6, 12, 24, and 36 months of irradiation at 30 kGy and 50 kGy (Figure 8 and Figure S1 in SI).

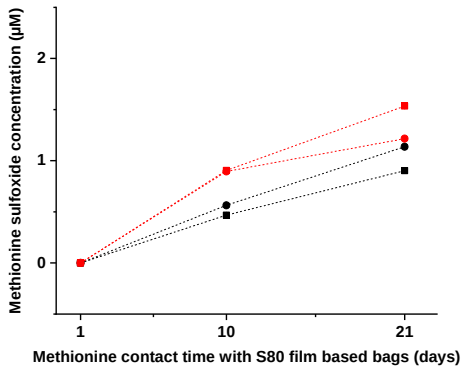


Figure 8: Methionine sulfoxide concentration (µM) in stored solution for 1, 10 and 21 days, 6 months after irradiation and analyzed by HPLC. Irradiation doses were 30 kGy (square), 50 kGy (circle). The irradiation process conducted in a single run is represented in red, while the process conducted in multiple runs is represented in black.

A regression model was developed to assess whether the irradiation process, post-irradiation aging, contact time with the solution, and dose significantly impacted the concentration of methionine sulfoxide formed.

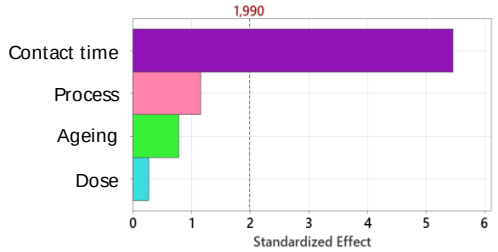


Figure 9: Pareto analysis of significant effects on methionine sulfoxide concentration: Dose (kGy) (blue), Ageing post irradiation (green), methionine contact time (days) (purple) and different process of gamma irradiation (pink)

The regression model (Figure 9) reveals that the contact time with the solution and the multilayer film significantly influence methionine oxidation. Post-irradiation ageing, dose and processing have no significant effect on methionine oxidation in contact with gamma irradiated samples.

## Conclusion

This study provides a comprehensive analysis of the effects of different irradiation technologies on PE/EVOH/PE multilayer films, crucial in the biotechnological and biopharmaceutical industries. ESR analysis highlights the generation of hydroxyalkyl radicals across gamma, X-ray, and electron beam irradiation, with similar decay kinetics observed in radical concentration post-irradiation. The study reveals that the dose rate does not significantly impact methionine sulfoxide formation, with the contact time with methionine solution is the main factor influencing oxidation.
A regression model examining different gamma irradiation processes reveals that the concentration of oxidized methionine remains statistically equivalent whatever the processes.
These findings highlight that the irradiation technologies have similar effects on PE/EVOH/PE films, as demonstrated by both analyses with doses up to 100 kGy.

The ESR study of the EVA/EVOH/EVA [1] and PE/EVOH/PE multilayer films revealed that hydroxyalkyl radicals are generated by irradiation in both films. Regardless of the technology used, the same radical is produced at equivalent concentrations for each material. The kinetics decays differ between the two films. In the EVA/EVOH/EVA film, the radicals decay within nine days post-irradiation, whereas in the PE/EVOH/PE film, they persist for up to 60 days. This difference is attributed to the thickness of the EVOH layer and to the -VOH contents. The thicker EVOH layer in the PE/EVOH/PE film likely contributes to the formation of more stable radicals over time [20].
The EVA/EVOH/EVA film generates more methionine sulfoxide in contact with the methionine solution than the PE/EVOH/PE film due to increased formation of peracids. In the EVA/EVOH/EVA film, hydroxyalkyl radicals react with oxygen to form peroxyl radicals, which then oxidize methionine. The

EVA/EVOH/EVA film produces more carboxylic acids, which react with hydrogen peroxide to form peracids, thereby increasing oxidation. In contrast, the PE/EVOH/PE film generates fewer carboxylic acids, limiting the formation of peracids and thus the oxidation of methionine[27,35].

For both films, the contact time of the methionine solution with the film is a significant factor. The dose rate to irradiate the EVA/EVOH/EVA film impacts the methionine oxidation *in fine*. It is not the case with the PE/EVOH/PE film. For both films processing has no significant effect on methionine oxidation in contact with gamma irradiated samples.

The EVA/EVOH/EVA film is impacted similarly by the three irradiation technologies (gamma, X-ray and e-beam). It is also the case for the PE/EVOH/PE film, with a different extent.

## Data availability

The data supporting this article have been included as part of the ESI.

## Conflicts of interest

There are no conflicts to declare.

## Acknowledgements

N.D., F.G. and S.R.A.M. are thankful to Aix-Marseille Université (AMU), Institut de Recherche pour le Développement (IRD) and Centre National pour la Recherche Scientifique (CNRS) for support.

## Notes and references

1 B. Krieguer, N. Ludwig, S. R. A. Marque, N. Dupuy, F. Girard, F. Kuntz and S. Dorey, Investigating dose rate effects and reactive species formation in irradiated EVA/EVOH/EVA multilayer films – part 1, submitted to *Phys. Chem. Chem. Phys,* 2024.

2 J. D. Vogel, The Maturation of Single-Use Applications, *BioProcess Int.*, 2012, 10–19.

3 E. Mahajan, G. Lye and R. Eibl-Schindler, Brinding polymer Science to Biotechnology Applications: A Single-Use Technology Conference Report, *BioProcess Int,* 2018._

4 ISO 11137-1; Sterilization of HealthCare Products-Radiation-Part 1: Requirements for Development, Validation and Routine control of a Sterilization Process for MedicalDevices. ISO: Geneva, Switzerland, 2006.

5 Guide to Irradiation and Sterilization Validation of Single-Use Bioprocess Systems, *BioProcess Int., 2008.*_

6 N. Dupuy, S. R. A. Marque, L. S. Fifield, M. Pharr, D. Staack, S. D. Pillai, L. Nichols, M. K. Murphy and S. Dorey, Supplementing Gamma Sterilization with X-Ray and E-Beam Technologies, *Bioprocess technical*, 2022, 20, 24–28.

7 BPAS Technical Guide, *X-rays Sterilization of single-Use BioProcess Equipment, Part 1: Industry Need*, Requirements&Risk Evaluation., 2021.

8 P. M. Armenante and O. Akiti, in *Chemical Engineering in the Pharmaceutical Industry*, eds. D. J. am Ende and M. T. am Ende, John Wiley & Sons, Inc., Hoboken, NJ, USA, 2019, pp. 311–379.

9 D. Darwis, Erizal, B. Abbas, F. Nurlidar and D. P. Putra, Radiation Processing of Polymers for Medical and Pharmaceutical Applications, *Macromolecular Symposia*, 2015, 353, 15–23.

10 H. De Brouwer, Comparison of the effects of x-ray and gamma irradiation on engineering thermoplastics, *Radiat. Phys. Chem.*, 2022, 193, 109999.

11 B. Croonenborghs, M. A. Smith and P. Strain, X-ray versus gamma irradiation effects on polymers, *Radiat. Phys. Chem.*, 2007, 76, 1676–1678.

12 T. K. Kroc, Monte Carlo Simulations Demonstrating Physics of Equivalency of Gamma, Electron- beam, and X-ray for Radiation Sterilization, *Radiat. Phys. Chem., 2023, 204, 110702.*_

13 G. Sadler, W. Chappas and D. E. Pierce, Evaluation of e-beam, **γ**- and X-ray treatment on the chemistry and safety of polymers used with pre-packaged irradiated foods: a review, *Food Addit. Contam.*, 2001, 18, 475–501.

14 W. D. Loveland, D. J. Morrissey and G. T. Seaborg, *Modern Nuclear Chemistry*, Wiley, 1st edn., 2017.

15 D. Lowe, L. Roy, M. A. Tabocchini, W. Rühm, R. Wakeford, G. E. Woloschak and D. Laurier, Radiation dose rate effects: what is new and what is needed?, *Radiat Environ Biophys*, 2022, 61, 507–543.

16 F. Gaston, N. Dupuy, S. R. A. Marque, M. Barbaroux and S. Dorey, Impact of γ-irradiation, ageing and their interactions on multilayer films followed by AComDim, *Analytica Chimica Acta*, 2017, **981**, 11–23.

17 F. Gaston, N. Dupuy, S. R. A. Marque, M. Barbaroux and S. Dorey, One year monitoring by FTIR of γ-irradiated multilayer film PE/EVOH/PE, *Radiation Physics and Chemistry*, 2016, **125**, 115–121.

18 S. Dorey, F. Gaston, N. Dupuy, M. Barbaroux and S. R. A. Marque, Reconciliation of pH, conductivity, total organic carbon with carboxylic acids detected by ion chromatography in solution after contact with multilayer films after γ-irradiation, *European Journal of Pharmaceutical Sciences*, 2018, **117**, 216–226.

19 F. Gaston, N. Dupuy, S. R. A. Marque and S. Dorey, Evaluation of multilayer film stability by Raman spectroscopy after gamma-irradiation sterilization process, *Vib. Spectrosc.*, 2018, 96, 52–59.

20 G. Audran, S. Dorey, N. Dupuy, F. Gaston and S. R. A. Marque, Degradation of γ-irradiated polyethylene-ethylene vinyl alcohol-polyethylene multilayer films: An ESR study, *Polym. Degrad. Stab.*, 2015, 122, 169–179.

21 S. Dorey, F. Gaston, S. R. A. Marque, B. Bortolotti and N. Dupuy, XPS analysis of PE and EVA samples irradiated at different γ-doses, *Applied Surface Science*, 2018, **427**, 966–972.

22 S. Dorey, F. Gaston, N. Girard-Perier, N. Dupuy, S. R. A. Marque and L. Delaunay, Generation of $O_2$ -Permeation Barrier during the Gamma-Irradiation of Polyethylene/Ethylene-Vinyl Alcohol/Polyethylene Multilayer Film, *Ind. Eng. Chem. Res.*, 2019, **58**, 14115–14123.

23 N. Girard-Perier, M. Claeys-Bruno, S. R. A. Marque, N. Dupuy, F. Gaston and S. Dorey, Effects of X-ray, electron beam and gamma irradiation on PE/EVOH/PE multilayer film properties, *Chem. Commun.*, 2021, 57, 11049–11051.

24 N. Girard-Perier, F. Gaston, N. Dupuy, S. R. A. Marque, L. Delaunay and S. Dorey, Study of the mechanical behavior of gamma-irradiated single-use bag seals, *Food Packaging Shelf .*, 2020, 26, 100582.

25 N. Girard-Perier, M. Claeys-Bruno, S. R. A. Marque, N. Dupuy, F. Gaston and S. Dorey, Effects of X-ray, electron beam and gamma irradiation on PE/EVOH/PE multilayer film properties, *Chem. Commun.*, 2021, 57, 11049–11051.

26 F. Gaston, N. Dupuy, N. Girard-Perier, S. R. A. Marque and S. Dorey, Comprehensive investigation on physical and chemical properties of γ-irradiated multilayer PE/EVOH/PE film: A multiscale approach, *Applied Research*, 2023, **2**, e202200065.



This journal is © The Royal Society of Chemistry 20xx

27 N. Girard-Perier, M. Claeys-Bruno, S. R. A. Marque, N. Dupuy, F. Gaston and S. Dorey, Monitoring of peroxide in gamma irradiated PE/EVOH/PE multilayer film using methionine probe, *Food Bioprod. Process.*, 2022, 132, 226–232.
28 N. Girard-Perier, S. Dorey, F. Gaston, F. Girard, S. R. A. Marque and N. Dupuy, One-year ageing FTIR monitoring of PE/EVOH/PE film after gamma or electron beam irradiation, *Polym. Degrad. Stab.*, 2022, 195, 109790.
29 N. Girard-Perier, S. R. A. Marque, N. Dupuy, B. Krieguer and S. Dorey, Gamma, E-Beam and X-ray Irradiations on PE/EVOH/PE Multilayer Film: An Industrial Point of View Regarding the Impact on Mechanical Properties, *Polymers*, 2023, 15, 2799.
30 T. Pędzinski, K. Grzyb, K. Skotnicki, P. Filipiak, K. Bobrowski, C. Chatgilialoglu and B. Marciniak, Radiation- and Photo-Induced Oxidation Pathways of Methionine in Model Peptide Backbone under Anoxic Conditions, *Int J Mol Sci*, 2021, 22, 4773.
31 V. Gold, Ed., *The IUPAC Compendium of Chemical Terminology: The Gold Book*, International Union of Pure and Applied Chemistry (IUPAC), Research Triangle Park, NC, 4th edn., 2019.
32 M. A. Rosenfeld, L. V. Yurina and A. D. Vasilyeva, Antioxidant role of methionine-containing intra- and extracellular proteins, *Biophys Rev*, 2023, 15, 367–383.
33 D. Tavella, D. R. Ouellette, R. Garofalo, K. Zhu, J. Xu, E. O. Oloo, C. Negron and P. M. Ihnat, A novel method for in silico assessment of Methionine oxidation risk in monoclonal antibodies: Improvement over the 2-shell model, *PLoS One*, 2022, 17, e0279689.
34 A. G. Davies, J. A. Howard and M. Lehnig, *Magnetic properties of free radicals- Organic O-, P-, Se-, Si-, Ge-, Sn-, Pb-, As-, Sb-Centered Radicals*, 1979, vol. 9 c2.
35 N. Girard-Perier, M. Claeys-Bruno, S. R. A. Marque, N. Dupuy, F. Gaston and S. Dorey, Monitoring of Peroxide in Gamma Irradiated EVA Multilayer Film Using Methionine Probe, *Polymers*, 2020, 12, 3024.

# Supporting information : Investigating dose rate effects and reactive species formation in irradiated multilayer films – part 2 PE/EVOH/PE

## Electron Spin Resonance

### Regression Analysis: generated radical

#### Method

Categorical predictor coding (1; 0)

#### Regression Equation

| Irradiation technologie | | | | |
|---|---|---|---|---|
| e-beam | Spin | = | 78669858412017568 - 1373536940976436 Ageing | + 17373531853056 Dose |
| Gamma | Spin | = | 78041793349616800 - 1373536940976436 Ageing | + 17373531853056 Dose |
| X-ray | Spin | = | 93688358923825104 - 1373536940976436 Ageing | + 17373531853056 Dose |

#### Coefficients

| Term | Coef | SE Coef | T-Value | P-Value | VIF |
|---|---|---|---|---|---|
| Constant | 7,80418E+16 | 1,84487E+16 | 4,23 | 0,000 | |
| Dose | 1,73735E+13 | 1,92651E+14 | 0,09 | 0,929 | 1,00 |
| Ageing post irradiation | -1,37354E+15 | 2,35733E+14 | -5,83 | 0,000 | 1,01 |
| Irradiation technologie | | | | | |
| e-beam | 6,28065E+14 | 1,19055E+16 | 0,05 | 0,958 | 1,43 |
| X-ray | 1,56466E+16 | 1,21552E+16 | 1,29 | 0,211 | 1,42 |

#### Model Summary

| S | R-sq | R-sq(adj) | R-sq(pred) |
|---|---|---|---|
| 2,49498E+16 | 62,60% | 55,80% | 43,28% |

#### Analysis of Variance

| Source | DF | Adj SS | Adj MS | F-Value | P-Value |
|---|---|---|---|---|---|
| Regression | 4 | 2,29204E+34 | 5,73011E+33 | 9,21 | 0,000 |
| Dose | 1 | 5,06254E+30 | 5,06254E+30 | 0,01 | 0,929 |
| Ageing post irradiation | 1 | 2,11337E+34 | 2,11337E+34 | 33,95 | 0,000 |
| Irradiation technologie | 2 | 1,40200E+33 | 7,01000E+32 | 1,13 | 0,342 |
| Error | 22 | 1,36948E+34 | 6,22493E+32 | | |
| Total | 26 | 3,66153E+34 | | | |

#### Fits and Diagnostics for Unusual Observations

| Obs | Spin | Fit | Resid | Std Resid | |
|---|---|---|---|---|---|
| 13 | 1,81976E+17 | 9,40522E+16 | 8,79236E+16 | 3,92 | R |

## Oxidation assay by high Performance Liquid Chromatography

## Comparison of irradiation technology

### Regression Analysis: Gamma, e-beam and X-ray

## Regression Equation

Methionine sulfoxide concentration = 0,132 + 0,00102 Dose - 0,0464 Ageing + 0,04487 Methionine contact time + 0,000002 Dose rate

## Coefficients

| Term | Coef | SE Coef | T-Value | P-Value | VIF |
|---|---|---|---|---|---|
| Constant | 0,132 | 0,171 | 0,77 | 0,444 | |
| Dose | 0,00102 | 0,00199 | 0,51 | 0,609 | 1,09 |
| Ageing | -0,0464 | 0,0298 | -1,56 | 0,124 | 1,01 |
| Methionine contact time | 0,04487 | 0,00515 | 8,71 | 0,000 | 1,00 |
| Dose rate | 0,000002 | 0,000006 | 0,29 | 0,776 | 1,09 |

## Model Summary

| S | R-sq | R-sq(adj) | R-sq(pred) |
|---|---|---|---|
| 0,389551 | 51,15% | 48,55% | 43,34% |

## Analysis of Variance

| Source | DF | Adj SS | Adj MS | F-Value | P-Value |
|---|---|---|---|---|---|
| Regression | 4 | 11,9178 | 2,9794 | 19,63 | 0,000 |
| Dose | 1 | 0,0401 | 0,0401 | 0,26 | 0,609 |
| Ageing | 1 | 0,3672 | 0,3672 | 2,42 | 0,124 |
| Methionine contact time | 1 | 11,5143 | 11,5143 | 75,88 | 0,000 |
| Dose rate | 1 | 0,0123 | 0,0123 | 0,08 | 0,776 |
| Error | 75 | 11,3813 | 0,1518 | | |
| Lack-of-Fit | 67 | 8,4520 | 0,1261 | 0,34 | 0,992 |
| Pure Error | 8 | 2,9292 | 0,3662 | | |
| Total | 79 | 23,2991 | | | |

## Fits and Diagnostics for Unusual Observations

| Obs | Methionine sulfoxide concentrat | Fit | Resid | Std Resid | |
|---|---|---|---|---|---|
| 4 | 0,000 | 0,960 | -0,960 | -2,56 | R |
| 8 | 0,000 | 0,986 | -0,986 | -2,61 | R |
| 72 | 2,861 | 1,014 | 1,847 | 4,95 | R |
| 76 | 0,000 | 0,849 | -0,849 | -2,30 | R |
| 80 | 0,000 | 0,875 | -0,875 | -2,36 | R |

*R Large residual*

# Regression Analysis: Gamma

## Regression Equation

Methionine sulfoxide concentration = -1,095 + 0,00252 Dose + 0,1875 Ageing post irradiation + 0,03953 Methionine contact time + 0,0610 Dose rate

## Coefficients

| Term | Coef | SE Coef | T-Value | P-Value | VIF |
|---|---|---|---|---|---|
| Constant | -1,095 | 0,356 | -3,07 | 0,006 | |
| Dose | 0,00252 | 0,00560 | 0,45 | 0,657 | 1,01 |
| Ageing post irradiation | 0,1875 | 0,0538 | 3,48 | 0,002 | 1,34 |
| Methionine contact time | 0,03953 | 0,00776 | 5,09 | 0,000 | 1,00 |
| Dose rate | 0,0610 | 0,0268 | 2,28 | 0,035 | 1,33 |

## Model Summary

| S | R-sq | R-sq(adj) | R-sq(pred) |
|---|---|---|---|

| | | | |
|---|---|---|---|
| 0,321626 | 67,23% | 60,33% | 45,77% |

### Analysis of Variance

| Source | DF | Adj SS | Adj MS | F-Value | P-Value |
|---|---|---|---|---|---|
| Regression | 4 | 4,03165 | 1,00791 | 9,74 | 0,000 |
| Dose | 1 | 0,02100 | 0,02100 | 0,20 | 0,657 |
| Ageing post irradiation | 1 | 1,25591 | 1,25591 | 12,14 | 0,002 |
| Methionine contact time | 1 | 2,68127 | 2,68127 | 25,92 | 0,000 |
| Dose rate | 1 | 0,53548 | 0,53548 | 5,18 | 0,035 |
| Error | 19 | 1,96542 | 0,10344 | | |
| Total | 23 | 5,99707 | | | |

## Regression Analysis: X-ray

### Regression Equation

Methionine sulfoxide = 0,384 - 0,00057 Dose_2 - 0,0750 Ageing post irradiation_2 + 0,04569 Methionine contact time_2 - 0,00028 Dose rate_2

### Coefficients

| Term | Coef | SE Coef | T-Value | P-Value | VIF |
|---|---|---|---|---|---|
| Constant | 0,384 | 0,128 | 3,00 | 0,006 | |
| Dose | -0,00057 | 0,00118 | -0,48 | 0,633 | 1,03 |
| Ageing post irradiation | -0,0750 | 0,0212 | -3,54 | 0,001 | 1,00 |
| Methionine contact time | 0,04569 | 0,00376 | 12,16 | 0,000 | 1,00 |
| Dose rate | -0,00028 | 0,00111 | -0,25 | 0,805 | 1,04 |

### Model Summary

| S | R-sq | R-sq(adj) | R-sq(pred) |
|---|---|---|---|
| 0,179672 | 85,63% | 83,50% | 80,56% |

### Analysis of Variance

| Source | DF | Adj SS | Adj MS | F-Value | P-Value |
|---|---|---|---|---|---|
| Regression | 4 | 5,19352 | 1,29838 | 40,22 | 0,000 |
| Dose | 1 | 0,00752 | 0,00752 | 0,23 | 0,633 |
| Ageing post irradiation | 1 | 0,40553 | 0,40553 | 12,56 | 0,001 |
| Methionine contact time | 1 | 4,77667 | 4,77667 | 147,97 | 0,000 |
| Dose rate | 1 | 0,00200 | 0,00200 | 0,06 | 0,805 |
| Error | 27 | 0,87161 | 0,03228 | | |
| Total | 31 | 6,06514 | | | |

### Fits and Diagnostics for Unusual Observations

| Obs | Methionine sulfoxide | Fit | Resid | Std Resid | |
|---|---|---|---|---|---|
| 7 | 1,1365 | 0,5839 | 0,5527 | 3,20 | R |

*R Large residual*

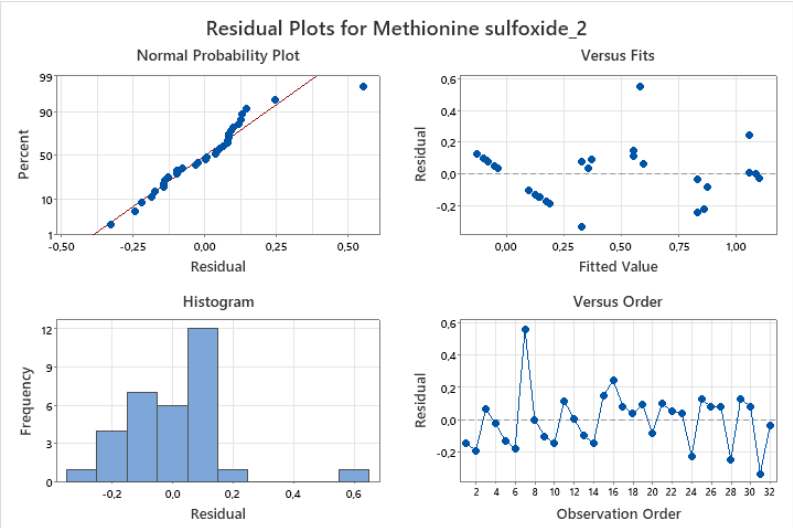


# Regression Analysis: e-beam

## Regression Equation

Methionine sulfoxide = 0,584 + 0,00367 Dose - 0,1858 Ageing post irradiation + 0,0491 Methionine contact time

## Coefficients

| Term | Coef | SE Coef | T-Value | P-Value | VIF |
|---|---|---|---|---|---|
| Constant | 0,584 | 0,458 | 1,28 | 0,217 | |
| Dose | 0,00367 | 0,00843 | 0,43 | 0,668 | 1,00 |
| Ageing post irradiation | -0,1858 | 0,0745 | -2,49 | 0,022 | 1,00 |
| Methionine contact time | 0,0491 | 0,0125 | 3,94 | 0,001 | 1,00 |

## Model Summary

| S | R-sq | R-sq(adj) | R-sq(pred) |
|---|---|---|---|
| 0,516446 | 52,28% | 45,13% | 24,71% |

## Analysis of Variance

| Source | DF | Adj SS | Adj MS | F-Value | P-Value |
|---|---|---|---|---|---|
| Regression | 3 | 5,8450 | 1,94832 | 7,30 | 0,002 |
| Dose | 1 | 0,0504 | 0,05044 | 0,19 | 0,668 |
| Ageing post irradiation | 1 | 1,6569 | 1,65685 | 6,21 | 0,022 |
| Methionine contact time | 1 | 4,1377 | 4,13766 | 15,51 | 0,001 |
| Error | 20 | 5,3343 | 0,26672 | | |
| Lack-of-Fit | 12 | 2,4051 | 0,20042 | 0,55 | 0,833 |
| Pure Error | 8 | 2,9292 | 0,36615 | | |
| Total | 23 | 11,1793 | | | |

## Fits and Diagnostics for Unusual Observations

| Obs | Methionine sulfoxide | Fit | Resid | Std Resid | |
|---|---|---|---|---|---|
| 16 | 2,861 | 1,242 | 1,619 | 3,51 | R |

*R Large residual*

# Regression Analysis: gamma radiation process

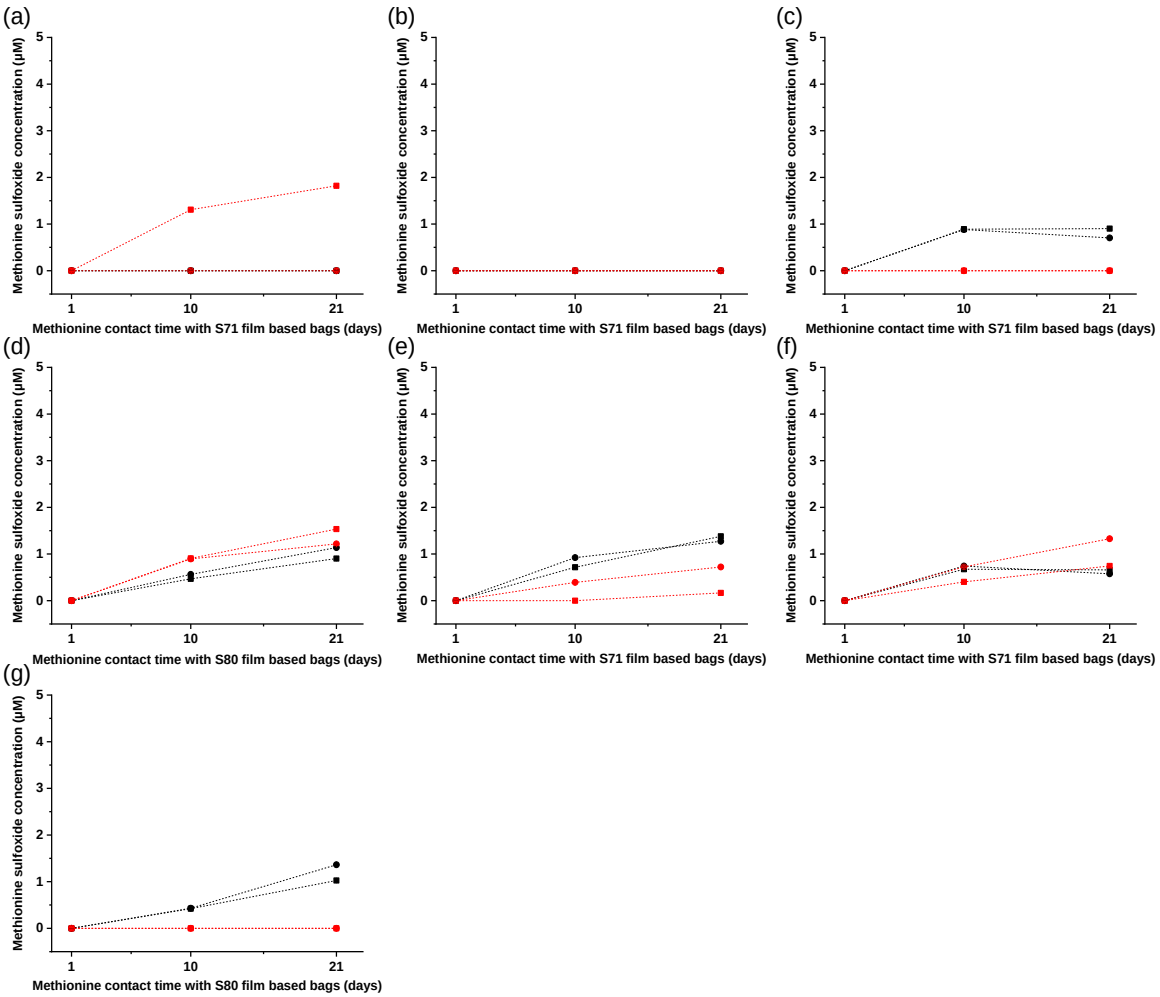


Figure S1: Methionine sulfoxide concentration (µM) in stored solution was measured at 0, 1, 10, and 21 days after gamma irradiation and analyzed by HPLC. The irradiation doses were 30 kGy (square) and 50 kGy (circle). The irradiation process conducted in a single run is represented in red, while the process conducted in multiple runs is represented in black. The measurements were taken at the following intervals after irradiation: (a) 1 month, (b) 2 months, (c) 3 months, (d) 6 months, (e) 12 months, (f) 24 months, and (g) 36 months.

## Method

| | |
|---|---|
| Categorical predictor coding | (1; 0) |

## Regression Equation

| Irradiation process | | | |
|---|---|---|---|
| S1 | methionine sulfoxide | = | 0,083 - 0,00125 Dose + 0,00295 Ageing post irradiation + 0,03074 Methionine contact time |
| S2 | methionine sulfoxide | = | -0,024 - 0,00125 Dose + 0,00295 Ageing post irradiation + 0,03074 Methionine contact time |

## Coefficients

| Term | Coef | SE Coef | T-Value | P-Value | VIF |
|---|---|---|---|---|---|
| Constant | 0,083 | 0,209 | 0,39 | 0,694 | |
| Dose | -0,00125 | 0,00461 | -0,27 | 0,787 | 1,00 |
| Ageing post irradiation | 0,00295 | 0,00375 | 0,79 | 0,434 | 1,00 |
| Methionine contact time | 0,03074 | 0,00563 | 5,46 | 0,000 | 1,00 |
| Irradiation process | | | | | |
| S2 | -0,1065 | 0,0921 | -1,16 | 0,251 | 1,00 |

## Model Summary

| S | R-sq | R-sq(adj) | R-sq(pred) |
|---|---|---|---|
| 0,422276 | 28,70% | 25,09% | 19,28% |

## Analysis of Variance

| Source | DF | Adj SS | Adj MS | F-Value | P-Value |
|---|---|---|---|---|---|
| Regression | 4 | 5,6701 | 1,41753 | 7,95 | 0,000 |
| Dose | 1 | 0,0131 | 0,01312 | 0,07 | 0,787 |
| Ageing post irradiation | 1 | 0,1104 | 0,11036 | 0,62 | 0,434 |
| Methionine contact time | 1 | 5,3086 | 5,30858 | 29,77 | 0,000 |
| Irradiation process | 1 | 0,2380 | 0,23804 | 1,33 | 0,251 |
| Error | 79 | 14,0870 | 0,17832 | | |
| Total | 83 | 19,7571 | | | |

## Fits and Diagnostics for Unusual Observations

| Obs | methionine sulfoxide | Fit | Resid | Std Resid |
|---|---|---|---|---|
| 8 | 1,308 | 0,249 | 1,059 | 2,57 R |
| 9 | 1,820 | 0,587 | 1,233 | 3,02 R |
| 45 | 1,534 | 0,602 | 0,932 | 2,27 R |

*R Large residual*

# Références Chapitre 4

1. Poirier, J. Estimateurs et tests d'hypothèses. *Instrumentation et méthodes de mesure* **1992**, doi:10.51257/a-v1-r250.

2. Girard-Perier, N.; Claeys-Bruno, M.; Marque, S.R.A.; Dupuy, N.; Gaston, F.; Dorey, S. Effects of X-Ray, Electron Beam and Gamma Irradiation on PE/EVOH/PE Multilayer Film Properties. *Chemical Communications* **2021**, *57*, 11049–11051, doi:10.1039/D1CC02871E.

3. Krieguer, B.; Ludwig, N.; Marque, S.R.A.; Dupuy, N.; Girard, F.; Kuntz, F.; Dorey, S. Investigating Dose Rate Effects and Reactive Species Formation in Irradiated EVA/EVOH/EVA Multilayer Films – Part 1. *Physical Chemistry Chemical Physics* **2024**.

4. Girard-Perier, N.; Claeys-Bruno, M.; Marque, S.R.A.; Dupuy, N.; Gaston, F.; Dorey, S. Monitoring of Peroxide in Gamma Irradiated PE/EVOH/PE Multilayer Film Using Methionine Probe. *Food and Bioproducts Processing* **2022**, *132*, 226–232, doi:10.1016/j.fbp.2022.02.001.

# Chapitre 5 : Comparaison de l'impact de l'irradiation gamma, rayons X et faisceau d'électrons sur les matériaux polymères

Dans ce chapitre nous avons choisi d'étudier le comportement après irradiations de matériaux constituants différentes pièces des solutions à usage unique du PP, du PE et du PA. Les matériaux formulés à partir de polyamides, connus pour leur résistance à l'abrasion, aux produits chimiques, à la corrosion et aussi pour leur flexibilité, sont couramment utilisés dans les colliers de serrage, les unions et pinces tri-clamp. Les polyoléfines, reconnu pour leurs excellentes performances, leurs stabilités chimiques, leurs propriétés mécaniques et thermiques sont fréquemment utilisées dans la production de pinces coulissantes, de connecteurs et de filtres.

Ce chapitre est structuré autour de trois études distinctes.

Le premier article est une analyse des radicaux générés post irradiation dans les matériaux formulés à partir de PP et de PE irradiés par rayons gamma et rayon X.

Le deuxième article est une évaluation complète des propriétés physiques, chimiques, thermiques et mécaniques du polypropylène irradié par rayons gamma, rayons X et faisceau d'électrons.

Enfin, le troisième article est une analyse des propriétés thermiques du polyamide et une analyse des radicaux générés post-irradiations par rayons gamma, rayons X et faisceau d'électrons.

Les informations essentielles à retenir de ce chapitre sont les suivantes :

- Chaque classe de polymères génère des radicaux, indépendamment de la technologie d'irradiation utilisée.
- Les additifs présents dans les polymères formulés peuvent modifier le comportement des polymères irradiés, indépendamment de la technologie d'irradiation utilisée.
- Les technologies d'irradiation gamma, rayons X et faisceau d'électrons sont équivalentes pour une même formulation de polymère jusqu'à une dose de 100 kGy.

# 5.1. Étude par résonnance paramagnétique électronique des radicaux générés dans les polyoléfines

Les radiations ionisantes, telles que les rayons gamma et les rayons X, sont largement utilisées dans l'industrie pour la stérilisation de matériaux, en particulier dans les secteurs médical et biopharmaceutique. Lorsqu'elles interagissent avec des polymères, ces radiations induisent l'apparition de radicaux libres, qui sont des espèces hautement réactives capables d'amorcer des modifications structurelles et chimiques dans les polymères. L'objectif principal de cette étude est de déterminer s'il existe des variations dans les radicaux produits lorsque le rayonnement de deux sources différentes interagit avec les matériaux. Si aucune différence n'est observée, on peut supposer que les matériaux irradiés présentent un comportement équivalent, quelle que soit la source de rayonnement.

Les radicaux libres sont produits par la rupture des liaisons chimiques dans les polymères sous l'effet des radiations ionisantes. Ce processus commence par l'absorption d'énergie par les polymères, ce qui entraîne l'excitation et l'ionisation des molécules. Les radicaux formés peuvent être classés en plusieurs types, notamment les radicaux alkyles et peroxyles, chacun ayant des propriétés et des réactivités distinctes. Les radicaux alkyles sont généralement formés par la rupture des liaisons C-H. Les radicaux peroxyles, quant à eux, se forment par réaction avec l'oxygène, ce qui est particulièrement pertinent pour les polymères exposés à l'air.

La RPE est une technique analytique utilisée pour identifier le type de radicaux produits pendant l'irradiation. Les quantifier et mesurer leurs cinétiques de disparition après irradiation par rayon X et gamma. Les signaux RPE des radicaux produits dans les polymères formulés sont complexes et évoluent au fil du temps. Le défi de la RPE réside dans l'identification des substances pures au sein d'un spectre qui présente un mélange de nombreuses espèces. Une analyse de résolution de courbe, spécifiquement la méthode SIMPLE-to-use Self-modeling Mixture Analysis (SIMPLISMA), a été employée afin d'identifier ces radicaux. Cette méthode permet d'extraire mathématiquement les signaux purs à partir d'un mélange complexe de plusieurs composés, tels que les polymères et les additifs, et fournit également leur profil de concentration. Il est important de noter que cette méthode ne nécessite aucune connaissance préalable du système étudié ni aucune hypothèse sur le nombre d'espèces présentes.

Dans cet article publié dans la revue *Journal of Applied Polymer Science* en 2024, des analyses RPE ont été réalisées sur chaque matériau sur une période de 380 jours après irradiation à 50 kGy. Les résultats montrent que, quelle que soit la technologie d'irradiation, un mélange de radicaux alkyles et allyles est observé dans les échantillons

de PP et des radicaux peroxyles sont observés dans les échantillons de PE. Pour chaque famille de polymères, des radicaux identiques sont produits en quantités équivalentes. Cependant, l'étude sur le PP révèle que les additifs présents dans les échantillons peuvent former des radicaux, en plus de ceux générés intrinsèquement dans le polymère, quelle que soit la technologie utilisée.

Ces matériaux étaient soit composés de PP, PE ou d'élastomère thermoplastique (TPE), soit constitués de mélanges de ces polymères. En testant 22 types de matériaux, PP, PE, TPE après irradiation par rayons gamma et rayons X, nous pouvons confirmer que l'interaction entre les photons et la matière est cohérente à travers tous les grades de polymères. La taille de notre échantillon, représentant les polymères les plus couramment utilisés, produit des résultats qui peuvent, de ce fait, être étendus à d'autres échantillons formulés à partir de ces polyoléfines.

Les résultats de cette étude ont des implications pratiques significatives pour l'industrie. La confirmation que les matériaux irradiés présentent un comportement équivalent, quelle que soit la source de rayonnement, permet une plus grande flexibilité dans le choix des méthodes de stérilisation. Cela est particulièrement important pour les fabricants de dispositifs médicaux et de produits biopharmaceutiques, qui peuvent choisir la méthode la plus adaptée à leurs besoins spécifiques sans compromettre la qualité ou la sécurité des matériaux. De plus, la compréhension des types de radicaux produits et de leur cinétique de décroissance peut aider à optimiser les formulations de polymères pour améliorer leur stabilité et leur performance après irradiation.

Malgré les avancées réalisées, plusieurs défis techniques subsistent dans l'étude des interactions entre les radiations ionisantes et les polymères. L'un des principaux défis est la complexité des signaux RPE, qui nécessitent des méthodes d'analyse sophistiquées pour être correctement interprétés. De plus, la variabilité des formulations de polymères et des conditions d'irradiation peut compliquer la généralisation des résultats. Il est également crucial de prendre en compte l'effet des additifs et des impuretés, qui peuvent influencer la génération et la stabilité des radicaux.

Les perspectives de la recherche dans ce domaine incluent le développement de nouvelles méthodes d'analyse pour améliorer la résolution et la précision des mesures RPE. L'intégration de techniques complémentaires, telles que la spectroscopie infrarouge et la chromatographie, pourrait fournir des informations supplémentaires sur les changements chimiques et structurels dans les polymères. De plus, l'exploration de nouveaux matériaux et formulations, ainsi que l'étude des effets à long terme des radiations, sont des domaines de recherche prometteurs. Enfin, l'application des résultats de cette étude à d'autres secteurs, tels que l'emballage alimentaire et les matériaux de construction, pourrait élargir l'impact de ces découvertes.

Check for updates

Received: 13 July 2023 | Revised: 15 November 2023 | Accepted: 9 December 2023

DOI: 10.1002/app.55098

RESEARCH ARTICLE

Applied Polymer SCIENCE WILEY

# Radical detection and electron-spin resonance (ESR) monitoring in polymer materials irradiated with gamma and X-rays: Polyethylene and polypropylene

Blanche Krieguer[1,2,3] | Sylvain R. A. Marque[2] | Samuel Dorey[1] | Nathalie Dupuy[3] | Fabien Girard[3] | Nina Girard-Perier[1] | Florent Kuntz[4] | Nicolas Ludwig[4]

[1]Sartorius Stedim FMT S.A.S, Z.I. Les paluds, Aubagne Cedex, France

[2]Aix Marseille Univ, CNRS, ICR, Case 551, Marseille, France

[3]IMBE, Aix Marseille Univ, Avignon Univ, CNRS, IRD, Marseille, France

[4]Aerial, Illkirch, France

Correspondence
Blanche Krieguer and Samuel Dorey, Sartorius Stedim FMT S.A.S, Z.I. Les paluds, Avenue de Jouques CS91051, Aubagne Cedex 13781, France.
Email: blanche.krieguer@sartorius.com and samuel.dorey@sartorius.com

Sylvain R. A. Marque, Aix Marseille Univ, CNRS, ICR, Case 551, Marseille 13397, France.
Email: sylvain.marque@univ-amu.fr

Nathalie Dupuy, IMBE, Aix Marseille Univ, Avignon Univ, CNRS, IRD, IMBE, Marseille, France.
Email: nathalie.dupuy@univ-amu.fr

## Abstract

When ionizing radiations interact with polymers, free radicals are generated and are known to be the initiating species for the modification in materials. Monitoring and identifying free radicals after irradiation allow assessing the impact of X-rays and gamma rays on materials. A comparative study has been performed on materials made from polypropylene and polyethylene after irradiation by the two irradiation technologies. Electron spin resonance (ESR) signal has been monitored up to 380 days when signal was still present. ESR signals, concentration profiles, and kinetics were observed after X-rays and gamma rays.

KEYWORDS

electron spin resonance (ESR), gamma rays, polymers materials, sterilization, X-rays

## 1 | INTRODUCTION

Commercial polypropylene (PP) and polyethylene (PE) materials were selected to compare interaction outputs between X-rays and gamma rays with matter. Both materials are known for their good mechanical and thermal properties[1] and are widely used in biopharmaceutical applications.[2] Among sterilization technologies for medical and biopharmaceutical devices, radiation remains one of the most widespread technics and especially the use of gamma irradiation.[3,4] Indeed, Cobalt 60 ($^{60}$Co) is presently the main source of radiation used for the sterilization of single-used plastic systems in biopharmaceutical industry accounting for 40%–45% of the global market in 2020. According to the current health context, a strong growth of products volume is intended for the pharmaceutical industry in the coming years and questions concerning gamma sterilization capacity are arising.[4]

This is an open access article under the terms of the Creative Commons Attribution-NonCommercial-NoDerivs License, which permits use and distribution in any medium, provided the original work is properly cited, the use is non-commercial and no modifications or adaptations are made.
© 2024 The Authors. Journal of Applied Polymer Science published by Wiley Periodicals LLC.

Thus, to guarantee the continuity of the production activities of these systems, alternative methods of radiation sterilization based on machine sources to complement gamma rays must be developed.[2] X-rays sterilization is considered as one possible technology which could absorb this market growth as proven by growing research on gamma rays and X-rays equivalency.[5-8]

X-ray and gamma rays exhibit very similar features as both are photons but produced from different sources.[8] Gamma rays refer to the production of photons by radioactive disintegration, whereas X-rays are produced with electron accelerator through conversion of electron energy into photons via Bremsstrahlung effect.[9] Their energy deposition profiles (i.e., dose profile) are very similar while in some cases,[7] X-rays irradiation can achieve a slightly better dose uniformity because of the higher photon energy present in X-rays spectrum. For these two irradiation technologies, delivered dose rates are very different (in the order of 1–2 kGy $h^{-1}$ for gamma rays and 12 kGy $h^{-1}$ for X-rays). Indeed, photons will generate secondary electrons through pair creation, Compton diffusion or photoelectric effect. These electrons will deposit their energy along their track in the matter. An energy of 10–500 eV can be deposited in a volume of the order of a cubic nanometer, which leads to the generation of free radicals in spurs.[10,11] When ionizing radiations interact with polymers, free radicals are generated. Free radicals are well known to be the starting point of modification, and several studies have investigated free radical in PP and PE through mechanical properties, Fourier Transform Infrared (FTIR), Gas Chromatography-Mass Spectroscopy (GC–MS), and electron spin resonance (ESR) (i.e., crosslinking, chain scission, and radiation oxidation).[12-16]

The energy of the source particles we are considering, that is, gamma and X photons, ranges between ~0.1 and ~ 7 MeV. The minimum energy required to create ionization is approximately 100 eV, which is 1000 to 70,000 times less than the energy of the source particles.[7] When these source particles collide with matter, such as a device to be sterilized, they trigger a cascade of photons and electrons. The number of particles increases while the energy per particle decreases as the cascade progresses. As the average energy per particle decreases, the number of ionizations proportionally increases.[7] This continues until the energy per particle falls below the energy needed to ionize an atom. At this point, the remaining energy is deposited in the matter as heat. The aim is to determine if there is a variation in the radicals generated when radiation from the two sources interacts with the products. If no differences are observed, it can be inferred that irradiated materials will exhibit similar behavior irrespectively of the radiation source.

Most generated radicals react very quickly when they exhibit sufficient mobility in matter. Others could be quite stable, especially in the crystalline phase and sometime in the amorphous phase of semicrystalline polymers, and, therefore, can be measured from minutes to days/weeks after irradiation.[17] ESR is a very powerful method to identify the type of radicals formed during irradiation and to monitor their quantity and decay after irradiation.[18,19] The effects of irradiation on PP and PE have been extensively studied by ESR.[13,20-22] However, very few studies have compared the effects of these irradiations on polymers. Free radical quantity and identification of radicals after irradiation help assess similarities on material impact between X-rays and gamma rays.

There are thousands of commercially available polymer grades potentially suitable for healthcare products, making it impractical to test them all. Consequently, we have selected several samples from these commercial polymer grades for our study. Our ESR study reveals that the type of radicals generated is dependent on the polymer type, although additives may also produce superimposed signals. Furthermore, while the qualitative data may vary based on the specific plastic recipe, this does not impact the decay kinetics. By testing a wide range of polymers, we can confirm that the interaction between photons and matter is consistent across all polymer grades when exposed to gamma and X-rays. Our sample size, representing the most commonly used plastics, will yield results that can be confidently extended to other polyolefins.

The ESR signals of formulated polymers are complex and change over time, depending on the conditions in which they are stored. The challenge in ESR spectroscopy lies in identifying the pure substances within a spectrum that displays a mixture of many species. To address this, a curve resolution analysis, specifically the SIMPLE-to-use Self-modeling Mixture Analysis (SIMPLISMA)[23-26] method, was employed. This method allows for the mathematical extraction of the pure signals from a complex mixture of several compounds, such as polymers and additives. It also provides their concentration profile. Importantly, this method does not require any prior knowledge about the system under study or any assumptions about the number of species present.

In this study, we investigated the effects of gamma and X-rays on 22 materials. These materials were either made of PP, PE, and thermoplastic elastomer (TPE), or composed of mixtures of these. ESR analyses were conducted on each material over a period of 380 days after irradiation. The aim was to monitor using ESR the free radicals generated after gamma and X-ray irradiations on each class of polymers.



10974628, 0, Downloaded from https://onlinelibrary.wiley.com/doi/10.1002/app.50098 by Cochrane France, Wiley Online Library on [18/01/2024]. See the Terms and Conditions (https://onlinelibrary.wiley.com/terms-and-conditions) on Wiley Online Library for rules of use; OA articles are governed by the applicable Creative Commons License

## 2 | MATERIALS AND METHODS

### 2.1 | Sample

The samples investigated in this article are PP, TPE, and PE of various types: high-density polyethylene (HDPE), low-density polyethylene (LDPE), linear low-density polyethylene (LLDPE),[15,27-29] and multilayer films. Their chemical structure is depicted in Figure 1, and Table 1 displays their properties: density and melting flow rate.

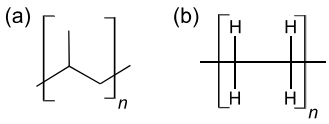


FIGURE 1 Chemical structure of (a) polypropylene and (b) polyethylene.

### 2.2 | Irradiations

#### 2.2.1 | Gamma ray irradiation

Irradiation with gamma rays produced from $^{60}$Co sources was performed at Ionisos, Dagneux, France, at a dose rate of 1–2 kGy h$^{-1}$. The samples were packed in craft boxes at room temperature. This together with the adapted

TABLE 1 Commercial of nonirradiated PP, TPE, and PE samples (density and MFI) and postirradiation features ($C_{max}$[a] and $t_{1/2}$[a]).

| Polymers | Identification number | Density (g·cm$^{-3}$) | MFI (g·10 min$^{-1}$)[b] | $C_{max}$ gamma (spin g$^{-1}$) | $C_{max}$ X-ray (spin g$^{-1}$) | $t_{1/2}$ gamma (days) | $t_{1/2}$ X-ray (days) |
|---|---|---|---|---|---|---|---|
| PP | 1 | 0.9 | 2.1 | 7·10$^{16}$ | 3·10$^{16}$ | ≈24 | ≈19 |
| | 2 | 0.9 | 18 | 8·10$^{16}$ | 3·10$^{16}$ | ≈23 | ≈27 |
| | 3 | 0.9 | 35 | 7·10$^{16}$ | 5·10$^{16}$ | >380 | >380 |
| | 4 | 0.9 | 10 | 8·10$^{16}$ | 4·10$^{16}$ | ≈24 | ≈26 |
| TPE | 5[c] | 0.9 | n.a.[d] | 6·10$^{16}$ | 3·10$^{16}$ | ≈25 | ≈31 |
| | 6 | 0.9 | n.a.[d] | n.a.[d] | 1·10$^{16}$ | n.a.[d] | <120 |
| HDPE | 7 | 0.960 | 7.6 | 1·10$^{17}$ | 9·10$^{16}$ | ≈13 | ≈12 |
| | 8 | 0.953 | 26 | 2·10$^{16}$ | 2·10$^{16}$ | ≈14 | >60 |
| | 9 | 0.954 | 0.25 | 2·10$^{16}$ | 3·10$^{16}$ | ≈33 | ≈31 |
| | 10 | 0.953 | 6.6 | 8·10$^{15}$ | 1·10$^{16}$ | >60 | >60 |
| | 11 | 0.962 | 13 | 5·10$^{16}$ | 6·10$^{16}$ | ≈22 | ≈15 |
| LLDPE | 12 | 0.925 | 1.9 | n.d.[e] | n.d.[e] | n.d.[e] | n.d.[e] |
| LDPE | 13 | 0.923 | 22 | n.d.[e] | n.d.[e] | n.d.[e] | n.d.[e] |
| | 14 | 0.922 | 0.33 | 5·10$^{16}$ | 6·10$^{16}$ | n.a.[d] | n.a.[d] |
| | 15 | 0.924 | n.a.[d] | n.d.[e] | n.d.[e] | n.d.[e] | n.d.[e] |
| | 16 | 0.920 | 1.5 | n.d.[e] | n.d.[e] | n.d.[e] | n.d.[e] |
| | 17 | 0.922 | n.a.[d] | n.d.[e] | n.d.[e] | n.d.[e] | n.d.[e] |
| | 18 | n.a.[d] | n.a.[d] | n.d.[e] | n.d.[e] | n.d.[e] | n.d.[e] |
| | 19 | n.a.[d] | n.a.[d] | n.a.[d] | n.a.[d] | n.a.[d] | n.a.[d] |
| PE/EVOH/PE[f] | 20 | n.a.[d] | n.a.[d] | 4·10$^{16}$ | 5·10$^{16}$ | ≈24 | ≈30 |
| EVA/EVOH/EVA[f] | 21 | n.a.[d] | n.a.[d] | 1·10$^{16}$ | 1·10$^{16}$ | n.d.[e] | n.d.[e] |
| PE/EVOH/PA/PET[f] | 22 | n.a.[d] | n.a.[d] | 9·10$^{16}$ | 1·10$^{17}$ | ≈40 | ≈44 |

Abbreviations: EVA, ethylene-vinyl acetate; EVOH, ethylene vinyl alcohol; HDPE, high-density polyethylene; LDPE, low-density polyethylene; LLDPE, linear low-density polyethylene; LOD, limit of detection; MFI, melt flow index; PA, polyamide; PE, polyethylene; PET, polyethylene terephthalate; TPE, thermoplastic elastomer.

[a]$C_{max}$: maximum concentration of radicals measured and $t_{1/2}$: half lifetime of radicals.

[b]MFI: 190°C × 2.16 kg$^{-1}$ for PE samples and 230°C × 2.16 kg$^{-1}$ for PP samples.

[c]Sample 5 is commercially available from Sartorius, that is, Tuflux® TPE.

[d]n.a.: not available.

[e]n.d.: not detected, LOD <3 × 10$^{15}$.

[f]Multilayer films proprietary of Sartorius. 20, 21, and 22 are commercially available as S80 (PE/EVOH/PE), S71 (EVA/EVOH/EVA), and S40 (PE/EVOH/PA/PET).



10974628, 0, Downloaded from https://onlinelibrary.wiley.com/doi/10.1002/app.55698 by Cochrane France, Wiley Online Library on [18/01/2024]. See the Terms and Conditions (https://onlinelibrary.wiley.com/terms-and-conditions) on Wiley Online Library for rules of use; OA articles are governed by the applicable Creative Commons License

packaging of plastic parts in thin craft boxes provides a good treatment uniformity.

Targeted dose was 50 kGy ± 10%. Dosimetry has been realized using alanine pellet and AerEDE Dosimetry software (Aerial, France) by placing dosimeters in cardboard box volume.

### 2.2.2 | X-ray irradiation

X-ray irradiation has been performed at Aerial-CRT on Feerix facilities. This facility is based on a Rhodotron (TT300–IBA) and delivers X-ray beams. In this study, 7-MV X-rays have been obtained from the conversion of 7 MeV electrons in a tantalum target. Irradiation has been performed with a vertical scan and a horizontal translation of products. This, together with the adapted packaging of plastic parts in thin craft boxes, provides good treatment uniformity. The average dose rate was about 12 kGy $h^{-1}$.

Targeted dose was 50 kGy ± 10% maximum which was verified by placing dosimeters in cardboard box volume. Dosimetry has been realized using alanine ESR dosimetry system with AerEDE software as well. Dose measurements performed are traceable to an international standard through appropriate calibration.

## 2.3 | ESR measurements

ESR measurement has been performed on a Magnettech MS5000X ESR spectrometer from Brucker, Switzerland with ESR studio controlling software. Samples have been prepared from irradiated dog bones or from irradiated material parts. Little pieces have been cut to be introduced in a glass probe of 4.2 mm of inner diameter. A height of about 4 cm and a sample mass of 100 to 200 mg were used.

All signals have been observed in the range of 322 to 340 mT magnetic field, corresponding to organic radicals. In this case, a subtraction of the ruby signal of the spectrometer has been performed. Spectra have been recorded with a modulation of 0.2 mT, 60 s of sweeping time, and a single scan.

Kinetics have been performed till the fading of the signal, over more than 1 year, and have been stopped earlier when the signal was too weak because of fading. Measurement days (D) are the following: D9, D15, D30, D60, D120, D180, and D380. For X-ray samples, D1 has been measured additionally. This wasn't possible with gamma irradiated samples because of delay caused by shipment. The intensity of the peaks was normalized with the sample mass, to use them in the chemometrics processing data. Total number of spins was directly calculated in ESR studio software. Only spin ½ is considered which could be verified later with SIMPLISMA analysis.

The LOD and the limit of quantification (LOQ) are defined as follows:

$$\mathrm{LOD} = \text{background signal(average of 10 measurements)} + 3 \times (\text{background standard deviation}).$$

$$\mathrm{LOQ} = \text{background signal(average of 10 measurements)} + 10 \times (\text{background standard deviation}).$$

The background signal depends on the range of measurement. For the range 322–340 mT, the average signal was $1 \times 10^{15}$ spins $\pm 2 \times 10^{14}$ spins. Obtained LOD and LOQ are, respectively, $2 \times 10^{15}$ and $3 \times 10^{15}$ spins. For the range 300–360 mT, a subtraction is realized for signal quantification, so that the background has been subtracted to another background of another day, obtain LOD and LOQ are, respectively, $3 \times 10^{15}$ and $7 \times 10^{15}$ spins. Each measurement is compared with the LOD and LOQ before normalization by the sample mass, and data are not reported in figures when inferior to LOD.

To obtain the variance of measurement for ESR signal a repeatability study has been realizing both on irradiation and measurement. 3 × 3 samples of the PE/EVOH/PE material (n°21) have been irradiated to 50 kGy in X-rays during three different irradiation sessions to generate a total number of nine samples for analyses in ESR. Measurement has been performed 1 day after irradiation, and the standard error of 11.4% was assessed.

Simulation of ESR spectra were performed with Pepper, a part of EasySpin program,[39] based on Matlab 7.14 (R2012a).

## 2.4 | Curve resolution method (SIMPLISMA)

The method used for self-modeling mixture analysis is the SIMPLISMA method described in the literature.[24-26,30-32] This method is used for self-modeling mixture analysis by resolving mixture data into pure component signal and concentration profiles without the help of prior information about the mixture. In the case of plastics, it's always a mixture of polymers and additives. SIMPLISMA will consider as "pure" either a monomaterial or a mixture that evolve in the same way after irradiation.[23] When the radicals have the same kinetic trend, the same *g*-factor, and same concentration profile, this tool is unable to differentiate the characteristics of

10974628, 0, Downloaded from https://onlinelibrary.wiley.com/doi/10.1002/app.55098 by Cochrane France, Wiley Online Library on [18/01/2024]. See the Terms and Conditions (https://onlinelibrary.wiley.com/terms-and-conditions) on Wiley Online Library for rules of use; OA articles are governed by the applicable Creative Commons License

**TABLE 2** Test for equivalency techniques measured with radical concentration in (2,2,6,6-tétraméthylpipéridin-1-yl)oxy (TEMPO) references.

| Concentration range applicability (spin $g^{-1}$) | Number of tests | Standard deviation | Six-sigma variation | Ratio lower limit[a] | Ratio upper limit[a] |
|---|---|---|---|---|---|
| $1.5 \times 10^{16}$ < concentration < $10^{17}$ | 8 | $4.6 \times 10^{15}$ | 112% | 0.1 | 2.2 |
| $10^{17} \leq$ concentration < $10^{18}$ | 8 | $9.7 \times 10^{15}$ | 50% | 0.4 | 1.6 |
| concentration $\geq 10^{18}$ | 8 | $2.2 \times 10^{17}$ | 21% | 0.7 | 1.3 |

[a]Ratio limit: mean ± 3 standard deviations.

different components. SIMPLISMA analysis is based on least squares optimization to determine the pure signal that has received the contributions from only one component. To properly handle noise, peak shift, and instrument drift, user interaction is required.[24]

The fitting of the SIMPLISMA results is calculated using the relative residual sum of squares (RRSSQ), square sum between the calculated and the original spectra. The number of species is incrementally increased until the reconstructed signal reaches 90% of the experimental signal. The SIMPLISMA procedure was performed with Matlab 7.14 (R2012a).

### 2.5 | Equivalency criteria

To evaluate the difference between gamma and X-ray irradiated samples, three criteria are defined: ESR pattern (type of radical), radical amount, and radical shelf life. The ESR signal (qualitative criterion) show the same signal shape at the same magnetic field for both gamma and X-ray irradiated samples highlighting the same type of radical (s). For the quantitative criterion, close amount for both gamma and X-ray irradiated samples are observed when concentration detected is higher than the LOQ (i.e., $>2 \times 10^{16}$ spin $g^{-1}$). Depending on the concentration measured, the equivalency is claimed when the ratio $[\text{Radicals}]_{\text{X-rays}}/[\text{Radicals}]_{\text{gamma}}$ is above the lower limit and below the upper limit (Table 2). These limits depend on the spin concentration range, as obtained after repeatability evaluation (cf. number of testing in Table 2). Regarding the shelf life criterion, the radical concentration should show the same kinetic decrease overtime for both gamma and X-ray irradiated samples.

### 2.6 | Storage condition

After irradiation and between measurements, samples were stored in a temperature and hygrometry-controlled environment (T: 22°C ± 2°C and RH: 45% ± 15%) in UV-free light.

## 3 | RESULTS

### 3.1 | Polyethylene

Different types of PE were analyzed: HDPE, LLDPE, and LDPE. The ESR signals for the LLDPE and LDPE samples couldn't be included in the quantitative study and processes by SIMPLISMA because they exhibit a too short lifetime, with concentrations rapidly fading under the LOD. The absence or the weak signal obtained for the LLDPE, and LDPE samples can be accounted by their low degree of crystallinity. The radicals can easily self-terminate as their mobility is higher in LDPE and LLDPE than in HDPE because of the higher amorphous phases in LDPE and LLDPE.[33]

Samples 20,21, and 22 (Table 1) are multilayer films with a contact layer of PE or EVA and with an embedded EVOH (ethylene vinyl alcohol) layer. These multilayer films have been intensively investigated and represent our reference materials.[3,17,23] The ESR signal of PE was not detected in these samples and the signal recorded is attributed to the $\text{EVOH}^{\bullet}$ species.[17]

#### 3.1.1 | Qualitative studies

Figure 2 displays the ESR signal of a HDPE at 9 days (Figure 2a) and 60 days (Figure 2b) after gamma and X-rays irradiations. Similar signals are observed for other samples and reported in Figure S1. There is no ESR signal in nonirradiated samples. These multiple signals afford a *g*-value of 2.003 corresponds to alkyl radicals which are ascribed to a mixture of superimposed signals of alkyl, allyl, and polyenyl radicals (Figure 3) according to the literature.[22,34-39] The multiplet signal changed overtime into a single line which is ascribed to the polyenyl radicals, as highlighted by signal at 60 days (Figure 2b). No change in the *g*-value is observed. Whatever the irradiation technology, ESR signal displayed the same pattern (Figures S1 and S2 in Supporting Information).



10974628, 0, Downloaded from https://onlinelibrary.wiley.com/doi/10.1002/app.55698 by Cochrane France, Wiley Online Library on [18/01/2024]. See the Terms and Conditions (https://onlinelibrary.wiley.com/terms-and-conditions) on Wiley Online Library for rules of use; OA articles are governed by the applicable Creative Commons License

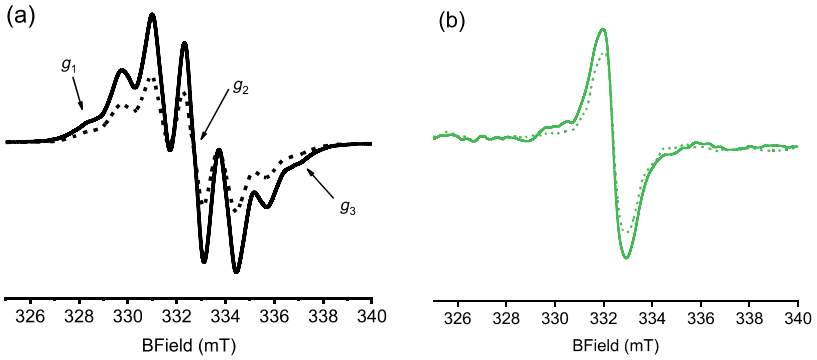


**FIGURE 2** (a) Electron spin resonance signal of HPDE-7, 9 days after gamma (full line) and X-rays (dotted line) irradiation corresponding to a mixture of allyl, alkyl, and polyenyl radicals. $g_1 = 2.021$, $g_2 = 2.003$, and $g_3 = 1.985$. (b) Signal of high-density polyethylene-7, 60 days after gamma (full line) and X-rays (dotted line) irradiation corresponding to a polyenyl radicals. [Color figure can be viewed at wileyonlinelibrary.com]

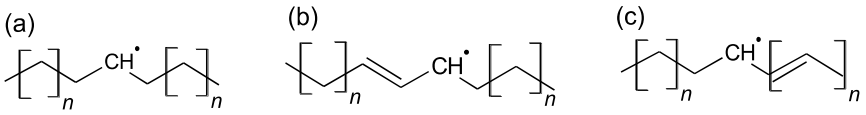


**FIGURE 3** Structure of (a) alkyl radical, (b) allyl radical, and (c) polyenyl in high-density polyethylene.

### 3.1.2 | Quantitative studies

Kinetics of all PEs are displays in Supporting Information (Figure S2). The equivalence tests were further applying on the quantitative ESR results between gamma and X-ray irradiated samples. The equivalency is claimed when the ratio $[\text{Radicals}]_{\text{X-rays}}/[\text{Radicals}]_{\text{gamma}}$ is in between the limits summarized in Table 2. The ratio is 0.8 for HPDE-7 9 days after irradiation for instance. The ratios for the other HPDEs are available in Table S1 in SI. For all HDPEs being irradiated with X-ray and gamma rays, the nature and quantity of radicals generated is equivalent.

### 3.1.3 | SIMPLISMA analysis

Given that ESR spectra are the superimposition of spectral contributions from various species present in the materials, we applied the SIMPLISMA treatment. This was carried out for the 26 spectra recorded over 380 days for gamma-irradiated samples and the 26 spectra recorded over the same period for X-ray samples, in order to separate each signal. This interactive method,[26] known as self-modeling mixture analysis, is used to resolve mixture data into pure spectra that are comparable with those of the mixture species. This is done without any prior information about the mixture. The method also provides associated concentration profiles, representing the relative contribution of each species in the mixture. The ability of SIMPLISMA curve resolution is to detect the wavenumbers or B field, with the highest intensity variations in the data set and it is these wavelength regions which will be most characteristic of each component in the mixture. It is applied for the analysis of FTIR and ESR,[24,40] and it is especially efficient in analyzing spectra containing both sharp and broad bands.[41,42]

Its concept is based on the determination of pure variables (e.g., a wavelength, a wavenumber in spectroscopic terms) that have contributions from only one component. By identifying the least correlated wavenumbers, which exhibit the largest variations, a 'pure variable' is defined. This is a wavenumber at which the contribution of an individual component to the spectral intensity is at its maximum, whereas the contributions from other components are minimal. Consequently, the intensity of the pure variable can be considered proportional to the contribution or relative "concentration" of that corresponding individual component in the mixture. Once the pure variables have been determined through interaction with the maximum ratio (referred to as 'purity') of standard deviation to mean intensity of each spectrum, the original dataset can be resolved into pure components and their contributions in the original mixture spectra. The SIMPLISMA algorithm has been described in detail elsewhere.[24,25] The results obtained from SIMPLISMA when applied to time evolving ESR data sets are pure kinetic and spectral profiles of the radicals present in the studied polymer. Resolved spectral profiles can be used to identify these radicals by comparing them with those reported in the work by Paul et al.[43] or by ESR spectra simulations (Figure 5). Afterward, the time profiles give the kinetic information of each radical and a description of the full-time-dependent process. For curve resolution methods, Abou Fadel et al.[40] use SIMPLISMA and then MCR-ALS. The main interest of MCR-ALS is to impose constraints,



10974628, 0, Downloaded from https://onlinelibrary.wiley.com/doi/10.1002/app.55698 by Cochrane France, Wiley Online Library on [18/01/2024]. See the Terms and Conditions (https://onlinelibrary.wiley.com/terms-and-conditions) on Wiley Online Library for rules of use; OA articles are governed by the applicable Creative Commons License

such as the nonnegativity on the concentration profiles. As all the profiles obtained in this work are positive, there is no interest presently in constraining and simplifying the digital part.

The SIMPLISMA procedure shows that the ESR signal is decomposed into three signals corresponding to three radicals species as given by $g = 2.003$: a signal ascribed to alkyl radical with $a_H = 2.152$ mT (Figure 4a), a signal ascribed to allyl radical with $a_H = 1.324$ mT (Figure 4b), and a signal corresponding to polyenyl mainly (Figure 4c) with some residual alkyl and allyl radical. To account for the variation in the data set (RRSSQ = 5%), three reconstructed signals are sufficient to avoid overfitting (decrease of the RRSSQ in Table S2 and their concentration profile in Figure S3).

Figure 4d shows the superimposition of the signal of alkyl (blue dotted line), allyl (red dotted line), and polyenyl radicals (black solid line). It's clear that the starred bands are because of the combination of signals of these radicals.

To complete the interpretation of the SIMPLISMA treatment, an ESR spectra simulation was performed with EasySpin. The signal provided may contain some combination of signals issued from the different radical species. Hence, the signals given by Easyspin simulation of allyl radicals match significantly with the signal given by SIMPLISMA (Figure 5). The differences are likely due to presence of alkyl and polyenyl radicals. Interestingly, SIMPLISMA affords an easy way to analyze several tenth of spectra. That so, it is possible to pinpoint two experiments displaying "pure" signals of allyl and alkyl radicals which are nicely modelized using EasySpin (see Figure S4). Therefore, SIMPLISMA is an efficient approach to decipher quickly species observed in the sample.

Same approach was performed for alkyl and polyenyl radicals, a nice agreement was observed for polyenyl radicals (see Figure S4). For alkyl radicals a good agreement

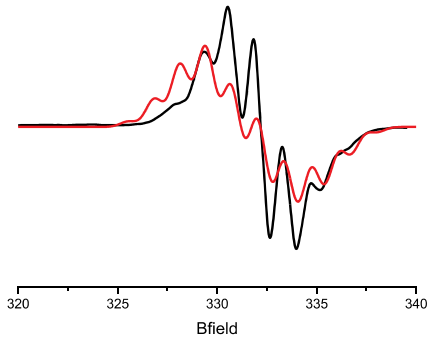


**FIGURE 5** Signal of allyl radical (red line) simulated with EasySpin and (black line) reconstructed with SIMPLISMA treatment. [Color figure can be viewed at wileyonlinelibrary.com]

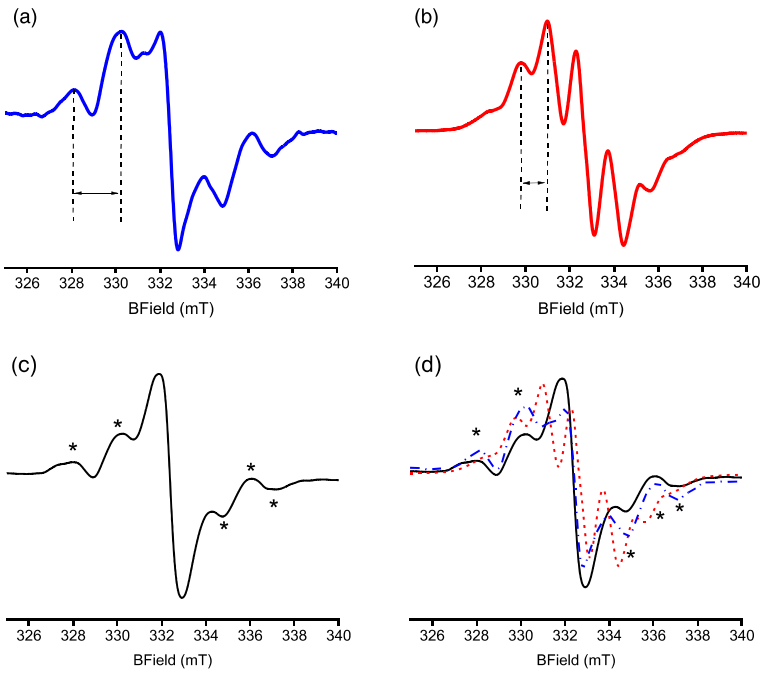


**FIGURE 4** "Pure" signal reconstructed with SIMPLSIMA analysis displays (a) alkyl radicals ($a_H = 2.152$mT), (b) allyl radical ($a_H = 1.3236$mT, (c) polyenyl radical, and (d) the superimposing of signals (a–c). Stars indicate alkyl and allyl radicals, blue dotted line represents alkyl radicals and red dotted line represents allyl radicals. [Color figure can be viewed at wileyonlinelibrary.com]



10974628, 0, Downloaded from https://onlinelibrary.wiley.com/doi/10.1002/app.55698 by Cochrane France, Wiley Online Library on [18/01/2024]. See the Terms and Conditions (https://onlinelibrary.wiley.com/terms-and-conditions) on Wiley Online Library for rules of use; OA articles are governed by the applicable Creative Commons License

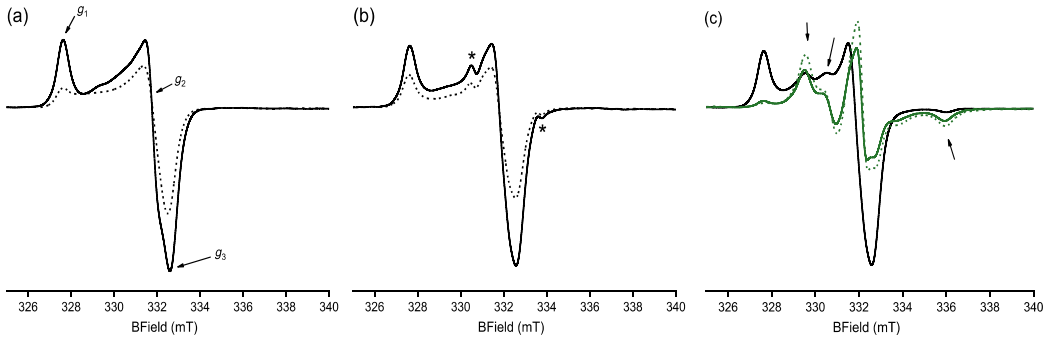


FIGURE 6 Electron spin resonance signal of polypropylene (PP) samples after gamma (full line) or X-rays (dotted line) irradiation at various times after irradiation: (a) PP-2 at day 9 corresponding to a peroxyl radical. $g_1 = 2.0339$, $g_2 = 2.0087$, and $g_3 = 2.0036$. (b) Thermoplastic elastomer-5 at day 9 corresponding to a mixture between a peroxyl radical and an unidentified radical (stars). (c) PP-3 at 9 days (back line) and 60 days (green line) arrows highlight nitroxide peaks (see SIMPLISMA analysis section). [Color figure can be viewed at wileyonlinelibrary.com]

was observed despite the presence of signal of allyl radicals.

Hence, whatever the irradiation technology, for all the analyzed PE samples, only HDPEs exhibit ESR signals 9 days after irradiation. Radicals (nature and quantity) generated in PE samples irradiated with gamma or X-rays are equivalent.

## 3.2 | PP and TPE

### 3.2.1 | Qualitative studies

There is no ESR signal in nonirradiated samples. ESR Signals of PP-2, PP-3, and TPE-5 are displayed in Figure 6 after gamma and X-ray irradiations at various times. Similar signals are observed for other PP and TPE samples and reported in Figure S5. The TPE samples (samples 5 and 6 in Table 1) signals (Figure 6b) mainly correspond to the signal observed in PPs (Figure 6a). The $g$ factor of the major radicals observed in Figure 6 is 2.015 ascribed to a peroxyl radical ($RO_2\bullet$, $g = 2.015$) (Figure 7a) according to the literature.[44,45] Interestingly, a nonidentified radical is observed for TPE-5 (stars in Figure 6b) with a signal superimposed to the signal of peroxyl radical. More puzzling is the significant signal of side product (arrows in Figure 6c) observed with the peroxyl signals for sample 3. Upon aging up to 60 days after irradiation (Figure 6c) this signal is persistent and becomes the main signal. The $g$-value of 2.004 is ascribed to a nitroxide, which is a radical side product. Indeed, sample 3 is loaded with hindered-amine light stabilizers (HALS) which are prone to afford the signal of nitroxide (Figure 6b,c).

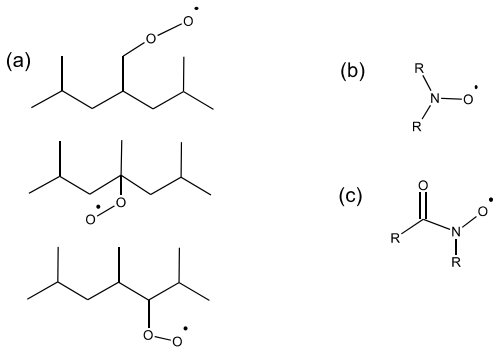


FIGURE 7 (a) Possible structures of the peroxyl radicals formed. (b) Structure of nitroxide radicals, and (c) structure of acyl nitroxide.

Taking into account the structure of PP, several peroxyl radicals are possible (Figure 7a) and cannot be distinguished. For PP-3, because of the presence of HALS, the presence of amines may quench the oxidation processes by scavenging radicals to generate many side products such as highly persistent nitroxide (Figure 7b) or acyl nitroxide (Figure 7c).

### 3.2.2 | Quantitative studies

Figure 8 displays ESR signal evolution overtime for PPs postirradiation, showing the decay of the signal of the peroxyl radical. Figure 9 plots radicals concentration measured by ESR at different times postirradiation. Whatever the irradiation technology, most PPs and TPEs exhibit similar trends in term of ESR signals, radical



10974628, 0, Downloaded from https://onlinelibrary.wiley.com/doi/10.1002/app.55098 by Cochrane France, Wiley Online Library on [18/01/2024]. See the Terms and Conditions (https://onlinelibrary.wiley.com/terms-and-conditions) on Wiley Online Library for rules of use; OA articles are governed by the applicable Creative Commons License

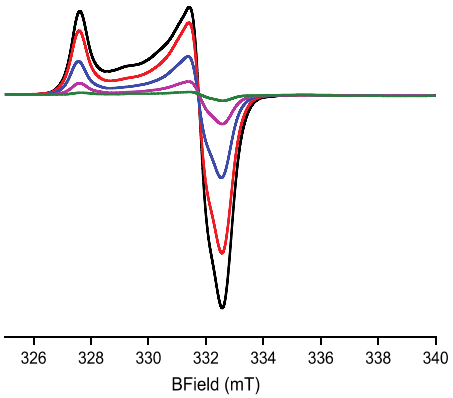


**FIGURE 8** Monitoring of electron spin resonance signal for polypropylene-4 after gamma irradiation and measured at 9 days (black line), at 15 days (red line), at 30 days (blue line), at 60 days (pink line), and at 120 days (green line). [Color figure can be viewed at wileyonlinelibrary.com]

decay kinetics, concentration profiles, except for PP-3 (Figure 9a–e**)**. Sample 6 couldn't have been measured after gamma irradiation (Figure 9f). All samples present a similar radical concentration decay and no more significant ESR signal is detected 120 days after irradiation, except for PP-3 (Figure 9c). ESR measurements were stopped at that stage. This comment holds for both for X-rays and gamma irradiated samples. For PP-3, assuming the oxidation of HALS by $RO_2^{\bullet}$ radicals, the plateau observed after 60 days denotes the full consumption of $RO_2^{\bullet}$ species as for other samples. For all PP samples being irradiated with X-ray and gamma rays, the quantity of radicals generated is equivalent (Table S3 in Supporting Information).

### 3.2.3 | SIMPLISMA analysis

The SIMPLISMA treatment was applied to the 23 spectra recorded over 380 days for gamma-irradiated samples

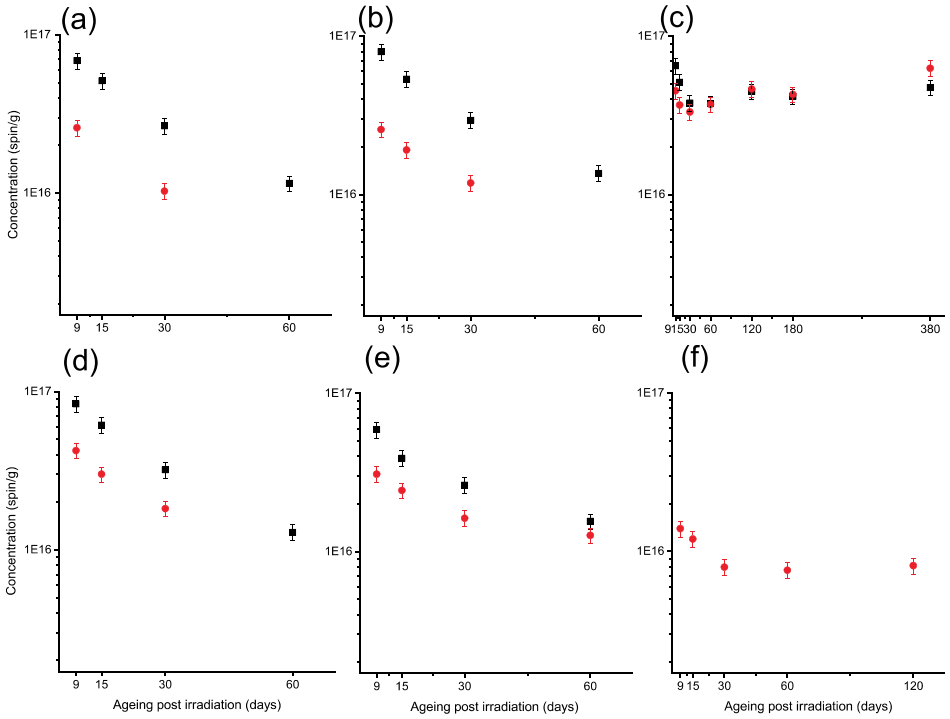


**FIGURE 9** Kinetics studies monitoring of the concentration of radicals for each polypropylene (PP) and thermoplastic elastomer (TPE) samples recorded by electron spin resonance as concentration (spin $g^{-1}$) verus aging post irradiation (days). (a) PP-1. (b) PP-2. (c) PP-3. (d) PP-4. (e) TPE-5. (f) TPE-6. Red circles correspond to samples irradiated by X-rays and black squares are samples irradiated by gamma rays. [Color figure can be viewed at wileyonlinelibrary.com]

10974628, 0, Downloaded from https://onlinelibrary.wiley.com/doi/10.1002/app.55698 by Cochrane France, Wiley Online Library on [18/01/2024]. See the Terms and Conditions (https://onlinelibrary.wiley.com/terms-and-conditions) on Wiley Online Library for rules of use; OA articles are governed by the applicable Creative Commons License

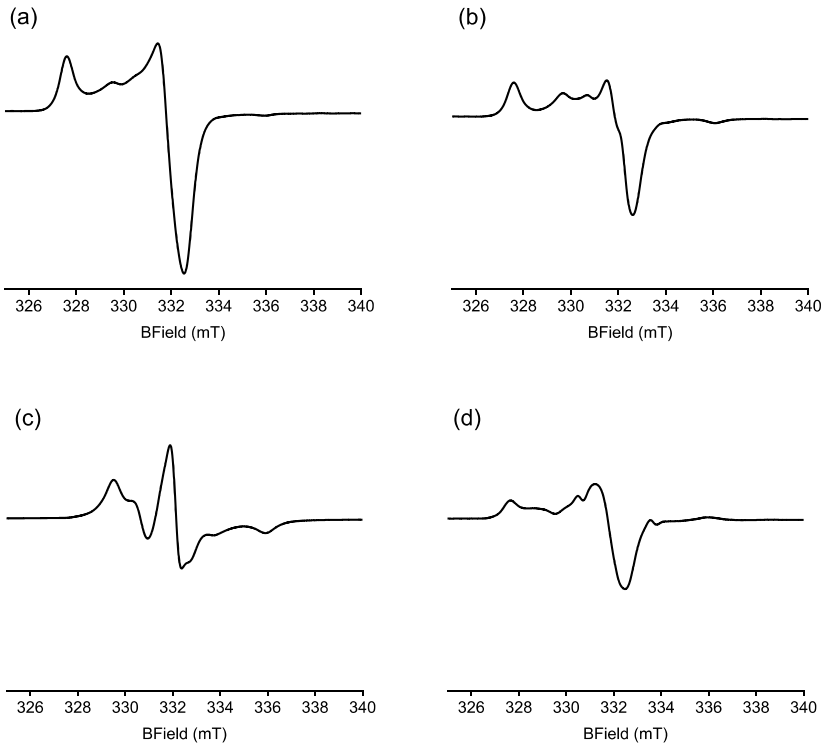


**FIGURE 10** "Pure" signals reconstructed with SIMPLISMA analysis displays peroxyl radical (a) in mobile and (b) in nonmobile phase. (c) "Pure" signal of nitroxyl radical. (d) "Pure" signal of a mixture of peroxyl and unidentified radicals.

and the 36 spectra recorded over the same period for X-ray samples, in order to separate the signal of each species. The changes in the data set (59 ESR spectra) are nicely described by four species affording different kinetics (RRSSQ is <9%) (decrease of the RRSSQ in Table S4). These four signals are assigned: two for peroxyl radicals (Figure 10a,b), one for the nitroxide (Figure 10c) and last one for the mixture of peroxyl radical and the unidentified radical observed in TPE-5 (Figure 10d). The concentration profiles of peroxyl radicals, nitroxide radicals, and the mixture of radicals are obtained for each irradiation technology at different aging after processing data with SIMPLISMA (Figure S6 in Supporting Information). In SIMPLISMA, absolute concentration cannot be determined because the signal intensity of pure radicals is unknown.

Peroxyl radicals in Figure 10a decayed faster than the ones in Figure 10b. PP exhibits two phases: amorphous and crystalline.[46,47] We hypothesize that the mobility of polymers is higher in the amorphous phase than in the crystalline phase,[33] which favors termination reactivity. Therefore, we attribute the signal in Figure 10a to peroxyl radicals in the amorphous phase of PP, and the signal in Figure 10b to peroxyl radicals in the crystalline phase of PP. Signal in Figure 10c is a mixture of peroxyl and nitroxyl radicals present in the sample 3. The concentration profiles display that the absolute concentration of nitroxide increases with aging post-irradiation (Figure S6 in Supporting Information).

## 4 | CONCLUSION

Given the vast number of commercially available polymer grades that could be utilized in healthcare products, it is not feasible to test them all. As such, we have chosen a selection of samples from these commercial polymer grades for our investigation. Our ESR study indicates that the type of radicals produced is contingent on the specific polymer, though additives may also generate overlapping signals. Additionally, while the qualitative data might fluctuate depending on the precise plastic composition, this does not influence the kinetics of decay. By examining a broad spectrum of polymers, we can affirm that the photon-matter interaction remains consistent across all polymer grades when subjected to gamma and X-rays. Our sample set, which encompasses the most frequently used plastics, will produce findings that can be confidently applied to other polyolefins.

Both groups of studied polymers generate featured radicals independently of the photon irradiation technologies. In sharp contrast to LDPE and LLDPE, the HDPE



10974628, 0, Downloaded from https://onlinelibrary.wiley.com/doi/10.1002/app.55698 by Cochrane France, Wiley Online Library on [18/01/2024]. See the Terms and Conditions (https://onlinelibrary.wiley.com/terms-and-conditions) on Wiley Online Library for rules of use; OA articles are governed by the applicable Creative Commons License

10974628, 0, Downloaded from https://onlinelibrary.wiley.com/doi/10.1002/app.55098 by Cochrane France, Wiley Online Library on [18/01/2024]. See the Terms and Conditions (https://onlinelibrary.wiley.com/terms-and-conditions) on Wiley Online Library for rules of use; OA articles are governed by the applicable Creative Commons License

samples display strong ESR signal after both gamma and X-ray irradiation, related to their density and their crystallinity. For all HDPE samples, alkyl, allyl, and polyenyl radicals are observed, and differentiated with their coupling constants. The results obtained with the SIMPLISMA treatment and the ESR simulation with EasySpin are correlated. For PP samples, similar ESR signal was observed for all samples attributed to a peroxyl radical. The radical nature depends first of all on the polymer family and second on some specific recipes. For one sample, nitroxide radical was identified because of nitrogen containing additives. A curve resolution analysis (SIMPLISMA) allows identifying peroxyl radicals. Among 22 different materials subjected to this work, divided in two groups (PE and PP), no significant differences of ESR signals have been observed between gamma and X-ray irradiation. There is no significant difference in amount and kinetics for the free radicals generated from PE and PP despite the generated radicals are different. No quantitative relationship was found between different the radiation source induced radicals and the material shelf life. The aim was to determine if there is a variation in the radicals generated when radiation from the two sources interacts with the products. If no differences are observed, it can be inferred that irradiated materials will exhibit similar behavior irrespectively of the radiation source. The similar ESR signals, kinetics, radical concentration profiles with both gamma and X-rays on PP and PE provide evidence about the same radiation interaction with condensed matter in link with theoretical physical considerations.[7]

## AUTHOR CONTRIBUTIONS

**Blanche Krieguer:** Data curation (equal); formal analysis (equal); investigation (equal); methodology (equal); project administration (equal); software (equal); validation (equal); visualization (equal); writing – original draft (equal). **Sylvain R. A. Marque:** Conceptualization (equal); data curation (equal); formal analysis (equal); investigation (equal); methodology (equal); project administration (equal); software (equal); supervision (equal); validation (equal); visualization (equal); writing – review and editing (equal). **Samuel Dorey:** Conceptualization (equal); data curation (equal); funding acquisition (lead); investigation (equal); methodology (equal); project administration (equal); resources (lead); software (equal); supervision (equal); validation (equal); visualization (equal); writing – review and editing (equal). **Nathalie Dupuy:** Conceptualization (equal); data curation (equal); investigation (equal); methodology (equal); project administration (equal); software (equal); supervision (equal); validation (equal); visualization (equal); writing – review and editing (equal). **Fabien Girard:** Conceptualization (equal); data curation (equal); investigation (equal); methodology (equal); project administration (equal); software (equal); supervision (equal); validation (equal); visualization (equal); writing – review and editing (equal). **Nina Girard-Perier:** Data curation (equal); investigation (equal); project administration (equal); software (equal); validation (equal); visualization (equal); writing – review and editing (equal). **Florent Kuntz:** Data curation (equal); investigation (equal); project administration (equal); software (equal); validation (equal); visualization (equal); writing – review and editing (equal). **Nicolas Ludwig:** Data curation (equal); formal analysis (equal); investigation (equal); project administration (equal); software (equal); validation (equal); visualization (equal); writing – original draft (equal).

## ACKNOWLEDGMENTS

Nathalie Dupuy, Fabien Girard and Sylvain R.A. Marque are thankful to Aix-Marseille University (AMU), Institut de Recherche pour le Développement (IRD) and Centre National pour la Recherche Scientifique (CNRS) A.M.U., I.R.D., and C.N.R.S. for support.

## DATA AVAILABILITY STATEMENT

The data that support the findings of this study are available from the corresponding author upon reasonable request.

## ORCID

*Blanche Krieguer* https://orcid.org/0009-0006-8756-8791
*Samuel Dorey* https://orcid.org/0000-0003-3178-2212
*Nathalie Dupuy* https://orcid.org/0000-0002-8739-2689
*Fabien Girard* https://orcid.org/0000-0001-9672-7658
*Nina Girard-Perier* https://orcid.org/0000-0002-5925-668X

## REFERENCES

[1] T. Chang, C. Yuan, Z. Guo, *Tribol. Int.* **2019**, *133*, 1.
[2] BPAS technical guide X-rays sterilization of single-use bioprocess equipment, part 1: industry need; requirements&risk evaluation. **2021**.
[3] N. Girard-Perier, M. Claeys-Bruno, S. R. A. Marque, N. Dupuy, F. Gaston, S. Dorey, *Chem. Commun.* **2021**, *57*, 11049.
[4] N. Dupuy, S. R. A. Marque, L. S. Fifield, M. Pharr, D. Staack, S. D. Pillai, L. Nichols, M. K. Murphy, S. Dorey, *Bioprocess Int.* **2022**, *20*, 24.
[5] H. De Brouwer, *Radiat. Phys. Chem.* **2022**, *193*, 109999.
[6] B. Croonenborghs, M. A. Smith, P. Strain, *Radiat. Phys. Chem.* **2007**, *76*, 1676.
[7] T. K. Kroc, *Radiat. Phys. Chem.* **2023**, *204*, 110702.
[8] In *Radiation Processing of Polymer Materials and its Industrial Applications*, John Wiley & Sons, Inc, Hoboken, NJ, USA **2011**, p. 1.

[9] G. Sadler, W. Chappas, D. E. Pierce, *Food Addit. Contam.* **2001**, *18*, 475.
[10] A. G. Chmielewski, *Advances in radiation chemistry of polymers*, IAEA, Vienna **2004**.
[11] O. Güven Ed., *Crosslinking and Scission in Polymers*, Springer, Dordrecht, Netherlands **1990**.
[12] D. Klepac, M. Ščetar, G. Baranović, K. Galić, S. Valić, *Radiat. Phys. Chem.* **2014**, *97*, 304.
[13] R. Tian, K. Li, Y. Lin, C. Lu, X. Duan, *Chem. Rev.* **2023**, *123*, 3007.
[14] A. E. Goulas, K. A. Riganakos, M. G. Kontominas, *Radiat. Phys. Chem.* **2004**, *69*, 411.
[15] A. L. Forster, Z. Tsinas, M. Al-Sheikhly, *Polymer* **2019**, *11*, 924.
[16] O. Tyapkova, M. Czerny, A. Buettner, *Polym. Degrad. Stab.* **2009**, *94*, 757.
[17] G. Audran, S. Dorey, N. Dupuy, F. Gaston, S. R. A. Marque, *Polym. Degrad. Stab.* **2015**, *122*, 169.
[18] E. T. Sarcan, A. Tas, M. Silindir-Gunay, A. Y. Ozer, S. Colak, B. Hekimoglu, *J. Pharm. Biomed. Anal.* **2020**, *188*, 113311.
[19] M. I. Chipara, *Nucl. Instrum. Methods Phys. Res. Sect. B* **1997**, *131*, 85.
[20] M. S. Jahan, M. C. King, W. O. Haggard, K. L. Sevo, J. E. Parr, *Radiat. Phys. Chem.* **2001**, *62*, 141.
[21] P. Silva, C. Albano, R. Perera, *Nucl. Instrum. Methods Phys. Res. Sect. B* **2007**, *265*, 300.
[22] P. Silva, C. Albano, D. Lovera, R. Perera, *Rev. Mex. Fis.* **2003**, *49*, 192.
[23] F. Gaston, N. Dupuy, S. R. A. Marque, S. Dorey, *Vib. Spectrosc.* **2018**, *96*, 52.
[24] W. Windig, D. A. Stephenson, *Anal. Chem.* **1992**, *64*, 2735.
[25] W. Windig, *Chemom. Intell. Lab. Syst.* **1994**, *23*, 71.
[26] W. Windig, *Chemom. Intell. Lab. Syst.* **1997**, *36*, 3.
[27] X. M. Zhang, S. Elkoun, A. Ajji, M. A. Huneault, *Polymer* **2004**, *45*, 217.
[28] C. France, P. J. Hendra, W. F. Maddams, H. A. Willis, *Polymer* **1987**, *28*, 710.
[29] Y. Morisawa, E. Tanimura, M. Ehara, H. Sato, *Appl. Spectrosc.* **2021**, *75*, 971.
[30] W. Windig, J. Guilment, *Anal. Chem.* **1991**, *63*, 1425.
[31] P. J. Gemperline, *J. Chemom.* **1989**, *3*, 549.
[32] J. C. Hamilton, P. J. Gemperline, *J. Chemom.* **1990**, *4*, 1.
[33] K. Yamamoto, K. Kato, Y. Sugino, S. Hara, Y. Miwa, M. Sakaguchi, S. Shimada, *Macromolecules* **2005**, *38*, 4737.
[34] F. J. Stadler, *Korean J. Chem. Eng.* **2011**, *28*, 2057.
[35] M. S. Jahan, K. McKinny, *S. Nucl. Instrum. Methods Phys. Res. Sect. B* **1999**, *151*, 207.
[36] Y. Ikada, K. Nakamura, S. Ogata, K. Makino, K. Tajima, N. Endoh, T. Hayashi, S. Fujita, A. Fujisawa, S. Masuda, H. J. Oonishi, *Polym. Chem.* **1999**, *37*, 159.
[37] E. M. Kornacka, G. Przybytniak, W. Święszkowski, *Radiat. Phys. Chem.* **2013**, *84*, 151.
[38] M. S. Mehmood, J. M. Shah, S. R. Mishra, B. M. Walters, *Radiat. Phys. Chem.* **2013**, *84*, 100.
[39] F. J. Stadler, *Korean J. Chem. Eng.* **2011**, *28*, 954.
[40] M. Abou Fadel, A. de Juan, N. Touati, H. Vezin, L. Duponchel, *J. Magn. Reson.* **2014**, *248*, 27.
[41] M. A. Fadel, A. de Juan, H. Vezin, L. Duponchel, *Anal. Chim. Acta* **2016**, *947*, 9.
[42] J.-H. Jiang, Y. Liang, Y. Ozaki, *Chemom. Intell. Lab. Syst.* **2004**, *71*, 1.
[43] H. Paul, H. Fischer, A. Berndt, Magnetic Properties of Free Radicals-Organic C-Centered Radicals. **1977** 9b.
[44] P. Silva, C. Albano, R. Perera, J. González, M. Ichazo, *Nucl. Instrum. Methods Phys. Res. Sect. B* **2004**, *226*, 320.
[45] A. G. Davies, J. A. Howard, M. Lehnig, *Magnetic Properties of Free Radicals- Organic O-, P-, Se-, Si-, Ge-, Sn-, Pb-, As-, Sb-Centered Radicals*. **1979** 9 c2.
[46] I. L. J. Dogué, N. Mermilliod, F. J. Genoud, *Polym. Sci. Part Polym. Chem.* **1994**, *32*, 2193.
[47] Y. Hori, S. Shimada, H. Kashiwabara, *J. Polym. Sci. Polym. Phys. Ed.* **1984**, *22*, 1407.

## SUPPORTING INFORMATION

Additional supporting information can be found online in the Supporting Information section at the end of this article.

**How to cite this article:** B. Krieguer, S. R. A. Marque, S. Dorey, N. Dupuy, F. Girard, N. Girard-Perier, F. Kuntz, N. Ludwig, *J. Appl. Polym. Sci.* **2024**, e55098. https://doi.org/10.1002/app.55098

10974628, 0, Downloaded from https://onlinelibrary.wiley.com/doi/10.1002/app.55098 by Cochrane France, Wiley Online Library on [18/01/2024]. See the Terms and Conditions (https://onlinelibrary.wiley.com/terms-and-conditions) on Wiley Online Library for rules of use; OA articles are governed by the applicable Creative Commons License

# Supporting Information : Radical detection and monitoring in polymer materials irradiated with gamma and X-rays: Polyethylene and Polypropylene

## Polyethylene

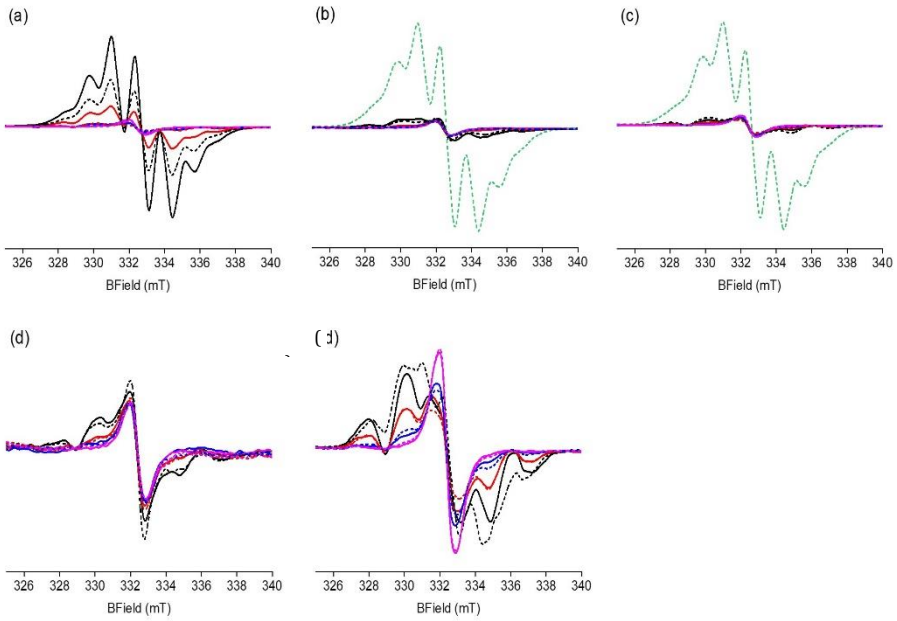


Figure S1: ESR signal of PP samples after gamma (solid line) and X-rays (dotted line) irradiation at various times after irradiation: 1 day (green line), 9 days (black line), 15 days (red line), 30 days (blue line), 60 days (pink line) for (a) HDPE-7, (b) HDPE-8, (c) HDPE-9, (d) HDPE-10, (e) HDPE-11.

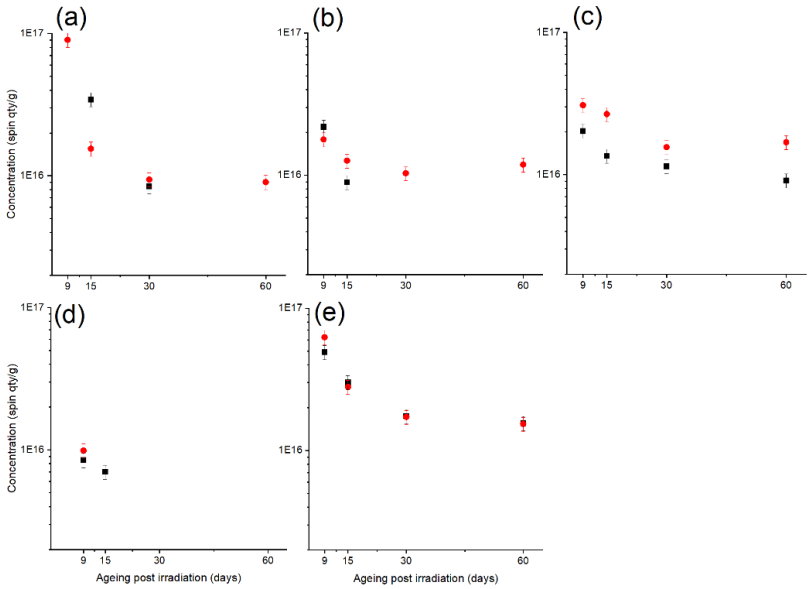


Figure S2: Kinetics studies monitoring of the concentration of radicals for each HDPE sample analyzed by ESR as concentration (spin/g) vs ageing (days). (a) Sample 7, (b) Sample 8, (c) Sample 9, (d) Sample 10, (e)

Sample 11. Red circles are samples irradiated with X-rays and black squares are samples irradiated with gamma ray.

| | RRSSQ |
|---|---|
| First component extracted | 50% |
| Second component extracted | 13% |
| Third component extracted | 5% |

Table S1: Equivalence test of irradiation technologies for PE samples.

| | $[radicals]_{X\text{-}rays}/[radicals]_{gamma}$ | | | |
|---|---|---|---|---|
| | D9 | D15 | D30 | D60 |
| Sample 7 | ✓ 0.8 | ✓ 0.5 | ✓ 1.1 | n.a. |
| Sample 8 | ✓ 0.8 | ✓ 1.4 | n.a. | n.a. |
| Sample 9 | ✓ 1.5 | ✓ 2.0 | ✓ 1.4 | ✓ 1.9 |
| Sample 10 | ✓ 1.2 | n.a. | n.a. | n.a. |
| Sample 11 | ✓ 1.3 | ✓ 0.9 | ✓ 1.0 | ✓ 1.0 |

Table S2: Variation in data set (RRSSQ) after extraction of each component

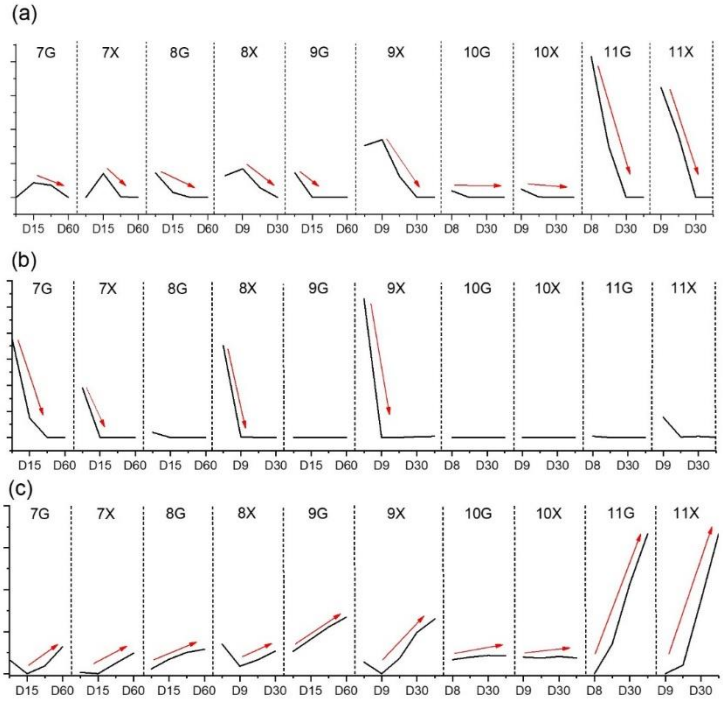


Figure S3: Concentration profile of (a) signal of Alkyl radical (b) allyl radical, (c) polyenyl radical obtained with SIMPLISMA treatment for the HDPE samples

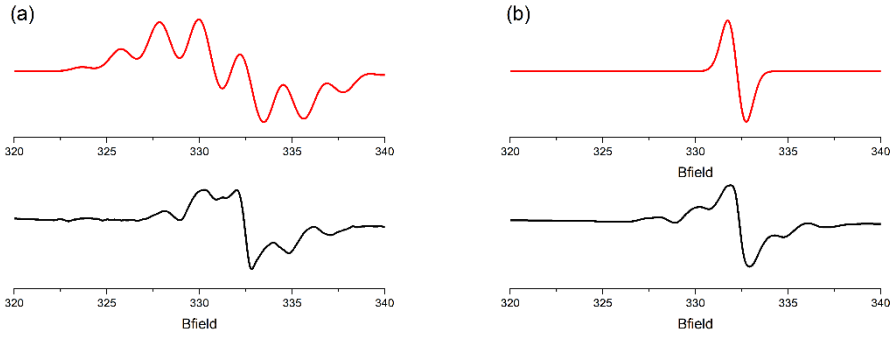


Figure S4: (a) Signal of alkyl radical (red line) simulated with Easyspin and (black line) reconstructed with SIMPLISMA treatment. (b) Signal of polyenyl radical (red line) simulated with Easyspin and (black line) reconstructed with SIMPLISMA treatment

## Polypropylene and thermoplastic elastomer

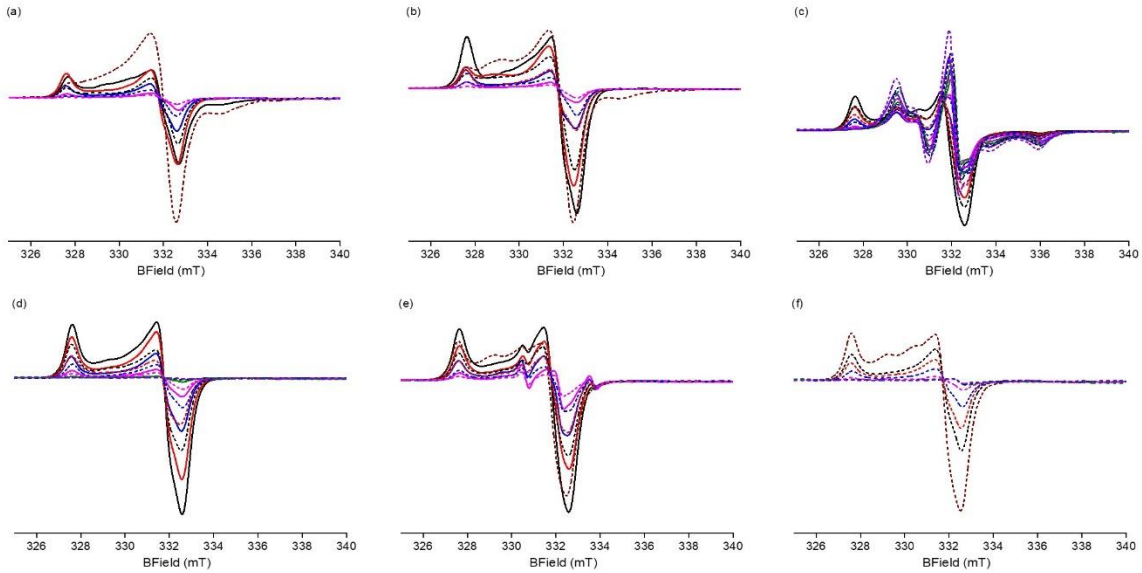


Figure S5: ESR signal of PP samples after gamma (solid line) and X-rays (dotted line) irradiation at various times after irradiation: 1 day (green line), 9 days (black line), 15 days (red line), 30 days (blue line), 60 days (pink line), 120 days (olive green line), 180 days (royal blue line) and 380 days (violet line) for (a) PP-1, (b) PP-2, (c) PP-3, (d) PP-4, (e)TPE-5, (f) TPE-6.

Table S3: Equivalence test of irradiation technologies for PP samples.

| | $[radicals]_{X\text{-}rays}/[radicals]_{gamma}$ | | | |
|---|---|---|---|---|
| | D9 | D15 | D30 | D60 |
| Sample 1 | ✓ 0.4 | n.a. | ✓ 0.4 | ✓ 0.5 |
| Sample 2 | ✓ 0.3 | ✓ 0.4 | ✓ 0.4 | ✓ 0.6 |
| Sample 3 | ✓ 0.7 | ✓ 0.7 | ✓ 0.9 | ✓ 1.0 |
| Sample 4 | ✓ 0.5 | ✓ 0.5 | ✓ 0.6 | ✓ 0.9 |
| Sample 5 | ✓ 0.5 | ✓ 0.6 | ✓ 0.6 | ✓ 0.8 |

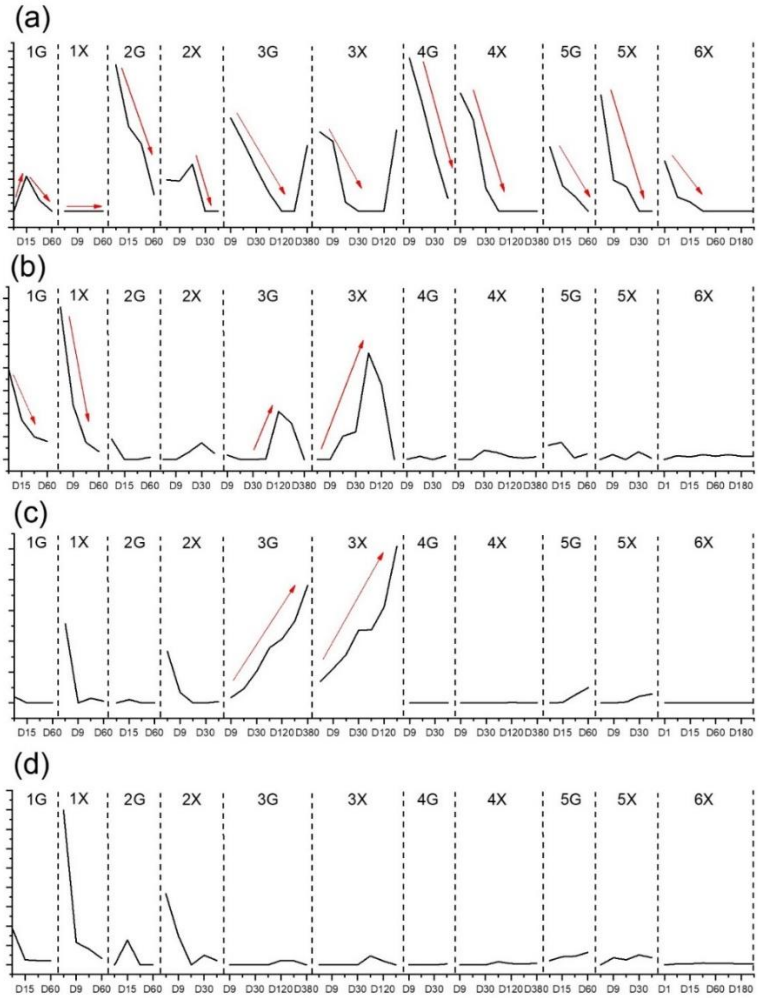


Figure S6: Concentration profile of (a)(b) signal of radical peroxyl, (c) nitroxide radical and (d) mixture of peroxyl radical and unidentified radical obtained with SIMPLISMA treatment for the PP and TPE samples.

Table S2: Variation in data set (RRSSQ) after extraction of each component

| | RRSSQ |
|---|---|
| First component extracted | 84% |
| Second component extracted | 80% |
| Third component extracted | 13% |
| Fourth component extracted | 9% |

## 5.2. Comportement du polypropylène après irradiation gamma, rayons X et faisceau d'électrons

Cet article, soumis dans la revue *Journal of Applied Polymer Science* en 2025, fournit une analyse approfondie des effets de l'irradiation par rayons gamma, rayons X et par faisceau d'électrons à 50 et 100 kGy sur les matériaux polymères, en se concentrant spécifiquement sur le polypropylène (PP). Les résultats ont des implications significatives pour les applications industrielles, notamment dans le secteur biopharmaceutique, où la stérilisation des matériaux à base de polymères est cruciale. Cette discussion étendue explore plus en détail les résultats de l'étude, leurs implications et leurs applications potentielles, tout en examinant le rôle de la formulation des polymères et des additifs dans l'influence de la réponse à l'irradiation. Le potentiel des diverses technologies d'irradiation a été évalué pour une utilisation interchangeable, mettant en évidence les limites de l'étude ainsi que les perspectives de recherche futures. La Figure 14. Illustre les différentes techniques analytiques utilisées dans l'article présenté ci-dessous.

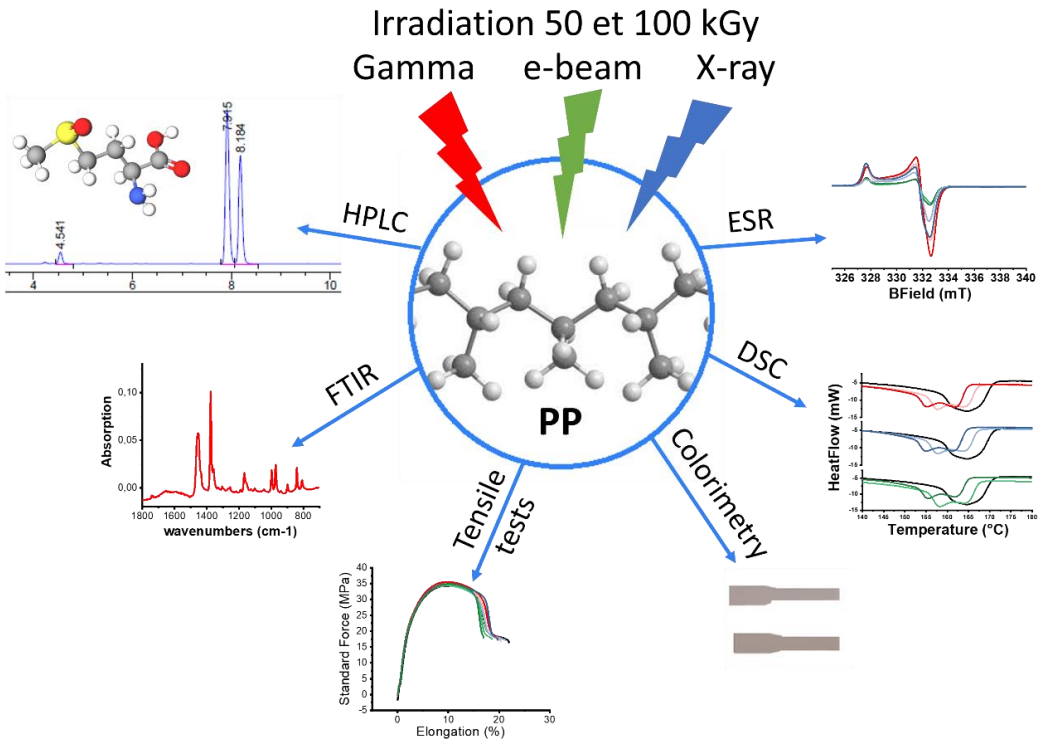


Figure 14 : Techniques analytiques utilisées sur les échantillons formulés à partir de PP après irradiation par rayons gamma, rayons X et faisceau d'électrons à 50 et 100 kGy

L'étude révèle que l'irradiation par rayons gamma, par rayons X et par faisceau d'électrons produisent des radicaux libres dans les matériaux polymères, qui sont essentiels pour amorcer des modifications dans ces matériaux. L'utilisation de la RPE a permis de surveiller et d'identifier ces radicaux sur une période prolongée. Les résultats indiquent que le type de radicaux générés dépend principalement du type de polymère, les additifs jouant également un rôle dans la production de signaux superposés. L'équivalence de l'irradiation par rayons gamma, X et faisceau d'électrons dans la production de radicaux similaires dans les PP est un résultat clé.

Les propriétés thermiques après irradiation par rayons gamma, X et faisceau d'électrons ont été examinées. Les changements de températures de transition et de capacité calorifique ont été déterminés par DSC pour évaluer la dégradation des matériaux. Les propriétés thermiques, représentés dans la figure 6 de l'article, sont équivalentes pour les trois technologies d'irradiation, bien qu'une légère réduction de la température de fusion ait été observée à des doses plus élevées.

Les propriétés mécaniques du PP ont été évaluées à l'aide de tests de traction, mesurant la résistance et l'élasticité des matériaux. Les propriétés mécaniques des échantillons étudiés restent constantes après irradiation par rayons gamma, rayons X et faisceau d'électrons. On observe une différence des valeurs d'élongation entre les quatre échantillons de PP étudiés dans la figure 7 de l'article.

Le jaunissement des PP formulés après irradiation, qui peut entraîner une modification de l'apparence, a été étudié par colorimétrie. Les résultats de l'ACP représenté dans la figure 8 révèlent qu'un échantillon analysé a un jaunissement plus important après irradiation par rayon gamma et X que par faisceau d'électrons, alors que le deuxième échantillon de PP analysés ne présente pas de différence entre les trois technologies d'irradiation. Le jaunissement du PP peut être attribué par la présence de certains additifs utilisés dans la formulation du polymère.

Une étude spectroscopique utilisant la FTIR a été menée pour identifier les modifications chimiques dans la structure des polymères. La FTIR permet de détecter les changements dans les liaisons chimiques et les groupes fonctionnels, fournissant ainsi des informations sur les altérations moléculaires causées par l'irradiation. Aucune modification de la structure chimique du PP après irradiation n'a été observée par spectroscopie infrarouge, bien que les spectres varient avec la nature et la quantité des additifs présents.

La génération de peroxydes et de peracides, résultant de la réactivité radicalaire post-irradiation, a été étudiée par l'oxydation de la méthionine (imitant l'oxydation des protéines) suivie par HPLC. Les concentrations de méthionine sulfoxyde dans la solution de méthionine en contact avec le PP révèlent des différences attribuées à la formulation du PP plutôt qu'à la technologie d'irradiation. Pour chaque échantillon de PP, les modèles

de régression dans la figure 11 montre qu'il n'y a aucune différence significative entre les trois technologies.

La formulation des polymères, y compris l'utilisation d'additifs, joue un rôle crucial dans l'influence de la réponse des matériaux à l'irradiation. Les additifs tels que les stabilisants à base d'amines encombrés (HALS) peuvent avoir un impact significatif sur le type et la stabilité des radicaux formés. Par exemple, la présence de HALS dans le PP-3 a conduit à la formation de radicaux nitroxyde, qui sont hautement persistants. Cela souligne l'importance de comprendre les formulations spécifiques des polymères utilisés dans les applications industrielles, car celles-ci peuvent affecter le comportement du matériau après irradiation. Les polymères ne sont pas des matériaux homogènes ; ils sont souvent mélangés avec divers additifs pour améliorer leurs propriétés mécaniques, thermiques et chimiques, ou pour répondre à des exigences spécifiques de performance. Ces additifs peuvent inclure des stabilisants, des plastifiants, des antioxydants et des agents de renforcement, chacun ayant un rôle distinct dans la modification des propriétés du polymère. Il est important de souligner que cette étude n'avait pas pour but de comparer les formulations entre-elles. Il s'agissait d'évaluer l'équivalence du comportement après irradiation gamma, rayons X et faisceau d'électrons des polypropylènes quel que soit leur formulation spécifique.

Cette équivalence suggère que l'irradiation par rayons X ou par faisceau d'électrons pourrait servir d'alternative viable à l'irradiation gamma, en particulier dans le contexte de la demande croissante de stérilisation dans l'industrie biopharmaceutique. Ces résultats ont des implications significatives pour le secteur biopharmaceutique, car ils suggèrent que l'interaction entre les photons et la matière est cohérente à travers différents grades de polymères lorsqu'ils sont exposés aux rayons gamma, X et faisceau d'électrons.

En conclusion, cette étude fournit des informations importantes sur les effets de l'irradiation par rayons gamma, X et faisceaux d'électrons sur les matériaux polymères comme le PP, avec des implications significatives pour les applications industrielles, notamment dans le secteur biopharmaceutique. L'équivalence démontrée des trois technologies d'irradiation dans le comportement des matériaux PP soutient le potentiel de leur utilisation interchangeable dans les processus de stérilisation.

**How X-rays, e-beam, and gamma irradiation change the chemical and physical properties of polypropylene**

*Blanche Krieguer, Sylvain R.A. Marque, Fabien Girard, Nathalie Dupuy, Nicolas Ludwig, Florent Kuntz, Samuel Dorey*

B. Krieguer, S. Dorey
Sartorius Stedim FMT S.A.S, Z.I. Les paluds, Avenue de Jouques CS91051, 13781, Aubagne Cedex, France
E-mail : blanche.krieguer@sartorius.com; samuel.dorey@sartorius.com

S.R.A. Marque
Aix Marseille Univ, CNRS, ICR, Case 551, 13397 Marseille, France;
E-mail : sylvain.marque@univ-amu.fr

N. Dupuy, F. Girard
Aix Marseille Univ, Avignon Univ, CNRS, IRD, IMBE, Marseille, France

N. Ludwig, F. Kuntz
Aerial, 250 Rue Laurent Fries, 67400 Illkirch, France

Keywords: Polypropylene, Irradiation technologies, ESR, DSC, FTIR, mechanical properties, HPLC

This study investigated the effects of gamma, e-beam, and X-ray irradiation on medical grade of polypropylene (PP) to assess their implications for pharmaceutical applications. Using an extensive suite of analytical techniques, the chemical and physical transformations of irradiated PP were evaluated. Key findings indicated that irradiation did not significantly alter the mechanical properties, with tensile strength and elongation at break remaining stable across all irradiation types and doses. Thermal analysis via DSC showed a slight decrease in melting temperature at higher doses. ESR detected peroxyl radicals, which decreased over time, with no significant differences attributable to irradiation type or dose. Colorimetric analysis showed yellowing in PP samples, particularly with gamma and X-ray irradiation, linked to specific additives. The chemical structure was not modified. HPLC demonstrated that oxidation potential was more dependent on the PP formulation than on the irradiation technology. The study concluded that while irradiation technology did not significantly impact PP properties, the polymer formulation played a crucial role in determining the material's response.

## 1. Introduction

Polymers are essential in the pharmaceutical industry, particularly in various single-use medical devices such as syringes, gloves, and disposable plastic bags. The type of polymer used can differ based on the application and required properties. Polypropylene, noted for its excellent performance, chemical stability, attractive mechanical and thermal properties and cost-effectiveness 1–3, is widely used in the production of slide clamps, connectors, and filters.

Among sterilization technologies for single used devices made of polymer, the usage of radiation is one of the most frequent. Currently, gamma radiation, provided by the isotope cobalt-60, is the most commonly used radiation technology for sterilizing medical devices and biopharmaceutical products 4. The current healthcare context leads to a strong growth in the manufacture of biopharmaceutical products. In addition, there are concerns about the capacity of sterilization using gamma radiation in future years. Two alternative technologies, e-beam and X-ray are being considered for use as additional technologies to gamma sterilization 4–7. Electron beam irradiation is generated when electrons are accelerated by an electro-magnetic field in an accelerator. X-rays are photons that are generated using an electron beam accelerator 8. The electron beam is converted to photons by accelerating the electrons into a high-density material (tungsten, tantalum). X-rays and gamma rays are both photons, but gamma rays come from radioactive sources and are emitted during a radioactive decay process 9. E-beam exhibit a different dose profile and a much limited penetration which implies reconsidering packaging or irradiation geometry when converting from photon irradiation to e-beam. For these irradiation technologies, the main difference resides in delivered average dose rates which are very different (in the order few kGy/h for gamma rays, kGy/min for X-rays and kGy/s for e-beam). The concept of Linear Energy Transfer (LET) is crucial in understanding the effects of these radiation types on polymers 10. LET measures the energy deposited by ionizing radiation per unit length of the material. High LET radiation, such as swift heavy ions, deposits energy in a dense track, leading to localized energy deposition and potentially more severe damage, including crosslinking and chain scission, compared to low LET radiation like gamma rays or e-beams. The presence of energy sinks, such as unsaturated bonds or aromatic rings within polymers, can capture transferred energy, influencing the radiation-induced behavior.

The exposure of polypropylene (PP) to ionizing radiation alter its performance characteristics 11,12. Various physical and physicochemical methods are available to assess the effects of such radiation doses 13. The ultimate radiative transformations that result in irreversible changes in the properties of irradiated PP are influenced by the irradiation conditions and the input dose. Previous studies on the radiolysis of PP have demonstrated chain scission, accompanied by chain crosslinking, increased chain unsaturation, and a reduction in crystallinity 14. Crosslinking of polymer chains leads to an increase in molecular weight and enhances the polymer's thermal stability and mechanical properties. Conversely, chain scission results in a decrease in molecular weight, thermal stability, melting temperature, and strength. In the case of PP, the coexistence of both chain scission and crosslinking generally results in an overall loss of matrix properties, medical grades (stabilized ones) are known to be able to handle typical sterilization dose 15 but the maximal acceptable dose must be carefully assessed for each grade and application.

In this study, irradiation doses of 50 kGy and 100 kGy were used and the primary objective was to compare the effects of the three different irradiation technologies. This research investigates the modifications in polymer structures resulting from these irradiation methods, aiming to provide insights into their general attributes for use in biopharmaceutical applications or interactions with biopharmaceutical solutions. The changes in transition temperatures and heat capacity were determined by Differential Scanning Calorimetry (DSC) as a marker of material degradation. The generation of reactive species such as peroxides and peracids, due to post-irradiation radical reactivity, was probed by the oxidation of methionine (mimicking protein oxidation) monitored by High-Performance Liquid Chromatography (HPLC). The yellowing of polypropylene was studied by colorimetry. A spectroscopic study using FTIR (Fourier Transform Infrared Spectroscopy) was conducted to identify chemical modifications in the polymer structure. FTIR allows the detection of changes in chemical bonds and functional groups, thus providing information on molecular alterations caused by irradiation. The mechanical properties of the polymers were studied using tensile tests, which measure the strength and elasticity of materials under tensile force. Finally, long-lived radicals were tracked by Electron Spin Resonance (ESR), a technique that allows the detection and quantification of radical species present in irradiated materials.

## 2. Materials and methods

### 2.1. Samples

The samples investigated (Figure 1) are composed of polypropylene (PP) and thermoplastic elastomer (TPE). Table 3 gathers the typical physical properties provided by resin suppliers.

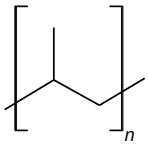

Figure 1: Chemical structure of Polypropylene

Table 3: Non-irradiated PP characteristics

| Polymers | Polypropylene (PP) | | | | | TPE |
|---|---|---|---|---|---|---|
| Identification number | PP-1 | PP-2 | PP-3 | PP-4 | PP-5 | TPE-6 |
| Typical industrial application | Slide clamp | Cartridge filters | Connector | Filter housing | Connector | TPE tubing |
| Density ($g \cdot cm^{-3}$) | 0.9 | 0.9 | 0.9 | 0.905 | 0.905 | 0.9 |
| Polymer type | Homopolymer | Homopolymer | Copolymer | Homopolymer | Homopolymer | Copolymer |

### 2.2. Samples packaging

The samples were packaged in cardboard boxes at room temperature at Sartorius Stedim FMT S.A.S, Aubagne. This method, combined with the appropriate arrangement of plastic components in thin cardboard boxes, ensured consistent treatment. The dose uniformity is monitored through dosimetry.

### 2.3. Samples irradiation

*Gamma rays*

Gamma ray irradiation, sourced from $^{60}Co$, was conducted at Ionisos in Dagneux, France, with an average dose rate of 2 kGy/h. The irradiation process spanned several days, accumulating the dose over multiple runs within the irradiation bunker.

*X-ray*

X-ray irradiation was carried out at Aerial-CRT using the feerix® facility, which is based on a Rhodotron (TT300 – IBA). A 7 MV X-ray field was produced by converting a 7 MeV electron beam using a tantalum target. The irradiation was performed horizontally with a

pallet conveyor, and multiple runs were conducted in the X-ray field to accumulate the dose. This process was completed in one day with an average dose rate of approximately 12 kGy/h.

*e-beam*

E-beam irradiation was conducted at Aerial-CRT using the same feerix® facility as the X-ray treatment. A 10 MeV vertical electron beam was utilized, with an average dose rate of 18 $MGy \cdot h^{-1}$ (5 kGy/s). The irradiation was performed in increments of 50 kGy to prevent critical temperature increases in the samples.

### 2.4. Dosimetry

The targeted delivered doses were approximately 50 kGy and 100 kGy, with the dose uniformity of ± 10%. Table 4 summarizes the effective doses. To accurately measure the absorbed dose, alanine pellets combined with ESR spectroscopy (Magnettech MS5000 ESR, Bruker) were used, along with AerEDE® dosimetry software (Aerial, France). Dosimetry readings were taken in a manner traceable to an international standard.

Three dosimeters were placed within the volume of the box containing the samples to establish dose uniformity within the sample box.

**Table 4:** Effective doses on samples irradiated by gamma-rays, X-ray and e-beam

| Target doses (kGy; ± 10%) | Effective doses (kGy; ± 10%) | | |
|---|---|---|---|
| | Gamma | X-ray | e-beam |
| 50 | 51 | 50 | 55 |
| 100 | 90 | 99 | 109 |

### 2.5. Electron Spin Resonance

ESR measurements were performed using a Magnettech MS5000X ESR spectrometer, manufactured by Bruker in Switzerland, and operated with ESR studio software for control. The samples were prepared from either irradiated dogbone specimens or parts of irradiated materials. Small pieces were cut to fit into a glass probe with an inner diameter of 4.2 mm. The samples, approximately 4 cm in height and weighing between 100 to 200 mg, were then ready for analysis.

First, the signal position was verified over a wide magnetic field range (150-400 mT). Then, the magnetic field range was narrowed to 320-340 mT around the sample, where the signal indicative of organic radicals was present. The spectra were recorded using a modulation

amplitude of 0.2 mT, a sweep time of 60 seconds, and a single scan. Measurements were taken from 1 to 60 days after sample irradiation, on the following days (D): D9, D15, D30, and D60. During this period, samples were kept in the dark at controlled temperature and humidity (25°C and 45% RH).

Signal amplitude (peak-to-peak) was measured on ESR spectra and calibrated using TEMPO (2,2,6,6-Tetramethylpiperidin-1-oxyl) standard samples with spin concentrations between $1 \cdot 10^{16}$ and $1 \cdot 10^{19}$ spins·$g^{-1}$. TEMPO and standard samples were prepared according to reported procedures [16]. TEMPO standards are very stable over time, and the calibration curve was measured eight times over several months to assess measurement variability. Therefore, ESR quantification in this paper should be considered as TEMPO equivalent, as the amplitude between the TEMPO radical and the probed radical in the polymer may differ.

### 2.6. Differential Scanning Calorimetry

Differential Scanning Calorimetry (DSC) was employed to analyze the physical and thermal properties of the polymers. In this process, a thermocouple within the furnace measures the temperature of the sample, while another thermocouple measures the temperature of a reference (an empty crucible). The heat flow variations observed during the melting transition were recorded, resulting in the creation of a thermogram. These DSC tests were conducted using a Sensys Evo131 thermal analyzer from Setaram.

For the DSC analysis, each sample, weighing approximately 20 mg, underwent three heating and cooling cycles. The temperature range for heating was set between -50°C and 200°C, with a heating rate of 10°C per minute for PP samples and for TPE the temperature range was set between room temperature and 220 °C, with a heating rate of 10 °C. A stabilization period was included before and after each cycle to ensure accuracy. Only the data from the second and third cycles were used for analysis, as the first cycle served to eliminate any previous thermal history of the material. The melting peak temperature and the onset of melting were both calculated and integrated using Calisto Processing software.

### 2.7. Tensile Test

Elongation, ultimate tensile strength (UTS), toughness, and the yields have been measured on the test sample. The mechanical properties of irradiated and nonirradiated samples were measured using a universal testing machine (Zwick Z005). The crosshead speed used was 50 mm/min (PP-1 and PP-2) and 500 mm/min. The initial gauge length was 100 mm. Five to

eight specimens were performed for each sample. Tensile strength tests were measured at 23 ± 3 °C and at 1 atm. Ultimate tensile strength (UTS) is then determined as the maximum stress the material can withstand and is calculated by dividing the maximum load by the original cross-sectional area of the specimen [17].

### 2.8. Colorimetry

Color measurements of the polymeric materials were outsourced to AERIAL.
Color measurements were performed using the CIELAB color space also referred to as L*a*b* with the CR 400 Konica Minolta chromameter. Verification measurements were done with white plaque CR A43 Konica Minolta. L*, a*, b* values were recorded for each sample. The measurement is valid only if the sample surface is plane, so that, measurements (from 2 to 5) were performed on different locations on the sample depending on the sample shape. The l*, a*, b* were measured for PP-1 and PP-2 samples prior to irradiation and after gamma and X-ray irradiation at 50 kGy.

### 2.9. Fourier Transform InfraRed

Samples were directly placed onto the Bruker "Golden Gate" Attenuated Total Reflectance (ATR) accessory, which features a diamond crystal, without any prior preparation. ATR-FTIR spectra of the polymer samples were captured in the range of 4000 to 650 $cm^{-1}$, with a resolution of 4 $cm^{-1}$ and 100 scans, using a Thermo Nicolet IS10 spectrometer. This spectrometer is equipped with an MCT/A detector, an Ever-Glo source, and a KBr/germanium beam splitter. The Mid-InfraRed (MIR) spectrometer was situated in an air-conditioned room maintained at 21°C.
To mitigate the potential effects of polymer inhomogeneity, three spectra were recorded for each sample. A background scan without samples, conducted under the same resolution and scanning conditions as the samples, was performed before each set of three acquisitions. The ATR crystal was thoroughly cleaned with ethanol to remove any residual traces from previous samples, and cleanliness was confirmed by recording a background spectrum. The penetration depth into the sample was only a few microns.

### 2.10. Oxidation essay by High Performance Liquid Chromatography

Each sample was cut into small pieces (2 mm) and placed in a vial . Vials were filled with a 50 µM solution of methionine in buffer (10 mM $NaH_2PO_4$, 10 mM $Na_2B_4O_7 \bullet 10H_2O$, 5 mM

$NaN_3$, pH 8.2). To determine the concentrations of methionine and methionine sulfoxide, an Agilent 1260 HPLC system (Waghaeusel-Wiesental, Germany) equipped with a quaternary pump (G1311C), an autosampler (G1329B), and a fluorescence detector (G1321B) was used. The automated online derivatization (in the autosampler) using an injection program is detailed in Figure 2. The derivatization reagent used was the ortho-phthaldehyde (OPA). The gradient program was as follows: 0–13.4 min, 2% phase B; 13.4 min, 57% phase B; 13.5–15.8 min, 100% phase B; 18 min, 2% phase B. Separation was carried out on an Agilent Poroshell HPH-C18 column (4.6 mm x 100 mm, 2.7 µm particles—Waghaeusel-Wiesental, Germany) used with a pre-column, UHPLC guard Poroshell HPH-C18, 4.6 mm. The column was maintained at 40 °C ± 0.8 °C in a thermostatted column compartment (G1316A) during the analyses. The fluorescence detector was set to an excitation wavelength of 340 nm and an emission wavelength of 450 nm. The total runtime of the method was 20 min. Chromatographic data were acquired and evaluated with the HPLC 1260 OpenLAB software (Waghaeusel-Wiesental, Germany). Internal calibration was done by spiking 20 µL of L-Norvaline in each sample and standard [18].

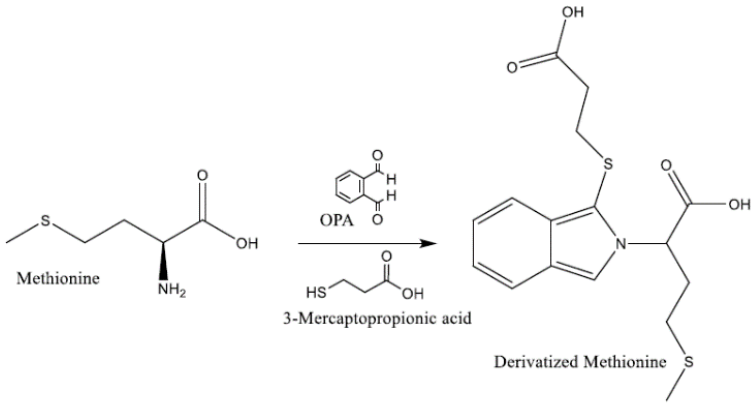


**Figure 2:** Automatic derivatization reaction for detecting methionine with a fluorescence detector

### 2.11. Equivalency analysis

*ESR and HPLC*

Regression models were performed using the Minitab® software to assess the effect of doses (50 and 100 kGy), the effect of ageing after irradiation, and the effect of the three irradiation technologies on the spin/g values measured by ESR for each sample or on the methionine

sulfoxide concentration. These models allow for the evaluation of the significant impact of each independent variable, with a confidence interval at 95% (α=0.05).

*Tensile test*

To assess the equivalency between gamma, X-ray, and e-beam irradiated samples, equivalence tests (TOST, two one-sided t-test [19]) were performed with Minitab® software. For the tensile tests, the equivalency is claimed when the ratio $[Radicals]_{X\text{-}ray\ or\ e\text{-}beam}/[Radicals]_{gamma}$ or $[Radicals]_{e\text{-}beam}/[Radicals]_{X\text{-}ray}$ is above the lower limit and below the upper limit. For the elongation, the criterion is 25% and for the yield the criterion is 15%.

### 2.12. Principal Component Analysis (PCA)

Principal component analysis (PCA) is a widely utilized technique in chemometrics [20,21] and has been detailed in a prior study [16]. Each principal component (PC) is designed to capture the maximum variance from the remaining data. By projecting the scores onto the space defined by the PCs, one can visualize the similarities and differences among the samples. The loadings, on the other hand, reveal which variables contribute the most information to each PC. In this study, we focused on PCs that accounted for more than 15% of the variance. Consequently, in some instances, only the first PC was significant, allowing the scores to be displayed as a bar chart. In other instances, the first two PCs were significant, and the scores were represented as a scatter plot.

PCA was conducted on spectra obtained via FTIR on PP and TPE samples non irradiated and irradiated by gamma rays, e-beam, and X-ray at doses of 50 and 100 kGy to emphasize the impact of the irradiation technology. The spectra were corrected using baseline correction and standard normal variate (SNV) pretreatment to address additive and multiplicative effects. PCA models were developed using the CAMO (Computer Aided Modelling, Trondheim, Norway) software UNSCRAMBLER X.1.

## 3. Results and discussion

### 3.1. Electron Spin Resonance

A first paper was published on polypropylene irradiated by X-ray and gamma at 50 kGy in 2024 [3]. The present study provides additional data recorded at higher doses for both X-ray and gamma, as well as new e-beam data. Figure 3 displays the ESR Signals of PP-2, PP-3 and TPE-6 after gamma, e-beam, and X-ray irradiations at 50 and 100 kGy, nine days post-

irradiation. No ESR signals were detected in non-irradiated samples. Similar signals to those of PP-2 were also observed for PP-1, PP-4 and PP-5 (figure S1).

The radicals detected in irradiated PP have a *g*-factor of 2.015, which is attributed to a peroxyl radical ($RO_2^{\bullet}$; $g$ = 2.015) as reported in the literature [22–24]. Additionally, an unidentified radical is present in TPE-6, and its signal overlaps with that of the peroxyl radical. A significant signal from a side product is observed alongside the peroxyl signals in PP-3. This signal persists and becomes dominant from 60 days of ageing post-irradiation. The *g*-value of 2.004 is attributed to a nitroxide, a radical side product.

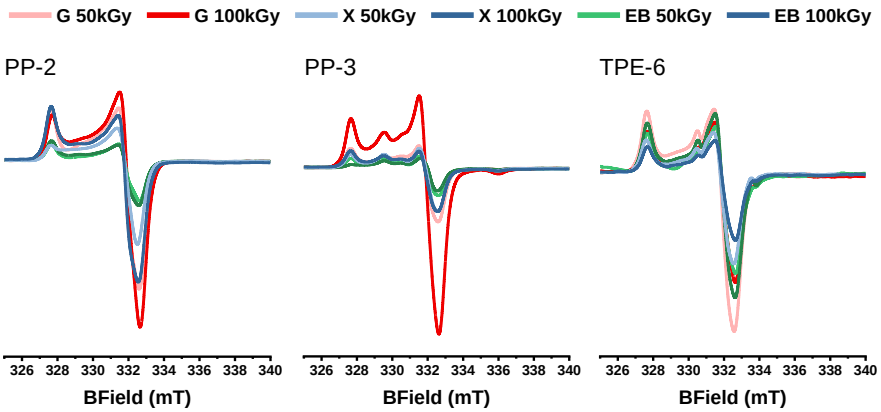


**Figure 3:** ESR signal of PP-2, PP-3 and TPE-6 nine days after irradiation at 50 kGy and 100 kGy by gamma irradiation (red line), X-ray (blue line) and e-beam (green line). Samples irradiated at 50 kGy are represented by pastel colors, and samples irradiated at 100 kGy by dark colors.

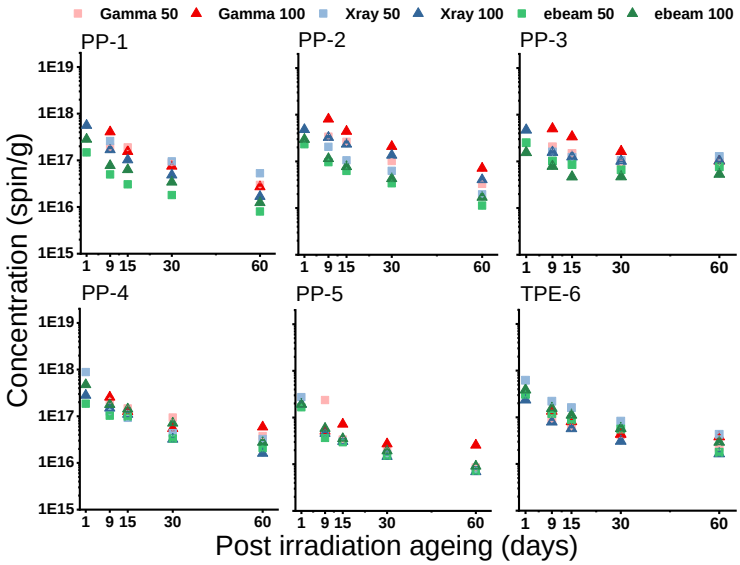


**Figure 4:** Monitoring of the concentration of radicals for PPs and TPE samples by ESR as concentration (spin/g) vs post irradiation ageing (days). Squares correspond to samples

irradiated at 50 kGy and up triangles correspond to samples irradiated at 100 kGy, red for gamma irradiation, blue for X-ray and green for e-beam

Figure 4 shows the concentration of radicals for each sample. Radical levels in samples exposed to gamma, X-ray, and e-beam irradiation at 50 kGy and 100 kGy were monitored for up to 60 days post-irradiation. The ESR signal and the quantity of radicals generated decrease after the three irradiation technologies.

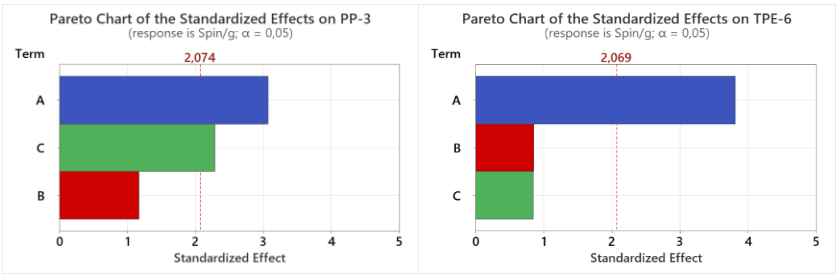


**Figure 5:** Pareto analysis of significant effects on radical concentration on PP-3 and TPE-6: Ageing after irradiation (A in blue), Dose (B in red) and Irradiation technologies (C in green)

Regression models were performed for each sample to determine whether the dose, post-irradiation ageing, and irradiation technologies significantly influence the quantity of radicals generated in the samples (Figure 5). A p-value greater than 0.05 indicates a non-significant effect. The Pareto chart represents the absolute values of the standardized effects from the largest to the smallest, along with a reference line indicating statistical significance. The reference line for statistical significance is based on the significance level (denoted by α), which is 1 minus the confidence level for the analysis [25].

Both post-irradiations, ageing and the irradiation technologies significantly affect the radical concentration for PP-3 (Figure 5a). Fewer radicals are generated in samples irradiated by X-ray and e-beam compared to gamma irradiation (see the model equation and coefficient in SI). For TPE-6 (Figure 5b), only post-irradiation ageing significantly affects the radical concentration, which decreases after irradiation. Similar results are observed for PP-1, PP-2,

PP-4, and PP-5 (see Figure S2). The equations and coefficients of the regression models obtained for each sample are reported in the SI.

### 3.2. Thermal behaviors

The DSC curves for PP-1, PP-2, and TPE-6 are shown in Figure 6a-c, while the DSC curves for PP-3, PP-4, and PP-5 are presented in Figure S3 in SI. The melting peak temperature are represented in Figure S4 in the SI. The DSC results reveal three distinct behaviors: some samples exhibit a single peak after irradiation, others develop a shoulder peak, and one PP develop a shoulder peak after gamma irradiation.

The shape of the DSC curves (Figure 6) provides valuable insights into the structural characteristics. Initially, all PP samples displayed a single melting peak. After irradiation, the melting peak shifted to a lower temperature and developed a shoulder peak for PP-1 and PP-5 (Figure 6a). Interestingly, PP-2 developed a shoulder peak after gamma irradiation, suggesting that gamma rays have a more significant impact on this sample (Figure 6b). For TPE-6, PP-3, and PP-4, the DSC curves for both non-irradiated and irradiated samples display only one melting peak (Figure 6c). All PPs tend to decrease in melting temperature and onset with increasing dose (up to 100 kGy) when compared to the non-irradiated samples used as the reference (Figure S4 in SI and Figure 6d and e). The TPE sample exhibits the same behavior as the PPs.

The decrease in melting peak temperature with higher doses of irradiation indicates an increase in the polymer's amorphous nature and structural modifications, such as crosslinking and oxidation [26,27]. The literature [28–30] reports that irradiation on PP causes molecular variations that shorten the polymer chains, thereby reducing the Tm values as a function of the absorbed dose.

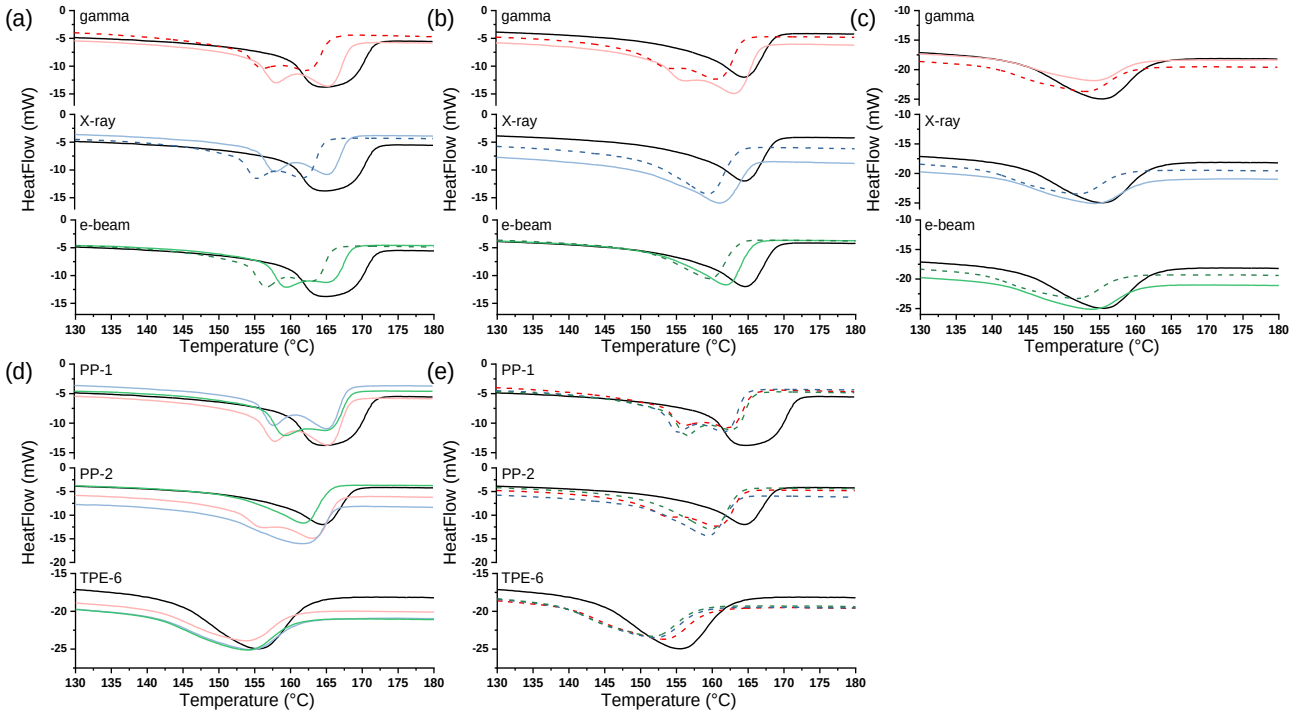


**Figure 6:** DSC thermograms for (a) PP-1, (b) PP-2 and (c) TPE-6 (d) materials irradiated at 50 kGy, (e) materials irradiated at 100 kGy. Black for non-irradiated, red for gamma irradiation, blue for X-rays and green for e-beam. Solid line for samples irradiated at 50 kGy are represented and dashed line for samples irradiated at 100 kGy.

### 3.3. Mechanical properties

The tensile tests were performed on PP-1 to PP-4. The tensile strength and elongation at break values are equivalent across all PP samples irradiated with gamma radiation, X-rays, and e-beam at doses of 50 and 100 kGy. No statistically significant effects of irradiation or doses up to 100 kGy were observed in the PP samples (Figure 7 and table S1). It has been reported that the loss of mechanical properties is closely related to the oxidative chain scission of polymers upon exposure to ionizing radiation [22,29,31].

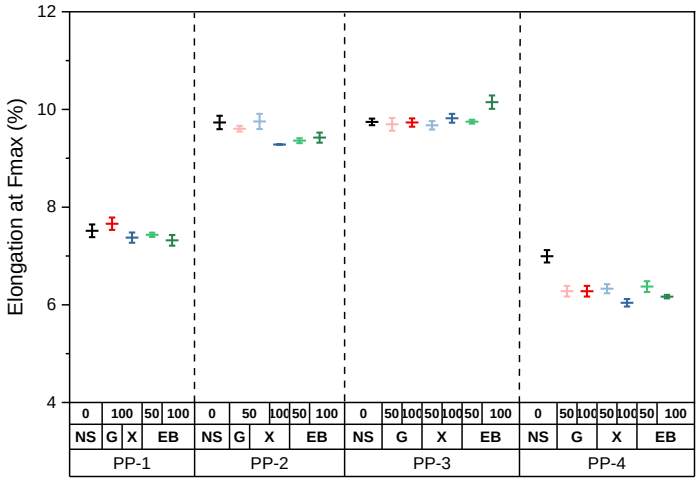


**Figure 7:** Elongation for PP-1, PP-2, PP-3 and PP-4 as a function of the irradiation technology and the dose. The mean is plotted with a confidence interval at 95%.

### 3.4. Colorimetry

This study focused on measuring the L*, a*, and b* values of PP-1 and PP-2 samples before and after irradiation at 50 kGy. L* indicates the brightness level between light and dark, a* represents the balance between green and red, and b* represents the balance between blue and yellow. According to the L*, a*, b* color diagram presented in the literature [32], when a color is expressed in CIELAB, a shift in the +a* direction indicates a red shift, while a shift in the +b* direction indicates a shift towards yellow. The central L* axis shows L* = 0 (black or total absorption) at the bottom. At the center of this plane is neutral gray.

A PCA was conducted using the results from the color analysis (Figure 8). The PCA reveals two distinct groups of samples for PP-1: Group 1 consists of non-irradiated samples and those irradiated by e-beam, while Group 2 consists of samples irradiated by gamma rays and X-ray. The b* values increase when PP-1 is irradiated with gamma rays and X-rays, resulting in a more yellow appearance compared to the non-irradiated and e-beam irradiated samples. In contrast, PP-2 showed a difference when irradiated but no difference between the three irradiation technologies, becoming less yellow than PP-1 after irradiation. For both PP-1 and PP-2, the L* values increase when the samples are irradiated. Consequently, irradiated samples appear brighter than non-irradiated samples.

The yellowing of PP (polypropylene) after irradiation can be attributed to the presence of certain additives used in the polymer[27,33,34].

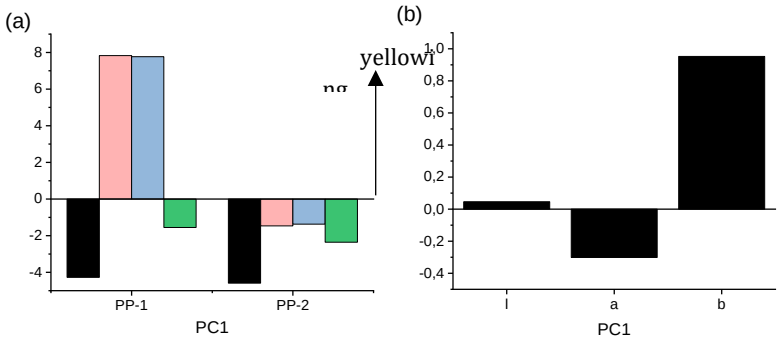


**Figure 8:** PCA of L*, a* and b* values obtained by color analysis on PP-1 and PP-2 non irradiated and irradiated by gamma, X-ray and e-beam at 50 kGy. (a) Score plot of PCA with irradiation technology (black: Non irradiated, pink: gamma, blue: X-ray, green: e-beam). (b) Loading plot of PC-1.

### 3.5. Infrared spectroscopy

The infrared spectra of the PP-1 non-irradiated and irradiated by gamma, e-beam, and X-ray at 50 and 100 kGy are displayed in Figure 9, and those of PP-2 to PP-5 are presented in the Figure S5 in SI. According to the literature [12,29,35,36], the main signal changes are observed in the carbonyl absorption region (1780-1680 cm-1). The IR assignments of the PP spectra are in accordance with the literature [37] and are represented in Figure 9.

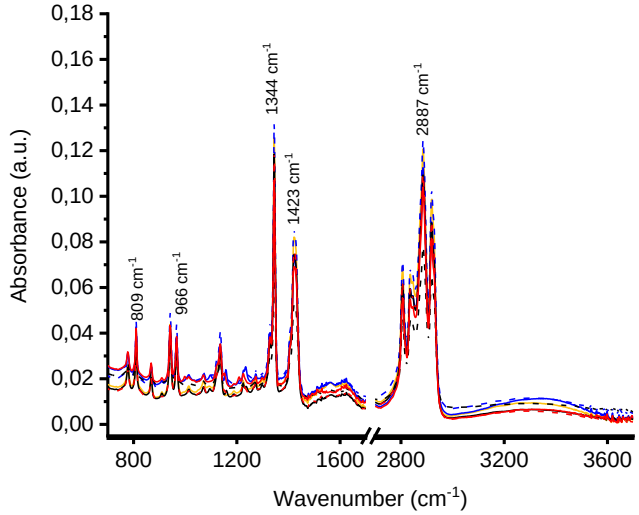


**Figure 9:** FTIR spectra of PP-2 non-irradiated (black line), irradiated by gamma (red line), by X-ray (blue line) and by e-beam (green line) at 50 kGy (solid line) and 100 kGy (dashed line).

PCA was performed on the 105 spectra representing the effects of all irradiation doses and technologies for all PP samples (Figure S6 in SI). For the FTIR fingerprint spectral region [1800-700 cm-1], the PP spectra were baseline corrected and normalized.

The separation of the samples in the PCA plot suggests that the different additives used in the PP formulations result in distinct spectral characteristics. Due to industrial confidentiality, the exact formulations of the PPs cannot be disclosed. The presence of additives in the PPs aligns with the results obtained from ESR and colorimetry analyses.

It is important to note that no significant effects of irradiation dose or technology were observed, as the samples do not cluster based on these variables. For all PPs, there is no broadband centered at 1745 $cm^{-1}$, which is characteristic of the stretching vibration of the carbonyl group C=O. With this technique, it is not possible to observe PP oxidation during the degradation after gamma, e-beam and X-ray irradiation.

### 3.6. Oxidation essay by High Performance Liquid Chromatography

Figure 10 represents the oxidation potential of PPs irradiated by X-ray, e-beam and gamma irradiation measured by the HPLC-detection of the methionine sulfoxide in the solution stored up to 63 days.

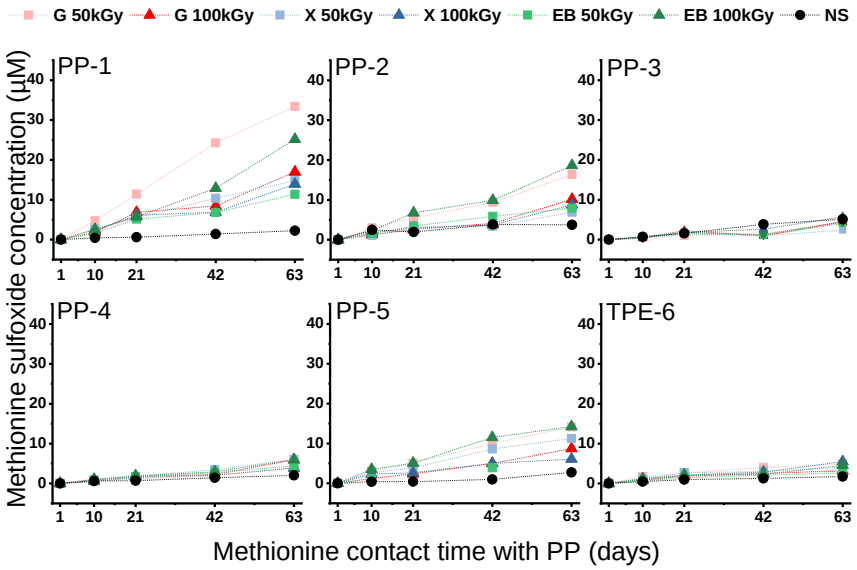


**Figure 10:** Methionine sulfoxide concentration (µM) in stored solution after 1, 10, 21, 42 and 63 days analyzed by HPLC for all PP samples. Irradiation doses were 50 and 100 kGy for gamma, X-ray and e-beam.

The Pareto charts are displayed in Figure 11. For all PPs, the irradiation dose did not significantly affect methionine sulfoxide concentration, whereas the solution contact time significantly increased it. Statistically significant differences in methionine sulfoxide concentration were observed between irradiated and non-irradiated samples for PP-1, PP-5 and TPE-6. However, there were no significant differences among the three irradiation technologies.

PP oxidation is due to the generation of peracids [38,39]. The variations among the PPs are attributed to their formulation and additive amounts, indicating that methionine solution oxidation depends more on the PP formulation than on the irradiation technology.

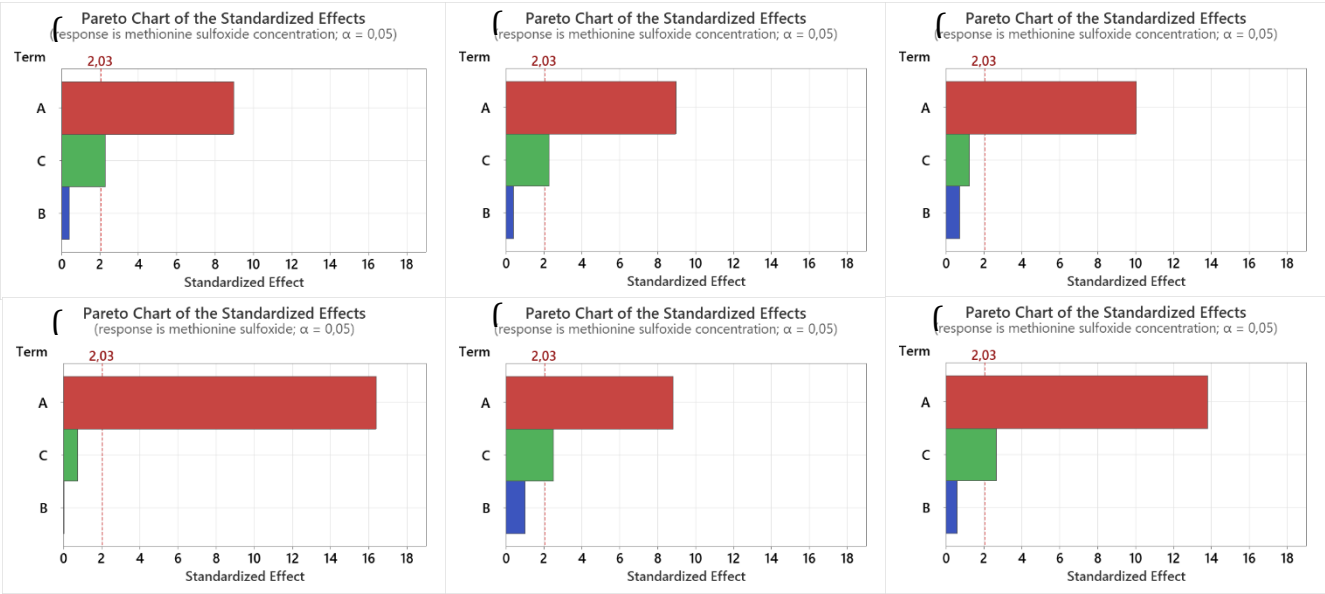


**Figure 11:** Pareto analysis of significant effects on methionine sulfoxide concentration: Methionine contact day (days) (A in red), Dose (kGy) (B in blue) and Irradiation technologies (C in green). (a) PP-1. (b) PP-2. (c) PP-3. (d) PP-4. (e) PP-5. (f) TPE-6.

## Conclusion

The study provides an analysis of the effects of X-ray, e-beam, and gamma irradiation on the chemical and physical properties of polypropylene and thermoplastic elastomer samples. ESR analysis revealed that the generation of peroxyl radicals in irradiated samples is not significantly influenced by the type of irradiation or dose, with these radicals decreasing over time. The formulation of PP can lead to the generation of additional radical species after irradiation. Thermal analysis through DSC demonstrated that the thermal properties of the samples remained consistent across all irradiation technologies, except for one PP sample

where gamma irradiation appeared to have a higher impact due to the formation of a shoulder peak. Although a slight reduction in melting temperature was observed at higher doses, the overall thermal stability was largely maintained. Mechanical testing further confirmed that tensile strength and elongation at break were unaffected by irradiation, preserving the mechanical integrity of PP. Colorimetric analysis indicated minor changes in brightness and color balance, with PP-1 exhibiting a yellowing effect post-irradiation, particularly in those irradiated by X-ray and gamma, due to the presence of certain additives. Infrared spectroscopy showed that the chemical structure of PP remained largely unaltered, with no significant spectral changes detected, although the spectra varied with the nature and amount of additives present. The study also assessed oxidation potential, with methionine sulfoxide concentrations revealing differences attributed to the PP formulation rather than the irradiation technology. This underscores the critical role of polymer formulation in determining the material's response to irradiation.

In conclusion, while irradiation technology does not significantly impact the properties of PP, the formulation of the polymer is a key factor in influencing its behavior post-irradiation. This insight emphasizes the importance of tailoring polymer formulations to optimize their performance and stability under various irradiation conditions, ensuring their suitability for diverse industrial applications.

**Supporting Information**

**Figure S1 :** ESR signal of (a) PP-1, (b) PP-4, and (c) PP-5 nine days after irradiation at 50 kGy and 100 kGy by gamma irradiation (red line), X-ray (blue line), and e-beam (green line). Samples irradiated at 50 kGy are represented by pastel colors, and those irradiated at 100 kGy by dark colors. **Table S1 :** Radical concentration (spins/g) of PP-1, PP-4, and PP-5 irradiated at 50 kGy and 100 kGy by gamma, X-ray, and e-beam. **Figure S2 :** Pareto analysis of significant effects on radical concentration on PP-1, PP-4, and PP-5: Aging after irradiation (A in blue), Dose (B in red), and Irradiation Technologies (C in green). **Table S2 :** Analysis of variance (ANOVA) for the radical concentration of PP-1, PP-4, and PP-5. **Figure S3 :** DSC thermograms for (a) PP-3, (b) PP-4, and (c) PP-5. Black for non-irradiated, red for gamma irradiation, blue for X-rays, and green for e-beam. Samples irradiated at 50 kGy are represented by pastel colors, and those irradiated at 100 kGy by dark colors. **Table S3 :** Melting temperature (Tm) and enthalpy of fusion (ΔHm) of PP-3, PP-4, and PP-5 samples non-irradiated and irradiated at 50 kGy and 100 kGy by gamma, X-ray, and e-beam. **Figure S4:** Peak melting temperature for PP and TPE samples. **Figure S5:** FTIR spectra of non-

irradiated PPs (black line), irradiated by gamma (red line), by X-ray (blue line), and by e-beam (green line) at 50 kGy (solid line) and 100 kGy (dashed line). **Table S4:** Carbonyl index (CI) and vinylene index (VI) of non-irradiated PP samples and those irradiated at 50 kGy and 100 kGy by gamma, X-ray, and e-beam. **Figure S6 :** PCA of spectra of non-irradiated and irradiated PPs by gamma, e-beam, and X-ray at 50 and 100 kGy. Spectra are baseline corrected and normalized.

**Acknowledgements**

N.D., F.G. and S.R.A.M. are thankful to Aix-Marseille University (AMU), Institut de Recherche pour le Développement (IRD) and Centre National pour la Recherche Scientifique (CNRS) A.M.U., I.R.D. and C.N.R.S. for support.

**References**

[1] BPAS Technical Guide, X-rays Sterilization of single-Use BioProcess Equipment, Part 1: Industry Need, Requirements&Risk Evaluation., 2021.

[2] Polypropylene Handbook: Morphology, Blends and Composites, Eds.: J. Karger-Kocsis, T. Bárány, Springer International Publishing: Cham, 2019.

[3] B. Krieguer, S. R. A. Marque, S. Dorey, N. Dupuy, F. Girard, N. Girard-Perier, F. Kuntz, N. Ludwig, Journal of Applied Polymer Science 2024, e55098.

[4] N. Dupuy, S. R. A. Marque, L. S. Fifield, M. Pharr, D. Staack, S. D. Pillai, L. Nichols, M. K. Murphy, S. Dorey, Bioprocess technical 2022, 20, 24.

[5] P. M. Armenante, O. Akiti, in Chemical Engineering in the Pharmaceutical Industry (Eds.: D. J. am Ende, M. T. am Ende), John Wiley & Sons, Inc.: Hoboken, NJ, USA, 2019, pp 311.

[6] H. De Brouwer, Radiation Physics and Chemistry 2022, 193, 109999.

[7] D. Darwis, Erizal, B. Abbas, F. Nurlidar, D. P. Putra, Macromolecular Symposia 2015, 353, 15.

[8] W. D. Loveland, D. J. Morrissey, G. T. Seaborg, Modern Nuclear Chemistry, 1st ed., Wiley, 2017.

[9] In Radiation Processing of Polymer Materials and its Industrial Applications, John Wiley & Sons, Inc.: Hoboken, NJ, USA, 2012, pp 1.

[10] M. Ferry, Y. Ngono, Radiation Physics and Chemistry 2021, 180, 109320.

[11] S. R. Allayarov, S. V. Demidov, A. T. Kapasharov, O. N. Golodkov, G. V. Malkov, M. P. Confer, D. A. Dixon, Radiation Physics and Chemistry 2024, 221.

[12] A. Rivaton, D. Lalande, J.-L. Gardette, Nuclear Instruments and Methods in Physics Research Section B: Beam Interactions with Materials and Atoms 2004, 222, 187.

[13] I. Krupa, A. S. Luyt, Polymer Degradation and Stability 2001, 72, 505.

[14] C. Vasile, E. Butnaru, in Applications of ionizing radiation in materials processing, 2017, Vol. 2, pp 117.

[15] AAMI TIR, 2017.

[16] G. Audran, S. Dorey, N. Dupuy, F. Gaston, S. R. A. Marque, Polymer Degradation and Stability 2015, 122, 169.

[17] S. Dorey, F. Gaston, N. Girard-Perier, N. Dupuy, S. R. A. Marque, L. Delaunay, Industrial & Engineering Chemistry Research 2019, 58, 14115.

[18] N. Girard-Perier, M. Claeys-Bruno, S. R. A. Marque, N. Dupuy, F. Gaston, S. Dorey, Polymers 2020, 12, 3024.

[19] Y. Ni, T. T. Bisel, M. K. Hasan, D. Li, W. K. Fuchs, S. K. Cooley, L. Nichols, M. Pharr, N. Dupuy, S. R. A. Marque, M. K. Murphy, S. D. Pillai, S. Dorey, L. S. Fifield, npj Mater Degrad 2023, 7.

[20] N. Kumar, A. Bansal, G. S. Sarma, R. K. Rawal, Talanta 2014, 123, 186.

[21] H. Martens, T. Naes, Multivariate Calibration, Wiley., 1989.

[22] A. C. Abraham, M. A. Czayka, M. R. Fisch, Radiation Physics and Chemistry 2010, 79, 83.

[23] G. Burlińska, J. Bojarski, J. Michalik, Radiation Physics and Chemistry 1996, 47, 449.

[24] P. Silva, C. Albano, R. Perera, J. González, M. Ichazo, Nuclear Instruments and Methods in Physics Research Section B: Beam Interactions with Materials and Atoms 2004, 226, 320.

[25] Minitab Statistical software, Minitab Help. Retrieved from https://support.minitab.com/en-us/minitab/21/help-and-how-to/ 2022.

[26] C. Aymes-Chodur, N. Betz, B. Legendre, N. Yagoubi, Polymer Degradation and Stability 2006, 91, 649.

[27] A. T. Fintzou, A. V. Badeka, M. G. Kontominas, K. A. Riganakos, Radiation Physics and Chemistry 2006, 75, 87.

[28] M. M. Hassan, N. A. El-kelesh, A. M. Dessouki, Polymer Composites 2008, 29, 883.

[29] H.-T. Wang, H.-Q. Jiang, R.-F. Shen, X.-J. Ding, C. Zhang, L.-F. Li, J.-Y. Li, Nuclear Science and Techniques 2018, 29, 87.

[30] N. Yagoubi, R. Peron, B. Legendre, J. L. Grossiord, D. Ferrier, Nuclear Instruments and Methods in Physics Research Section B: Beam Interactions with Materials and Atoms 1999, 151, 247.

[31] K. A. Riganakos, W. D. Koller, D. A. E. Ehlermann, B. Bauer, M. G. Kontominas, Radiation Physics and Chemistry 1999, 54, 527.

[32] X-rite, Pantone, A guide to understanding color, 2016, p 40.

[33] F. Gaston, N. Dupuy, S. R. A. Marque, D. Gigmes, S. Dorey, Journal of Applied Polymer Science 2018, 135, 46114.

[34] H. B. Thorat, C. S. Prabhu, S. Kumar, M. V. Pandya, Journal of Applied Polymer Science 1996, 11, 1769.

[35] S. Mouaci, M. Saidi, N. Saidi-Amroun, Micro & Nano Letters 2017, 12, 478.

[36] E. Bormashenko, R. Pogreb, A. Sheshnev, S. Sutovski, A. Shulzinger, L. Nachum, R. Kerbel, Applied Surface Science 2003, 220, 125.

[37] J. Fang, L. Zhang, D. Sutton, X. Wang, T. Lin, Journal of Nanomaterials 2012, 2012, 1.

[38] P. Gijsman, R. Fiorio, Polymer Degradation and Stability 2023, 208, 110260.

[39] N. Girard-Perier, M. Claeys-Bruno, S. R. A. Marque, N. Dupuy, F. Gaston, S. Dorey, Chemical Communications 2021, 57, 11049.

# Supporting information : How X-rays, e-beam, and gamma irradiation change the chemical and physical properties of polypropylene

## Electron Spin resonance

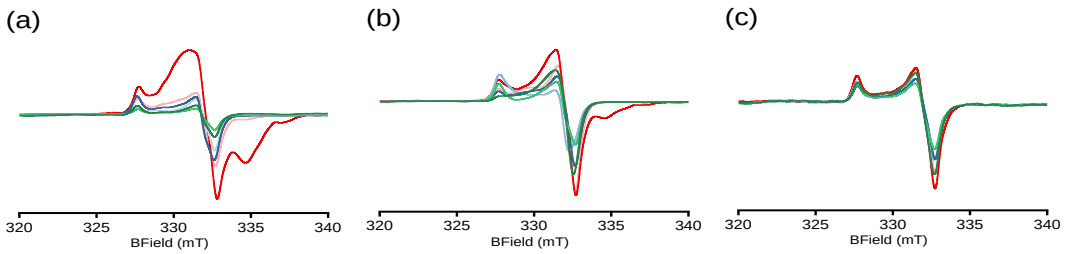


Figure S1: ESR signal of (a) PP-1, (b) PP-4 and (c)PP-5 nine days after irradiation at 50 kGy and 100 kGy by gamma irradiation (red line), X-ray (blue line) and e-beam (green line). Samples irradiated at 50 kGy are represented by pastel colors, and samples irradiated at 100 kGy by dark colors.

## Regression analysis : PP-3

### Method

Categorical predictor (1; coding 0)

### Regression Equation

**3Irradiation technologies**

e-beam Spin/g = 94908770665714720 - 2701854411506068 3Ageing after irradiation + 841651217176317 3Dose

gamma Spin/g = 219760414520728416 - 2701854411506068 3Ageing after irradiation + 841651217176317 3Dose

X-ray Spin/g = 166102863794247808 - 2701854411506068 3Ageing after irradiation + 841651217176317 3Dose

### Coefficients

| Term | Coef | SE Coef | T-Value | P-Value | VIF |
|---|---|---|---|---|---|
| Constant | 2,19760E+17 | 6,88992E+16 | 3,19 | 0,004 | |
| Ageing after irradiation | -2,70185E+15 | 8,80374E+14 | -3,07 | 0,006 | 1,01 |
| Dose | 8,41651E+14 | 7,19480E+14 | 1,17 | 0,255 | 1,00 |
| Irradiation technologies | | | | | |
| e-beam | -1,24852E+17 | 4,44628E+16 | -2,81 | 0,010 | 1,43 |
| X-ray | -5,36576E+16 | 4,53951E+16 | -1,18 | 0,250 | 1,42 |

### Model Summary

| S | R-sq | R-sq(adj) | R-sq(pred) |
|---|---|---|---|
| 9,31784E+16 | 44,37% | 34,25% | 15,43% |

### Analysis of Variance

| Source | DF | Adj SS | Adj MS | F-Value | P-Value |
|---|---|---|---|---|---|
| Regression | 4 | 1,52344E+35 | 3,80859E+34 | 4,39 | 0,009 |
| Ageing after irradiation | 1 | 8,17748E+34 | 8,17748E+34 | 9,42 | 0,006 |
| Dose | 1 | 1,18811E+34 | 1,18811E+34 | 1,37 | 0,255 |

| | | | | | |
|---|---|---|---|---|---|
| Irradiation technologies | 2 | 6,99287E+34 | 3,49643E+34 | 4,03 | 0,032 |
| Error | 22 | 1,91009E+35 | 8,68221E+33 | | |
| Total | 26 | 3,43352E+35 | | | |

### Fits and Diagnostics for Unusual Observations

| Obs | Spin/g | Fit | Resid | Std Resid | |
|---|---|---|---|---|---|
| 5 | 5,00242E+17 | 2,79609E+17 | 2,20633E+17 | 2,64 | R |
| 13 | 4,68033E+17 | 2,47566E+17 | 2,20467E+17 | 2,63 | R |

*R Large residual*

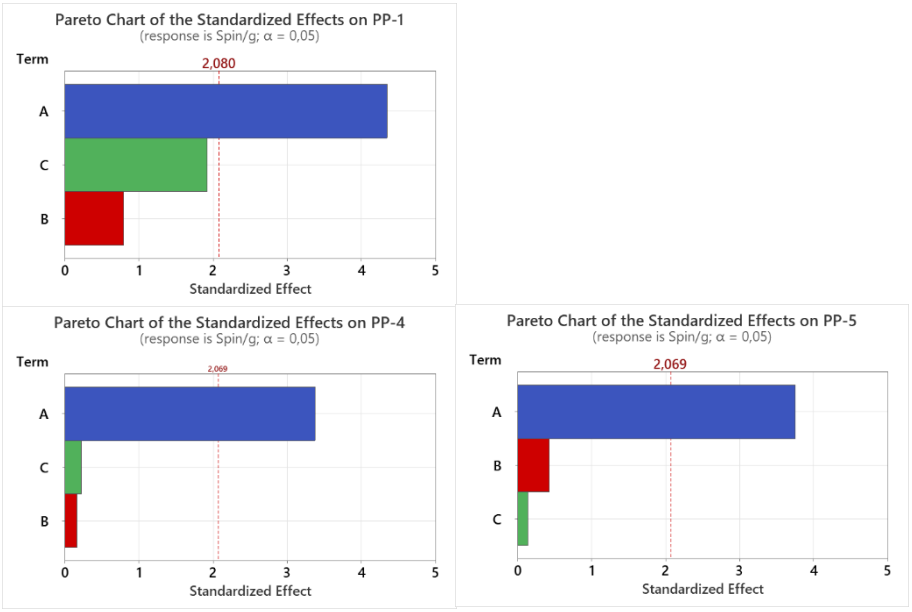


Figure S2: Pareto analysis of significant effects on radical concentration on PP-1, PP-4 and PP-5: Ageing after irradiation (A in blue), Dose (B in red) and Irradiation technologies (C in green).

## Regression analysis : PP-1

### Method

Categorical predictor (1; coding 0)

### Regression Equation

**1Irradiation technologies**

e-beam 1pin/g = 119068385763730976
- 4048258730167399 1Ageing after irradiation
+ 619331543584455 1Dose

gamma Spin/g = 213921687228625216
- 4048258730167399 1Ageing after irradiation
+ 619331543584455 1Dose

X-ray Spin/g = 220703923742588416
- 4048258730167399 1Ageing after irradiation
+ 619331543584455 1Dose

### Coefficients

| Term | Coef | SE Coef | T-Value | P-Value | VIF |
|---|---|---|---|---|---|
| Constant | 2,13922E+17 | 7,43063E+16 | 2,88 | 0,009 | |
| Ageing after irradiation | -4,04826E+15 | 9,31548E+14 | -4,35 | 0,000 | 1,02 |
| Dose | 6,19332E+14 | 7,77474E+14 | 0,80 | 0,435 | 1,02 |
| Irradiation technologies | | | | | |
| e-beam | -9,48533E+16 | 4,67232E+16 | -2,03 | 0,055 | 1,40 |
| X-ray | 6,78224E+15 | 4,92098E+16 | 0,14 | 0,892 | 1,40 |

### Model Summary

| S | R-sq | R-sq(adj) | R-sq(pred) |
|---|---|---|---|
| 9,79072E+16 | 53,84% | 45,05% | 29,03% |

### Analysis of Variance

| Source | DF | Adj SS | Adj MS | F-Value | P-Value |
|---|---|---|---|---|---|
| Regression | 4 | 2,34840E+35 | 5,87101E+34 | 6,12 | 0,002 |
| Ageing after irradiation | 1 | 1,81032E+35 | 1,81032E+35 | 18,89 | 0,000 |
| Dose | 1 | 6,08280E+33 | 6,08280E+33 | 0,63 | 0,435 |
| Irradiation technologies | 2 | 5,85865E+34 | 2,92932E+34 | 3,06 | 0,068 |
| Error | 21 | 2,01302E+35 | 9,58582E+33 | | |
| Total | 25 | 4,36143E+35 | | | |

### Fits and Diagnostics for Unusual Observations

| Obs | Spin/g | Fit | Resid | Std Resid | |
|---|---|---|---|---|---|
| 12 | 5,59624E+17 | 2,78589E+17 | 2,81035E+17 | 3,21 | R |

## Regression Analysis: PP-2

### Method

Categorical predictor (1; coding 0)

### Regression Equation

**Irradiation technologies**

e-beam Spin/g = 119507193113294688 - 4335417153663521 2Ageing after irradiation + 1241098800637626 2Dose

gamma Spin/g = 226380195165124992 - 4335417153663521 2Ageing after irradiation + 1241098800637626 2Dose

X-ray Spin/g = 171374155114655808 - 4335417153663521 2Ageing after irradiation + 1241098800637626 2Dose

### Coefficients

| Term | Coef | SE Coef | T-Value | P-Value | VIF |
|---|---|---|---|---|---|
| Constant | 2,26380E+17 | 6,42977E+16 | 3,52 | 0,002 | |
| Ageing after irradiation | -4,33542E+15 | 8,54891E+14 | -5,07 | 0,000 | 1,01 |
| Dose | 1,24110E+15 | 6,86831E+14 | 1,81 | 0,087 | 1,01 |
| Irradiation technologies | | | | | |
| e-beam | -1,06873E+17 | 4,26825E+16 | -2,50 | 0,022 | 1,46 |
| X-ray | -5,50060E+16 | 4,34386E+16 | -1,27 | 0,221 | 1,44 |

### Model Summary

| S | R-sq | R-sq(adj) | R-sq(pred) |
|---|---|---|---|
| 8,36722E+16 | 62,84% | 55,01% | 41,19% |

### Analysis of Variance

| Source | DF | Adj SS | Adj MS | F-Value | P-Value |
|---|---|---|---|---|---|
| Regression | 4 | 2,24914E+35 | 5,62285E+34 | 8,03 | 0,001 |
| Ageing after irradiation | 1 | 1,80054E+35 | 1,80054E+35 | 25,72 | 0,000 |
| Dose | 1 | 2,28599E+34 | 2,28599E+34 | 3,27 | 0,087 |
| Irradiation technologies | 2 | 4,40258E+34 | 2,20129E+34 | 3,14 | 0,066 |
| Error | 19 | 1,33020E+35 | 7,00104E+33 | | |
| Total | 23 | 3,57934E+35 | | | |

### Fits and Diagnostics for Unusual Observations

| Obs | Spin/g | Fit | Resid | Std Resid | |
|---|---|---|---|---|---|
| 20 | 4,96412E+17 | 2,39282E+17 | 2,57130E+17 | 3,45 | R |

# Regression Analysis: PP-4

## Method

Categorical predictor (1; coding 0)

## Regression Equation

**4Irradiation technologies_4**

e-beam Spin/g = 257712410645497024 - 4780708173478873 4Ageing after irradiation - 190951321703356 4Dose

gamma Spin/g = 274487085397061568 - 4780708173478873 4Ageing after irradiation - 190951321703356 4Dose

X-ray Spin/g = 300761521298999168 - 4780708173478873 4Ageing after irradiation - 190951321703356 4Dose

## Coefficients

| Term | Coef | SE Coef | T-Value | P-Value | VIF |
|---|---|---|---|---|---|
| Constant | 2,74487E+17 | 1,10322E+17 | 2,49 | 0,021 | |
| Ageing after irradiation | -4,78071E+15 | 1,41682E+15 | -3,37 | 0,003 | 1,01 |
| Dose | -1,90951E+14 | 1,16155E+15 | -0,16 | 0,871 | 1,00 |
| Irradiation technologies | | | | | |
| e-beam | -1,67747E+16 | 7,33018E+16 | -0,23 | 0,821 | 1,46 |
| X-ray | 2,62744E+16 | 7,33018E+16 | 0,36 | 0,723 | 1,46 |

## Model Summary

| S | R-sq | R-sq(adj) | R-sq(pred) |
|---|---|---|---|
| 1,53658E+17 | 34,36% | 22,94% | 3,58% |

## Analysis of Variance

| Source | DF | Adj SS | Adj MS | F-Value | P-Value |
|---|---|---|---|---|---|
| Regression | 4 | 2,84234E+35 | 7,10584E+34 | 3,01 | 0,039 |
| Ageing after irradiation | 1 | 2,68823E+35 | 2,68823E+35 | 11,39 | 0,003 |
| Dose | 1 | 6,38092E+32 | 6,38092E+32 | 0,03 | 0,871 |
| Irradiation technologies | 2 | 9,39318E+33 | 4,69659E+33 | 0,20 | 0,821 |
| Error | 23 | 5,43048E+35 | 2,36108E+34 | | |
| Total | 27 | 8,27282E+35 | | | |

## Fits and Diagnostics for Unusual Observations

| Obs | Spin/g | Fit | Resid | Std Resid | |
|---|---|---|---|---|---|
| 9 | 8,81788E+17 | 2,86433E+17 | 5,95354E+17 | 4,27 | R |

# Regression Analysis: PP-5

## Method

Categorical predictor (1; coding 0)

## Regression Equation

**Irradiation technologies**

e-beam Spin/g = 123562831093529600
- 2214417510030617 5Ageing after irradiation_5
- 209526800270816 5Dose_5

gamma Spin/g = 138066562235694160
- 2214417510030617 5Ageing after irradiation_5
- 209526800270816 5Dose_5

X-ray Spin/g = 133114467447114896
- 2214417510030617 5Ageing after irradiation_5
- 209526800270816 5Dose_5

## Coefficients

| Term | Coef | SE Coef | T-Value | P-Value | VIF |
|---|---|---|---|---|---|
| Constant | 1,38067E+17 | 4,59164E+16 | 3,01 | 0,006 | |
| Ageing after irradiation | -2,21442E+15 | 5,89684E+14 | -3,76 | 0,001 | 1,01 |
| Dose | -2,09527E+14 | 4,83438E+14 | -0,43 | 0,669 | 1,00 |
| Irradiation technologies | | | | | |
| e-beam | -1,45037E+16 | 3,05084E+16 | -0,48 | 0,639 | 1,46 |
| X-ray | -4,95209E+15 | 3,05084E+16 | -0,16 | 0,872 | 1,46 |

## Model Summary

| S | R-sq | R-sq(adj) | R-sq(pred) |
|---|---|---|---|
| 6,39528E+16 | 38,52% | 27,83% | 9,15% |

## Analysis of Variance

| Source | DF | Adj SS | Adj MS | F-Value | P-Value |
|---|---|---|---|---|---|
| Regression | 4 | 5,89355E+34 | 1,47339E+34 | 3,60 | 0,020 |
| Ageing after irradiation | 1 | 5,76767E+34 | 5,76767E+34 | 14,10 | 0,001 |
| Dose | 1 | 7,68276E+32 | 7,68276E+32 | 0,19 | 0,669 |
| Irradiation technologies | 2 | 9,89093E+32 | 4,94546E+32 | 0,12 | 0,887 |
| Error | 23 | 9,40691E+34 | 4,08996E+33 | | |
| Total | 27 | 1,53005E+35 | | | |

## Fits and Diagnostics for Unusual Observations

| Obs | Spin/g | Fit | Resid | Std Resid | |
|---|---|---|---|---|---|
| 1 | 2,36197E+17 | 1,07660E+17 | 1,28536E+17 | 2,24 | R |
| 9 | 2,73581E+17 | 1,20424E+17 | 1,53158E+17 | 2,64 | R |

## Thermal behaviors :

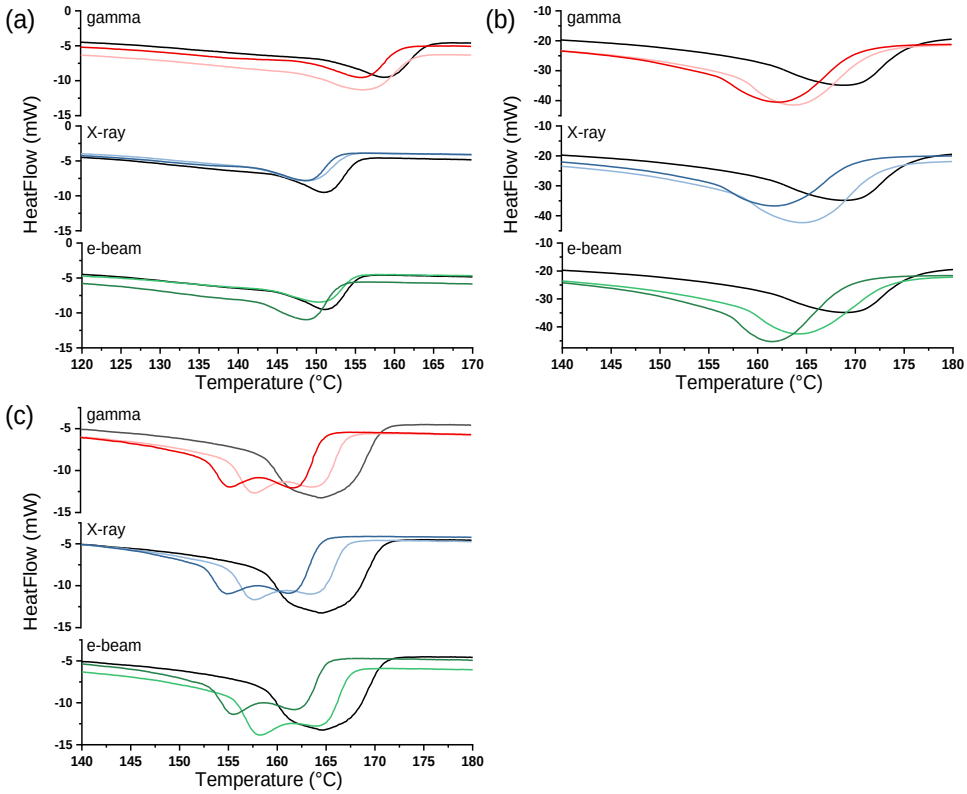


Figure S3: DSC thermograms for (a) PP-3, (b) PP-4 and (c) PP-5. Black for non-irradiated, red for gamma irradiation, blue for X-rays and green for e-beam. Samples irradiated at 50 kGy are represented by pastel colors, and samples irradiated at 100 kGy by dark colors.

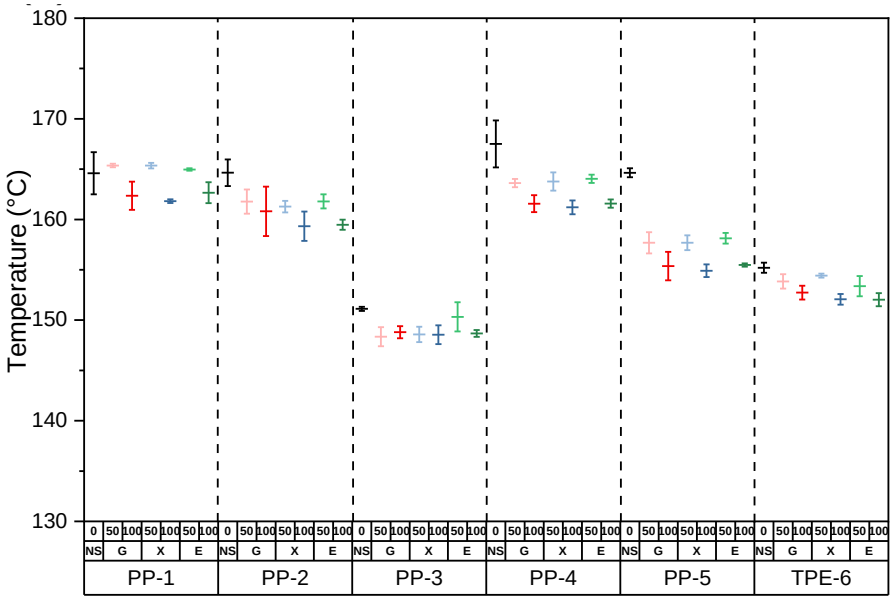


Figure S4: Melting peak temperature for PPs and TPE samples

## Mechanical properties:

*Table S1: Equivalence test summary. ✓: equivalence*

| | | | | Gamma | | X-ray | | e-beam | |
|---|---|---|---|---|---|---|---|---|---|
| | | | | 50 kGy | 100 kGy | 50 kGy | 100 kGy | 50 kGy | 100 kGy |
| PP-1 | Elongation | Non-irradiated | | | ✓ | | ✓ | ✓ | ✓ |
| | | Gamma | 100 | | | | ✓ | ✓ | ✓ |
| | | X-ray | 100 | | | | | ✓ | ✓ |
| | | e-beam | 50 | | | | | | ✓ |
| | UTS | Non-irradiated | | | ✓ | | ✓ | ✓ | ✓ |
| | | Gamma | 100 | | | | ✓ | ✓ | ✓ |
| | | X-ray | 100 | | | | | ✓ | ✓ |
| | | e-beam | 50 | | | | | | ✓ |
| PP-2 | Elongation | Non-irradiated | | ✓ | | ✓ | ✓ | ✓ | ✓ |
| | | Gamma | 50 | | | ✓ | ✓ | ✓ | ✓ |
| | | X-rays | 50 | | | | ✓ | ✓ | ✓ |
| | | | 100 | | | | | ✓ | ✓ |
| | | e-beam | 50 | | | | | | ✓ |
| | UTS | Non-irradiated | | ✓ | | ✓ | ✓ | ✓ | ✓ |
| | | Gamma | 50 | | | ✓ | ✓ | ✓ | ✓ |
| | | X-rays | 50 | | | | ✓ | ✓ | ✓ |
| | | | 100 | | | | | ✓ | ✓ |
| | | e-beam | 50 | | | | | | ✓ |
| PP-3 | Elongation | Non-irradiated | | ✓ | ✓ | ✓ | ✓ | ✓ | ✓ |
| | | Gamma | 50 | | ✓ | ✓ | ✓ | ✓ | ✓ |
| | | | 100 | | | ✓ | ✓ | ✓ | ✓ |
| | | X-rays | 50 | | | | ✓ | ✓ | ✓ |
| | | | 100 | | | | | ✓ | ✓ |
| | | e-beam | 50 | | | | | | ✓ |
| | UTS | Non-irradiated | | ✓ | ✓ | ✓ | ✓ | ✓ | ✓ |
| | | Gamma | 50 | | ✓ | ✓ | ✓ | ✓ | ✓ |
| | | | 100 | | | ✓ | ✓ | ✓ | ✓ |
| | | X-rays | 50 | | | | ✓ | ✓ | ✓ |
| | | | 100 | | | | | ✓ | ✓ |
| | | e-beam | 50 | | | | | | ✓ |
| PP-4 | Elongation | Non-irradiated | | ✓ | ✓ | ✓ | ✓ | ✓ | ✓ |
| | | Gamma | 50 | | ✓ | ✓ | ✓ | ✓ | ✓ |
| | | | 100 | | | ✓ | ✓ | ✓ | ✓ |
| | | X-rays | 50 | | | | ✓ | ✓ | ✓ |
| | | | 100 | | | | | ✓ | ✓ |
| | | e-beam | 50 | | | | | | ✓ |
| | UTS | Non-irradiated | | ✓ | ✓ | ✓ | ✓ | ✓ | ✓ |
| | | Gamma | 50 | | ✓ | ✓ | ✓ | ✓ | ✓ |
| | | | 100 | | | ✓ | ✓ | ✓ | ✓ |
| | | X-rays | 50 | | | | ✓ | ✓ | ✓ |
| | | | 100 | | | | | ✓ | ✓ |
| | | e-beam | 50 | | | | | | ✓ |

## Infrared spectroscopy

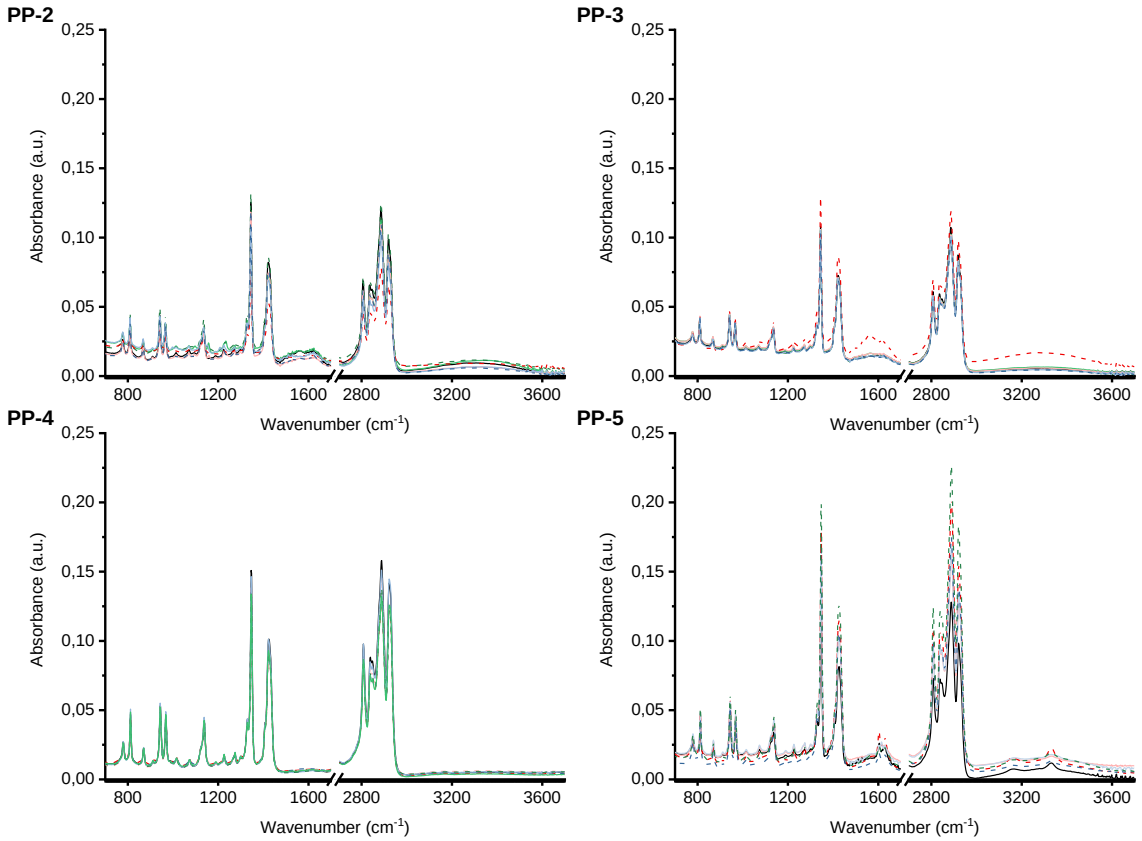


Figure S5: FTIR spectra of PPs non-irradiated (black line), irradiated by gamma (red line), by X-ray (blue line) and by e-beam (green line) at 50 kGy (solid line) and 100 kGy (dashed line).

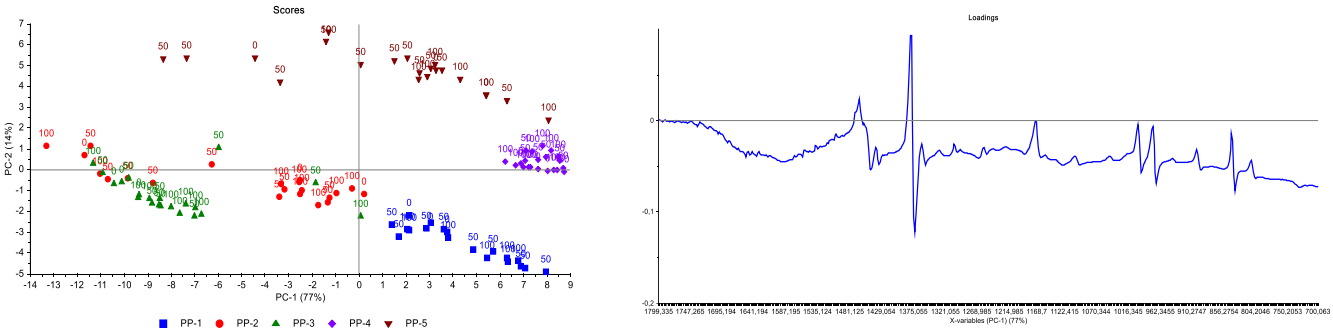


Figure S6: PCA of PPs spectra of non-irradiated and gamma, e-beam and X-ray irradiated samples at 50 and 100 kGy. Spectra are baseline corrected and normalized.

## 5.3. Comportement du Polyamide après irradiation gamma, rayons X et faisceau d'électrons

Dans ce manuscrit nous avons souligné que l'irradiation des polymères est une technique largement utilisée pour la stérilisation, en particulier dans les industries médicale et pharmaceutique. Les technologies d'irradiation, telles que les rayons gamma, les rayons X et le faisceau d'électrons, peuvent modifier de manière positive ou néfaste, les propriétés des matériaux polymères, notamment leur résistance, leur durabilité et leur compatibilité biologique. L'étude en question se concentre sur l'analyse des effets de ces technologies sur les polyamides 6.6 et les polyamides 12, un groupe de polymères largement utilisé dans diverses applications industrielles.

Tableau 6 : Dose et débit de dose d'irradiation du PA par rayons gamma, rayons X et faisceau d'électrons.

| **Techniques analytiques** | **Gamma** | | **Rayons X** | | **Faisceau d'électrons** | |
|---|---|---|---|---|---|---|
| | Dose (kGy) | Débit de dose (kGy/h) | Dose (kGy) | Débit de dose (kGy/h) | Dose (kGy) | Débit de dose (kGy/h) |
| **RPE** | 50, 100 | 2 | 50, 100 | 12 | 50, 100 | 18000 |
| **DSC** | 50, 100 | 2 | 50, 100 | 12 | 50, 100 | 18000 |

Lorsqu'un polymère est exposé à des radiations ionisantes, l'énergie absorbée peut provoquer la rupture des liaisons chimiques, générant ainsi des radicaux libres. Ces radicaux sont des espèces hautement réactives qui peuvent initier des réactions chimiques, conduisant à des modifications de la structure du polymère. Dans le cas des polyamides, les radicaux alkyles sont les principaux types de radicaux détectés. Ces radicaux se forment généralement par la rupture des liaisons C-H dans la chaîne polymère, et leur réactivité peut être influencée par la présence d'additifs et la structure cristalline du matériau.

L'étude utilise la RPE pour identifier, quantifier et suivre la cinétique des radicaux générés par les irradiations gamma, faisceau d'électrons et rayons X. En complément, la DSC est utilisée pour étudier les propriétés thermiques des polyamides irradiés. Cette méthode permet de mesurer les variations de température de fusion, fournissant des informations sur la stabilité thermique et la structure cristalline des matériaux.

Les résultats de l'étude montrent que le type de radicaux formés est identique pour tous les polyamides étudiés, indépendamment de la technologie d'irradiation utilisée. Des radicaux alkyles ont été détectés dans tous les échantillons, et aucune différence significative dans la concentration en radicaux n'a été observée. Cela suggère que les interactions entre les radiations et les polyamides étudiés sont cohérentes, quelle que soit la source de rayonnement. Cependant, la présence d'additifs dans les formulations de polyamide peut entraîner la formation d'espèces radicalaires supplémentaires, soulignant l'importance de la composition chimique dans la réponse des matériaux à l'irradiation.

Les analyses DSC révèlent que les températures de fusion des polyamides restent constantes, quelle que soit la technologie d'irradiation utilisée, et correspondent aux valeurs rapportées pour les matériaux non irradiés. Cela indique que la structure cristalline des matériaux n'est pas modifiée par l'irradiation, et que leurs propriétés thermiques ne sont pas affectées. L'équivalence des températures de fusion, des signaux RPE, de la cinétique de décroissance et des profils de concentration de radicaux après les trois technologies d'irradiation renforce l'hypothèse d'une interaction standardisée des rayonnements gamma, X et faisceau d'électrons avec la matière condensée.

Les résultats de cette étude ont des implications importantes pour l'industrie, en particulier dans le domaine de la stérilisation des systèmes à usage unique et des matériaux d'emballage, le PA étant souvent utilisé pour cette application. L'équivalence des effets des trois technologies d'irradiation sur les polyamides suggère que les industriels peuvent choisir la méthode la plus adaptée à leurs besoins spécifiques sans compromettre la qualité ou la sécurité des matériaux. Cela offre une plus grande flexibilité dans le choix des technologies de stérilisation, permettant de s'adapter aux contraintes de production et aux exigences réglementaires.

De plus, la capacité des polyamides à maintenir leurs propriétés thermiques et structurelles après irradiation est un atout majeur pour leur utilisation dans des applications exigeantes, où la stabilité et la durabilité sont essentielles. Les résultats de l'étude pourraient également être extrapolés à d'autres polymères non étudiés, à condition encore une fois de prendre en compte les spécificités de chaque matériau, notamment en termes de formulation et de structure chimique.

Open Access Article. Published on 23 July 2024. Downloaded on 7/30/2024 10:18:57 AM.
This article is licensed under a Creative Commons Attribution-NonCommercial 3.0 Unported Licence.

PCCP

ROYAL SOCIETY OF CHEMISTRY

PAPER

View Article Online
View Journal

Check for updates

Cite this: DOI: 10.1039/d4cp02358g

# Thermal properties and radical monitoring after gamma, X-ray, and electron beam irradiation in polyamides†

Blanche Krieguer, *[acd] Nicolas Ludwig,[b] Samuel Dorey, *[a] Nathalie Dupuy, [c] Fabien Girard, [c] Nina Girard-Perier, [a] Florent Kuntz[b] and Sylvain R. A. Marque *[d]

Received 10th June 2024,
Accepted 22nd July 2024

DOI: 10.1039/d4cp02358g

rsc.li/pccp

Ionizing radiation induced transformations in materials were monitored through tracking of the generation and degradation processes of radical species. Consequently, the types and quantities of radicals were determined by electron spin resonance (ESR). Subsequently, differential scanning calorimetry (DSC) was utilized to assess the impact of irradiation on the material crystallinity. The effects of gamma rays, X-rays, and electron beams were investigated on different polyamides, which exhibit an ESR signal up to 60 days. DSC results showed no significant effect of irradiation on the melting peak temperature of the materials, indicating that the amount of radicals generated was not large enough to induce a significant alteration of the material's macrostructure.

## Introduction

Polymers play a crucial role in the pharmaceutical industry, being involved in a wide array of single-use medical devices such as syringes, gloves, and disposable plastic bags. Polymers can be of various natures depending on their applications and their desired properties.[1] Materials formulated from polyamides, known for their resistance to abrasion, chemicals, and corrosion, as well as their flexibility, are commonly used in cable ties,[2] tri-clamp unions and clamps among other components.

Gamma irradiation is used to sterilize almost half of the market of medical devices of biopharmaceutical single-use plastic systems.[3,4] With the pharmaceutical sector poised for rapid growth, there is a large strain to expand sterilization capacity.[5] The development of radiation sterilization alternatives to gamma rays is essential to manage the increasing volume of biopharmaceutical systems.[1] Currently, two alternative irradiation technologies are available: electron beam and X-ray irradiation.[6–12]

Electron-beam irradiation is a continuous process that utilizes an electron accelerator to convert electricity into a radiation beam. Electron accelerators can be used for direct electron beam irradiation or to produce X-ray fields which are generated through the Bremsstrahlung[13] effect generally in a tantalum converter. Both X-ray and gamma-rays are photons[12] but gamma-rays originate from radioactive sources and are emitted during disintegration. Due to their similar nature, X-ray and gamma-rays energy deposition patterns (dose profiles) are fairly similar resulting in a potentially easy conversion from gamma-rays to X-ray technologies.[9–12] X-ray may even achieve better dose uniformity because of their higher photon energy[11] and their easily tunable radiation field properties. In similarly irradiated material, electron beam exhibits much less penetration compared to photons as their interaction with matter is much stronger. Therefore, products packaging and/or geometry must be adapted for electron beam treatment when converting a gamma-ray irradiation process to an electron beam irradiation process.

From an interaction point of view, photon interaction with matter leads to the generation of secondary electrons through pair production, Compton effect and photoelectric effect[14] which will deposit their energy. Regardless of the irradiation technology, the electron will transfer its energy to the matter by ionizing or exciting processes. These interactions will lead to chemical bond breaking and will generate free radicals in polymers which are the seeds of material modification (cross-linking, chain scission, radiation oxidation, *etc.*).[7,15,16]

Electron spin resonance (ESR) is an effective technique for detecting radicals generated during irradiation and their

[a] *Sartorius Stedim FMT S.A.S, Z.I. Les paluds, Avenue de Jouques CS91051, 13781, Aubagne Cedex, France. E-mail: blanche.krieguer@sartorius.com, samuel.dorey@sartorius.com*
[b] *Aerial, 250 Rue Laurent Fries, 67400 Illkirch, France*
[c] *Aix Marseille Univ, Avignon Univ, CNRS, IRD, IMBE, Marseille, France*
[d] *Aix Marseille Univ, CNRS, ICR, Case 551, 13397 Marseille, France. E-mail: sylvain.marque@univ-amu.fr*

† Electronic supplementary information (ESI) available. See DOI: https://doi.org/10.1039/d4cp02358g

Open Access Article. Published on 23 July 2024. Downloaded on 7/30/2024 10:18:57 AM.
This article is licensed under a Creative Commons Attribution-NonCommercial 3.0 Unported Licence.

subsequent decay. As most radicals are unstable, they react rapidly.[17,18]

The impact of gamma irradiation on polyamide (PA) has already been investigated using ESR.[17,19–21] However, very few studies have compared the effects of gamma, e-beam and X-ray irradiations on polymers. The identification and quantification of post-irradiation radicals is essential to assess the similarity of effects on materials among the three irradiation technologies.

In our study, we investigated four different polyamide materials with varying formulations, including glass-reinforced PA, PA6.6, and PA12. We performed ESR analyses on each material for a period of 60 days after irradiation. The objective was to use ESR to monitor the free radicals generated by gamma, electron beam, and X-ray irradiations. Additionally, we performed differential scanning calorimetry (DSC) to compare the thermal properties of the irradiated PA, providing insights into changes in melting temperature regarding to the different types of irradiations. Hence, our approach provides data concerning the type, nature, and stability of radicals as well as the impact of irradiations on the thermal stability of the materials.

## Materials and methods

### Samples

The samples investigated (Fig. 1) are composed of various types of polyamides: glass-reinforced polyamide, polyamide 6.6 (PA6.6) and polyamide 12 (PA12). Table 1 gathers the typical density values provided by resin suppliers.[22]

### Samples packaging

The samples were packed in craft boxes at room temperature at Sartorius Stedim FMT S.A.S, Aubagne. This packaging along with the suitable arrangement of plastic components in thin craft boxes, ensured a uniform treatment. The dose uniformity was controlled by dosimetry.

### Samples irradiation

**Gamma rays.** Irradiation using gamma rays generated from $^{60}$Co sources was carried out at Ionisos, Dagneux, France at an average dose rate of 1–2 kGy h$^{-1}$. Irradiation was performed over several days by accumulation of the dose through many runs in the irradiation bunker.

**X-rays.** X-ray irradiation was performed at Aerial-CRT using the feerix® facility based on a Rhodotron (TT300 – IBA). A 7 MV X-ray beam is generated by converting a 7 MeV electron beam in a tantalum target. Irradiation was performed horizontally with a pallet conveyor; several runs are realized in an X-ray field to realize a dose accumulation. Irradiation was conducted for one day with an average dose rate about 12 kGy h$^{-1}$.

**e-beam.** E-beam irradiation was performed at Aerial-CRT using the same feerix® facility as for X-rays treatment. A 10 MeV vertical electron-beam was used with an average dose rate of 18 MGy h$^{-1}$ (5 kGy s$^{-1}$). Irradiation was performed per lap of 50 kGy in order to avoid critical temperature elevation in the samples.

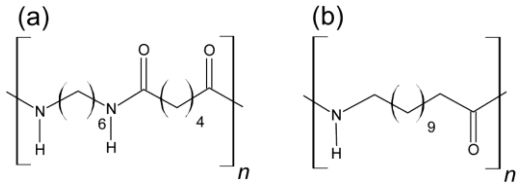


Fig. 1 Chemical structure of (a) polyamide 6.6 and (b) polyamide 12.

### Dosimetry

The targeted delivered doses were ≈50 kGy and ≈100 kGy with a target dose uniformity of ±10% and the Table 2 gathers the effective doses. To accurately measure the absorbed dose, alanine pellets combined with EPR spectroscopy (Magnettech MS5000 ESR, Brucker) were used with AerEDE® dosimetry software (Aerial, France). Dosimetry readings were taken in a manner that was traceable to an international standard.

The dosimeters were placed within the volume of the box containing samples to establish dose uniformity in the sample box.

### ESR measurements

ESR measurements were conducted using a Magnettech MS5000X ESR spectrometer manufactured by Brucker, Switzerland, and operated with ESR studio software for control. The samples were prepared from either irradiated dogbone specimens or part of irradiated products. Small pieces were cut to introduce them into a glass probe of 4.2 mm inner diameter. The samples, with a height of approximately 4 cm and a mass ranging from 100 to 200 mg, were then ready for analysis.

Firstly, the position of the signal was verified in a large magnetic field range (150–400 mT). Secondly the magnetic field range was narrowed from 320 mT to 340 mT around the sample, where the signal was present which is indicative of organic radicals. The spectra were recorded using a modulation amplitude of 0.2 mT, a sweep time of 60 seconds, and a single scan. Measurements were performed from 1 to 60 days after sample irradiation, at following days (D): D9, D15, D30, D60. During this time, samples were kept without light and at controlled temperature and humidity (25 °C and 45% RH).[23]

Signal amplitude (highest peak to peak signal) was measured on ESR spectra and calibrated using TEMPO (2,2,6,6-tétraméthylpipéridin-1-yl)oxy standard samples at spin concentration between $1 \times 10^{16}$ and $1 \times 10^{19}$ spin per g. TEMPO and standard samples were prepared according to the reported procedures.[24] TEMPO standards are very stable over time and the calibration curve was measured 8 times over several months in order to assess variabilities of measurements. Thus, ESR quantifications in this paper must be considered as TEMPO equivalent as the amplitude between TEMPO radical and probed radical in polymer may differ.

The ESR signals were measured for all PA samples prior to irradiation. The PA-4 sample was analyzed after gamma and X-ray irradiation at 50 kGy. The PA-1, PA-2, and PA-3 samples

Open Access Article. Published on 23 July 2024. Downloaded on 7/30/2024 10:18:57 AM.
This article is licensed under a Creative Commons Attribution-NonCommercial 3.0 Unported Licence.

Table 1 Non-irradiated PA commercially available (density)

| Polymers | Polyamide (PA) | | | |
|---|---|---|---|---|
| Identification number | PA-1 | PA-2 | PA-3 | PA-4 |
| Type of polyamide | Glass reinforced PA | PA6.6 | PA 12 | PA6.6 |
| Typical industrial application | Clamp/unions | Black cable tie | Black cable tie | Blue cable tie |
| Density (g cm$^{-3}$) | 1.38 | 1.14[a] | 1.01[a] | 1.14[a] |

[a] Standard density of polyamides 6, 6.6, and 12 are given in the literature.[22]

Table 2 Effective doses on samples irradiated by gamma-rays, X-rays and e-beam

| | Effective doses (kGy; ±10%) | | |
|---|---|---|---|
| Target doses (kGy; ±10%) | Gamma | X-rays | e-beam |
| 50 | 51 | 50 | 55 |
| 100 | 90 | 99 | 109 |

were analyzed after gamma, X-ray, and e-beam irradiation at 50 and 100 kGy.

### Differential scanning calorimetry (DSC)

Differential scanning calorimetry analyses were performed to characterize the physical and thermal properties of polymers. In a furnace, a thermocouple measures the temperature of the sample and another thermocouple measures one of the references (empty crucible). The heat variations observed during the glass transition and the melting temperature were also measured and a thermogram was established using these data. DSC tests were performed using a Sensys Evo131 thermal analyzer from Setaram.

For the DSC analysis, 3 cycles (heating and cooling) were performed on ~20 mg. The range of heating was −50 to 200 °C. The ramp of temperature was 10 °C min$^{-1}$ and a stabilization step was set before and after each cycle. For the results interpretation, only the 2nd and the 3rd cycles were considered, since the first cycle was performed to erase the thermal past of the material. The melting peak temperature and the melting onset temperature were both integrated and determined using the Calisto Processing software.

### Equivalency analysis

**ESR.** Regression models were performed using the Minitab software to assess the effect of doses (50 and 100 kGy), the effect of ageing after irradiation, and the effect of the three irradiation technologies on the spin per mg values measured by ESR for each sample. This model allows for the evaluation of the significant impact of each independent variable, with confidence interval at 95% ($\alpha$ = 0.05).

**DSC.** To assess the equivalency between gamma, X-rays, and e-beam irradiated samples, equivalence tests (TOST, two one-sided *t*-test[25]) were performed with Minitab® software. The melting peak and melting onset temperatures of the samples either irradiated by Gamma, X-ray or e-beam were considered equivalent if results were within the equivalence interval defined with equivalency criterium (±5 °C) confidence interval at 95% ($\alpha$ = 0.05).

## Results and discussion

### Electron spin resonance

ESR was performed after gamma, X-ray and e-beam radiation at 50 and 100 kGy for PA-1, PA-2 and PA-3. PA-4 was analyzed by gamma and X-ray at 50 kGy.

The literature describes a well-defined multiplet ESR signal for polyamide when ESR analysis is performed immediately following gamma irradiation.[17,26,27] In our case, Fig. 2 displays the ESR signal of polyamide samples one day after exposure to X-rays and e-beam at 100 kGy. Prior to irradiation, a broad singlet was observed in PA-2 and PA-3, in sharp contrast to PA-1.

Both PA-1 and PA-2 exhibit similar ESR signals as depicted in Fig. 2, while PA-3 displays a poorly resolved signal that more closely aligns with those reported in the literature. The ESR pattern observed for PA-1–3 is presumed to result from the superimposition of two signals: a multiplet ascribed to the radical –$CH_2CONHC^{\bullet}HCH_2$– and a singlet present in the polymer prior to irradiation.

In our study, the alkyl radical is only detected after X-ray and e-beam irradiation because ESR measurements are performed within one day post-irradiation. In contrast, measurements after gamma irradiation are performed several days later due to the time required for sample transportation.

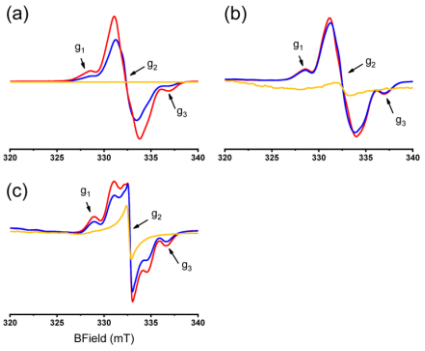


Fig. 2 Signal of (a) PA-1, (b) PA-2 and (c) PA-3, non-irradiated (yellow line) and one day after irradiation at 100 kGy by X-rays (red line) and e-beam (blue line). Arrows are to point peaks corresponding to the expected radical ($g \approx 2.003$).

Open Access Article. Published on 23 July 2024. Downloaded on 7/30/2024 10:18:57 AM.
This article is licensed under a Creative Commons Attribution-NonCommercial 3.0 Unported Licence.

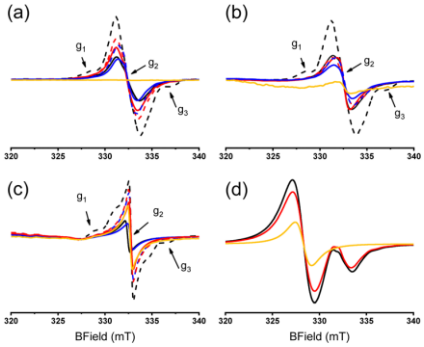


Fig. 3 Signal of (a) PA-1, (b) PA-2, (c) PA-3 and (d) PA-4, non-irradiated (yellow line) and nine days after irradiation at 50 kGy (solid line) and 100 kGy (dotted line) by gamma irradiation (black line), X-rays (red line) and e-beam (blue line). Arrows are to point peaks corresponding to the expected radical ($g \approx 2.003$).

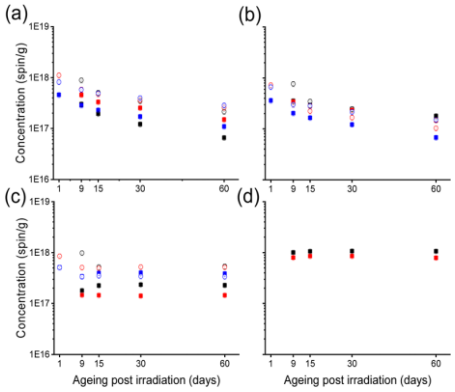


Fig. 4 Monitoring of the concentration of radicals for each PA sample by ESR as concentration (spin per g) *vs.* ageing (days). (a) PA-1. (b) PA-2. (c) PA-3. (d) PA-4. Filled squares correspond to samples irradiated at 50 kGy and open circles correspond to samples irradiated at 100 kGy, black for gamma irradiation, red for X-rays and blue for e-beam.

Fig. 3 displays the ESR signal of polyamide samples nine days after exposure to gamma, X-rays, and e-beam at 50 and 100 kGy. For PA-1, PA-2 and PA-3, a singlet is observed for gamma, e-beam and X-rays regardless of the dose. The singlet signal is attributed to the radical $-CH_2CHO^{\bullet}NHCH_2-$ ($g = 2.003$).[17,28]

After gamma irradiation at 100 kGy, a small signal was detected and ascribed to the expected multiplet radical, *i.e.* $-CH_2C^{\bullet}HCONHCH_2-$.[17,26,29] Similar signals are observed for other samples aged after irradiation and are reported in Fig. S1 (ESI†).

PA-4 displays two radical species (Fig. 3d), with the signal at $g = 2.03$ being observed before irradiation and does not decaying upon ageing (Fig. 3d and Fig. S1, ESI†). According to the literature,[30,31] the signal at $g = 2.03$ can be tentatively ascribed to the blue additive, which likely contains a sulfur-centered radical. For industrial reasons the formulation of the material cannot be obtained. The second weak signal of PA-4 (Fig. 3d) perfectly matches the singlet observed in PA-1, PA-2 and PA-3.

Fig. 4 displays the concentration of radicals for each PA and the maximum concentration is reported in Table 3. The ESR signal and the quantity of radicals generated exhibit a decrease after irradiation, a trend that holds across the different irradiation technologies applied to samples PA-1 and PA-2. The amount of radicals remains constant in PA-3 nine days after irradiation (Fig. 4).

For PA-4, the sulfur radical maintains a constant concentration within the formulated polymer, and due to its predominance, the kinetics of the singlet radical cannot be observed with the technique utilized.

Radical levels in samples exposed to gamma, X-ray, and e-beam irradiation at doses of 50 kGy and 100 kGy were monitored for a period of up to 60 days post-irradiation.

Regression models were developed for each sample to determine the influence of dose, ageing, and irradiation technology on radical production. These models allow us to assess whether the dose, ageing after irradiation, and irradiation technologies can have a significant effect on the quantity of radicals generated in the sample. Indeed, with *p*-values less than 0.05, it indicates a significant effect. The Pareto chart shows the absolute values of the standardized effects from the largest to the smallest effect. The chart also plots a reference line that indicates if the effects are statistically significant. The reference line for statistical significance depends on the significance level (denoted by α). The significance level is 1 minus the confidence level for the analysis.[32]

Post-irradiation time (*i.e.*, kinetics) shows a significant effect, with radical levels decreasing with increasing post-irradiation time for PA-1 and PA-3 (Fig. 5a and c). For the PA-1 and PA-2 samples (Fig. 5a and c), an increase in dose was correlated with a rise in radical concentration.

When comparing X-ray and e-beam with gamma irradiation, the Pareto charts for each sample showed no notable differences among the irradiation technologies. The equations and coefficients of the regression models obtained for each sample are reported in ESI.† No regression model was generated for PA-4 due to the lack of data.

Table 3 Maximum radical concentration ($C_{max}$, spin per g) in polyamide samples

| Irradiation technology | Dose (kGy) | Maximum radical concentration (spin per g; in $10^{17}$) PA-1 | PA-2 | PA-3 | PA-4 |
|---|---|---|---|---|---|
| Gamma | 50 | 3 | 4 | 2 | 10 |
| | 100 | 8 | 8 | 10 | n.a.[a] |
| X-ray | 50 | 5 | 3 | 1 | 8 |
| | 100 | 6 | 3 | 5 | n.a.[a] |
| e-beam | 50 | 3 | 2 | 5 | n.a.[a] |
| | 100 | 6 | 3 | 5 | n.a.[a] |

[a] n.a.: non available data.

## Thermal properties (DSC)

The PA-2 and PA-4 samples are formulated from polyamide 6.6, while the PA-3 sample is formulated from polyamide 12.


This journal is © the Owner Societies 2024

Open Access Article. Published on 23 July 2024. Downloaded on 7/30/2024 10:18:57 AM.
This article is licensed under a Creative Commons Attribution-NonCommercial 3.0 Unported Licence.

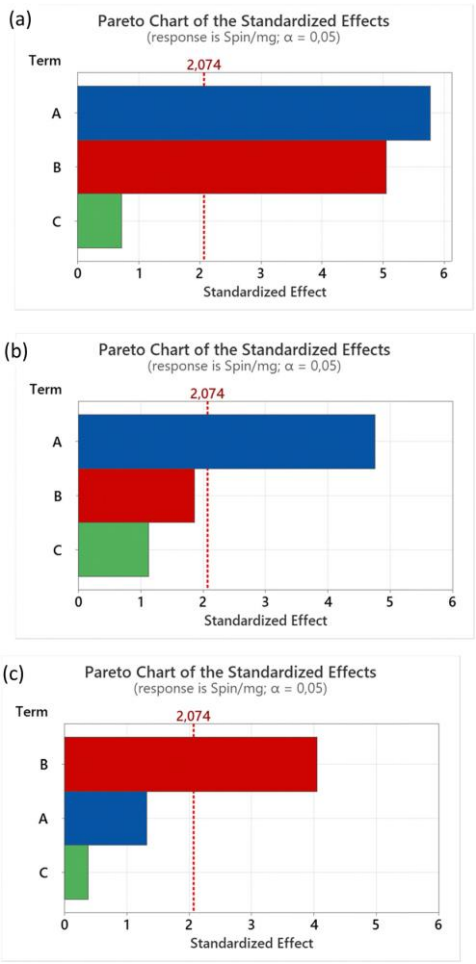


Fig. 5 Pareto analysis of significant effects on radical concentration: ageing after irradiation (term A in blue), dose (term B in red) and irradiation technologies (term C in green). (a) PA-1. (b) PA-2. (c) PA-3.

PA6.6 has a higher crystallinity than PA12. This is attributed to the higher hydrogen-bonding density in PA6.6, which facilitates faster crystallization compared to PA12. Despite PA12 having a more flexible chain structure, which could potentially lead to faster crystallization at lower temperatures, PA6.6 still crystallizes slightly faster than PA12.[33]

The DSC results (Fig. 6) regarding the evaluation of the thermal properties of polyamide show that the melting temperature of the PA-1, PA-2 and PA-4 samples (PA6.6) is about 260 °C, while for PA-3 (PA12), the melting temperature is about 180 °C; these results are consistent with the literature.[34–37]

The melting temperatures of PA remain consistent regardless of the irradiation technology used (at 50 and 100 kGy) and correspond to the values reported for non-irradiated materials. This indicates that their thermal properties are unchanged. Consequently, the structure of the materials is not altered, and

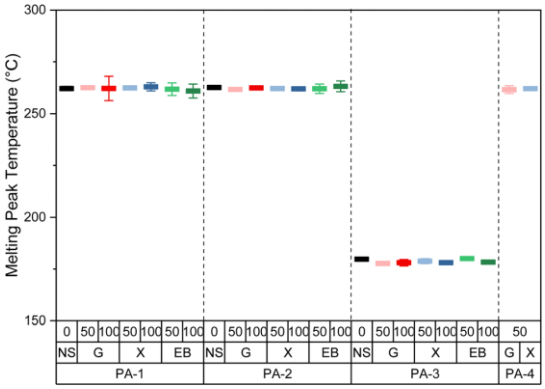


Fig. 6 Melting peak temperature for all PA samples non irradiated (black) and irradiated by gamma (red), X-ray (blue) and e-beam (green) at 50 and 100 kGy.

their thermal properties are not affected. Examples of thermograms and melting onset temperature are displayed in ESI.†

## Conclusions

Electron spin resonance measurements were used to investigate the radicals generated in these polymers when exposed to different sources of radiation. The results indicate that the type of radicals generated is similar for all PA but the presence of additives can also affect the ESR signals. Indeed, alkyl radicals were present in all PA samples. No significant differences in radical concentration were found when comparing the effects of gamma, e-beam, and X-ray irradiation on these materials.

The generation and decay of free radicals in PA appeared equivalent, even though the specific radicals varied.

The thermal properties of polyamides were also investigated using DSC, and no significant differences were observed in the melting temperature regardless of the irradiation technologies or the doses.

The objective was to determine whether the type of radiation source influences the radicals generated during material interaction. The lack of differences suggests that the behavior of the materials after irradiation is likely to be similar regardless of the radiation source used. The melting temperature, the ESR signals uniformity, the kinetics decay and the radical concentration profiles with gamma, e-beam, and X-rays in PA lend credence to the hypothesis of a standardized radiation interaction with condensed matter.

## Data availability

The data supporting this article have been included as part of the ESI.†

## Conflicts of interest

There are no conflicts to declare.

Open Access Article. Published on 23 July 2024. Downloaded on 7/30/2024 10:18:57 AM.
This article is licensed under a Creative Commons Attribution-NonCommercial 3.0 Unported Licence.

## Acknowledgements

N. D., F. G. and S. R. A. M. are thankful to Aix-Marseille Université (AMU), Institut de Recherche pour le Développement (IRD) and Centre National pour la Recherche Scientifique (CNRS) for support.

## Notes and references

1 BPAS Technical Guide, X-rays Sterilization of single-Use BioProcess Equipment, Part 1: Industry Need, Requirements & Risk Evaluation, 2021.
2 S. A. Umoren, M. M. Solomon and V. S. Saji, *Polymeric Materials in Corrosion inhibition fundamentals and applications*, 2022, pp. 541–563.
3 N. Girard-Perier, M. Claeys-Bruno, S. R. A. Marque, N. Dupuy, F. Gaston and S. Dorey, Effects of X-ray, electron beam and gamma irradiation on PE/EVOH/PE multilayer film properties, *Chem. Commun.*, 2021, **57**, 11049–11051.
4 N. Dupuy, S. R. A. Marque, L. S. Fifield, M. Pharr, D. Staack, S. D. Pillai, L. Nichols, M. K. Murphy and S. Dorey, Supplementing Gamma Sterilization with X-Ray and E-Beam Technologies, *Bioprocess Technol.*, 2022, **20**, 24–28.
5 M. Wellesley, BBC publishing, 2020.
6 P. M. Armenante and O. Akiti, in *Chemical Engineering in the Pharmaceutical Industry*, ed. D. J. Am Ende and M. T. Am Ende, John Wiley & Sons, Inc., Hoboken, NJ, USA, 2019, pp. 311–379.
7 D. Darwis Erizal, B. Abbas, F. Nurlidar and D. P. Putra, Radiation Processing of Polymers for Medical and Pharmaceutical Applications, *Macromol. Symp.*, 2015, **353**, 15–23.
8 S. Moondra, N. Raval, K. Kuche, R. Maheshwari, M. Tekade and R. K. Tekade, *Dosage form design parameters*, Elsevier, 2018, pp. 467–519.
9 H. de Brouwer, Comparison of the effects of x-ray and gamma irradiation on engineering thermoplastics, *Radiat. Phys. Chem.*, 2022, **193**, 109999.
10 B. Croonenborghs, M. A. Smith and P. Strain, X-ray versus gamma irradiation effects on polymers, *Radiat. Phys. Chem.*, 2007, **76**, 1676–1678.
11 T. K. Kroc, Monte Carlo simulations demonstrating physics of equivalency of gamma, electron-beam, and X-ray for radiation sterilization, *Radiat. Phys. Chem.*, 2023, **204**, 110702.
12 K. Makuuchi and S. Cheng, *Radiation Processing of Polymer Materials and its Industrial Applications*, John Wiley & Sons, Inc., Hoboken, NJ, USA, 1st edn, 2012.
13 G. Sadler, W. Chappas and D. E. Pierce, Evaluation of e-beam, γ- and X-ray treatment on the chemistry and safety of polymers used with pre-packaged irradiated foods: a review, *Food Addit. Contam.*, 2001, **18**, 475–501.
14 *Applications of ionizing radiation in materials processing*, ed. A. G. Chmielewski and Y. Sun, Institute of Nuclear Chemistry and Technology, Warszawa, 2017, vol. 1.
15 J. Ahmed, J. Wu, S. Mushtaq and Y. Zhang, Effects of electron beam irradiation and multi-functional monomer/co-agents on the mechanical and thermal properties of ethylene-vinyl acetate copolymer/polyamide blends, *Mater. Today Commun.*, 2020, **23**, 100840.
16 M. Morino, Y. Nishitani, T. Kitagawa and S. Kikutani, Thermal, Mechanical and Tribological Properties of Gamma-Irradiated Plant-Derived Polyamide 1010, *Polymers*, 2023, **15**, 3111.
17 P. Simon, A. Rocketm and M. Azori, Esr Study Of 7-Irradiated Nylon-6; Conformational Isomerism Of Free Radicals, *Eur. Polym. J.*, 1977, **13**, 189–192.
18 M. I. Chipara, ESR investigations on ion beam irradiated polymers, *Nucl. Instrum. Methods Phys. Res., Sect. B*, 1997, **131**, 85–90.
19 R. Tian, K. Li, Y. Lin, C. Lu and X. Duan, Characterization Techniques of Polymer Aging: From Beginning to End, *Chem. Rev.*, 2023, **123**, 3007–3088.
20 H. Yoshida and B. Rånby, Electron spin resonance studies on oriented polyoxymethylene, *J. Polym. Sci., Part A: Gen. Pap.*, 1965, **3**, 2289–2302.
21 A. Oshima, T. Seguchi and Y. Tabata, Radiation-induced free radicals and their behaviour in crosslinked polytetrafluoroethylene (PTFE), *Polym. Int.*, 1999, **48**, 996–1003.
22 P. A. Polyamides, **https://www.techniques.ingenieur.fr/base-documentaire/materiaux-th11/matieres-thermoplastiques-monographies-42147210/polyamides-pa-a3360/**, accessed May 31, 2024.
23 B. Krieguer, S. R. A. Marque, S. Dorey, N. Dupuy, F. Girard, N. Girard-Perier, F. Kuntz and N. Ludwig, Radical detection and electron-spin resonance (ESR) monitoring in polymer materials irradiated with gamma and X-rays: Polyethylene and polypropylene, *J. Appl. Polym. Sci.*, 2024, e55098.
24 G. Audran, S. Dorey, N. Dupuy, F. Gaston and S. R. A. Marque, Degradation of γ-irradiated polyethylene-ethylene vinyl alcohol-polyethylene multilayer films: An ESR study, *Polym. Degrad. Stab.*, 2015, **122**, 169–179.
25 Y. Ni, T. T. Bisel, M. K. Hasan, D. Li, W. K. Fuchs, S. K. Cooley, L. Nichols, M. Pharr, N. Dupuy, S. R. A. Marque, M. K. Murphy, S. D. Pillai, S. Dorey and L. S. Fifield, Compatibility of ethylene vinyl acetate (EVA)/ethylene vinyl alcohol (EVOH)/EVA films with gamma, electron-beam, and X-ray irradiation, *npj Mater. Degrad.*, 2023, **7**, 93.
26 C. T. Graves and M. G. Ormerod, The Radiation Chemistry of Some Polyamides, *Electron Spin Reson.*, 1963, **4**, 81–91.
27 B. Li and L. Zhang, Dependence of decaying of trapped radicals on aggregates of polyamide 1010, *Radiat. Phys. Chem.*, 1997, **49**, 395–397.
28 A. G. Davies, J. A. Howard and M. Lehnig, *Magnetic properties of free radicals- Organic O-, P-, Se-, Si-, Ge-, Sn-, Pb-, As-, Sb-Centered Radicals*, 1979, vol. 9c2.
29 H. Paul, H. Fischer and A. Berndt, *Magnetic properties of free radicals- Organic C-Centered Radicals*, 1977, vol. 9b.
30 N. Gobeltz, A. Demortier, J. P. Lelieur and C. Duhayon, Correlation between EPR, Raman and colorimetric characteristics of the blue ultramarine pigments, *Faraday Trans.*, 1998, **94**, 677–681.
31 S. D. McLaughlan and D. J. Marshall, Paramagnetic resonance of sulfur radicals in synthetic sodalites, *J. Phys. Chem.*, 1970, **74**, 1359–1363.

Open Access Article. Published on 23 July 2024. Downloaded on 7/30/2024 10:18:57 AM.
This article is licensed under a Creative Commons Attribution-NonCommercial 3.0 Unported Licence.

32 Minitab software.
33 T. Wang, X. Li, R. Luo, Y. He, S. Maeda, Q. Shen and W. Hu, Effects of amide comonomers on polyamide 6 crystallization kinetics, *Thermochim. Acta*, 2020, **690**, 178667.
34 J. Simek, V. Dockalova, Z. Hrdlicka and V. Duchacek, Effect of liquid butadiene rubber on mechanical properties of polyamide 11/polyamide 12 blends, *J. Polym. Eng.*, 2015, **35**, 349–357.
35 H. Ghasemi, A. Mirzadeh, P. J. Bates and M. R. Kamal, Effect of Polyamide 66 on the Mechanical and Thermal Properties of Post-Industrial Waste Polyamide 6, *Polym.-Plast. Technol. Eng.*, 2014, **53**, 1794–1803.
36 C. Menchaca, A. Alvarez-Castillo, G. Martinez-Barrera, H. Lopez-Valdivia, H. Carrasco and V. M. Castano, Mechanisms for the modification of nylon 6,12 by gamma irradiation, *IJMPT*, 2003, **19**, 521.
37 M. C. Evora, L. D. B. Machado, V. L. Lourenço, O. L. Gonçalez and H. Wiebeck, Thermal Analysis of Ionizing Radiation Effects on Recycled Polyamide-6, *J. Therm. Anal. Calorim.*, 2002, **67**, 327–333.

# Supporting information: Thermal properties and radical monitoring after gamma, X-ray, and electron beam irradiation in Polyamide

## Electron Spin Resonance

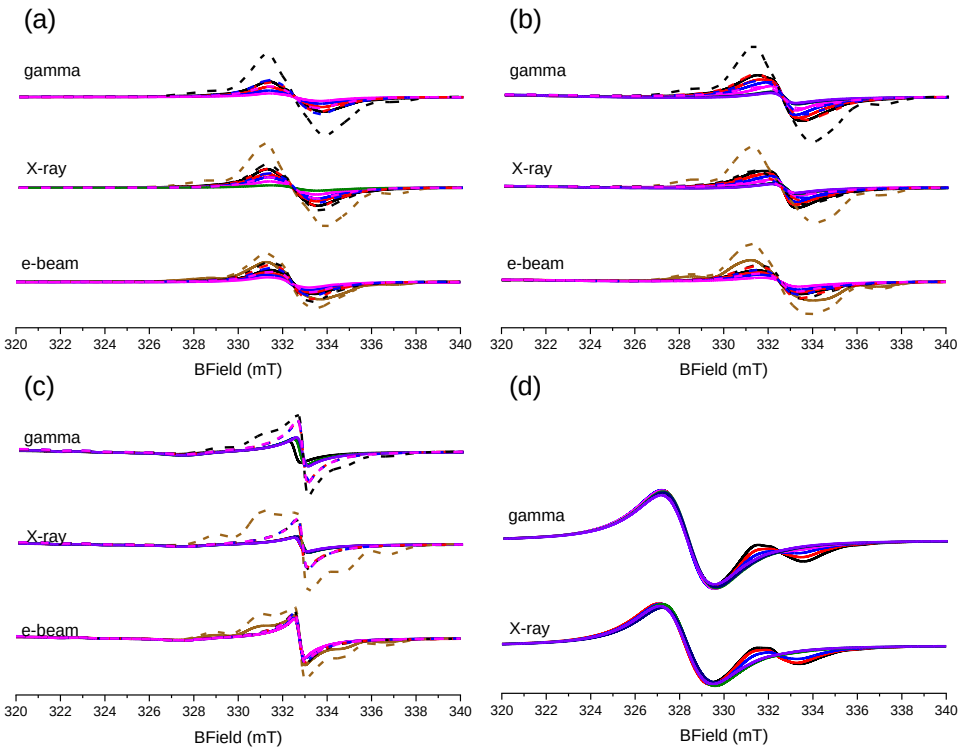


Figure S1: ESR signal of irradiated PA samples by gamma, X-ray and e-beam at 50 kGy (solid line) and 100 kGy (dotted line) ESR signal were recorded at one day (brown line) 9 days (black line), 15 days (red line), 30 days (blue line), 60 days (pink line), 120 days (green line), 180 days (navy line) and 380 days (purple line). (a) PA-1. (b) PA-2. (c) PA-3. (d) PA-4.

## Model regression results of PA-1

### Method

Categorical predictor (1; coding 0)

### Regression Equation

| Irradiation technologies | | | | |
|---|---|---|---|---|
| e-beam | Spin/mg | = | 154982362322843 + 5306709765816 Dose | - 7417296941425 Ageing after irradiation |
| gamma | Spin/mg | = | 143404658668274 + 5306709765816 Dose | - 7417296941425 Ageing after irradiation |
| X-ray | Spin/mg | = | 217719144189160 + 5306709765816 Dose | - 7417296941425 Ageing after irradiation |

### Coefficients

| Term | Coef | SE Coef | T-Value | P-Value | VIF |
|---|---|---|---|---|---|
| Constant | 1,43405E+14 | 1,00518E+14 | 1,43 | 0,168 | |
| Ageing after irradiation | -7,41730E+12 | 1,28439E+12 | -5,77 | 0,000 | 1,01 |

| | | | | | |
|---|---|---|---|---|---|
| Dose | 5,30671E+12 | 1,04966E+12 | 5,06 | 0,000 | 1,00 |
| Irradiation technologies | | | | | |
| e-beam | 1,15777E+13 | 6,48673E+13 | 0,18 | 0,860 | 1,43 |
| X-ray | 7,43145E+13 | 6,62274E+13 | 1,12 | 0,274 | 1,42 |

### Model Summary

| S | R-sq | R-sq(adj) | R-sq(pred) |
|---|---|---|---|
| 1,35939E+14 | 74,57% | 69,94% | 61,42% |

### Analysis of Variance

| Source | DF | Adj SS | Adj MS | F-Value | P-Value |
|---|---|---|---|---|---|
| Regression | 4 | 1,19204E+30 | 2,98009E+29 | 16,13 | 0,000 |
| Ageing after irradiation | 1 | 6,16293E+29 | 6,16293E+29 | 33,35 | 0,000 |
| Dose | 1 | 4,72327E+29 | 4,72327E+29 | 25,56 | 0,000 |
| Irradiation technologies | 2 | 2,81628E+28 | 1,40814E+28 | 0,76 | 0,479 |
| Error | 22 | 4,06546E+29 | 1,84794E+28 | | |
| Total | 26 | 1,59858E+30 | | | |

### Fits and Diagnostics for Unusual Observations

| Obs | Spin/mg | Fit | Resid | Std Resid | |
|---|---|---|---|---|---|
| 5 | 8,91608E+14 | 6,07320E+14 | 2,84288E+14 | 2,33 | R |
| 13 | 1,11068E+15 | 7,40973E+14 | 3,69703E+14 | 3,02 | R |

## Model regression results of PA-2

### Method

| | |
|---|---|
| Categorical predictor coding | (1; 0) |

### Regression Equation

| Irradiation technologies | | | | |
|---|---|---|---|---|
| e-beam | Spin/mg | = | 246928278495736 + 1824114350704 Dose | - 5708020409260 Ageing after irradiation |
| gamma | Spin/mg | = | 347424098552292 + 1824114350704 Dose | - 5708020409260 Ageing after irradiation |
| X-ray | Spin/mg | = | 283556043325953 + 1824114350704 Dose | - 5708020409260 Ageing after irradiation |

### Coefficients

| Term | Coef | SE Coef | T-Value | P-Value | VIF |
|---|---|---|---|---|---|
| Constant | 3,47424E+14 | 9,38518E+13 | 3,70 | 0,001 | |
| Ageing after irradiation | -5,70802E+12 | 1,19921E+12 | -4,76 | 0,000 | 1,01 |
| Dose | 1,82411E+12 | 9,80049E+11 | 1,86 | 0,076 | 1,00 |
| Irradiation technologies | | | | | |
| e-beam | -1,00496E+14 | 6,05655E+13 | -1,66 | 0,111 | 1,43 |
| X-ray | -6,38681E+13 | 6,18355E+13 | -1,03 | 0,313 | 1,42 |

### Model Summary

| S | R-sq | R-sq(adj) | R-sq(pred) |
|---|---|---|---|
| 1,26924E+14 | 56,25% | 48,29% | 34,17% |

### Analysis of Variance

| Source | DF | Adj SS | Adj MS | F-Value | P-Value |
|---|---|---|---|---|---|
| Regression | 4 | 4,55622E+29 | 1,13905E+29 | 7,07 | 0,001 |
| Ageing after irradiation | 1 | 3,64978E+29 | 3,64978E+29 | 22,66 | 0,000 |
| Dose | 1 | 5,58080E+28 | 5,58080E+28 | 3,46 | 0,076 |
| Irradiation technologies | 2 | 4,47425E+28 | 2,23713E+28 | 1,39 | 0,270 |
| Error | 22 | 3,54413E+29 | 1,61097E+28 | | |
| Total | 26 | 8,10035E+29 | | | |

### Fits and Diagnostics for Unusual Observations

| Obs | Spin/mg | Fit | Resid | Std Resid | |
|---|---|---|---|---|---|
| 5 | 7,65649E+14 | 4,78463E+14 | 2,87186E+14 | 2,52 | R |
| 13 | 7,25191E+14 | 4,60259E+14 | 2,64931E+14 | 2,32 | R |

| | | | | | |
|---|---|---|---|---|---|
| 23 | 6,63203E+14 | 4,23632E+14 | 2,39572E+14 | 2,08 | R |

*R Large residual*

# Model regression results of PA-3

## Method

Categorical predictor coding (1; 0)

## Regression Equation

| Irradiation technologies | | | | |
|---|---|---|---|---|
| e-beam | Spin/mg | = 55944561495113 + 5099031780666 Dose | - 2042747866180 Ageing after irradiation | |
| gamma | Spin/mg | = 105905108987982 + 5099031780666 Dose | - 2042747866180 Ageing after irradiation | |
| X-ray | Spin/mg | = 41581151504161 + 5099031780666 Dose | - 2042747866180 Ageing after irradiation | |

## Coefficients

| Term | Coef | SE Coef | T-Value | P-Value | VIF |
|---|---|---|---|---|---|
| Constant | 1,05905E+14 | 1,20464E+14 | 0,88 | 0,389 | |
| Ageing after irradiation | -2,04275E+12 | 1,53926E+12 | -1,33 | 0,198 | 1,01 |
| Dose | 5,09903E+12 | 1,25795E+12 | 4,05 | 0,001 | 1,00 |
| Irradiation technologies | | | | | |
| e-beam | -4,99605E+13 | 7,77393E+13 | -0,64 | 0,527 | 1,43 |
| X-ray | -6,43240E+13 | 7,93694E+13 | -0,81 | 0,426 | 1,42 |

## Model Summary

| S | R-sq | R-sq(adj) | R-sq(pred) |
|---|---|---|---|
| 1,62914E+14 | 46,44% | 36,70% | 19,01% |

## Analysis of Variance

| Source | DF | Adj SS | Adj MS | F-Value | P-Value |
|---|---|---|---|---|---|
| Regression | 4 | 5,06191E+29 | 1,26548E+29 | 4,77 | 0,006 |
| Ageing after irradiation | 1 | 4,67439E+28 | 4,67439E+28 | 1,76 | 0,198 |
| Dose | 1 | 4,36081E+29 | 4,36081E+29 | 16,43 | 0,001 |
| Irradiation technologies | 2 | 1,89681E+28 | 9,48403E+27 | 0,36 | 0,704 |
| Error | 22 | 5,83902E+29 | 2,65410E+28 | | |
| Total | 26 | 1,09009E+30 | | | |

## Fits and Diagnostics for Unusual Observations

| Obs | Spin/mg | Fit | Resid | Std Resid | |
|---|---|---|---|---|---|
| 5 | 9,86742E+14 | 5,97424E+14 | 3,89319E+14 | 2,66 | R |
| 13 | 8,54593E+14 | 5,49442E+14 | 3,05152E+14 | 2,08 | R |

*R Large residual*

## Thermal properties (DSC)

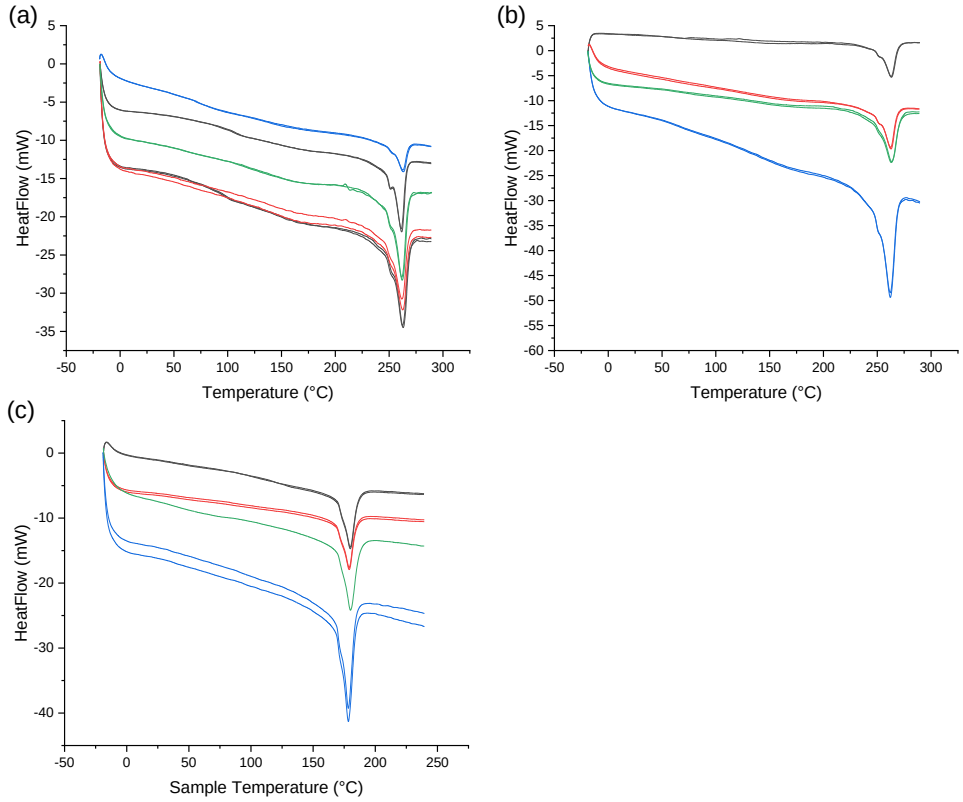


Figure S2: Representative DSC responses of PA non-irradiated (black) and irradiated by gamma (red), X-ray (blue) and e-beam (green) at 50 kGy. Data were taken from the second heating ramp. (a) PA-1. (b) PA-2. (c) PA-3.

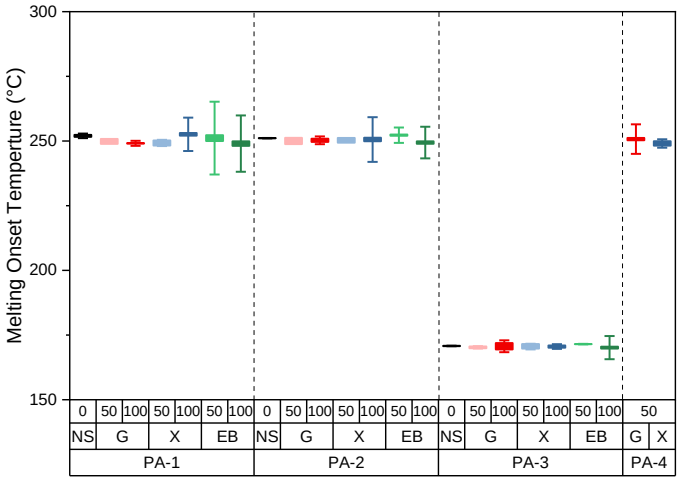


Figure S3: Melting Onset temperature for the PA-1, PA-2, PA-3, and PA-4 non-irradiated (black) and irradiated by gamma (red), X-ray (blue) and e-beam (green) at 50 and 100 kGy. The error bar represents the 95% confidence interval.

# Conclusion et perspectives

Les polymères revêtent une importance cruciale dans l'industrie biopharmaceutique grâce à leur polyvalence et à leur adaptabilité à une multitude d'usage. Ces matériaux sont essentiels pour la fabrication de produits à usage unique, d'emballages, et de systèmes de délivrance de médicaments. Leur stabilité chimique, leurs propriétés mécaniques, et leur faculté à être adaptés à des fonctions spécifiques en font des choix idéaux pour des environnements où la stérilité et la fiabilité sont des priorités absolues. Leur capacité à être stérilisés sans perdre leurs propriétés est un atout remarquable. Par exemple, les systèmes à usage unique, tels que les seringues, les cathéters, et les tubes, sont souvent élaborés à partir de polymères en raison de leur coût relativement bas et de leur facilité de production en masse. Ces produits doivent être stériles pour éviter toute contamination, et les polymères permettent d'atteindre ce niveau de stérilité grâce à des procédés de fabrication contrôlés.

Les polymères présentent plusieurs avantages qui les rendent incontournables dans l'industrie biopharmaceutique. Leur légèreté et leur flexibilité permettent de concevoir des dispositifs qui sont non seulement efficaces mais aussi confortables pour les patients. De plus, les polymères peuvent être formulés pour résister à des conditions environnementales variées, telles que des températures extrêmes ou des expositions chimiques, ce qui est crucial pour les applications biopharmaceutiques.

La société Sartorius est une figure de proue de l'industrie biopharmaceutique, maîtrisant l'art de la fabrication de divers polymères pour concevoir une vaste gamme de produits indispensable. Parmi ces produits, on trouve des systèmes de filtration, des poches de stockage, et des équipements de traitement à usage unique. Ces produits sont conçus pour répondre aux normes rigoureuses de stérilité et de sécurité, un aspect crucial dans le domaine biopharmaceutique.

Les systèmes de filtration, par exemple, utilisent des membranes polymères pour séparer les impuretés des produits biopharmaceutiques. Ces membranes doivent être chimiquement stables et capables de résister à des pressions élevées sans se dégrader. Les poches de stockage fabriquées à partir de polymères doivent également être stériles et capables de contenir des substances sensibles sans réagir avec elles.

Malgré leurs nombreux avantages, l'utilisation des polymères dans l'industrie biopharmaceutique présente également des défis. Un des principaux défis est la nécessité de garantir que les polymères utilisés ne libèrent pas de substances nocives dans les produits biopharmaceutiques tout en gardant leur intégrité. Cela nécessite des tests rigoureux et des contrôles de qualité pour s'assurer que les matériaux soient sûrs.

Les récentes innovations dans le domaine des polymères visent à surmonter ces défis. Par exemple, le développement de polymères à haute performance qui peuvent résister à des conditions de stérilisation plus rigoureuses sans se dégrader est une avancée significative. De plus, l'utilisation de technologies avancées de fabrication, telles que l'impression 3D, permet de créer des dispositifs polymères avec des structures complexes qui étaient auparavant impossibles à réaliser.

Pour mener à bien notre étude, nous avons été confrontés au défi de ne pas pouvoir effectuer une analyse exhaustive de tous les types de polymères employés dans le domaine des biotechnologie pharmaceutiques. Nous avons donc dû sélectionner des polymères d'intérêt selon plusieurs critères. Ces critères incluent les matériaux en contact avec des fluides, la durée de contact avec la solution, les polymères les plus couramment utilisés avec une forte représentativité, et la présence d'additifs dans la composition des polymères. Cette sélection nous a permis de concentrer nos efforts sur les polymères les plus pertinents pour l'industrie. Les films multicouches et les principaux polymères (Polypropylène, PP ; Polyéthylène, PE ; Polyamide, PA) font partie de cette sélection.

Depuis une dizaine d'années, notre équipe s'est spécialisée dans l'analyse des films multicouches, tels que EVA/EVOH/EVA (le film Sartorius S71) et PE/EVOH/PE (le film Sartorius S80), en raison de leur utilisation courante dans l'emballage biopharmaceutique. Ces films sont essentiels pour protéger les produits biologiques sensibles grâce à leurs propriétés barrières et leur résistance mécanique, les préservant de l'oxygène et de tout autre échange gazeux. Les films EVA/EVOH/EVA et PE/EVOH/PE sont particulièrement prisés pour leur efficacité. L'alcool éthylène-vinyle (EVOH) est utilisé comme couche barrière pour ses excellentes propriétés de protection contre l'oxygène, importante pour maintenir l'efficacité des produits biopharmaceutiques. Nous avons étudié les modifications de ces films en analysant leurs caractéristiques physico-chimiques à travers une étude multi-échelle, comparant l'impact des trois technologies d'irradiation.

Notre équipe a entrepris une étude approfondie des propriétés physico-chimiques de ces films post-stérilisation. L'objectif était de comprendre comment les différentes technologies d'irradiation affectent ces matériaux. L'irradiation est couramment utilisée pour stériliser les matériaux biopharmaceutiques. Cependant, elle peut également induire des modifications dans les propriétés des films. Notre étude a comparé l'impact de trois technologies d'irradiation : les rayons gamma, les rayons X et le faisceau d'électrons. Chacune de ces méthodes a ses propres avantages et inconvénients, et il est fondamental de comprendre comment elles influencent les propriétés des films multicouches.

Les rayons gamma sont largement utilisés pour leur capacité à pénétrer profondément dans les matériaux. Ils peuvent provoquer des changements dans la structure chimique des polymères. Les rayons X, bien qu'ils aient une pénétration similaire, pourraient avoir des effets différents en raison de leur énergie différente. Le faisceau d'électrons, quant à lui, est souvent utilisé pour des applications plus superficielles de stérilisation ou de faible densité.

Les résultats de notre recherche ont des implications pratiques importantes pour l'industrie biopharmaceutique : comprendre comment les différentes technologies d'irradiation affectent les matériaux et permettre aux fabricants de choisir la méthode la plus appropriée pour leurs besoins spécifiques. Toutefois, l'utilisation de ces technologies, soulève des défis, notamment la formation des radicaux libre qui peuvent affecter la stabilité des polymères. Il est donc essentiel de continuer à explorer des moyens de minimiser ces effets indésirables tout en maximisant les avantages de l'irradiation.

L'intégration de technologies de pointe, telles que l'analyse spectroscopique, peut fournir des informations plus détaillées sur les modifications induites par l'irradiation.

L'approche analytique multi-échelle employée dans les articles décrits précédemment fournit une compréhension complète de l'impact de l'irradiation. Nous avons examiné les changements à l'échelle moléculaire, macro-moléculaire et à l'échelle du matériau (Figure 15), cette méthode d'analyse nous a permis d'obtenir des informations sur les transformations chimiques et physiques se produisant après l'irradiation afin de déterminer l'impact et l'équivalence des trois technologies d'irradiations [1].

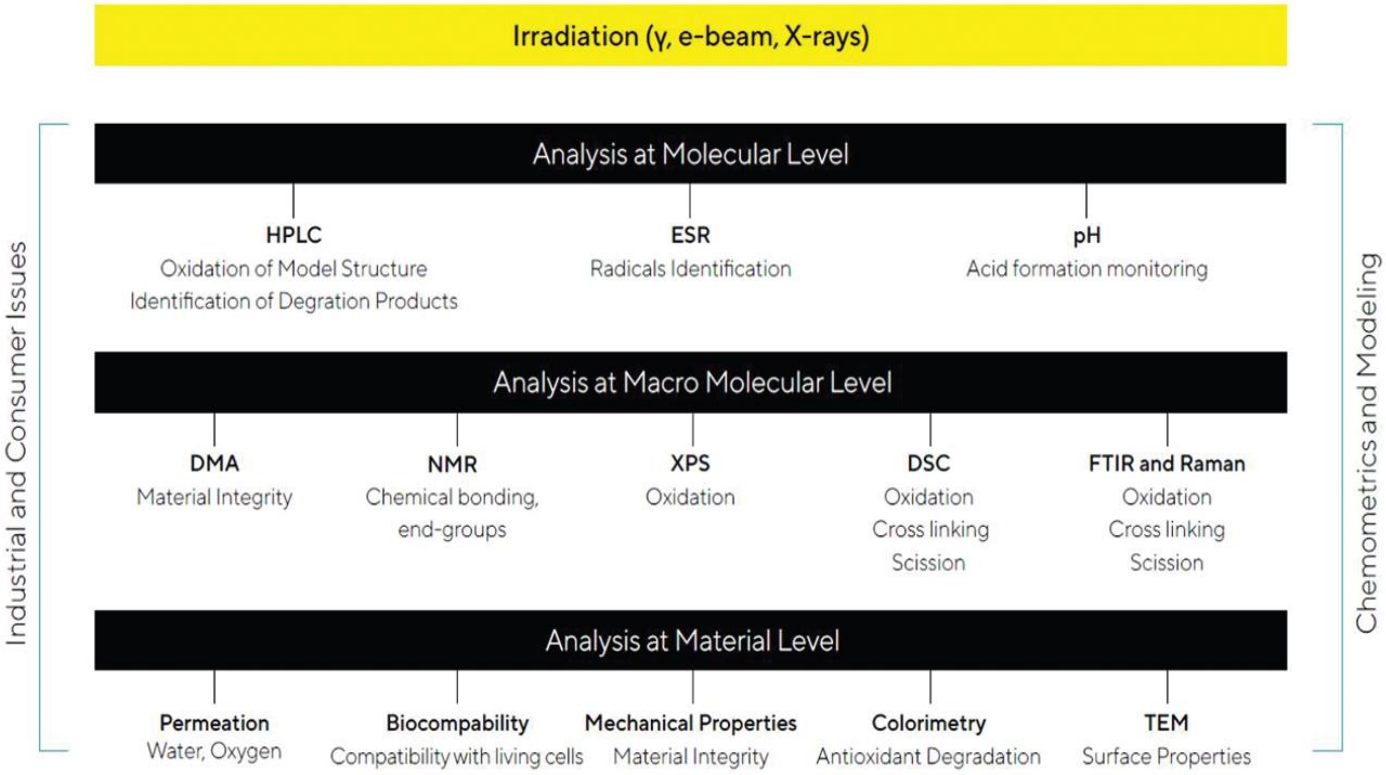


Figure 15 : Analyse multi-échelle pour caractériser les matériaux après irradiations gamma, rayons X et faisceau d'électrons [1]

Cette approche multi-échelle fait partie d'un effort conjoint entre l'industrie et le milieu universitaire pour répondre à la demande croissante de capacité de stérilisation et aux limites des méthodes traditionnelles, comme l'irradiation gamma et l'oxyde d'éthylène (EO). Nous avons participé à l'effort d'élaboration de cette approche multi-échelle et nous l'avons appliquée. L'intégration des disciplines, incluant la chimie, la physique, la mécanique, la science des matériaux et les mathématiques est cruciale pour comprendre les effets variés des différentes méthodes de stérilisation sous les matériaux. L'analyse multi-échelle se concentre sur plusieurs aspects. Au niveau moléculaire, elle examine les processus chimiques et les espèces radicalaires formées lors de l'irradiation, en utilisant des techniques comme la RPE, l'HPLC et la pH-métrie. Au niveau macromoléculaire, elle

étudie les changements dans les liaisons chimiques et l'intégrité des matériaux à l'aide de la DMA, de la DSC et de la spectroscopie photoélectronique X (XPS). Au niveau des matériaux, elle évalue les propriétés critiques pour les utilisateurs finaux, telles que les propriétés mécaniques, la colorimétrie, la qualité de surface et la biocompatibilité. La démarche d'étude globale du projet team NABLO, analyse l'impact de l'irradiation, gamma, faisceau d'électrons, et des rayons X sur les polymères et les composants médicaux, incluant les essais de biocompatibilité, de caractérisation, des matériaux et de fonctionnalités. Les informations basées sur les données sont générées et analysées à l'aide de méthodes chimiométriques comme l'analyse en composantes principales et la conception de plan d'expériences, aidant à comprendre les changements à l'échelle moléculaire et macromoléculaire qui pourraient affecter les propriétés des matériaux. La collaboration industrielle et académique est stratégique, impliquant des fabricants de systèmes à usage unique et de produits biopharmaceutiques, des fabricants d'équipements faisceau d'électrons et rayons X, des laboratoires nationaux pour garantir que les résultats soient pertinents et
applicables à l'industrie des produits de santé. La validation et la caractérisation incluent la validation des méthodes de stérilisation en comparant les effets des différentes technologies d'irradiation sur les propriétés des matériaux et la fonctionnalité des dispositifs, identifiant des alternatives viables à l'irradiation gamma. Cette approche multi-échelle vise à fournir une compréhension approfondie de la manière dont les différentes méthodes de stérilisation affectent les matériaux à divers niveaux, garantissant que des technologies alternatives comme le faisceau d'électrons et les rayons X peuvent être utilisées efficacement et surement aux côtés de la stérilisation gamma traditionnelle. Revoyons maintenant les principales conclusions érigées à chaque échelle.

Au niveau moléculaire, nous avons analysé la formation des radicaux plusieurs jours après les différentes irradiations. L'étude des radicaux est déterminante, car la formation d'espèces radicalaires est à la base de toutes les modifications des polymères. Ces études nous ont permis de démontrer que pour chaque classe de polymères, des radicaux sont formés, et chaque classe de polymères génère des radicaux avec une cinétique de décroissance propre à sa classe.

Pour chaque classe de polymères, l'identification, la concentration et la cinétique des radicaux générés après irradiation sont équivalentes pour les trois technologies d'irradiation (gamma, rayons X et faisceau d'électrons) pour une dose allant jusqu'à 100 kGy.

L'étude sur la formation des radicaux a permis de montrer que la composition des matériaux impacte la concentration en radicaux ou engendre des radicaux supplémentaires. Les films multicouches, présentent une variation de concentration en radicaux entre le film EVA/EVOH/EVA et le film PE/EVOH/PE en raison de l'épaisseur et de la formulation de la couche EVOH. Pour le PP ou le PA, la présence d'additifs dans certains échantillons analysés induit des espèces radicalaires au sein des matériaux. Ces variations sont observées quelle que soit la technologie d'irradiation utilisée.

L'étude de l'oxydation d'une solution de méthionine en contact avec les matériaux a permis d'identifier les produits de dégradation à l'échelle moléculaire. Cette analyse a été faite avec les films multicouches et avec le PP.

Les résultats obtenus avec le film multicouche PE/EVOH/PE ont montré que la formation de radicaux et l'oxydation de la méthionine étaient principalement influencées par le temps de contact avec la solution, plutôt que par le débit de dose ou la technologie d'irradiation. Pour le PP, la technologie d'irradiation impacte de manière équivalente l'oxydation de la méthionine. Les analyses ont révélé que la formulation du PP, notamment la présence d'additifs, jouait un rôle dans l'oxydation de la solution de méthionine.

Les analyses au niveau macro-moléculaire permettent d'obtenir des informations sur l'intégrité des matériaux. Les analyses DMA du film PE/EVOH/PE ont démontré que les propriétés viscoélastiques du film irradié dans des conditions industrielles sont équivalentes pour les trois technologies d'irradiation. Nous avons également examiné les modifications potentielles des propriétés thermiques par DSC des matériaux après irradiation. Aucune modification n'a été observée pour le PA après irradiation par les trois technologies. Pour le PP, nous avons noté une diminution de la température de fusion des matériaux irradiés, avec un effet de dose : plus le PP est irradié à une forte dose, plus sa température de fusion diminue, indiquant une modification de sa structure.

L'irradiation peut provoquer l'oxydation, la réticulation et la rupture de chaînes dans les matériaux polymères. Pour le film EVA et le PP, aucune modification n'a été détectée après l'application des trois technologies d'irradiation, selon les analyses effectuées par spectroscopie infrarouge. Cependant, les spectres infrarouges ont révélé que les différents échantillons de PP possèdent des formulations variées, incluant des additifs.

Les données obtenues par spectroscopie ont permis de modéliser la dose absorbée par le film EVA et de déterminer l'impact de l'irradiation. Les résultats ont montré que l'irradiation par rayons gamma et X a un impact équivalent, tandis que l'irradiation par faisceau d'électrons a un impact plus faible sur le film.

Au niveau du matériau, nous avons analysé les propriétés mécaniques du PP et du film PE/EVOH/PE en réalisant des tests de traction. Nous avons pu conclure que les trois technologies d'irradiation à 50 kGy n'influencent pas les propriétés mécaniques du film. Les propriétés mécaniques du PP sont équivalentes après irradiation par les trois technologies.

Le jaunissement du matériau après irradiation est également un indicateur de la modification du polymère. Nous avons analysé le jaunissement de deux échantillons de PP par colorimétrie. Cette étude a montré que le matériau irradié par rayons X et gamma présente un jaunissement plus prononcé que celui irradié par faisceau d'électrons pour un échantillon, tandis que l'autre ne montre pas de différence significative entre les trois technologies. Le jaunissement est dû à la dégradation des additifs au sein des matériaux, et non à la chaîne polymère du PP.

Le vieillissement des polymères sous irradiation est un processus complexe qui dépend de nombreux facteurs, tels que la dose de radiation, la durée d'exposition et les conditions environnementales. Le vieillissement après irradiations ionisantes, par exemple, est le résultat d'un processus compétitif de scission de chaînes et de post-réticulation, qui peut altérer les propriétés mécaniques et chimiques du matériau. Les mécanismes de dégradation des polymères sous irradiation sont complexes et multifactoriels. Par exemple, la photo-oxydation implique des interactions entre les polymères et l'oxygène, ainsi que des réactions secondaires qui peuvent influencer les propriétés du matériau. Comprendre pleinement ces mécanismes a nécessité des études approfondies et multidisciplinaires.

Une des principales limites des études actuelles est la variabilité des conditions expérimentales. Les résultats peuvent varier en fonction des types de polymères étudiés, des sources de radiation utilisées et des conditions environnementales (température, humidité, etc.). Cette variabilité pourrait rendre difficiles la généralisation des résultats et la prédiction des comportements des polymères dans toutes les conditions réelles. La plupart des études sur les effets de l'irradiation sont menées sur des périodes relativement courtes, ce qui peut ne pas refléter les effets à long terme de l'exposition aux radiations. Les polymères peuvent subir des changements progressifs qui ne sont pas détectables dans des études à court terme, mais qui peuvent avoir des impacts significatifs sur leur durabilité et leur performance à long terme. Pour cette raison, nous avons mené des études jusqu'à trois ans post-irradiation.

La recherche s'est concentrée sur un éventail restreint de grades et de formulations de polymères, ce qui pourrait ne pas refléter pleinement la diversité des matériaux utilisés dans les applications industrielles. Les recherches futures pourraient élargir la variété des polymères et des additifs étudiés pour obtenir une compréhension plus complète des facteurs influençant la génération et la stabilité des radicaux. La recherche pourrait également se concentrer sur le développement de nouveaux polymères et composites résistants aux radiations. Cela pourrait inclure l'incorporation d'additifs stabilisants, la modification chimique des polymères existants ou la conception de nouveaux matériaux avec des structures moléculaires optimisées pour résister aux effets de l'irradiation. Cet axe de recherche n'est cependant pas possible au vu des applications biopharmaceutiques visées, pour lesquelles un changement de formulation entraînerait une requalification complète. D'un point de vue industriel, ce n'est pas réaliste.

Les techniques de modélisation et de simulation pourront certainement contribuer à la compréhension des effets de l'irradiation sur les polymères. Les modèles numériques ont le potentiel de prédire les comportements des matériaux sous différentes conditions de radiation et à identifier les mécanismes de dégradation clés. Ces outils peuvent également être utilisés pour optimiser la conception des polymères et améliorer leur résistance aux radiations. C'est une piste que nous n'avons pas pu explorer dans le cadre de cette thèse.

Enfin, l'application des résultats de cette étude à d'autres secteurs, tels que les dispositifs médicaux, l'industrie alimentaire, l'aérospatiale et l'électronique, pourrait élargir l'impact de ces découvertes. Comprendre comment les formulations spécifiques influencent la réponse à l'irradiation dans ces contextes peut aider à optimiser les matériaux pour des performances améliorées et une sécurité accrue.

En conclusion, l'étude des interactions entre les radiations ionisantes et les polymères est essentielle pour comprendre et optimiser les processus de stérilisation dans l'industrie. L'utilisation de la RPE et de méthodes d'analyse avancées a permis d'identifier et de quantifier les radicaux générés, fournissant des informations précieuses sur les mécanismes sous-jacents et les implications pratiques de ces interactions. Les résultats obtenus confirment que les matériaux irradiés présentent un comportement équivalent, quelle que soit la source de rayonnement, offrant ainsi une plus grande flexibilité et sécurité dans le choix des méthodes de stérilisation. Les défis techniques et les perspectives de la recherche dans ce domaine ouvrent la voie à de nouvelles innovations et applications, renforçant ainsi l'importance de cette étude pour l'industrie et la recherche scientifique.

La faculté de substituer l'irradiation par rayons X et faisceau d'électrons à l'irradiation gamma pourrait améliorer considérablement la flexibilité et l'efficacité des procédés de stérilisation. Cela pourrait entraîner des économies de coûts et une réduction de la dépendance au cobalt 60, la principale source de rayons gamma, qui est soumise à des contraintes d'approvisionnement.

Bien que ces études fournissent des informations précieuses sur les effets de l'irradiation sur les matériaux polymères, elles présentent également des limites qui potentiellement mériteraient d'être explorées davantage. L'étude s'est concentrée sur un nombre limité de grades et de formulations de polymères, ce qui peut ne pas capturer pleinement la diversité des matériaux utilisés dans les applications industrielles. Les recherches futures pourraient élargir la gamme de polymères et d'additifs étudiés pour fournir une compréhension plus complète des facteurs influençant la génération et la stabilité des radicaux. Le fond de la question est de savoir dans quelle mesure l'industrie a confiance ou au contraire, est incertaine quant à la nécessité ou non d'étudier d'autres systèmes pour tirer une conclusion générale sur l'équivalence des propriétés après irradiation, gamma, rayons X et faisceau d'électrons. Un niveau de confiance a-t-il été atteint ? Des exceptions sont-elles possibles ? Pouvons-nous accepter les exceptions potentielles qui pourraient nécessiter des ressources considérables, mais qui serait peu utile, voire inutiles ?

# Résumé

Les systèmes en plastique à usage unique sont conçus pour les industries biopharmaceutiques afin de stocker, transporter ou mélanger des solutions biopharmaceutiques. Ces systèmes, fabriqués à partir de polymères, sont actuellement stérilisés par rayonnement gamma. Le contexte sanitaire actuel entraîne une croissance de la production de produits destinés à l'industrie pharmaceutique. Des préoccupations émergent quant à la capacité de stérilisation par rayonnement gamma dans les années à venir. L'irradiation par faisceau d'électrons et par rayonnement X sont comparées pour être utilisées en tant que méthodes alternatives à la stérilisation gamma.

L'objectif de cette thèse est d'examiner l'impact potentiel des irradiations par rayons gamma, rayons X et faisceau d'électrons sur deux types de films (PE/EVOH/PE et EVA/EVOH/EVA) ainsi que sur des matériaux formulés à partir de polypropylène, de polyéthylène et de polyamide.

Les échantillons irradiés ont été analysés à l'aide d'une approche multi-échelle : au niveau moléculaire, macro-moléculaire et au niveau du matériau. Les résultats montrent que, quel que soit le polymère, les trois technologies d'irradiation produisent des effets équivalents : les mêmes types de radicaux sont générés, il n'y a pas de modification de la structure et de la composition des polymères observés dans les conditions d'analyse. Les variations observées entre les différentes classes de polymères sont principalement dues à la composition des matériaux.

# Abstract

Single-use plastic systems are intended for the biopharmaceutical industries to store, transport, or mix biopharmaceutical solutions. These systems, made from polymers, are currently sterilized by gamma radiation. The current health context is leading to an increase in the production of products intended for the pharmaceutical industry. Concerns are emerging about the capacity for gamma radiation sterilization in the coming years. Electron beam irradiation and X-ray irradiation are being compared as alternative methods to gamma sterilization.

The objective of this thesis is to examine the potential impact of gamma, X-ray, and electron beam irradiations on two types of films (PE/EVOH/PE and EVA/EVOH/EVA) as well as on materials formulated from polypropylene, polyethylene, and polyamide.

The irradiated samples were analyzed using a multi-scale approach: at the molecular, macromolecular, and material levels. The results show that, regardless of the polymer, the three irradiation technologies produce equivalent effects: the same types of radicals are generated, and there is no modification of the structure and composition of the polymers observed under the analysis conditions. The variations observed between the different classes of polymers are mainly due to the composition of the materials.